UNIVERSITY OF SOUTHAMPTON

Faculty of Engineering and Physical Sciences
Department of Physics and Astronomy

Modelling galaxy and black hole evolution via DECODE: Discrete statistical sEmi-empiriCal mODEl

by

Hao Fu

Supervisor: Prof. F. Shankar

A thesis submitted for the degree of
Doctor of Philosophy

April 2025

University of Southampton

Abstract

Faculty of Engineering and Physical Sciences
Department of Physics and Astronomy

Doctor of Philosophy

Modelling galaxy and black hole evolution via DECODE: Discrete statistical sEmi-empiriCal mODEl

by Hao Fu
Supervisor: Prof. F. Shankar

In a dark matter-dominated Universe, where structures grow hierarchically, galaxies are thought to live inside dark matter haloes with their evolution being intimately connected. In traditional models of galaxy evolution, galaxies build up their stellar mass via the interplay among several physical processes such as mergers, star formation and quenching, implying that all the observables characterizing galaxy evolution should be strictly linked to each other. These quantities include, for example, the galaxy stellar mass function, merger rates, star formation histories, satellite abundances and intracluster light. The failure in simultaneously fitting distinct observational probes may be attributed to shortcomings in the underlying modelling, or to disagreements in different data sets. Indeed, the systematic errors affecting observations still prevent universal and uniform measurements of, for instance, the stellar mass functions and the star formation rates, inevitably preventing theoretical models to compare with multiple data sets efficiently and simultaneously. Therefore, the need of well calibrated, homogeneous and self-consistent observational data sets is of vital importance for all types of theoretical galaxy evolution models, especially for data-driven models like semi-empirical ones. The goal of this thesis is to build a holistic perspective among all the aforementioned quantities in galaxy evolution via a semi-empirical approach, exploring the role of each involved physical process.

In this thesis, I will present DECODE, the Discrete statistical sEmi-empiriCal mODEl, and its contribution to the field of galaxy evolution. DECODE runs on top of object-by-object dark matter merger trees (hence discrete) generated from (sub)halo mass and infall redshifts distributions (hence statistical), without relying on full N-body simulations. Merger trees are then converted into galaxy assembly histories via abundance matching, using different stellar mass functions as input. First, I will apply DECODE to show the dependence of the output quantities on the input stellar mass function, probing that only specific characteristics of the latter can predict galaxy merger rates and star formation histories self-consistently with the latest observational data sets. Secondly, I will also show how DECODE can also efficiently predict other observables via simple merger models, such as the elliptical abundances, bulge-to-total distributions and intracluster light. Finally, I will present an updated version of DECODE, which grows galaxies via input star formation rate functions along with physically motivated quenching prescriptions, and will show the role of various quenching mechanisms in the stellar mass assembly histories of galaxies.

Contents

List of Figures

List of Tables

Definitions and Abbreviations

DECODE	Discrete statistical sEmi-empiriCal mODEl
AGN	Active Galactic Nucleus
BCG	Brightest Cluster Galaxy
BHAR	Black Hole Accretion Rate
B/T	Bulge-to-Total
FOF	Friend-Of-Friends
GMLR	Gas Mass Loss Rate
HAR	Halo Accretion Rate
(S)HMF	(Sub) Halo Mass Function
ICL	IntraCluster Light
IMF	Initial Mass Function
IR	InfraRed
ΛCDM	Λ Cold Dark Matter
LF	Luminosity Function
SAM	Semi-Analytical Model
SED	Spectral Energy Distribution
SEM	Semi-Empirical Model
SFH	Star Formation History
(s)SFR	(specific) Star Formation Rate
SMBH	SuperMassive Black Hole
SMF	Stellar Mass Function
SMHM	Stellar Mass-Halo Mass
UV	UltraViolet

Declaration of Authorship

I declare that this thesis and the work presented in it is my own and has been generated by me as the result of my own original research.

I confirm that:

1. This work was done wholly or mainly while in candidature for a research degree at this University;
2. Where any part of this thesis has previously been submitted for a degree or any other qualification at this University or any other institution, this has been clearly stated;
3. Where I have consulted the published work of others, this is always clearly attributed;
4. Where I have quoted from the work of others, the source is always given. With the exception of such quotations, this thesis is entirely my own work;
5. I have acknowledged all main sources of help;
6. Where the thesis is based on work done by myself jointly with others, I have made clear exactly what was done by others and what I have contributed myself;
7. Parts of this work have been published as:
   Fu et al. (2022) and Fu et al. (2024)

Signed:..... Date:.....

Acknowledgements

This PhD received funding from the European Union's Horizon 2020 research and innovation programme under the Marie Skłodowska-Curie grant agreement No. 860744 for the BiD4BESt project (Coordinator: F. Shankar).

I would like to thank my supervisor, Prof. Francesco Shankar, for this wonderful opportunity, his great patience and careful supervision. His passion for research and astrophysics motivated me a lot, especially during the early stage of my PhD, and I have learned a lot working with him. I would like to thanks also my co-supervisor, Prof. Andrea Lapi, for his supervision and help for the last part of my PhD.

I warmly thank Prof. Antony Bird and Dr. Aldo Rodriguez-Puebla for having gone so thoroughly through my thesis and for having assessed my defence.

I am very grateful to Dr. Mohammadreza Ayromlou, Prof. Mariangela Bernardi and all other collaborators for providing data for my work and for the useful discussion.

People from the BiD4BESt project made my PhD much more instructive, funnier and enjoyable.

I thank Dr. Lorenzo Zanisi who helped my a lot at the beginning of my PhD in understanding my research and finding my direction.

Un grande grazie a Dr. Lumen Boco con cui, oltre ad essere collaboratore, siamo diventati amici. Ho imparato molto lavorando insieme e mi sono divertito molto durante la tua visita a Southampton e la mia visita in SISSA. Dobbiamo tornare al Cricketers.

My other friends played a crucial role in my PhD. In particular, Maria, Georgios, Matt, Giorgio, Alessandro, Jakub, and Yingying made my time in Southampton much more pleasant and enjoyable. Grazie anche Zio Max e Luca, che avete reso i miei due periodi a Monaco più piacevoli e indimenticabili.

A special thank to Maria, who is not only a colleague or office mate, but also a great friend and companion for fun, hanging out and post-PhD desperation.

Inutile dire il ruolo di Ivan e Niko. Senza di voi sarebbe stato impossibile passare i periodi di lockdown più duri. Ringrazio poi la comparsa di Lorenza che ha reso questa città molto più vivace e piena di cose da fare.

Un enorme abbraccio al mio fratello Alfonso. Non dimenticherò mai il lockdown passato insieme, le nostre uscite e le birre di nascosto. Ti ringrazio anche un sacco per le visite a Monaco, Southampton e Trieste durante il mio dottorato, inutile dire quanto ci siamo divertiti.

我感谢我爸妈还有我妹妹的支持、鼓励和信任，这在这一路上起到了很大的关键作用。

Chapter 1

The thesis at a glance

Since the most ancient times, the night sky has inspired profound curiosity in humanity, evoking feelings of vastness, solitude, a serene sense of belonging, and a quest for meaning. These themes have always recurred in poetry, arts, and philosophy operas of all cultures throughout centuries and millennia.

A very fascinating old citation from the civilized era comes from the Greek monk from Alexandria, Cosmas Indicopleustes, who stated:

"The crystal-made sky sustains the heat of the Sun, the moon, and the infinite number of stars; otherwise, it would have been full of fire, and it could melt or set on fire."

This serves as a precursor of the problem of infinite stars, which is one of the most enchanting and captivating paradox of modern astronomy: the *Olbers' paradox*. The paradox can be formulated as follows:

if the Universe is infinite, homogeneous at large scales and isotropic, any line of sight from the Earth should intersect a star sooner or later. Then, why the night sky is not uniformly bright?

Throughout history, astronomers and more generally scientists relied on their eyes to perceive the world around us and to begin explaining the causes of natural phenomena. Over the last millennia, human eyes allowed to observed the Sun and planets in our solar system, and to understand their motions. Astronomers also observed several stars within our own Galaxy, the Milky Way. The Milky Way is the observed galaxy, and indeed the term 'galaxy' comes from ancient Greek $\gamma\alpha\lambda\alpha$ (milk), because of the fully and milky appearance of our Galaxy when it was observed with naked eyes. The advancement of new technology and the use of more modern telescopes allowed astronomers to observe and identify objects situated more distant from us, such as other galaxies, intergalactic stars, dust, and more. The start of the study of celestial objects outside the Milky Way marked the birth of extragalactic astronomy and galaxy evolution.

1.1 Scientific background and state-of-the-art

The advent of state-of-the-art telescopes and the abundance of information at our disposal have ushered in a new era of refined models for the evolution of galaxies. Recent developments in galaxy surveys and simulations have unveiled intriguing insights. They have highlighted that galaxies, categorized by their morphology and properties, as classified by E. P. Hubble, exhibit varying degrees of abundance or rarity at different stellar masses and epochs in the Universe's history.

Galaxies grow in mass by converting their cold gas reservoir into stars, commonly referred to as *star formation*. The rate across cosmic time at which stars are formed depends on the different morphology and mass of the galaxy, and therefore on the available gas. Additionally, there is also a moment when galaxies reach the peak rate of star formation and after which it gradually extinguishes, a process typically known as *quenching*. Quenching can be attributed to several physical processes that prevent gas from cooling, including shock heating or feedback from the central supermassive black hole. Understanding the nature and the relative significance of each process in quenching galaxies of different stellar masses at different epochs remains still one of the main challenges of astrophysics.

Galaxies also grow their mass through hierarchical processes such as *mergers* with other smaller neighbouring galaxies, known as satellite galaxies. The rate at which the stellar mass is accreted through mergers also varies with the age and present-day mass of each individual galaxy. The relative amount of stellar mass that galaxies acquire from star formation and mergers is also a matter of hot discussion in astrophysics and is one of the main problems that I will address in this thesis.

Several modelling tools have been developed over the last decades to investigate these physical mechanisms that govern galaxy evolution. These tools are mostly based on the ΛCDM model and encompass semi-analytical models (SAMs), hydrodynamical simulations and semi-empirical models (SEMs). Semi-analytical models and hydrodynamical simulations aim to capture a wide range of astrophysical processes relevant to galaxy evolution, often resulting in complex models with numerous parameters. Semi-analytical models can achieve this goal without explicitly including spatial information, while hydrodynamical simulations provide explicit spatial details, which can be invaluable for model constraints, but they come with a significant computational cost that hinders quick exploration. In contrast, semi-empirical models rely on empirical but theoretically informed scaling relationships between dark and visible matter as input. Typically, these relationships are established by assuming that larger or more massive galaxies inhabit correspondingly larger and more massive dark matter haloes, in line with the ΛCDM theory. Semi-empirical models can generate data-driven predictions using fewer parameters and limited physical modelling, making them a powerful complementary tool to study galaxy evolution, as I will show in this thesis.

1.2 Questions we seek to answer

In this scientific context, the primary goal of this thesis is to understand the relative role of star formation and mergers in building-up the stellar mass of galaxies at different mass ranges and redshifts. The main scientific questions that I aim to address in this thesis can be summarized as follows:

- How much mass do galaxies acquire from star formation and mergers respectively?
- What physical mechanisms halt star formation in galaxies?
- How do supermassive black holes grow within their host galaxies?

To address these questions, I developed and made use of DECODE, the Discrete statistical sEmi-empiriCal mODEl. DECODE presents a huge advantage with respect to previous semi-empirical models, which is the capability of generating from the ground up a population of *individual* discrete galaxies statistically without simulating on top of N-body simulations. By design, this removes any volume and mass resolution limitations, allowing fast simulation of galaxies of any stellar mass even those in the most massive clusters. In the first version of DECODE, stellar mass assembly histories are generated stochastically, allowing to study only the *mean* growths per stellar mass bin, while the second version of DECODE allows to generate the accretion tracks individually galaxy-by-galaxy. DECODE represents a complementary model to existing tools and is publicly available to the community.

1.3 Outline of the thesis

In this thesis, I will present DECODE and show how it is used to address such issues in galaxy evolution as a complementary tool to existing ones. This manuscript is structured as follows.

First of all, in Chapter 2 I will provide a more detailed introduction to the theoretical background and tools available. In particular, I will describe the hierarchical ΛCDM Universe, and how galaxies and black holes grow in such a cosmological model. I will also provide an overview on the observational surveys and theoretical tools available to the community.

In Chapter 3 I will describe the methodology employed in this work and the specifics of the two versions of DECODE. I will provide details on how I generate the catalogue of dark matter haloes and their merger trees, perform the abundance matching, populate

dark matter haloes with galaxies and build up their stellar mass. I will also describe the physical recipes implemented for the quenching processes.

In Chapter 4 I will check that DECODE can fairly reproduce the statistics of dark matter haloes and merger trees from dark matter-only simulations. I will also test the performance and inner consistency of DECODE against a comprehensive model such as the TNG hydrodynamical simulation.

In Chapter 5 I will show the implications of different input photometries on the connection between galaxies and dark matter haloes, galaxy merger rates, morphologies and bulge-to-total distributions.

In Chapter 6 I will show how DECODE can provide a holistic perspective on quantities related to galaxy evolution self-consistently between each other. These include satellite abundances, merger histories, star formation histories and intracluster light.

In Chapter 7 I will address the problem of quenching, focusing on the halo quenching, and discussing also the black hole quenching, major mergers and morphological quenching.

Finally, in Chapter 8 I will discuss the main results of this thesis and draw the conclusions.

1.4 Original sources

Most of the work presented in this thesis has been published or submitted for publication. The original journal articles are listed below:

- H. Fu et al., "Testing the key role of the stellar mass-halo mass relation in galaxy merger rates and morphologies via DECODE, a novel Discrete statistical sEmi-empiriCal mODEl", 2022, MNRAS, 516, 3206.
- H. Fu et al., "Unveiling the (in)consistencies among the galaxy stellar mass function, star formation histories, satellite abundances and intracluster light from a semi-empirical perspective", 2024, submitted to MNRAS.
- H. Fu et al. 2024, paper III, in prep.

Additional papers to which I have contributed during my PhD are listed below:

- F. Shankar et al., "Probing black hole accretion tracks, scaling relations, and radiative efficiencies from stacked X-ray active galactic nuclei", 2020, MNRAS, 493, 1500.

- L. Zanisi et al., "The evolution of compact massive quiescent and star-forming galaxies derived from the $R_e - R_h$ and $M_{star} - M_h$ relations", 2021, MNRAS, 505, 4555.
- C. Marsden et al., "The weak dependence of velocity dispersion on disc fractions, mass-to-light ratio, and redshift: implications for galaxy and black hole evolution", 2022, MNRAS, 510, 5639.
- A. V. Afanasiev et al., "The galaxy mass-size relation in CARLA clusters and proto-clusters at $1.4 < z < 2.8$: Larger cluster galaxy sizes", 2023, A&A, 670, 95.
- L. Boco et al., "TwO Parameters Semi Empirical Model (TOPSEM): Galaxy Evolution and Bulge/Disk Dicothomy from Two-stage Halo Accretion", 2023, ApJ, 954, 97.
- P. Dimauro et al., "Chasing the Intra-Cluster Light at $z \geq 2$", in prep.
- V. Allevato et al., "Building an AGN mock catalog for survey planning", in prep.

DECODE, along with a full documentation file, is publicly available for download at https://github.com/haofu94/DECODE.

DECODE 2.0 is available for download at https://github.com/haofu94/DECODE2.

During the course of my PhD, I have published also the following paper on my Master's work on the CMB spectral distortions, which is unrelated to this thesis, but listed below for completeness:

H. Fu et al., "Unlocking the synergy between CMB spectral distortions and anisotropies", 2021, JCAP, 12, 050.

Chapter 2

The dark and visible Universe

Galaxies are a result of the combination of several physical mechanisms, and the way they have formed and evolved has been widely studied in the literature both from a theoretical and observational point of view. In this Chapter I will provide a brief review on the observations and tools that are relevant to the work of this thesis. In particular, I will describe the Lambda Cold Dark Matter (ΛCDM) model and how galaxies grow following their host dark matter haloes, as well as the present and upcoming observational facilities. I will then describe how supermassive black holes grow following their host galaxies. I will also review the currently developed galaxy formation and evolution models. The reader familiar with these notions may wish to skip this Chapter.

2.1 Lambda cold dark matter model

The two main ways we can study galaxy formation and evolution are through theoretical models or direct observations, which are complementary tools to each other. In theoretical models, the cosmological initial conditions are provided by the ΛCDM model, such as the dark matter and baryons fraction, the properties of the dark matter haloes and their hierarchical evolution. In a ΛCDM Universe, galaxy modelling is based on the assumption that galaxies live inside dark matter haloes and their evolution are generally described following the evolution of their host haloes. Figure 2.1 shows a cartoon of how galaxies grow in a hierarchical ΛCDM model. Within this framework, each galaxy lives inside one dark matter halo and the growth of the two are intimately connected. In particular, larger galaxies typically live in larger haloes and formed earlier growing their mass both by merging with other smaller galaxies (*ex-situ* processes) or by *in-situ* baryonic processes, such as the formation of stars. Smaller galaxies, that live in smaller haloes, formed at later epochs growing their mass mostly *in-situ*. The description of the complex physics behind these processes lies beyond the purposes of

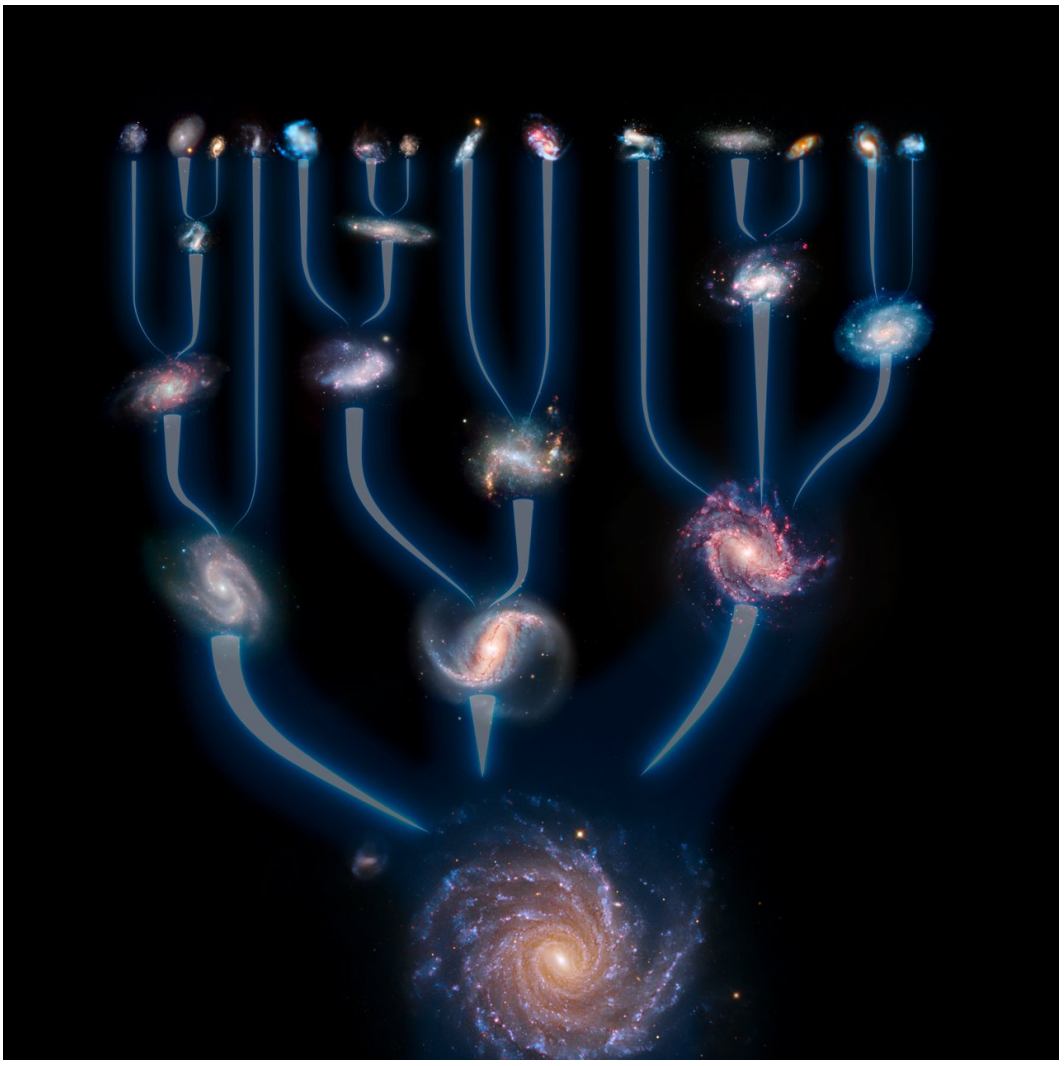

FIGURE 2.1: Artistic realization of a galaxy merger tree. Smaller galaxies are formed first during the early epochs and they merge with other galaxies to form larger structures. Image credit: ESO/L. Calçada.

this thesis. The interested reader can find a more thorough discussion in Somerville et al. (2015), King and Pounds (2015) and Wechsler and Tinker (2018).

The tools available nowadays to theoretically model galaxy formation and evolution in a ΛCDM framework are several. A first example is given by cosmological hydrodynamical simulations, which are designed to follow step by step the coevolution of baryons and dark matter particles across cosmic time and space. Secondly, there are semi-analytical models, which treat the baryonic physics with a set of analytical prescriptions and initial assumptions on top of a pre-existing dark matter halo evolution model. Lastly, in more recent years we have witnessed the advent of semi-empirical models, which evolve galaxies with their dark matter haloes by linking them via data-driven relations. I will describe these theoretical models more in detail in Section 2.4.

2.1.1 The halo mass function

I now go one step deeper in the dark matter sector and present the halo mass function (HMF), which contains the information about the mass assembly evolution of dark matter haloes. The HMF describes the number density of dark matter haloes per unit of comoving volume as a function of their mass. To compute the HMF from simulations, it is crucial to have a way of identifying haloes in the simulation and defining their mass. There are two main ways of identifying dark matter haloes and assigning their mass: 1) the method based on the overdensity and 2) the Friends-Of-Friends (FOF) algorithm. The reader can find a more thorough review in White (2001) and Voit (2005).

The overdensity method consists in finding regions with density above a certain threshold with respect to the critical density $\rho_c = 3H^2/8\pi G$, or to the background density, $\rho_b = \Omega_m \rho_c$. The mass of the halo M_Δ is defined to be the mass within the radius R_Δ where the mean spherical density inside is Δ times the critical density (e.g., Press and Schechter 1974; Jenkins et al. 2001). The halo mass defined in such a way can be interpreted also as the mass contained within the radius where the material is virialized and the mass outside is collapsing onto it. Different works suggest this to happen at different values of Δ, e.g., 200, 500 or 1000. Sheth et al. (2001) also extended the Press and Schechter (1974) formalism assuming that haloes have an elliptical, instead of spherical, configuration.

The FOF algorithm, instead, consists in finding neighbours and neighbours of neighbours of particles (Davis et al. 1985). The neighbouring particles are identified via the linking length, b, defined as the mean space between particles, for which the most commonly used value is $b = 0.2$ (Jenkins et al. 2001). In this method, the mass of the halo is just computed as the sum of the mass of all the neighbouring particles.

The HMF has an exponential behaviour as a function of halo mass, whose general fitting function can be described as follows (Jenkins et al. 2001; Tinker et al. 2008)

$$\frac{\mathrm{d}n}{\mathrm{d}M} = f(\sigma)\frac{\rho_m}{M}\frac{\mathrm{d}\ln\sigma^{-1}}{\mathrm{d}M}\,, \tag{2.1}$$

where

$$f(\sigma) = A\left[\left(\frac{\sigma}{c}\right)^{-a} + 1\right]e^{-d/\sigma^2}\,, \tag{2.2}$$

with a, c and d as free parameter depending on the halo definition and cosmology. The variance of the linear density field σ is computed as follows

$$\sigma = \frac{\mathrm{d}^2(z)}{2\pi^2}\int k^2 P(k) W^2(k) k^2 \mathrm{d}k \tag{2.3}$$

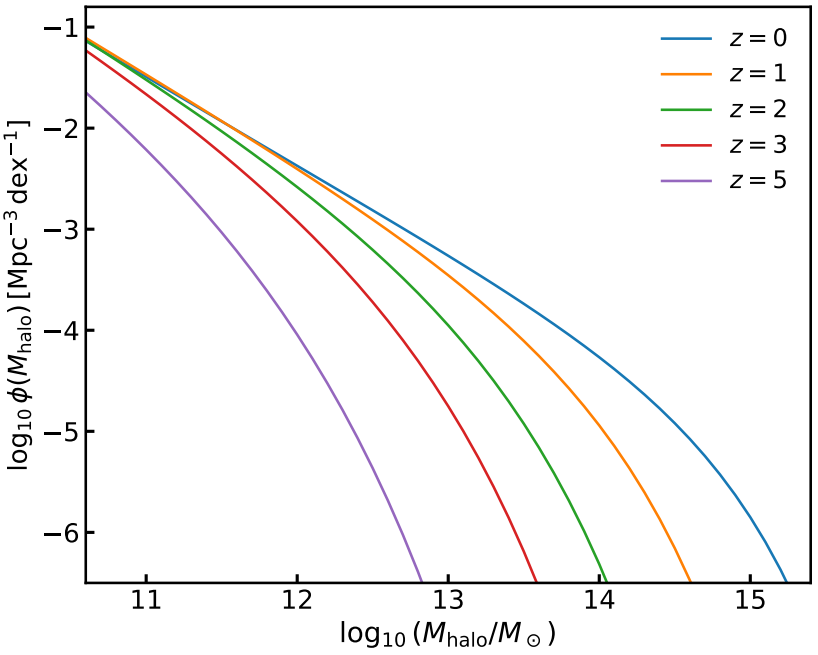

FIGURE 2.2: Halo mass function from Tinker et al. (2008) at redshifts $z = 0, 1, 2, 3$ and 5.

where $P(k)$ is the linear matter power spectrum and W is the real space top-hat filter function. Figure 2.2 shows the analytical fit to the HMF from Tinker et al. (2008), that I adopt in this thesis, at different redshifts.

2.1.2 The subhalo mass function

Numerical simulations have shown that in a ΛCDM model, each dark matter halo contains a population of smaller haloes, called *subhaloes*, which are surviving self-bound structures that have merged with the bigger halo (e.g., Giocoli et al. 2008; Jiang and van den Bosch 2014, 2016). Such subhaloes are subject to dynamical friction which can make them losing their orbital energy and angular momentum, and to tidal forces which can strip their mass.

The number density of the subhaloes is described by the subhalo mass function (SHMF). Same as for parent haloes, in order to compute the mass function, a way of identifying subhaloes in simulations is needed. A very popular method is the SUBFIND algorithm (Springel et al. 2001), based on which each FOF halo has one central subhalo, and the rest of the subhaloes are labelled as satellite subhaloes. The SUBFIND algorithm considers a minimum number of particles $n_{\rm min} = 20$ for identifying subhaloes. The time when a subhalo last changes its type from central to satellite is called *infall time*. Figure 2.3 shows an example of identification of FOF haloes and subhaloes in the S2 cluster simulation from Springel et al. (2001). The upper left panel shows the big structure of self-bound dark matter, while the upper right and lower left panels show the central

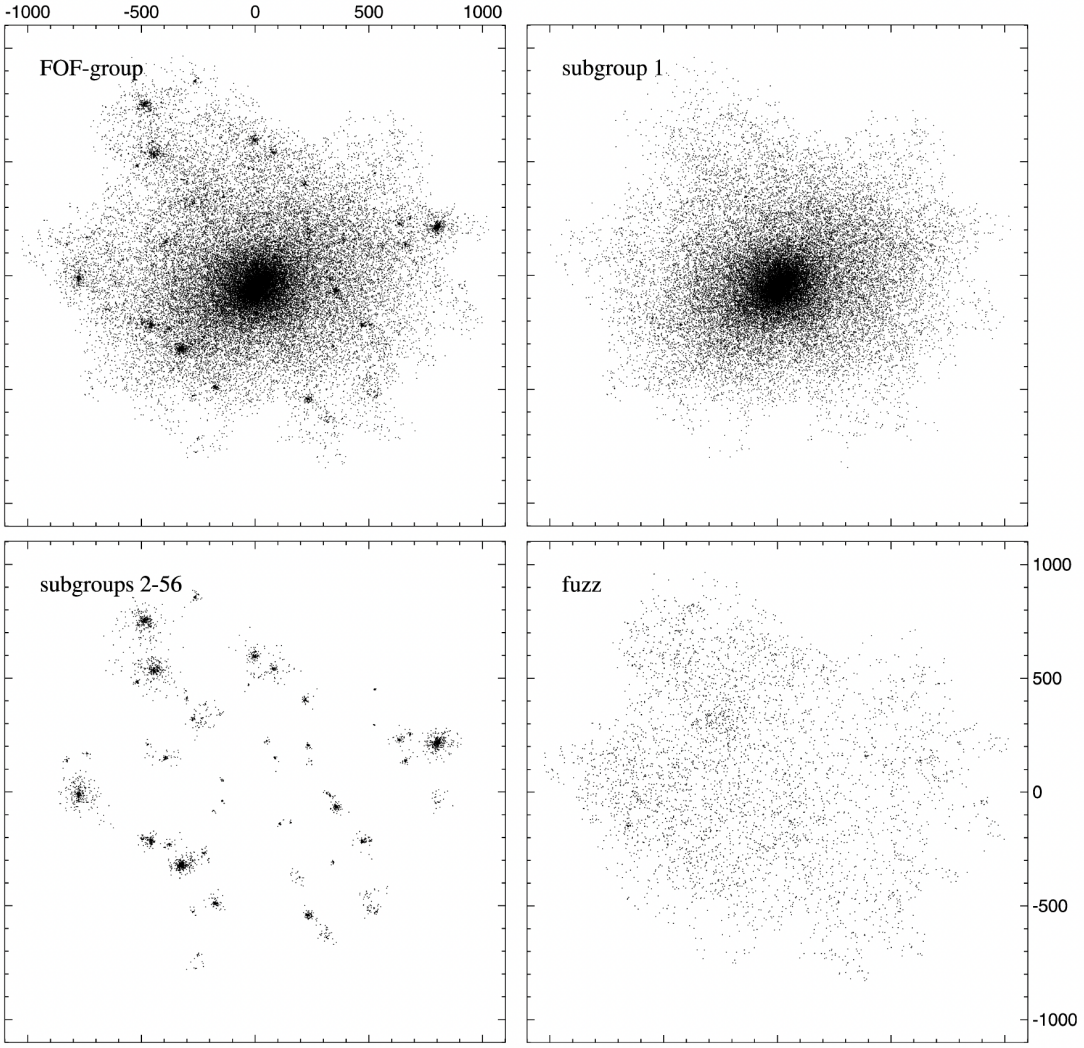

FIGURE 2.3: Example of a subhalo identification with SUBFIND. The upper left panel shows a small FOF group identified at redshift $z = 0$ in the vicinity of the S2 cluster. SUBFIND identifies 56 subhaloes within this group, the largest one forms the central subhalo or parent halo (upper right panel), while the other 55 form the satellite subhaloes (lower left panel). Particles not bound to any of the subhaloes form 'fuzz' dark matter (lower right panel). Image from Springel et al. (2001).

halo and subhaloes, respectively. Lastly, the lower right panel shows the fuzz dark matter which is not bound to any subhalo. Hereafter, I will refer to the central subhaloes as *parent* haloes, while I will refer to the satellite subhaloes simply as subhaloes.

Depending on their mass and whether the subhaloes have merged with the parent halo, the definition of the SHMF can be several. Jiang and van den Bosch (2016) proposed the following classification of the SHMF:

- *evolved total* SHMF, which includes all subhaloes that have ever accreted onto the main progenitor, including those that have been disrupted since the infall, as a function of their mass at redshift z;

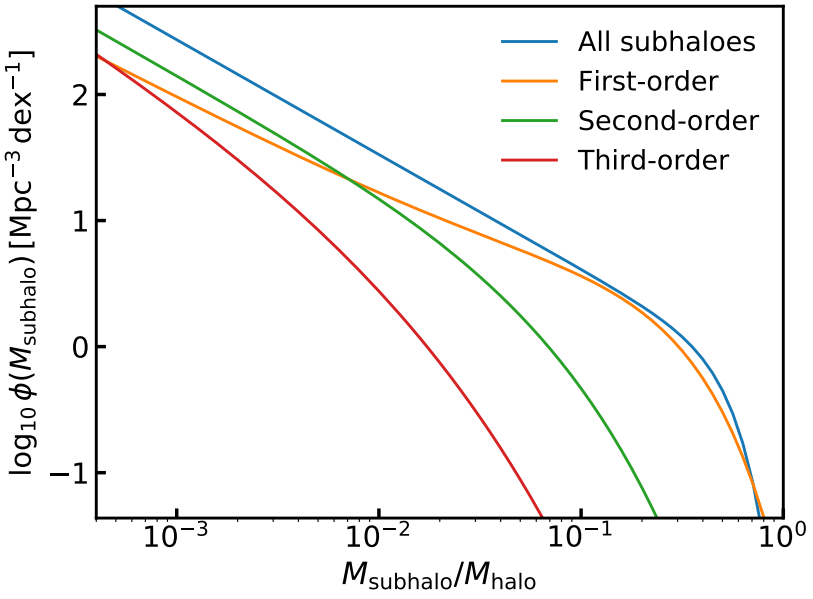

FIGURE 2.4: Unevolved total subhalo mass function from Jiang and van den Bosch (2016) for all (blue line), first-order (orange line), second-order (green line) and third-order (red line) subhaloes.

- *unevolved total* SHMF, which is the same as the evolved total SHMF but as a function of the mass at infall;
- *evolved surviving* SHMF, which is the same as the evolved total SHMF but for subhaloes surviving at redshift z;
- *unevolved surviving* SHMF, which is the same as the evolved surviving SHMF but as a function of the mass at infall.

Figure 2.4 shows the analytical fit to the universal unevolved SHMF from Jiang and van den Bosch (2016) valid at any redshift, which well describes the abundances of subhaloes from the Bolshoi simulation (Klypin et al. 2011). The figure shows the mass function for all subhaloes as well as the one distinguished by order, i.e., subhaloes of other subhaloes, as a function of the mass ratio with respect to the parent halo mass. The SHMF is found to be the same regardless of the mass of the parent halo, within the resolution of the simulation.

2.2 Population of galaxies

Having introduced the ΛCDM cosmology and how dark matter haloes are structured in such hierarchical model, in this Section I now describe how galaxies form and grow within this framework. I will also describe the quantities that contain information on the evolution of galaxies, such as the stellar mass function and main sequence, and will

describe the systematics affecting the measurement of these observables. I will then provide a brief overview on the ongoing and upcoming galaxy surveys.

2.2.1 The stellar mass assembly

As mentioned in Section 1.1, in a ΛCDM Universe galaxies grow their stellar mass both *in-situ* and *ex-situ*. *In-situ* processes mainly originate from the cooling of the infalling gas which fuels the star formation in galaxies. Instead, the *ex-situ* growth is predominantly provided by mergers with other galaxies. Indeed, each merger between two dark matter haloes could potentially trigger a merger between their hosted galaxies, even though cosmological models suggest that in several cases the dynamical timescale is longer than the age of the Universe, resulting in the smaller galaxy orbiting as satellite of the more massive one (e.g., Khochfar and Burkert 2006; Fakhouri et al. 2010; McCavana et al. 2012).

In traditional models of galaxy evolution, galaxies are evolved following the hierarchical growth of their host dark matter haloes, tending to build up via mergers more massive systems at later epochs (e.g., Guo and White 2008; Oser et al. 2010; Cattaneo et al. 2011; Lackner et al. 2012; Rodriguez-Gomez et al. 2016; Pillepich et al. 2018a; Monachesi et al. 2019; Grylls et al. 2020a; Fu et al. 2022, 2024). However, in stellar archaeological findings and star formation histories analysis via spectral energy distribution (SED) fitting (e.g., Thomas et al. 2019; Sánchez et al. 2019; Bellstedt et al. 2020), galaxies are observed to follow a downsizing trend, with more massive galaxies forming at earlier times, possibly triggered by large bursts of star formation, and less massive galaxies forming at later times with progressively lower star formation rates probably induced by an overall "cosmic starvation" caused by the general reduction of the cold gas available to feed galaxies (e.g., Larson et al. 1980; Gunn and Gott 1972; Cowie and Songaila 1977). The primary physical processes responsible for such rapid quenching are still unclear, with theories supporting the combination of internal and external processes, such as stellar and AGN feedback, halo quenching, morphological quenching, mergers, ram-pressure stripping (e.g., Granato et al. 2004; Dekel and Birnboim 2006; Shankar et al. 2006; Dekel and Birnboim 2008; Martig et al. 2009; Lilly et al. 2013; Schawinski et al. 2014; Lapi et al. 2018; Xu and Peng 2021).

2.2.2 The stellar mass function

Similarly to the HMF, the main information on the galaxy mass assembly history across cosmic time is contained in the stellar mass function (SMF), i.e. the comoving number density of galaxies as a function of their stellar mass. Understanding the shape and evolution of the SMF is still one of the most challenging goals in galaxy evolution and several works supports even contradicting results, as I will discuss in more detail in

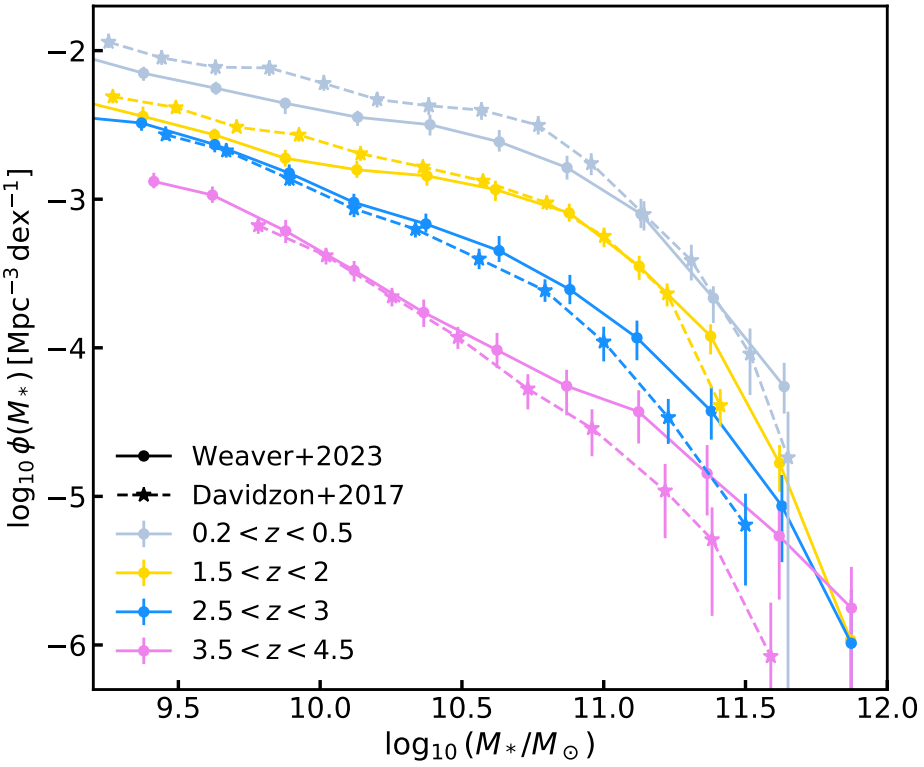

FIGURE 2.5: Evolution up to redshift $z \sim 4$ of the stellar mass functions from the COSMOS2015 (Davidzon et al. 2017, coloured stars) and COSMOS2020 (Weaver et al. 2023, coloured dots) surveys.

Section 5.1. Figure 2.5 shows the latest measured COSMOS2020 SMF as presented in Weaver et al. (2023) and the previous COSMOS2015 SMF from Davidzon et al. (2017) at different redshifts. As shown in Figure 2.5, the COSMOS determinations suggest that the SMF evolves gradually with redshifts in normalization, slope and position of the knee. On the other hand, other works, such as Kawinwanichakij et al. (2020), interestingly suggested a lack of evolution up to redshift $z \sim 1.5$. Later in this thesis, I will discuss and show what such different kinds of evolution will imply on the galaxy evolution in our semi-empirical framework.

Generally, the shape of the SMF is well described by a double power law, and well represented analytically by the combination of two Schechter functions as follows:

$$\phi(M_\star) = \frac{\exp(-M_\star/M_0)}{M_0} \cdot \left[\phi_1 \left(\frac{M_\star}{M_0}\right)^{\alpha_1} + \phi_2 \left(\frac{M_\star}{M_0}\right)^{\alpha_2}\right], \tag{2.4}$$

where M_0 is the position of the knee, ϕ_1 and ϕ_2 the normalizations, α_1 and α_2 the slopes at the low- and high-mass ends, respectively.

Figure 2.6 shows the SMF distinguished by star-forming and quiescent galaxies measured by COSMOS2020 as presented in Weaver et al. (2023). The population of the star-forming galaxies dominates at the faint end at every redshift, with the shape and

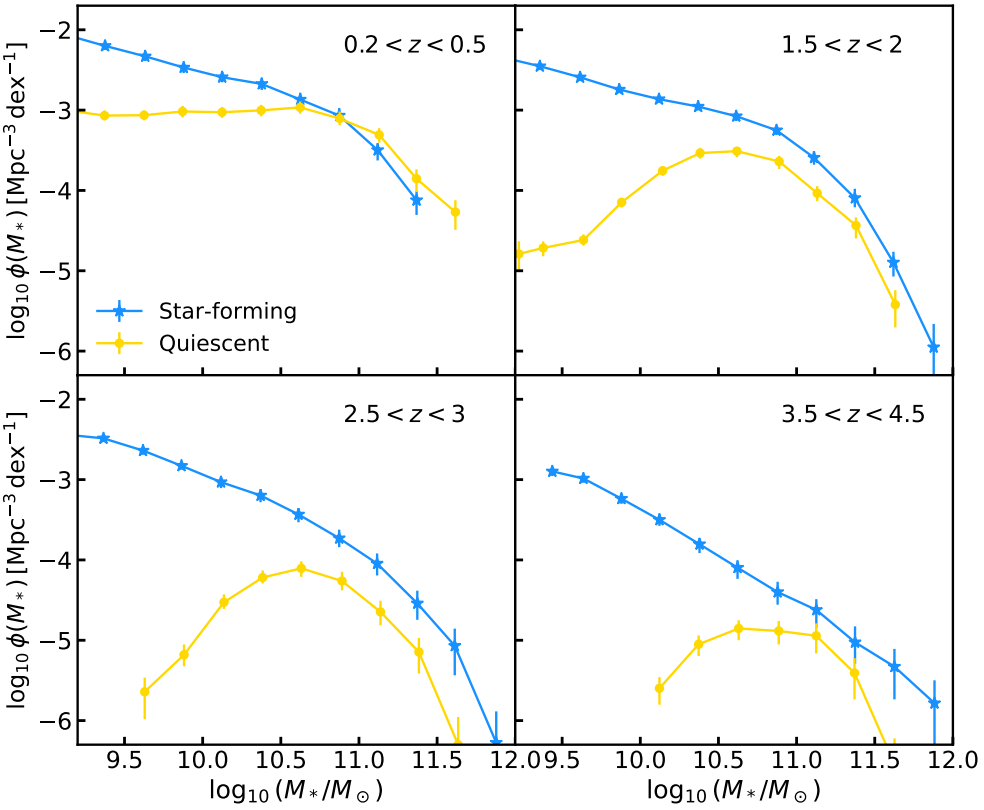

FIGURE 2.6: Stellar mass functions from COSMOS2020 (Weaver et al. 2023) for star-forming and quiescent galaxies up to redshift $z \sim 4$.

evolution similar to that of the SMF of the total population. On the other hand, the star-forming galaxies are being quenched gradually across cosmic time building-up the population of quiescent galaxies. Towards low redshifts, most massive galaxies are quenched above the knee of the SMF around solar masses $M_\star \gtrsim 10^{11}\, M_\odot$. Similar results are found also by other observational determinations of the SMF.

2.2.3 The star-forming sequence

As mentioned in Section 1.1, one of the main physical processes through which galaxies acquire their mass is by converting their cold gas reservoir into stars. The rate at which stars are formed is proportional to the amount of the cold gas content available in the halo (Kennicutt 1998). Indeed, observational surveys and numerical simulations found that the star formation rate (hereafter SFR) and the galaxy stellar mass are connected via a monotonically increasing power law relation, called star-forming main sequence (MS), which is valid at any redshift (e.g., Whitaker et al. 2014; Speagle et al. 2014; Ilbert et al. 2015; Leja et al. 2022; Popesso et al. 2023). Determining the shape and evolution of the main sequence, along with the SMF, is one of the toughest challenges in galaxy evolution, as I will further discuss in Section 6.3.3. Figure 2.7 shows the fit to the SFR-stellar mass relation from several UV, IR, optical and radio surveys as presented in Popesso

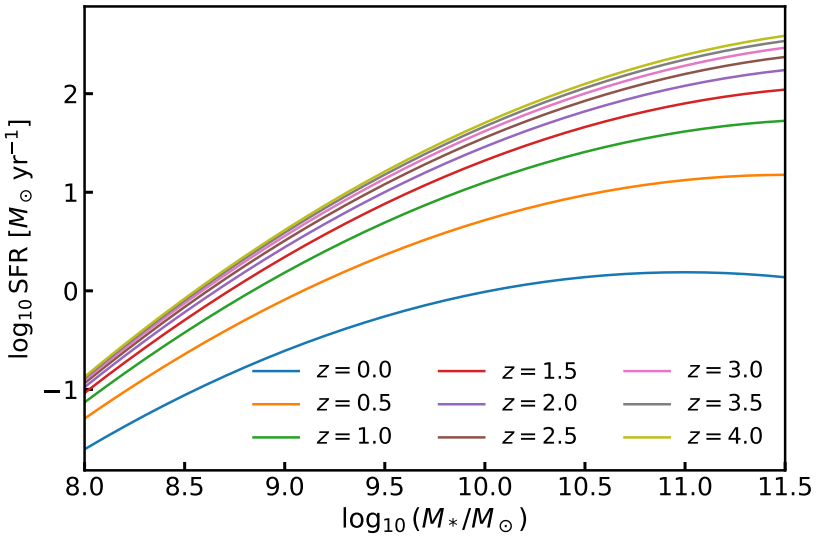

FIGURE 2.7: Main sequence of star forming galaxies from Popesso et al. (2023) at different redshifts.

et al. (2023). Remarkably the main sequence presents a trend which is proportional to the galaxy stellar mass. As also found by other works, at high stellar masses the main sequence can present a turnover in slope, although some other determinations found a simple single power law increasing relation. The nature of such a break in slope, if present at all, is hypothesized to be due to the presence of many quenched galaxies and mergers happening, as I will show later in this thesis.

Most of the star-forming galaxies lie on the mean main sequence relation, while others do not follow the relation at all. For instance, older galaxies have a much lower SFR with respect to the average, and starburst galaxies form stars at even roughly 10 times higher rate than the main sequence. Star formation and quenching are topics of very hot debate in astrophysics and the physical mechanisms that quench star formation are several, including the activity of the central supermassive black holes and virial shock heating (Birnboim and Dekel 2003; Dekel and Birnboim 2006; Dekel et al. 2009; King and Pounds 2015; Martín-Navarro et al. 2018). The importance of each mechanism is still poorly known, and testing such quenching mechanisms is also one of the key goals of this thesis.

2.2.4 Systematics

Currently, obtaining an accurate measurement of the SMF and its evolution across cosmic time is challenging due to uncontrolled systematic errors. On the observational side, several factors influence the determination of galaxy luminosities, particularly at the brightest end. These factors include the choice of the aperture used for measuring

light and the selection of photometric fits for the light profile (see, e.g., Simard et al. 2011; Meert et al. 2013; Bernardi et al. 2013; Kravtsov et al. 2018).

Additionally, the conversion of luminosity into stellar mass through the mass-to-light ratio depends on several assumptions, including the initial mass function (IMF), stellar population synthesis models, dust obscuration, and star formation history. Indeed, different IMFs yield different estimates of stellar masses. For instance, the IMF from Salpeter (1955) produces higher estimates due to the presence of more long-lived dwarf stars, compared to the IMFs from Kroupa (2001) and Chabrier (2003). Furthermore, it remains unclear whether the IMF is constant or varies with redshift (see, e.g., Sonnenfeld et al. 2017), and radial gradients in the IMF and their impact on the SMF have been widely studied in Domínguez Sánchez et al. (2019) and Bernardi et al. (2018a,b). Moreover, the selection of a specific stellar population synthesis model can introduce variations of up to 0.3 dex in number density at the high-mass end of the SMF, as shown by Bernardi et al. (2017). Finally, the impact of distinct star formation histories on stellar mass estimates has been studied in Lower et al. (2020).

2.2.5 Galaxy surveys

In the last couple of decades huge amounts of astronomical data have become available thanks to the advent of modern surveys with advanced technology. Galaxy surveys have opened a window to the Universe, and constitute an essential ingredient to calibrate semi-empirical models, as data-driven tools, since their robustness highly depends on the quality of the available data. In the bygone era of astronomical imaging and redshift surveys, which spanned the last century, the primary tools at our disposal were photographic techniques, and the instruments predominantly employed were optical telescopes. However, as the dawn of the new millennium broke, a transformative shift occurred in the field of astronomy, ushering in the age of contemporary surveys.

Modern observations of galaxies consist in gaining imaging and spectral data from telescopes and extracting physical and structural properties from them. Galaxy surveys, depending on the wideness, deepness and band of the field, can be either ground-based or in the space, and sometimes balloon-borne. Indeed, to study thoroughly the properties of a galaxy a multi-wavelength observation covering a wide band range is needed. For instance, the light emitted by stars are mainly concentrated in the ultraviolet (UV) and near infrared (NIR) bands, while interstellar molecular gas in the far infrared (FIR) and millimetric, and supermassive black holes in the X-rays. Ground-based telescopes provides a wide field for the surveys but are limited to the optical and NIR, because other wavelengths are absorbed or deviated by Earth's atmosphere. The other spectral bands are accessible through space telescopes, which face other challenges, such as the high costs or travel risks. Furthermore, depending on its specifics, a survey can be classified as wide or deep. A wide survey covers a large area of the sky to observe a

statistically large sample of usually brighter objects. On the other hand, a deep survey covers a smaller portion of the sky with the gain of being able to observe fainter and more distant galaxies, accessing higher redshifts.

Below I briefly introduce a few examples of the most renowned galaxy surveys relevant to the work of this thesis.

2.2.5.1 Past and present surveys

One of the pioneering examples of the ground-breaking modern surveys is the *Sloan Digital Sky Survey* (SDSS; York et al. 2000), that revolutionized astronomical research with its comprehensive imaging and spectroscopic observations. Unlike its predecessors, SDSS broke new ground by conducting both imaging and spectroscopy experiments across a spectrum of five distinct wavelength bands, covering roughly from 3550 Å to 9000 Å. A noteworthy milestone in the history of SDSS is the release of its most recent and publicly accessible data set, Data Release 18 (DR18; Almeida et al. 2023). This latest release stands as a testament to the ongoing progress and evolution of modern astronomical surveys, continuing to unlock the secrets of our Universe through its comprehensive and cutting-edge approach.

Several other prominent astronomical surveys have also made significant contributions to our understanding of the Universe. The Hubble Space Telescope[1] (HST), orbiting above Earth's atmosphere, has provided stunning images and invaluable data, unravelling the mysteries of distant galaxies, nebulae, and celestial objects, with the CANDELS (Cosmic Assembly Near-infrared Deep Extragalactic Legacy Survey; Grogin et al. 2011) and 3D-HST (Brammer et al. 2012) surveys. The Herschel Space Observatory[2], with its sensitive IR detectors, delved into the cold, dusty regions of the Universe, unveiling the secrets of star formation and the evolution of galaxies. The Atacama Large Millimeter/submillimeter Array[3] (ALMA) offered us a unique glimpse into the coldest, darkest corners of space, enabling the study of cosmic phenomena in unprecedented detail. The Galaxy and Mass Assembly Survey (GAMA; Driver et al. 2011) investigated the large-scale structure of the universe, mapping the distribution of galaxies over cosmic time. The Cosmic Evolution Survey[4] (COSMOS), conducted with space-based and ground-based telescopes, has probed the Universe's evolution, from the early Cosmos to the present day, shedding light on the formation and growth of galaxies. The James Webb Space Telescope[5] (JWST) will unveil the secrets of the early Universe, study exoplanet atmospheres for signs of habitability, and transform our understanding of celestial phenomena with its unprecedented capabilities in IR astronomy.

[1] https://science.nasa.gov/mission/hubble/
[2] https://www.esa.int/Science_Exploration/Space_Science/Herschel_overview
[3] https://www.eso.org/public/unitedkingdom/teles-instr/alma/
[4] https://cosmos.astro.caltech.edu/
[5] https://webb.nasa.gov/

Recently, the Euclid[6] space telescope has been launched. During my PhD I have worked within the Euclid Collaboration to create the AGN mock catalogue (Appendix F). Euclid represents a significant space mission with a specific focus on advancing our understanding of cosmology, the enigmatic nature of dark matter, and the intricate processes governing galaxy evolution. This mission is equipped with two instrumental components, known as VIS (VISible instrument) and NISP (Near Infrared Spectrometer and Photometer), which are designed to observe a wide region spanning 15,000 deg^2. Within this extensive field, Euclid will capture objects with extremely faint apparent magnitudes, extending our view into the optical and near-infrared spectrum. Furthermore, Euclid will push the boundaries of exploration even further, probing depths down to magnitudes of 26 but within a smaller area of 40 deg^2. Together, these surveys have expanded our cosmic horizons and enriched our understanding of the Universe.

2.2.5.2 Upcoming surveys

In the current modern era of astronomical observation, we are witnessing the advent of cutting-edge observing facilities that will revolutionize our understanding of the Cosmos. Over the course of the next decade, these forthcoming observing facilities will open up unprecedented opportunities for astronomers, offering a wealth of high-quality data that was previously inaccessible.

The Large Synoptic Survey Telescope[7] (LSST) stands as a ground-breaking observatory with immense potential to revolutionize our knowledge of the Universe. LSST, with its vast 8.4-meter mirror and a 3.2-gigapixel camera, will be one of the most powerful survey telescopes in the world. With its wide field of view and rapid surveying capabilities, LSST will capture the entire visible southern sky repeatedly over a ten-years period. This ambitious project is set to generate an unprecedented amount of data, making it possible to detect transient events, study dark matter and dark energy, and create the most comprehensive three-dimensional map of our Universe to date.

The ESO Extremely Large Telescope[8] (ELT), with a colossal primary mirror measuring up to 39 meters in diameter, is set to be the largest optical and IR telescope ever constructed. This monumental instrument, equipped with state-of-the-art adaptive optics and multiple specialized instruments, will enable astronomers to peer deeper into the Universe, providing unprecedented insights into the formation and evolution of galaxies, the characterization of exoplanets, and the study of dark matter and dark energy.

[6] https://www.esa.int/Science_Exploration/Space_Science/Euclid
[7] https://www.lsst.org/
[8] https://elt.eso.org/

2.3 Supermassive black holes

All galaxies, including also the Milky Way, host a supermassive black hole (SMBH) at their centers. These black holes grow their mass via the infalling gas that accretes onto them and their evolution is tightly linked to that of their host galaxies. In this Section, I will briefly review the co-evolution of SMBHs within their host galaxies and the main quantities related to the latter, such as the black hole mass-stellar mass and black hole mass-stellar velocity dispersion relations.

2.3.1 Super massive black holes and host galaxies co-evolution

SMBHs are classified as black holes with mass ranging from millions up to billions solar masses ($10^6\,M_\odot \lesssim M_{\rm BH} \lesssim$ few $\times\, 10^{9-10}\,M_\odot$, Gültekin et al. 2009). SMBHs are usually located at the centre of a galaxy, with usually one observed SMBH for each galaxy. SMBHs triggers the active galactic nuclei (AGNs), which are dense regions at the centre of galaxies that emits electromagnetic radiation at a wide wavelengths range. The bolometric luminosity is proportional to the mass accretion rate of the SMBH, $L_{\rm bol} = \epsilon c^2 \dot{M}_{\rm acc}$, with ϵ being the radiative efficiency. Therefore, in principle it is possible access to the mass growth history of a SMBH through the evolution of the AGN across cosmic time.

There is now plenty of evidence that the evolution of SMBHs is connected to that of their host galaxies. Numerous studies have shown the existence of scaling relations between the masses of SMBHs and the properties of their host galaxies. The initial discovery in this field was carried out by Dressler and Richstone (1988), who employed the stellar dynamical method to calculate the masses of SMBHs at the centre of two neighbouring galaxies, M31 and M32. Their work discussed an upper limit of approximately $10^9\,M_\odot$ for SMBHs in galaxies with the largest spheroids, based on the black hole mass-bulge stellar mass ratio, thus introducing the concept of a potential relationship between these two quantities.

Subsequently, Kormendy and Richstone (1995) identified a linear correlation between black hole mass and bulge stellar mass using only six galaxies. Significant advances in galaxy observations occurred after the launch of the Hubble Space Telescope in 1990. Specifically, Magorrian et al. (1998) proposed a single power law relationship to model the data relating to $M_{\rm BH}$ and $M_{\star,\rm bulge}$, with the help of the HST data. With an ever-increasing sample of objects, numerous other studies have reported nearly log-linear relationships between black hole mass and stellar mass (see, e.g., Ho 1999; Häring and Rix 2004; Ferrarese and Ford 2005; Graham et al. 2007; Gültekin et al. 2009; Sani et al. 2011a,b; Kormendy and Ho 2013).

The findings above show a substantial agreement within the scientific community regarding the existence of a relationship between the mass of a central SMBH and the mass of the surrounding spheroid. However, another aspect of interest pertains to the potential scaling relationships with the overall properties of the galaxy, specifically the total stellar mass or the stellar velocity dispersion. Studying scaling relations plays a pivotal role in unravelling the dynamic relationship between the growth of galaxy properties and the mass of black holes. Such studies offer valuable insights into a range of research areas, including the regulation of materials (such as gas and dust) within galaxies through AGN feedback, the interplay between black hole growth and the galaxy SFR, which in turn is linked to the availability of cold gas, and even the morphology of galaxies (see, e.g., Marconi et al., 2008; Volonteri and Ciotti, 2013; Heckman and Best, 2014; Calvi et al., 2018; King, 2019). Furthermore, the correlations between SMBHs and galaxies established within the local Universe provide a reference point for studies seeking to investigate the evolution of these relationships at higher redshifts (e.g., Bennert et al., 2011; Sexton et al., 2019). Lastly, scaling relations are an invaluable tool for calculating the black hole mass function in the local universe (e.g., Driver et al., 2007), estimating timescales for black hole mergers (e.g., Biava et al., 2019), and constraining the rates at which such mergers occur (e.g., Chen et al., 2019).

2.3.2 The black hole mass-stellar mass relation

Läsker et al. (2014) used both Early-Type Galaxies (ETGs) and Late-Type Galaxies (LTGs) to infer a relationship between the mass of the central SMBH and the total luminosity of the galaxy, which proved to be as robust as the one observed with the spheroid component. Furthermore, the discovery of numerous galaxies lacking a distinct bulge but still hosting a central black hole has provided support for the idea of a connection between the black hole mass and the total galaxy stellar mass (e.g., Reines et al. 2011; Secrest et al. 2012; Simmons et al. 2013; Schramm et al. 2013; Satyapal et al. 2014; Reines and Volonteri 2015; Shankar et al. 2016).

Nonetheless, it remains unclear whether an $M_{\rm BH} - M_{\star}$ relation applies universally to all types of galaxies, encompassing both ETGs and LTGs. It is possible that there exists a morphological dependence similar to the $M_{\rm BH} - M_{\star,\rm bulge}$ relation, as discussed in Savorgnan and Graham (2016a,b) and Sahu et al. (2019). With the determination of a reliable relationship with the total stellar mass of galaxies, it would greatly facilitate the determination of SMBH masses, even for distant galaxies that are challenging to resolve.

Figure 2.8 shows the latest determinations of the $M_{\rm BH} - M_{\star}$ relation from Kormendy and Ho (2013), Reines and Volonteri (2015), Shankar et al. (2006), Savorgnan et al. (2016) and Baron and Ménard (2019). As we can see from the plot, the results from different works are often in disagreement, even though all works found that the relation is well

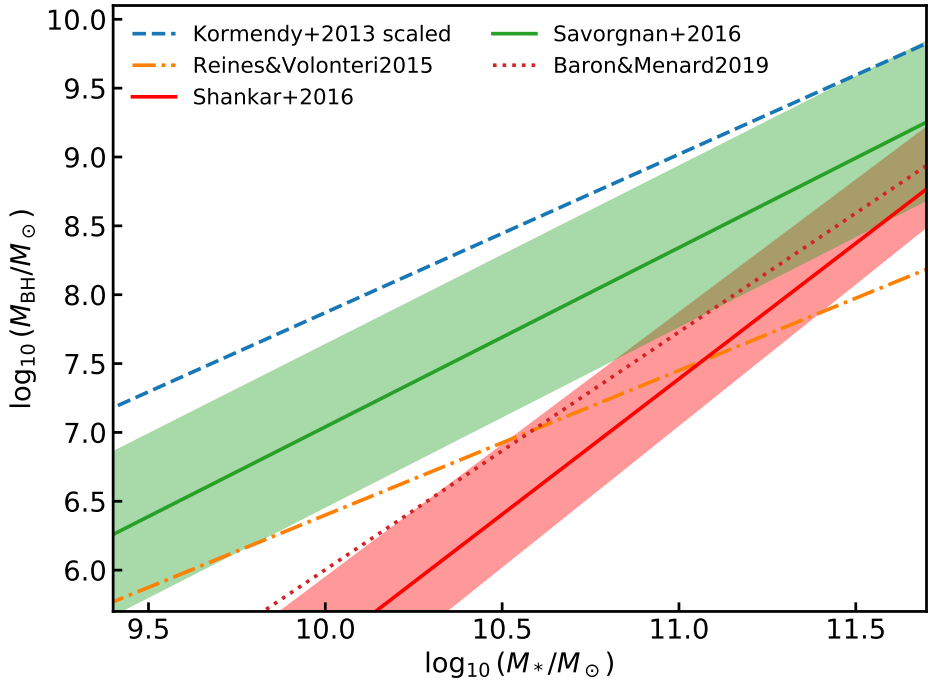

FIGURE 2.8: Local scaling relation between black hole mass and host galaxy total stellar mass. The blue dashed, orange dash-dotted and red dotted lines show the fits from Kormendy and Ho (2013), Reines and Volonteri (2015) and Baron and Ménard (2019), respectively. The red and green solid lines with shaded areas show the relations and uncertainties from Shankar et al. (2016) and Savorgnan et al. (2016).

represented by a single power law with slope roughly ~ 1. However, a unique relation valid globally for all galaxies regardless of their type and morphology is not yet solidly determined.

2.3.3 The black hole mass-stellar velocity dispersion relation

Another remarkable relation between galactic and black hole properties is the black hole mass-stellar velocity dispersion ($M_{\rm BH} - \sigma_\star$) relation. Galaxies, as self-gravitating systems, respect the virial theorem, as represented by the following equation (Busarello et al., 1992; Ferrarese and Merritt, 2000)

$$M_\star \propto R \frac{V^2_{\rm rms}}{G}\,, \tag{2.5}$$

where $V^2_{\rm rms}$ stands for the observed root-mean-square velocity, which is typically a combination of two velocity components: the stellar velocity dispersion $\sigma_\star$ and the line-of-sight rotational velocity ($V_{\rm rot}$), expressed as

$$V^2_{\rm rms} = \sqrt{\sigma^2_\star + \frac{V^2_{\rm rot}}{\sin^2\vartheta}} \tag{2.6}$$

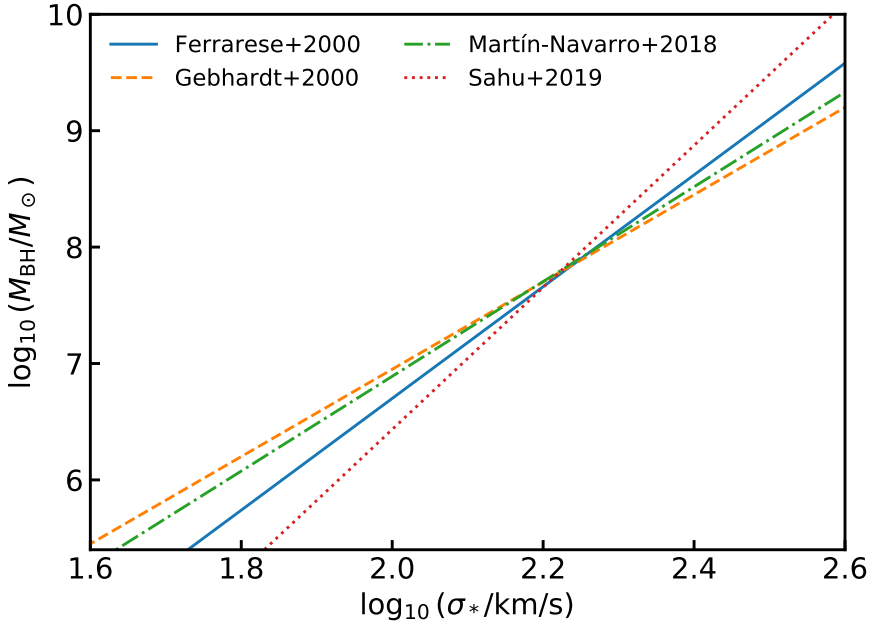

FIGURE 2.9: Local scaling relation between black hole mass and host galaxy stellar velocity dispersion from different works in the literature: Ferrarese and Merritt (2000), Gebhardt et al. (2000), Martín-Navarro et al. (2018) and Sahu et al. (2019), as labelled.

with ϑ being the inclination angle of the galaxy. In this context, the virial theorem establishes a connection between the velocity dispersion and the enclosed mass within a specific radius R in galactic bulges. In combination with observed relationships between black hole mass and the stellar mass of the host bulge, Equation (2.5) prompted the exploration of a potential connection between the mass of the central black hole and the galaxy velocity dispersion. The earliest indications of this relationship are attributed to Ferrarese and Merritt (2000) and Gebhardt et al. (2000), who proposed that there might be a fundamental connection between the central black hole and its host galaxy.

Figure 2.9 shows the $M_{\rm BH} - \sigma_\star$ relations from Ferrarese and Merritt (2000) and Gebhardt et al. (2000), along with the latest determinations from Martín-Navarro et al. (2018) and Sahu et al. (2019). Despite the slightly different slopes, all works seem to agree that the $M_{\rm BH} - \sigma_\star$ relation, similarly to the $M_{\rm BH} - M_\star$ relation, is well represented by a single power law as well.

2.4 Theoretical tools

As described in the previous sections, the formation and evolution of galaxies and SMBHs involve a huge variety of physical processes and often non-linear physics. Consequently, a fully analytic approach alone falls short in addressing thoroughly this problem. To surmount this challenge, astronomers have developed a diverse variety of

tools, such as hydrodynamical simulations, semi-analytical models and, more recently, semi-empirical models. In this Section, I provide a concise overview of the aforementioned tools and discuss their respective strengths and limitations, providing a few prominent examples and references to these models.

2.4.1 Hydrodynamical simulations

Hydrodynamical simulations represent a powerful tool in galaxy evolution research. They evolve simultaneously baryonic and dark matter particles by directly numerically solving the non-linear equations of the physics involved in galaxy evolution. The primary advantage of hydrodynamical simulations is the fact that they are able to follow step-by-step the co-evolution of galaxies and dark matter haloes, offering in-depth insights into the physics, dynamics and any properties of each single galaxy and host dark matter halo directly. The outputs are saved as a set of data containing galactic and halo properties, divided into time intervals, called *snapshots*. However, these simulations come with a significant downside. Indeed, they require very high computational times and man power to design, run the simulation and analyze the outputs.

One of the most remarkable recent hydrodynamical simulation is the IllustrisTNG[9] project, which I also extensively make use of in this thesis to test DECODE. The IllustrisTNG simulation is a set of 18 simulations consisting of three box volumes of roughly 50, 100 and 300 Mpc side length. Each individual simulation differs for the size, mass resolution and complexity of the physics. The choice of the box size allows to focus on particular aspects of galaxy formation. For example, the largest box facilitates the study of galaxy clustering and large-scale structures, such as clusters of galaxies. On the other hand, the smallest box, having a better resolution, enables investigations into smaller structural properties, such as the gas inside galaxies. Finally, the intermediate volume offers a balanced compromise between size of the sample and resolution. In this thesis, I make heavy usage of data from the TNG100 to validate my model. More details are provided in Section 3.4.2.

2.4.2 Semi-analytical models

Semi-analytical models exploit analytical approximations for the non-linear physics to evolve galaxies on top of existing dark matter-only N-body simulations that give the foundational dark matter halo evolution data. These models come with a notable advantage, i.e., their much cheaper computational cost compared to simulations, allowing to study substantially much larger samples of galaxies. As a consequence, semi-analytical models also allow to rapidly explore new parameters and physics, eliminating the need to run from scratch a full simulation.

[9] https://www.tng-project.org/

However, there is a trade-off to this efficiency. The primary drawback of semi-analytical models is their reliance on analytical approximations and a multitude of input assumptions/parameters. These approximations and assumptions can introduce a level of uncertainty and complexity that might cause the model to become entangled in the degeneracy of a high number of parameters. Thus, while these models offer practical advantages in terms of computational resources and speed, they should be taken with caution, particularly when confronting the intricate web of galaxy evolution processes and their interactions.

The earliest attempts to build a fully self-consistent semi-analytical model began in the early nineties, marking a significant milestone in the field of galaxy evolution. Pioneering works from that era, including those by White and Frenk (1991), Cole (1991) and Lacey and Silk (1991), laid the foundation for subsequent developments in this field. Over the years, numerous research groups have expanded upon these foundational efforts, resulting in the creation of robust and sophisticated models.

Some notable models that have emerged from this ongoing evolution include GALFORM introduced by Cole et al. (2000), the Munich model developed by Croton et al. (2006), GAEA as conceived by De Lucia and Blaizot (2007), and the Santa-Cruz model initiated by Somerville et al. (2008) and updated in Somerville et al. (2015). The Morgana model developed by Monaco et al. (2007) and the GALICS model (Hatton et al. 2003; Cattaneo et al. 2017, 2020; Koutsouridou and Cattaneo 2022) have also made significant contributions to our understanding of galaxy evolution. L-Galaxies (Henriques et al. 2015, 2020; Ayromlou et al. 2021a) also adds to the diversity of available tools. Finally, SHARK (Lagos et al. 2018, 2022), as well as SatGen (Jiang et al. 2021; Green et al. 2022a), represent the latest entries in this set of models.

2.4.3 Semi-empirical models

In the recent decades, semi-empirical models have emerged as a supplementary tool alongside existing methods. Semi-empirical models rely on *data-driven* empirical relations between a galaxy property and a halo property, to assign and evolve galaxies within dark matter haloes, without explicitly modelling the baryon physics in first principle. The major advantage of semi-empirical models, besides the low computational requirements, lies in their simplicity when used in their most basic form, as they involve only a minimal set of input parameters, being the relation between galaxies and dark matter haloes and the scatter in this relation. Subsequently, additional layers of complexity and physics can be incrementally incorporated, characterizing them with a high degree of flexibility and transparency, which permits users to thoroughly examine the effect of each individual physical process on the galactic evolution.

The mappings between galactic and halo properties used to assign galaxies to dark matter haloes are several. Among these, the most commonly employed relation is the one between the masses, called stellar mass-halo mass (SMHM) relation, which is adopted in the semi-empirical models by Hopkins et al. (2009a), Conroy and Wechsler (2009), Behroozi et al. (2010), Moster et al. (2010), Yang et al. (2012), Zavala et al. (2012), Behroozi et al. (2013), Moster et al. (2013), Shankar et al. (2014a), Rodríguez-Puebla et al. (2017), Tollet et al. (2017), Grylls et al. (2019) and Fu et al. (2022). Then, more recently people have begun using mappings involving the derivative of the masses, either between the star formation rate and halo accretion rate (e.g., Moster et al. 2018) or between the specific accretion rates (e.g., Boco et al. 2023). The recent work of Contreras et al. (2021) also used the relation between the galaxy stellar mass and the halo peak circular velocity.

A popular and traditional approach to build a connection between galaxies and dark matter haloes is via abundance matching. This technique consists in matching the statistical distributions or number densities of a galaxy-related quantity ($X_{\rm gal}$) and of a halo-related quantity ($X_{\rm halo}$). Abundance matching is based on the assumption of a monotonically increasing relationship between the two quantities and allows to compute the mean empirical relation. However, in the real world galaxies are not perfectly distributed along such relation and there is a certain scatter around the mean in the $X_{\rm gal} - X_{\rm halo}$ plane, which constitutes also an input assumption in the abundance matching itself.

Abundance matching can be performed either numerically by directly matching the number densities or by assuming a parametric form for the empirical relation. The former approach enables the computation of the mapping straightforwardly where the only assumption is the scatter (e.g., Behroozi et al. 2010; Tollet et al. 2017; Fu et al. 2022; Boco et al. 2023). The second approach, instead, is based on extensive Monte Carlo simulations to fit the model's parameters with the observed quantities (e.g., Moster et al. 2018; Behroozi et al. 2019; Grylls et al. 2020a). The complexity of such a model depends on the number of parameters and quantities designed to be fitted. Since these models incorporate observational inputs, a robust semi-empirical model should be internally self-consistent by design between its input and output quantities with the observed ones.

2.4.3.1 Some semi-empirical models in the literature

Among the most remarkable models in the literature that employed the SMHM relation to assign galaxies to haloes, we recall the works of Behroozi et al. (2013), Moster et al. (2013), Rodríguez-Puebla et al. (2017) and Grylls et al. (2019). In these models the authors constrained the SMHM relation by fitting observational SMFs at each redshift, along with star formation histories and cosmic SFRs, using an MCMC approach. The

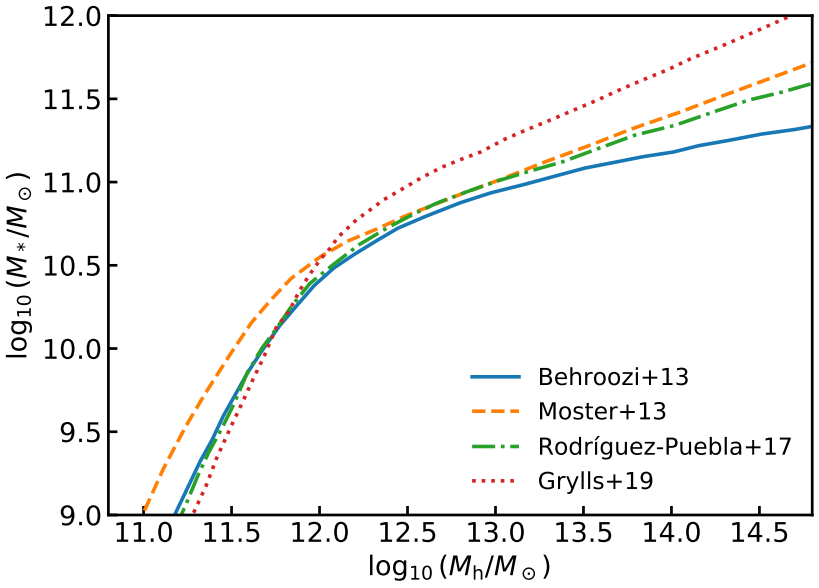

FIGURE 2.10: Stellar mass-halo mass relation at redshift $z = 0$ from the semi-empirical models of Behroozi et al. (2013), Moster et al. (2013), Rodríguez-Puebla et al. (2017) and Grylls et al. (2019), as labelled.

shape assumed for the SMHM relation is that of a double power law of the form

$$M_\star \propto N\left[\left(\frac{M_{\rm halo}}{M_0}\right)^{-\beta} + \left(\frac{M_{\rm halo}}{M_0}\right)^{\gamma}\right]^{-1}, \tag{2.7}$$

where N, M_0, β and γ are parameters that depends on redshift and regulate the normalization, position of the knee and slope of the relation, respectively. Figure 2.10 shows the local SMHM relation from the aforementioned models. The SMHM relation is characterized by a steeper faint end which is thought to be produced by AGN feedback and a flatter bright end caused by mergers.

Among more recent models we recall EMERGE (Empirical ModEl for the foRmation of GalaxiEs, Moster et al. 2018) and UNIVERSEMACHINE (Behroozi et al. 2019). EMERGE builds up galaxies by assigning SFRs to dark matter haloes via a parametric SFR-HAR relation described by a double power law, similar in shape to Equation (2.7), constrained by observational SMFs, SFR densities and quenched fractions. The interesting characteristic is the fact that the SMHM relation and its scatter is a prediction of the model. UNIVERSEMACHINE assumes a parameterized SFR which, along with a quenched fraction, is used to assign a SFR probability distribution to each dark matter halo. These distributions are then used to assign SFRs to haloes, so that later haloes host more star forming galaxies, and the SFRs are integrated to derive the galaxy stellar mass growth. The galaxy SMF, cosmic SFRs, correlation functions and other quantities are predicted as outputs of the model. UNIVERSEMACHINE is designed with 44 parameters, which is a massive number of parameters close to that of a semi-analytical model. To fit the model to the observational data, a set of 100 MCMC walkers was run

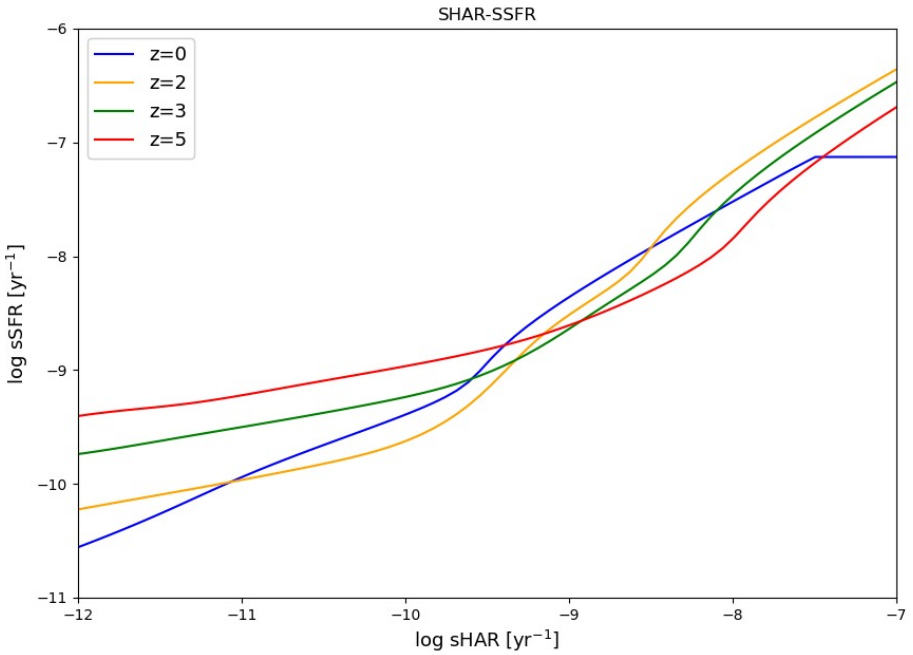

FIGURE 2.11: Specific star formation rate-specific halo accretion rate relation computed via the abundance matching at different redshifts from Boco et al. (2023). Image used with permission from Lumen Boco.

for a total of several hundred thousands CPU hours. The best-fitting parameters that minimizes the χ^2 allows to reproduce all the targeted observed quantities (see Table 1 in Behroozi et al. 2019).

Very recently, TOPSEM (TwO Parameters Semi Empirical Model; Boco et al. 2023) has been published, which populates dark matter haloes with galaxies via abundance matching between the specific SFR and dark matter specific halo accretion rate (sHAR). Halo accretion rates are taken from the Hearin et al. (2021) DIFFMAH model designed to fit halo accretion histories from N-body simulations, while specific SFR distributions are computed by convolving the observed SMF and main sequence at each redshift. Galaxies are initialized at redshift $z = 0$ via an input SMF. Then, galaxies are evolved backwards in time using the specific SFRs and quenching is modelled separately empirically using the observed fraction of quenched.

Figure 2.11 shows the sSFR-sHAR relation from Boco et al. (2023) at different redshifts. TOPSEM is able to reproduce the observed populations of galaxies up to redshift $z \sim 5$, supporting the assumption of a monotonic increasing relationship between the specific accretion rates of galaxies and dark matter haloes. The model can also excellently reproduce the observed mass functions of bulges and ellipticals.

Chapter 3

Methodology

3.1 Why is there a need of a statistical discrete model?

One of the major limitations in galaxy modelling is the compromise among speed, resolution and transparency. As I mentioned in Chapter 2, hydrodynamical simulations are an extremely good tool to study galaxy formation since they follow their evolution object-by-object throughout the entire history of the Universe, but are severely limited by the available CPU power and mass or volume resolution. Semi-analytical models and multi parameter semi-empirical models, on the other hand, are characterized by a high number of parameters controlling the physical processes, which makes them extremely heavy to run and prone to degeneracies.

In this thesis, I propose a new complementary *statistical* and *discrete* semi-empirical approach, which differs from previous discrete semi-empirical models for a number of reasons. First of all, previous discrete semi-empirical models run on top of dark matter simulations, which makes them less flexible to handle since they model the evolution of each galaxy following the merger tree of each group/cluster in the simulation, which are not only expensive to run but often affected by serious mass and volume resolutions as described in Chapter 2. Instead, my approach relies on analytic subhalo mass distributions, allowing for a precise and complete implementation of the merger histories and satellite abundances of galaxies. Secondly, in most previous semi-empirical models the baryonic physics parameters connected to the dark matter are calibrated to fit observational data, while in my methodology I use directly input observed stellar mass or luminosity functions to build galaxies inside dark matter haloes. Lastly, in my approach I can include each physical process one at a time allowing for a transparent investigation of the impact of each modelling choice on the outputs. A more detailed discussion on how DECODE compares to other semi-empirical models in the literature can be found in Appendix E.

In this Chapter, I will describe the specifications of my semi-empirical model, DECODE, discussing its design, self-consistency and performance.

3.2 DECODE's implementation

DECODE has been designed to eliminate volume and mass resolution limitations like in more traditional models. To this purpose, many modules in DECODE, such as the generation of the *stochastic* merger trees, are designed in C seeking a higher computational performance. This high computational speed of DECODE allows to simulate rapidly and easily also large samples of the most massive cluster haloes.

The main body of the code is written in Python to make it more accessible to the community, especially to the youngest students. All the input parameters are read from a text file to make it as user friendly as possible and the basic user should not need to tackle with the code at all.

Below I describe the main components of DECODE, highlighting its advantages and high flexibility. In brief, DECODE aims at predicting the galaxy stellar mass assembly histories, in terms of both mergers and star formation rates (SFR), starting from a mean SMHM relation. Full details are provided in the next Sections.

3.2.1 Workflow of DECODE

Figure 3.1 shows a handmade cartoon sketching the idea behind DECODE, which gives an overview on how different shapes and evolution of the input stellar mass function (SMF), therefore stellar mass-halo mass (SMHM) relation, can impact my predictions. Ideally, semi-empirical models, developed on top of a dark matter-dominated hierarchical Universe, are designed to be self-consistent between their inputs and output observables. This means, in the case of DECODE, that the input observed SMF should produce a SMHM relation that predicts SFHs, merger rates, morphologies, ICL, satellite abundances and so on, self-consistent among each other when compared simultaneously with observational data. Therefore, simultaneously matching robust and homogeneous data sets via semi-empirical hierarchical models like DECODE, will not only allow to test the input assumptions on, e.g., infall timescales and amount of stellar stripping, but also will probe the full effectiveness of the standard cosmological model of galaxy evolution. However, these are challenging goals for a number of reasons. First of all, observations are not fully consistent between themselves, e.g., integrated SFHs have often resulted in the literature to overestimate the stellar mass in galaxies when compared to the SMFs at any given epoch, as I will further discuss in this thesis. Furthermore, several observables predicted by DECODE depend not only on the input

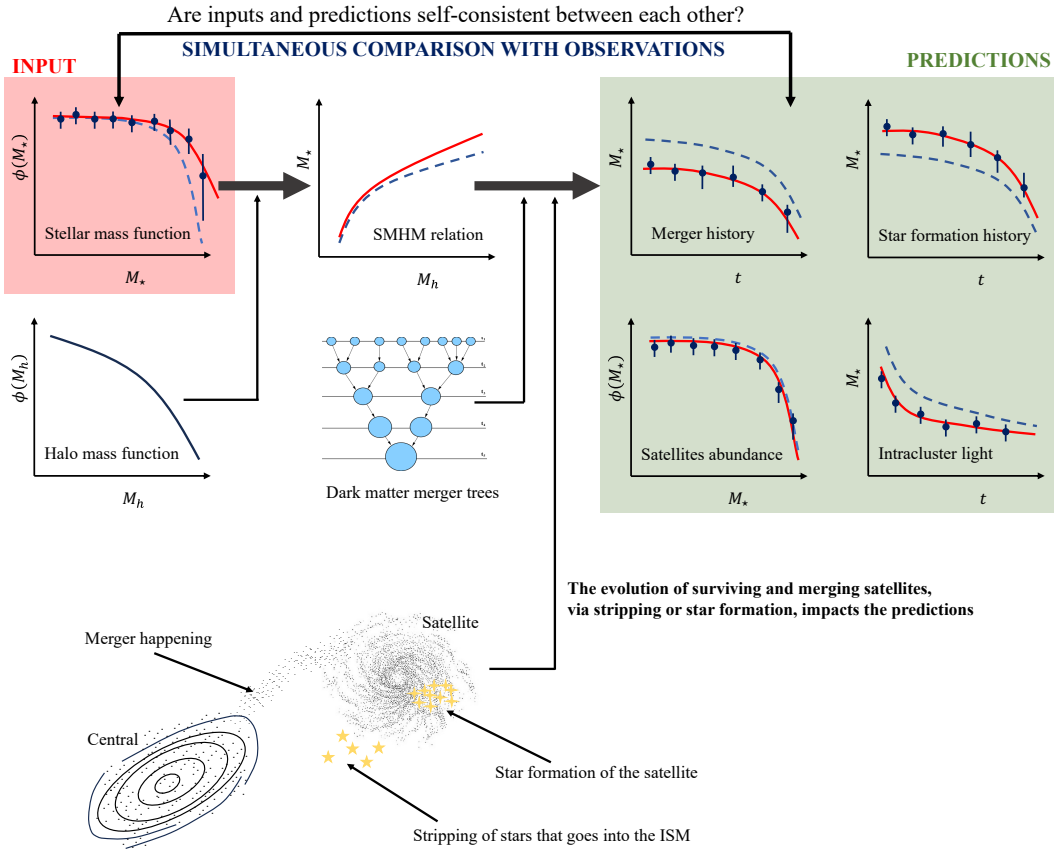

FIGURE 3.1: Cartoon of DECODE's conception in forming and evolving galaxies, as described in Section 3.2.1. The galaxy stellar mass function and dark matter halo mass function are taken as inputs in DECODE to calculate the SMHM relation via abundance matching (Section 3.2.3). The SMHM relation, along with the halo merger trees, is used in DECODE to predict galaxy merger histories and satellite abundances. The star formation histories are computed from the difference between the total mass growth and the merger history (Section 3.2.4). Different photometries, or different input stellar mass functions, will produce different SMHM relations, merger histories, star formation histories and other quantities such as elliptical fractions, B/T ratios and intracluster light, as shown by the example red solid and blue dashed lines in the cartoon. The red lines in the cartoon are shown to line up with all data. However, in reality, the data sets in the green panel are highly heterogeneous, derived using distinct methods and assumptions, and possibly susceptible to a number of diverse systematic errors.

SMF, but also on the way satellites evolution is modelled, which can be affected by a number of, sometime degenerate, physical processes (e.g., star formation, quenching, stripping). Therefore, one should also choose parameters that rules satellites evolution in such a way to be self-consistent between inputs and produced outputs, which is not a trivial task at all. I will discuss in this thesis that some observables are more dependent than others on post-infall satellite evolution.

As shown in Figure 3.1, the working flow of DECODE is practically from the left to the right, i.e., predicting galaxy properties using an input SMF and satellites modelling. However, conceptually, things can be seen also in the other way around and the galaxy

observables can be considered as input quantities, which DECODE uses to constrain the galaxy SMF and satellites evolution. In this thesis, I will discuss what are the insights on the SMF that SFHs can provide and, afterwards, I will show the predictions for my SMF models.

3.2.2 Dark matter halo catalogue

First of all, I generate a catalogue of dark matter parent and sub- haloes, on top of which I run my semi-empirical simulation. The main steps followed in DECODE can be summarized as follows:

- generation of the dark matter parent halo population (Section 3.2.2.1);
- generation of the dark matter subhalo population (Sections 3.2.2.2 and 3.2.2.3);
- evolution of subhaloes after infall (Section 3.2.2.4).

Figure 3.2 shows DECODE's general framework to generate the population of dark matter haloes and subhaloes, which I will describe in detail below.

3.2.2.1 Generating parent haloes

The DECODE analysis is based on a statistical catalogue of dark matter haloes extracted from the HMF. In this thesis, I adopt the definition and parameterization of the HMF of Tinker et al. (2008)[1], which accounts only for central (or largest) subhaloes in each FOF group. I extract haloes and their masses in my catalogue from the cumulative HMF multiplied by an input cosmological volume, so that the mass distribution of the haloes in the generated catalogue follows exactly the input mass function. I choose a reference volume box of 250 Mpc on a side, which represents a good balance between speed and accuracy.

I then assign an average mass accretion history to each parent halo, computed using the methodology described in van den Bosch et al. (2014), who fitted the mean halo accretion histories from the Bolshoi simulation (Klypin et al. 2011). Since the van den Bosch et al. (2014) formalism allows to compute only the mean accretion history for a given parent halo mass at $z = 0$, instead of computing the growth for each single halo in the catalogue, I predefine a fine halo mass grid of 0.1 dex width and assign the same mean history to all the dark matter haloes contributing to the same cell in the grid. The choice of using average accretion histories and a predefined grid allows also to save computational time. I have tested that my average results do not alter at all

[1] I make use of the `lss.mass_function` module in the Python `colossus` package (Diemer 2018).

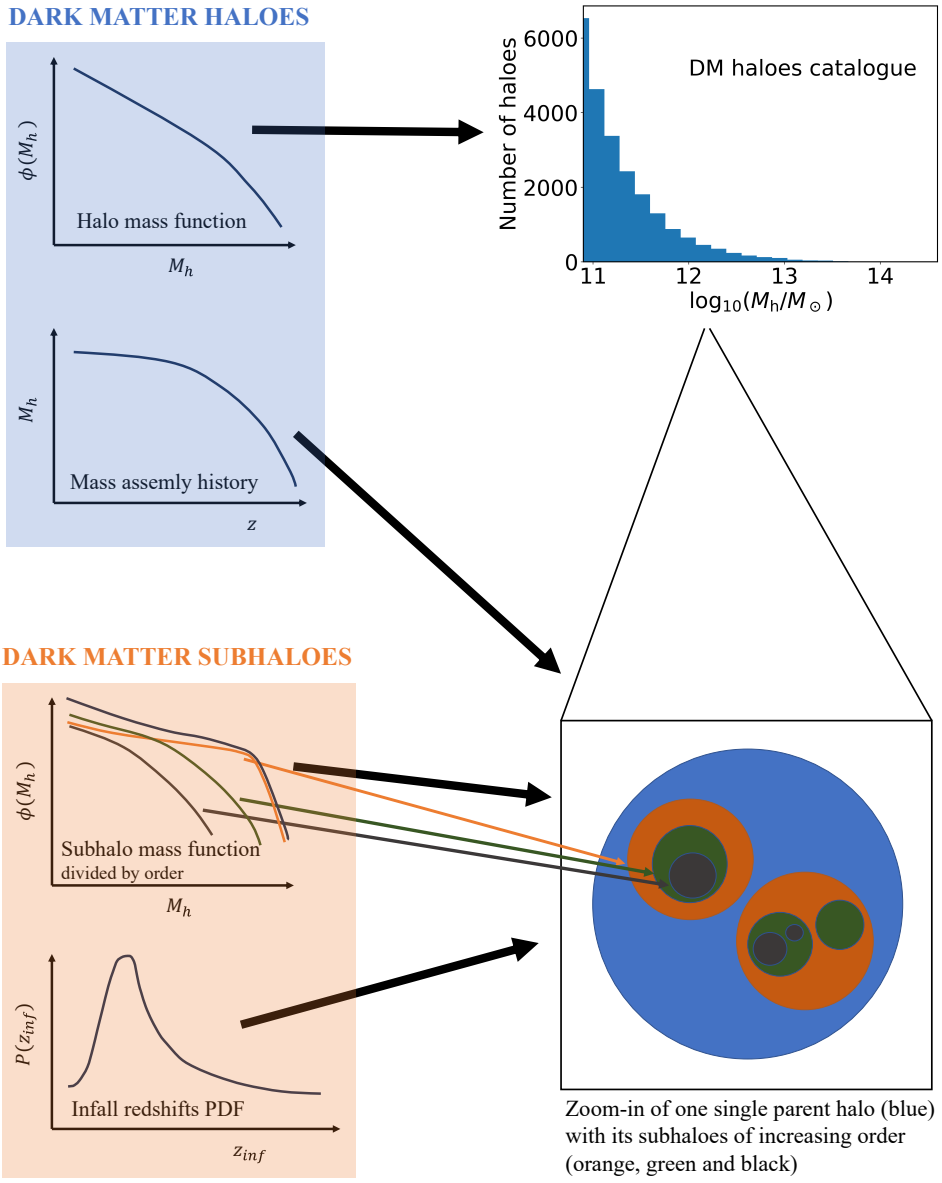

FIGURE 3.2: Cartoon scheme of DECODE for the dark matter side as described in Section 3.2.2. Top: halo mass function used to generate the parent haloes catalogue (represented by the histogram in mass bins). The halo mass function is used as probability distribution to generate the masses of the dark matter haloes, and a mean accretion history is assigned to each halo through van den Bosch et al. (2014)'s analytic fit. In this way, I build a set of main progenitors discretely, each of them characterized by a mean accretion history. The histogram in the top right side represents a stochastic realization of the halo mass function. Bottom: statistical distributions used to assign the subhaloes to the parent haloes. For each parent halo, I compute the subhalo mass function for all subhaloes as well as divided by order, and use it as probability density distribution for generating the subhalo population. The order of the subhaloes in the merger tree is assigned using the subhalo mass functions distinguished by order (coloured lines), and in this thesis I limit my attention up to the second-order. Finally, the redshifts of infall are assigned to the subhaloes via analytic formulas that I fit from N-body simulations, depending on their order and mass (see Figure 3.4 for the distinction for different orders and masses). In this way, the merging structure of each halo is known, i.e., the infalling subhaloes' order, mass and time at infall.

by assigning individual accretion histories to each halo using the DIFFMAH code from Hearin et al. (2021). In Section 3.3, I will present an upgraded version of DECODE, which is able to decipher galaxies on an object-by-object basis.

3.2.2.2 Generating subhaloes of different orders

The average number of subhaloes of a given mass that fall onto each parent halo at any given time is given by the SHMF. Here, I adopt the definition of unevolved SHMF distinguished by "order" of accretion in the merger tree (Jiang and van den Bosch 2014, 2016). The first-order subhaloes are those that fall directly onto the main branch, the second-order subhaloes those that are already satellites in the first-order subhaloes at the redshift of accretion onto the main branch, and so on. The redshift at which a subhalo falls into its progenitor is referred to as infall redshift.

I use the same methodology applied to parent haloes to calculate the number and mass of all the subhaloes that have ever fallen onto each given parent halo, by using the cumulative total unevolved SHMF from Jiang and van den Bosch (2016, see Appendix A), whose fitting function is

$$\frac{\mathrm{d}N}{\mathrm{d}\ln\psi} = \gamma\psi^{\alpha}\exp[-\beta\psi^{\zeta}] \tag{3.1}$$

with $\psi = M_{\rm h,sub}/M_{\rm h,par}$ being the ratio between masses of the infalling subhalo and parent halo, and best-fitting parameters $(\gamma, \alpha, \beta, \zeta) = (0.22, -0.91, 6, 3)$.

Once the number of subhaloes and their mass have been computed, I need to assign the order to each of them. The order of the subhaloes is assigned through the SHMF distinguished by order. In particular, I use the ratio between the generic n-th order SHMF and total SHMF in a given subhalo mass bin as the probability that a given subhalo of that mass is of n-th order. I use the first-order SHMF and the higher orders SHMF from Jiang and van den Bosch (2014, see Equations 17 and 19 therein), according to which the best-fitting parameters to Equation (3.1) for the former are $(\gamma, \alpha, \beta, \zeta) = (0.18, -0.80, 12.27, 3)$ and the latter is computed using

$$\begin{aligned}\frac{\mathrm{d}N_{n-\rm th}}{\mathrm{d}\ln\psi}(M_{\rm h,sub}|M_{\rm h,par}) = \\ \int_0^{M_{\rm h,par}} \frac{\mathrm{d}N_{1-\rm st}}{\mathrm{d}\ln\psi}(M_{\rm h,sub}|M'_{\rm h})\frac{\mathrm{d}N_{n-1-\rm th}}{\mathrm{d}\ln\psi}(M'_{\rm h}|M_{\rm h,par})\frac{\mathrm{d}M'_{\rm h}}{M'_{\rm h}}\,.\end{aligned} \tag{3.2}$$

3.2.2.3 Assigning infall redshifts

To predict a robust merger history for both galaxies and dark matter haloes, one needs to correctly know the infall redshifts ($z_{\rm inf}$) of the merging satellite galaxies and subhaloes. In this thesis, I define the infall redshift as the time when a dark matter halo became a subhalo for the *first* time, or in other words when it entered the virial radius of another halo. I assign infall redshifts to the subhaloes in a statistical way and I apply two different recipes for the first-order and higher-order subhaloes.

For the first-order subhaloes, I use directly the first-order SHMF as redshift probability distribution. In particular, at any given redshift z, for a parent halo that grows by $\mathrm{d}M_{\rm h,par}(z)$ from redshift $z + \mathrm{d}z$ to z, the derivative of the SHMF with respect to the redshift provides the probability distribution function (PDF) of the infall redshifts of the subhaloes of mass $M_{\rm h,sub}$ that have accreted onto this progenitor:

$$\mathrm{PDF}(z_{\rm inf}) \propto \frac{\mathrm{d}}{\mathrm{d}z}\phi(M_{\rm h,sub}, M_{\rm h,par}(z)) \ . \tag{3.3}$$

In other words, this is equivalent to view the SHMF as a function of redshift, instead of mass, at fixed subhalo mass and given parent halo. Therefore, for any subhalo mass bin, the SHMF seen in such a way will provide the number of subhaloes that have accreted onto this parent halo at any infall redshift. Then, the redshifts of infall for subhaloes of any given mass $M_{\rm h,sub}$ are generated by randomly extracting them from the PDF given in Equation (3.3).

To explain this concept more clearly, let us consider a parent halo of mass at present day $M_{\rm h,par} = 10^{14}\,M_\odot$ with an hypothetical infalling subhalo of mass $M_{\rm h,sub} = 10^{11}\,M_\odot$ at infall and I want to assign its redshift of infall. The upper left panel of Figure 3.3 shows the mass assembly history of the parent halo and the hypothetical mass ratio at given infall redshift between the subhalo and parent halo. Given these two ingredients, I compute the value of the first-order SHMF at any redshift for this specific subhalo mass and parent halo, which is shown by the colour code in the upper right panel of the Figure. Then, the probability density function, shown in the lower panel, used to assign the actual infall redshift to the subhalo is simply given by the derivative of the SHMF with respect to redshift.

The methodology described previously to assign the infall redshifts to subhaloes can be applied to first-order subhaloes only. This is due to the fact that the SHMF only provides information on the subhaloes that accrete onto the parent or zero-order halo. Instead, for instance, for a second-order subhalo I am interested in the epoch when it was accreted for the first time as subhalo inside its host first-order subhalo, and not inside the zeroth-order halo. For second-order subhaloes, I first generate the full merger tree associated to a given parent halo by following its mass assembly history backwards in cosmic time and, using the recipe described above, computing the population

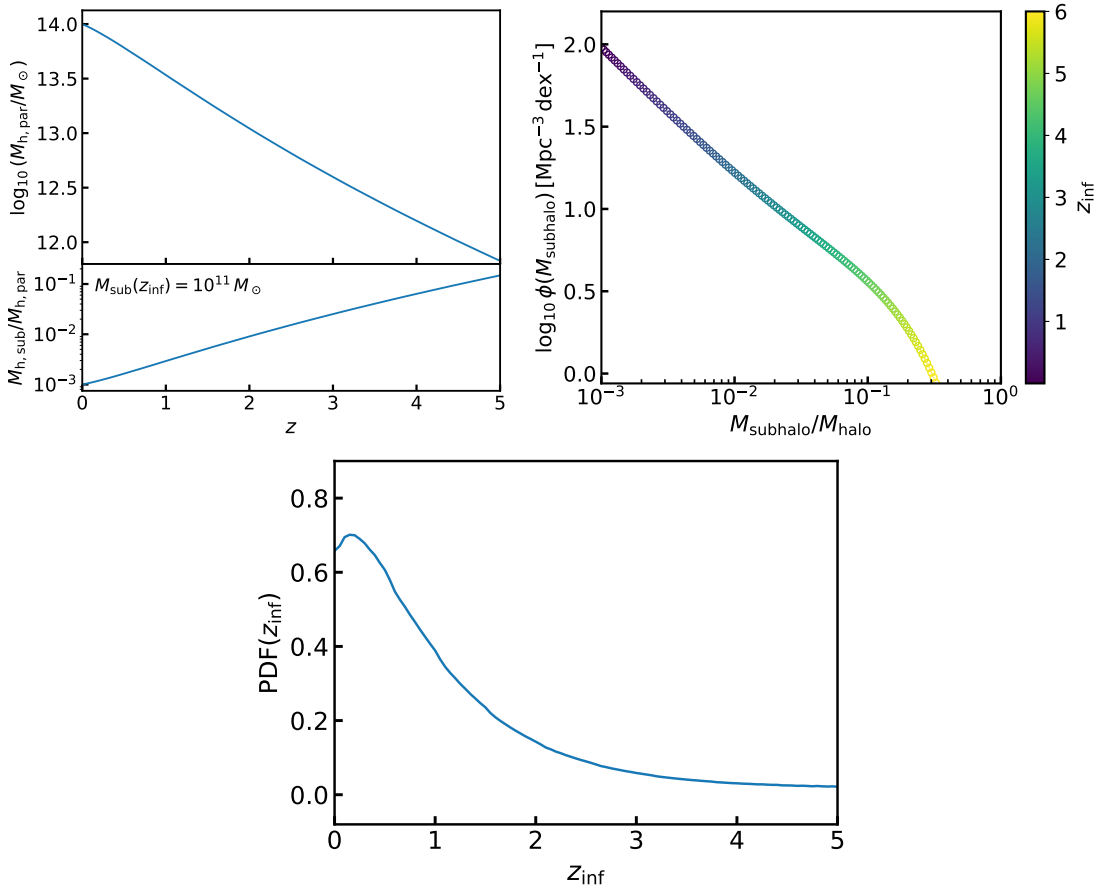

FIGURE 3.3: Upper left panel: example of accretion history of one halo of present-day mass $M_{\rm h,par}(z = 0) = 10^{14}\,M_\odot$, and evolution of the mass ratio between one hypothetical subhalo of mass $M_{\rm h,sub}(z_{\rm inf}) = 10^{11}\,M_\odot$ at infall and the parent halo. Upper right panel: first-order subhalo mass function, with colour bar representing the redshift of infall. Lower panel: resulting probability density function of the redshift of infall for the subhalo of infall mass $M_{\rm h,sub}(z_{\rm inf}) = 10^{11}\,M_\odot$ accreting onto the parent halo of mass $M_{\rm h,par}(z = 0) = 10^{14}\,M_\odot$.

of first-order subhaloes and their redshifts of infall from the first-order SHMF. For each first order subhalo, I then follow its mass and satellite accretion history using again the first-order SHMF. The satellites of the first-order subhalo will be second-order subhaloes with respect to the parent halo. I repeat this loop up to the third-order for sake of completeness, as orders higher than the third have insignificant contribution to the total amount of subhaloes (Jiang and van den Bosch 2014). I have tested that orders higher than the second have negligible contribution to the amount of both halo-halo and galaxy-galaxy mergers. Therefore, for the purposes of this thesis I limit my investigation to the second-order subhaloes.

In order to speed up the computational time, I first run fine merger histories with all relevant second- and third-order subhaloes. I then sample and compute analytic fits to

Sub. order	mass range	A	α	β	γ	δ
second	$10^{10}\,M_\odot < M_{\rm h,sub} < 10^{11}\,M_\odot$	$10.06^{+3.51}_{-3.86}$	$1.07^{+0.16}_{-0.14}$	$13.78^{+3.51}_{-5.78}$	$1.86^{+9.25}_{-7.80}$	$1.77^{+0.44}_{-0.37}$
second	$10^{11}\,M_\odot < M_{\rm h,sub} < 10^{12}\,M_\odot$	$24.93^{+6.24}_{-10.31}$	$1.77^{+0.22}_{-0.18}$	$8.87^{+3.39}_{-3.64}$	$0.42^{+6.22}_{-6.71}$	$1.94^{+0.43}_{-0.35}$
second	$M_{\rm h,sub} > 10^{12}\,M_\odot$	$24.81^{+5.64}_{-9.19}$	$2.67^{+0.26}_{-0.21}$	$2.31^{+0.88}_{-0.87}$	$-2.60^{+2.52}_{-4.08}$	$1.86^{+0.45}_{-0.34}$
third	$10^{10}\,M_\odot < M_{\rm h,sub} < 10^{11}\,M_\odot$	$8.37^{+2.76}_{-3.36}$	$1.50^{+0.21}_{-0.18}$	$13.50^{+3.74}_{-5.79}$	$3.00^{+10.33}_{-8.75}$	$3.29^{+0.53}_{-0.51}$
third	$M_{\rm h,sub} > 10^{12}\,M_\odot$	$23.71^{+7.73}_{-12.63}$	$2.54^{+0.31}_{-0.31}$	$3.41^{+1.57}_{-1.70}$	$-3.56^{+4.59}_{-4.65}$	$3.12^{+0.70}_{-0.49}$

TABLE 3.1: Best-fitting parameters to the infall redshift distribution parameterization from Equation (3.4), for different subhalo orders and mass ranges.

the probability distribution of their redshifts of infall. I adopt the following parameterization which allows to well fit the infall redshift distribution

$$\mathcal{P}(z) = A z^{\alpha} \frac{1}{\delta e^{\beta z} - \gamma}\,, \tag{3.4}$$

where A, α, β, γ and δ are dimensionless free fitting parameters, with best-fit values reported in Table 3.1. I use the analytic PDF of Equation (3.4) to assign the infall redshifts statistically to all second- and third-order subhaloes, especially when simulating large boxes and cluster-sized parent haloes. Furthermore, for each group or cluster, a generic subhalo of the $n-$th order must have fallen inside its (n-1)-th subhalo at a redshift $z_{\rm inf,n}$ higher than the redshift $z_{\rm inf,n-1}$ at which the latter has fallen inside its progenitor. I therefore set the infall redshift of the (n-1)-th order subhalo as a lower bound for the n-th order subhalo redshift, i.e.,

$$z_{\rm inf,n} = \mathrm{RAND}\left[z_{\rm inf,n-1}, +\infty\right]. \tag{3.5}$$

Figure 3.4 illustrates the $z_{\rm inf}$ probability density functions predicted by DECODE (shown as histograms) and the fits (shown as coloured lines) to Equation (3.4) for different subhalo masses and orders, as labelled.

3.2.2.4 Merging timescales and surviving subhaloes

After a subhalo has fallen into its host halo, it is affected by tidal stripping and dynamical friction, resulting in an overall net mass loss and disruption at the end. The amount of mass lost and whether the subhalo will be disrupted by such processes depends on its orbital energy and angular momentum (e.g., Hayashi et al. 2003; Taffoni et al. 2003; Taylor and Babul 2004; Peñarrubia and Benson 2005; van den Bosch et al. 2005; Zentner et al. 2005; Giocoli et al. 2008; Angulo et al. 2009; Gan et al. 2010; Klypin et al. 2015; Jiang and van den Bosch 2016; van den Bosch et al. 2016; van den Bosch 2017; Green and van den Bosch 2019). In van den Bosch et al. (2005) the authors have found that the

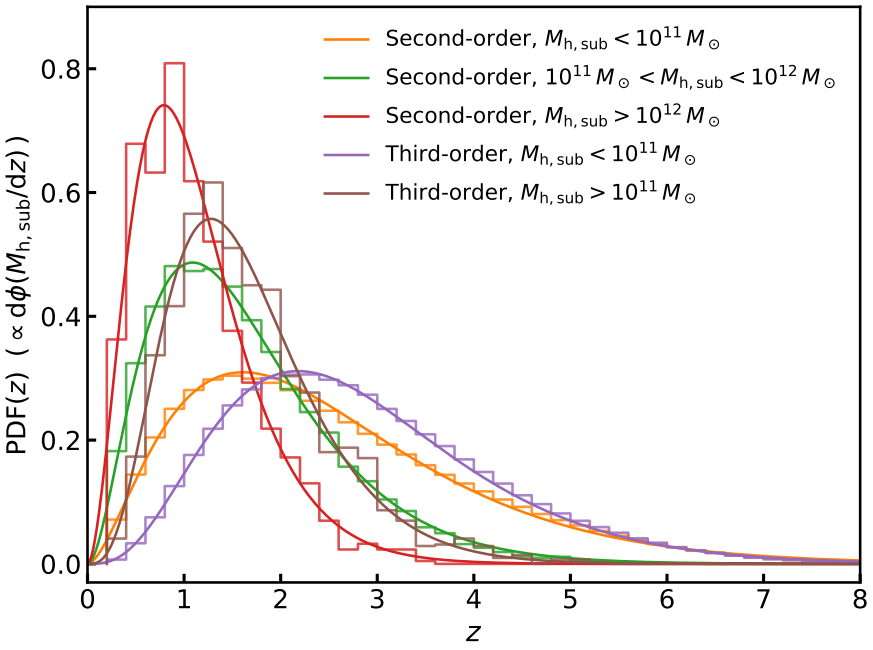

FIGURE 3.4: Analytic normalized probability distributions of the infall redshifts adopted in this thesis to generate the mock catalogues. The results are organized for different subhalo orders and mass ranges, as labelled. The histograms show the results from the merger tree and the coloured lines show the best fits to Equation (3.4).

average mass loss rate of satellite subhaloes can be analytically expressed as

$$\dot{M}_{\rm h,sub} = -\mathcal{A}\frac{M_{\rm h,sub}}{\tau_{\rm dyn}}\left(\frac{M_{\rm h,sub}}{M_{\rm h,host}}\right)^{\zeta}, \tag{3.6}$$

where $\mathcal{A} = 1.54$ and $\zeta = 0.07$. $M_{\rm h,sub}$ and $M_{\rm h,host}$ are the masses of the subhalo and its host halo, respectively. $\tau_{\rm dyn}$ is the halo dynamical friction timescale given by

$$\tau_{\rm dyn}(z) = 1.628\,h^{-1}\,{\rm Gyr}\left[\frac{\Delta_{\rm vir}(z)}{178}\right]^{-1/2}\left[\frac{H(z)}{H_0}\right]^{-1}, \tag{3.7}$$

with $H(z)$ being the Hubble's parameter at redshift z and $\Delta_{\rm vir}$ the virial parameter taken from Equation (6) of Bryan and Norman (1998). The typical timescale that a subhalo needs in order to fully merge with its progenitor from the time of first accretion is well described by the following merging timescale formula given by Equation (5) of Boylan-Kolchin et al. (2008)

$$\tau_{\rm merge} = \tau_{\rm dyn}A\frac{(M_{\rm h,host}/M_{\rm h,sub})^{b}}{\ln(1+M_{\rm h,host}/M_{\rm h,sub})}\exp\left[c\frac{J}{J_c(E)}\right]\left[\frac{r_c(E)}{R_{\rm vir}}\right]^{d}, \tag{3.8}$$

where $J/J_c(E) \stackrel{\rm def}{=} \xi$ represents the orbital circularity, $r_c/R_{\rm vir}$ the orbital energy and (A, b, c, d) are free parameters that govern the dependence of the merging timescale on the mass ratio. In Equation (3.8) I adopt the fitting parameters to N-body simulations

provided by McCavana et al. (2012). I also assume that galaxies living in the same dark matter haloes will merge with the same timescale, based on the assumption that a merger between haloes triggers the merger between their hosted galaxies.

In order to apply Equation (3.8), I assign an orbital circularity ξ to galaxies according to Khochfar and Burkert (2006), by extracting a random value from a Gaussian distribution centered in $\bar{\xi} = 0.5$ and with standard deviation $\sigma_\xi = 0.23$, and compute the ratio between the average radius of the orbit r_c and the host halo virial radius $R_{\rm vir}$

$$\frac{r_c}{R_{\rm vir}} = \frac{\xi^{2.17}}{1-\sqrt{1-\xi^2}} \,. \tag{3.9}$$

However, the analytic recipes described above are an approximation to the complex dynamics of dark matter haloes extracted from numerical simulations, which may themselves suffer from resolution or incompleteness problems. To allow for some flexibility in the merging timescales, I include a fudge factor (e.g., Grylls et al. 2019), which is a numerical correction factor applied to the merging timescale $f_{\rm dyn}$ in Equation (3.8), $\tau_{\rm merge} \rightarrow f_{\rm dyn}\tau_{\rm merge}$, to fit the population of surviving subhaloes at any redshift. I assume the fudge factor to be slightly dependent on parent halo mass, as I will describe in Section 4.1. To test the validity of this assumption, I analyze the population of the surviving subhaloes at redshift $z = 0$ via the unevolved surviving SHMF (Jiang and van den Bosch 2016), which is the number density of the surviving subhaloes that have not merged yet as a function of their mass at the time of first accretion. I again assume that subhaloes of third-order or higher are not statistically significant to the surviving population (Jiang and van den Bosch 2014).

The next step in building my merger tree is to assign merging timescales to all subhaloes of different orders, which I implement in DECODE in the following way. For any parent halo of mass $M_{\rm P0}(z)$, with a first-order subhalo of mass $M_{\rm S1}$ and a second-order subhalo of mass $M_{\rm S2}$:

1. I first compute the time that the first-order subhalo takes to merge with its parent halo, which depends on the ratio between their masses at the time of infall $M_{\rm P0}(z_{\rm inf})/M_{\rm S1}(z_{\rm inf})$;

2. I assign the merging timescale to the second-order subhalo which depends on the ratio between their masses at the time when it did infall into its host first-order subhalo $M_{\rm S1}(z_{\rm inf,2})/M_{\rm S2}(z_{\rm inf,2})$;

3. depending on the first accretion redshift and the merging timescale, I consider and implement in DECODE the three following possibilities: 1) the first-order subhalo has survived today and I assume at this step that its higher-order subhaloes inside still exist; 2) the higher-order subhaloes have been tidally disrupted before their first-order subhalo has merged; 3) the first-order subhalo has not survived

and it releases all its higher-order subhaloes to the parent[2] (Jiang and van den Bosch 2016);

4. finally, to the second-order subhaloes that are released from a first-order to the parent I assign a new merging timescale using the ratio between their masses at the new time of infall $M_{\rm P0}/M_{\rm S2}$[3], when released to the parent halo.

In Section 4.1, I will compare DECODE's predicted abundances of local unmerged subhaloes, described in terms of the surviving SHMF, with the analytic fit of Jiang and van den Bosch (2016) and with the resolved SHMF from the Millennium simulation, showing very good agreement when adopting a mass-dependent fudge factor, even though by simply adopting $f_{\rm dyn} \sim 1$ does not alter any of the main findings of this thesis.

3.2.2.5 Stochasticity of DECODE

As described in this Section, due to the *statistical* nature of DECODE, dark matter haloes in my mock catalogue are stochastic realizations of the input analytic HMF. Then, I generate a stochastic merger tree of subhaloes for each given *mean* parent halo mass following its mean accretion history $M_{\rm h,par}(z)$. In other words, DECODE produces a stochastic distribution of subhaloes merging on a mean halo. As quantitatively proven and discussed in Appendix A, when averaged over a large population of subhaloes, this approach is equivalent to an average one in which discrete subhaloes are replaced by statistical weights given by the SHMF, as carried out in Grylls et al. (2019). The main advantage of building halo assembly histories via discrete sources resides in the extreme flexibility of working with discrete objects and not with statistical weights, especially when transitioning to galaxies and the modelling of baryonic physics. Indeed, when working with discrete objects, it is straightforward to implement specific physical processes to evolve galaxies, although the stochastic characteristics limits our analysis only to mean quantities.

However, when investigating the quenching mechanisms in Chapter 7, whilst I still generate the parent halo catalogue stochastically, I will not use anymore mean accretion histories for them, favouring individual mass assembly histories for each dark matter halo via Hearin et al. (2021)'s DIFFMAH code. Furthermore, I will also abandon the stochastic fashion when generating subhaloes in merger trees and will make use of analytical merger trees generated via the Jiang et al. (2021)'s SatGen code to implement single mergers. The reason of these choices is the fact that, because of its stochasticity,

[2] I investigate also different ways of treating the evolution of higher-order subhaloes after the time of infall. In particular, I explored two additional possibilities: 1) every higher-order subhaloes merge together with their host first-order subhalo, 2) higher-order subhaloes have a dynamical friction longer than the age of the Universe and never merge. In both cases, there is not any appreciable difference in terms of satellite abundances and mergers.

[3] The evolved mass of the second-order subhalo, $M_{\rm S2}$, is computed according to Equation (3.6)

DECODE can only make predictions on the mean quantities for the *entire* galaxy population in each stellar mass bin, regardless of their type. Instead, when investigating the galaxy quenching, I need to make a clear distinction between star-forming and quiescent galaxies, along with their own individual mergers and growth history.

3.2.3 Abundance matching

I now present the abundance matching technique, used to compute the empirical scaling relations to populate dark matter haloes with galaxies. The main idea behind the abundance matching in semi-empirical models is that there is a monotonic connection between some galactic property and the host dark matter halo property, assuming that each halo or subhalo hosts one galaxy. For example, the very common assumption is that there is a relationship between galaxy stellar mass and host dark matter halo mass or, in other words, that the more (less) massive galaxies live inside more (less) massive haloes. This assumption is used in many semi-empirical models to assign galaxies to dark matter haloes via the SMHM relation (e.g., Behroozi et al. 2010; Moster et al. 2013; Grylls et al. 2019). However, the distribution of the galaxies in the stellar mass versus halo mass plane is not represented by a perfect monotonic function, but they are scattered around the mean relation. When deriving the mapping between the masses, the scatter in stellar mass at fixed halo mass is an assumption of the abundance matching which should be chosen a priori. Assuming different input scatter in stellar mass may bring non negligible changes in the predicted quantities, as I will discuss more in detail in Chapter 5. Instead, more recently several semi-empirical models are adopting the connection between the galaxy SFR and the halo accretion rate (e.g., Moster et al. 2018; Boco et al. 2023), which allows an actual prediction of the scatter in stellar mass, and the input scatter in SFR at fixed halo accretion rate within reasonable ranges has a smaller impact on the predictions. Below I describe how I perform the abundance matching to compute the SMHM relation and the inputs used for it.

3.2.3.1 Stellar mass-halo mass relation

In DECODE I assume a connection between the galaxy stellar mass and host dark matter halo mass. The SMHM relation is computed via abundance matching between the dark matter HMF and the observed galaxy SMF, using the formalism from Equation (37) of Aversa et al. (2015), reported below

$$\int_{\log M_\star}^{+\infty} \phi(M'_\star, z) \mathrm{d}\log M'_\star = \int_{-\infty}^{+\infty} \frac{1}{2} \mathrm{erfc}\left\{ \frac{\log M_\mathrm{h}(M_\star) - \log M'_\mathrm{h}}{\sqrt{2}\tilde{\sigma}_{\log M_\star}} \right\} \cdot \phi(M'_\mathrm{h}, z) \mathrm{d}\log M'_\mathrm{h} \,, \tag{3.10}$$

where $\tilde{\sigma}_{\log M_*} = \sigma_{\log M_*}/\mu$. Here, $\sigma_{\log M_*}$ is the Gaussian scatter in stellar mass at fixed halo mass, and $\mu = \mathrm{d}\log M_*/\mathrm{d}\log M_h$ is the derivative of the stellar mass with respect to halo mass. Equation (3.10) is tested to provide accurate results for values of the input scatter values below $\sigma_{\log M_*} \lesssim 0.3$. This recipe provides a fast and flexible tool to compute the SMHM relation numerically with only two ingredient (the HMF and SMF) and one input parameter, the scatter in stellar mass at fixed halo mass, without any pre-defined analytic fitting formula which requires a heavy MCMC exploration of the parameter space. The SMHM relation computed from Equation (3.10) is then used to assign galaxies to dark matter haloes.

3.2.3.2 Input halo mass function

In Equation (3.10), I make use of the total HMF which accounts for both the population of parent haloes and subhaloes

$$\phi(M_{\mathrm{h,tot}}) = \phi(M_{\mathrm{h,par}}) + \phi(M_{\mathrm{h,sub}}) \,, \tag{3.11}$$

where $\phi(M_{\mathrm{h,sub}}) \propto \phi(M_{\mathrm{h,par}})$ is the subhalo term, and it is proportional to the parent HMF at each redshift. This term allows to include all unstripped and unmerged subhaloes down to redshift z, as predicted by DECODE following the recipe detailed in Section 3.2.2.4. To determine the proportionality factor, I first compute the abundances of unstripped and surviving subhaloes at any redshift from DECODE and then fit it to following the expression from Behroozi et al. (2013, see Appendix G therein)

$$\frac{\phi(M_{\mathrm{h,sub}})}{\phi(M_{\mathrm{h,par}})} \sim C(a) \log\left(\frac{M_{\mathrm{cutoff}}(a)}{M_{\mathrm{h}}}\right) , \tag{3.12}$$

where $a = 1/(1+z)$ is the scale factor. The fit from DECODE's outputs provides the following fitting formulae for the two free parameters in Equation 3.12

$$\log(C(a)) = -2.42 + 11.68a - 28.88a^2 + 29.33a^3 - 10.56a^4 \,, \tag{3.13}$$

$$\log(M_{\mathrm{cutoff}}(a)) = 10.94 + 8.34a - 0.36a^2 - 5.08a^3 + 0.75a^4 \,, \tag{3.14}$$

where I have refitted only the parameters at redshift $z = 0$ and kept the same redshift evolution as in Behroozi et al. (2013). I show in Figure 3.5 the Tinker et al. (2008) HMF for parent haloes only, along with the total HMF with the correction for including unstripped surviving (i.e., unmerged) subhaloes, and I compare them with the numerical mass functions calculated from DECODE. I find that the new total HMF $\phi(M_{\mathrm{h,tot}})$, inclusive of the surviving subhaloes, is similar to the parent HMF $\phi(M_{\mathrm{h,par}})$ but with a slightly steeper low mass end, similarly to what was shown in Behroozi et al. (2013). More discussion on the completeness of the HMF can be found in Appendix B.

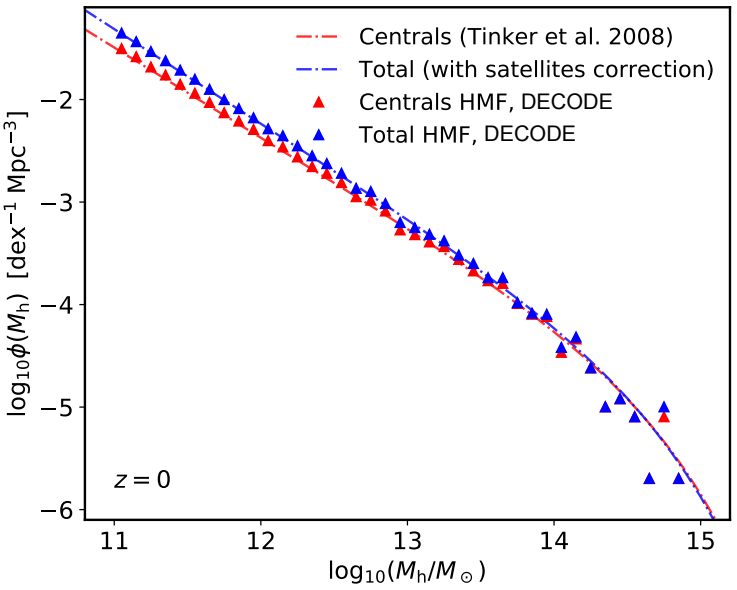

FIGURE 3.5: Halo mass function for parent dark matter haloes of Tinker et al. (2008) (red dash-dotted line) and the total HMF obtained by applying the correction with subhaloes from Equation 3.12 (blue dash-dotted line), compared to the numerical halo mass functions calculated from DECODE (triangles).

I will show in Sections 5.1 and 6.1 the observational SMFs that I consider for the abundance matching in this thesis and the resulting SMHM relation models.

3.2.4 Galaxy mass assembly

Once I have assigned the central galaxies to the parent haloes and satellite galaxies to the subhaloes, I proceed to the mass assembly history of central galaxies. As already described, galaxies grow their mass both via *in-situ* and *ex-situ* processes. *In-situ* processes are related to the internal properties of the galaxies, while *ex-situ* processes take place by interacting with external objects. The *in-situ* and *ex-situ* processes that I consider in this thesis are the star formation and mergers, respectively, which I assume to be the predominant components in the stellar mass growth of a galaxy.

Given the merger tree of a central galaxy, which is built with the subhalo merger tree and the SMHM relation, its merger history is derived by simply computing the cumulative sum of the merging satellites masses accounting for the time delay from Equation (3.8). I assume that a constant fraction of 20% of the stellar mass of satellites is lost during each merger and transferred to the intracluster light (e.g., Contini et al. 2014; Moster et al. 2018; Koutsouridou and Cattaneo 2022). Moreover, the galaxy total mass growth is derived by simply mapping its host dark matter halo mass assembly history into stellar mass via the SMHM relation. Given these two ingredients, the stellar mass formed

via star formation is simply provided by the difference between the two of them

$$M_\star^{\rm SF}(t) = M_\star^{\rm tot}(t) - M_\star^{\rm mer}(t) \ . \tag{3.15}$$

From the star formation history computed in terms of cumulative stellar mass from Equation (3.15), I compute the SFR at each redshift as the derivative with respect to stellar mass. When estimating the SFR, I account for the gas lost by stars which goes into the inter-stellar medium (ISM), described with the global gas mass loss rate (GMLR) following the formalism from Leitner and Kravtsov (2011, see Section 3.2 therein). For sake of clearness, I report below the main equation that I make use of

$$\mathrm{GMLR}(t) = \int_{t_0}^{t} \dot{M}_\star^{\rm SF}(t') \dot{f}_{\rm ML}(t - t') \mathrm{d}t' \ , \tag{3.16}$$

where $\dot{M}_\star^{\rm SF} = \mathrm{d}M_\star^{\rm SF}/\mathrm{d}t$ is the SFR, and $f_{\rm ML}$ is the fraction of mass lost given by Equation (1) of Leitner and Kravtsov (2011).

3.2.4.1 Satellites evolution

The merger history directly depends on the evolution of satellite galaxies from the infall until the time of their merger, and therefore also the star formation history will consequently depend on it. In most parts of this thesis, I assume that the stellar mass of satellite galaxies remains mostly constant after infall (frozen model). This assumption allows to rapidly predict in first approximation the galaxy merger rates, satellite abundances and morphology, saving much computational time simultaneously. However, the stellar mass of each individual satellite is expected to evolve via several physical processes such as stellar stripping, star formation and quenching (e.g., Cattaneo et al. 2011; Wetzel et al. 2013; Fillingham et al. 2016; Smith et al. 2016; Shi et al. 2020; Wright et al. 2022; Engler et al. 2023), even though a frozen model gives already an extremely good fit to the mean merger histories theoretically. I will show and discuss how these processes impact the prediction of the satellite abundances, merger rates and star formation histories of central galaxies. Below, I provide a brief detailing of how I model these processes in DECODE.

- Stellar stripping:
  I apply the recipe for stellar stripping according to the results from the N-body simulations by Smith et al. (2016)

  $$f_{\rm str} = \exp(1 - 14.2 f_{\rm DM}) \ , \tag{3.17}$$

  where $f_{\rm DM}$ the ratio between the mass of the subhalo at given redshift z and its peak mass, for which I assume to be in good approximation equal to the mass of

the subhalo at infall, and $f_{\rm str}$ is the fraction of the satellite's stellar mass at redshift z after stripping.

- Satellites star formation:
  to growth satellites via star formation, I use the main sequence SFR-$M_\star$ relation, that I predict for central galaxies, as input for the satellites in DECODE. I assume that the satellites have enough gas reservoirs to sustain this SFR until a given quenching timescale defined below. I stress that in DECODE the SFR for centrals is a prediction, while for the satellites it is an input assumption. Obviously, the prediction of the former depends on the latter according to the prescription of Section 3.2.4, since the star formation histories of centrals depend on the merger histories, and therefore on the way I treat satellites evolution. However, satellite mergers are negligible for low-mass galaxies and the mass of massive satellites remains mostly constant since their infall and, therefore, I simply rely on a frozen satellites model when predicting the main sequence. I also allow the possibility to include a scatter in the SFR-$M_\star$ relation as well. However, I found that by adding a scatter up to 0.25 dex, the results do not change at all.

- Satellites quenching:
  I quench the star formation in satellites following the recipe from Wetzel et al. (2013) of the "delayed-then-rapid" quenching, according to which galaxies continue to form stars for a period equal to the delay timescale $\tau_{\rm delay}$ and after it they undergo a rapid quenching where the SFR is truncated exponentially.

3.3 Quenching implementation

In this Section, I present the recipe for studying the quenching mechanisms in central galaxies. Quenching is thought to have a crucial role in shaping galactic properties, such as colours and morphologies (e.g., Blanton et al. 2003; Baldry et al. 2004; Brinchmann et al. 2004; Kauffmann et al. 2004; Muzzin et al. 2013; Davies et al. 2019). The physical processes that can halt star formation in galaxies are several and still matter of intense debate.

Quenching scenarios are typically classified into two categories: 1) internal quenching and 2) environmental quenching. Internal quenching, or mass quenching (Peng et al. 2010, 2012) includes all those mechanisms related to internal galactic processes, such as gas heating and outflow due to stellar winds, supernova feedback (e.g., Larson 1974; Dekel and Silk 1986), and/or active galactic nucleus (AGN) feedback from the central supermassive black hole (SMBH, e.g., Silk and Rees 1998; Granato et al. 2004; Bower et al. 2006; Croton et al. 2006; Somerville et al. 2008; Fabian 2012; Fang et al. 2013; Cicone et al. 2014; Lapi et al. 2018). Environmental quenching includes several distinct mechanisms due to the interaction between the galaxy and the environment.

Renowned quenching mechanisms fall in this category, such as halo quenching, where the hot gas of the galaxy is prevented from cooling when the mass of the host halo goes above a certain threshold (also known as *golden halo mass*, see, e.g., Birnboim and Dekel 2003; Dekel and Birnboim 2006), ram-pressure stripping, starvation and strangulation (e.g., Larson et al. 1980; Gunn and Gott 1972; Cowie and Songaila 1977).

To test the processes involved in quenching star formation, I develop an updated version of DECODE (DECODE 2.0, Fu, Boco et al. in prep.). In DECODE 2.0, there are two main differences with respect to the first version. Firstly, instead of using the abundance matching between the masses, I adopt the abundance matching between the halo accretion rate (HAR) and SFR, and assign galaxies to dark matter haloes via the SFR-HAR relation. This key feature allows to explicitly implement physical quenching processes and to directly study their role in galaxy evolution. Secondly, I make use of the DIFFMAH code from Hearin et al. (2021) to grow galaxies individually and merger trees are also generated individually using the SatGen code from Jiang et al. (2021) and Green et al. (2022a).

In this Section, I describe DECODE 2.0 and how I use it to evolve galaxies following their host dark matter haloes. The main steps of the methodology are summarized as follows:

- computing the SFR-HAR relation;
- assigning SFRs to galaxies;
- quenching the star formation;
- building galaxies stellar mass growth histories.

On top of this semi-empirical baseline, I will test the halo quenching mechanism. Furthermore, I will also discuss the role of the major mergers, SMBH feedback and morphological quenching. The specific implementation of these quenching mechanisms is described in Section 3.3.4. These quenching scenarios applied on top of DECODE 2.0 will generate a diverse set of outputs which will be compared with up-to-date observational data.

Figure 3.6 shows a cartoon-like scheme of DECODE 2.0. In brief, I firstly compute the SFR-HAR relation via abundance matching between the dark matter HAR function and the SFR function derived from observed luminosity functions. Secondly, galaxies are assigned with a SFR as a function of redshift via the SFR-HAR relation following the mass accretion history of their host haloes, and their star formation is quenched following the tested quenching recipe. Finally, I make my predictions for the galaxy SMF, quenched fraction and SMHM relation, and I compare them with the same observed quantities.

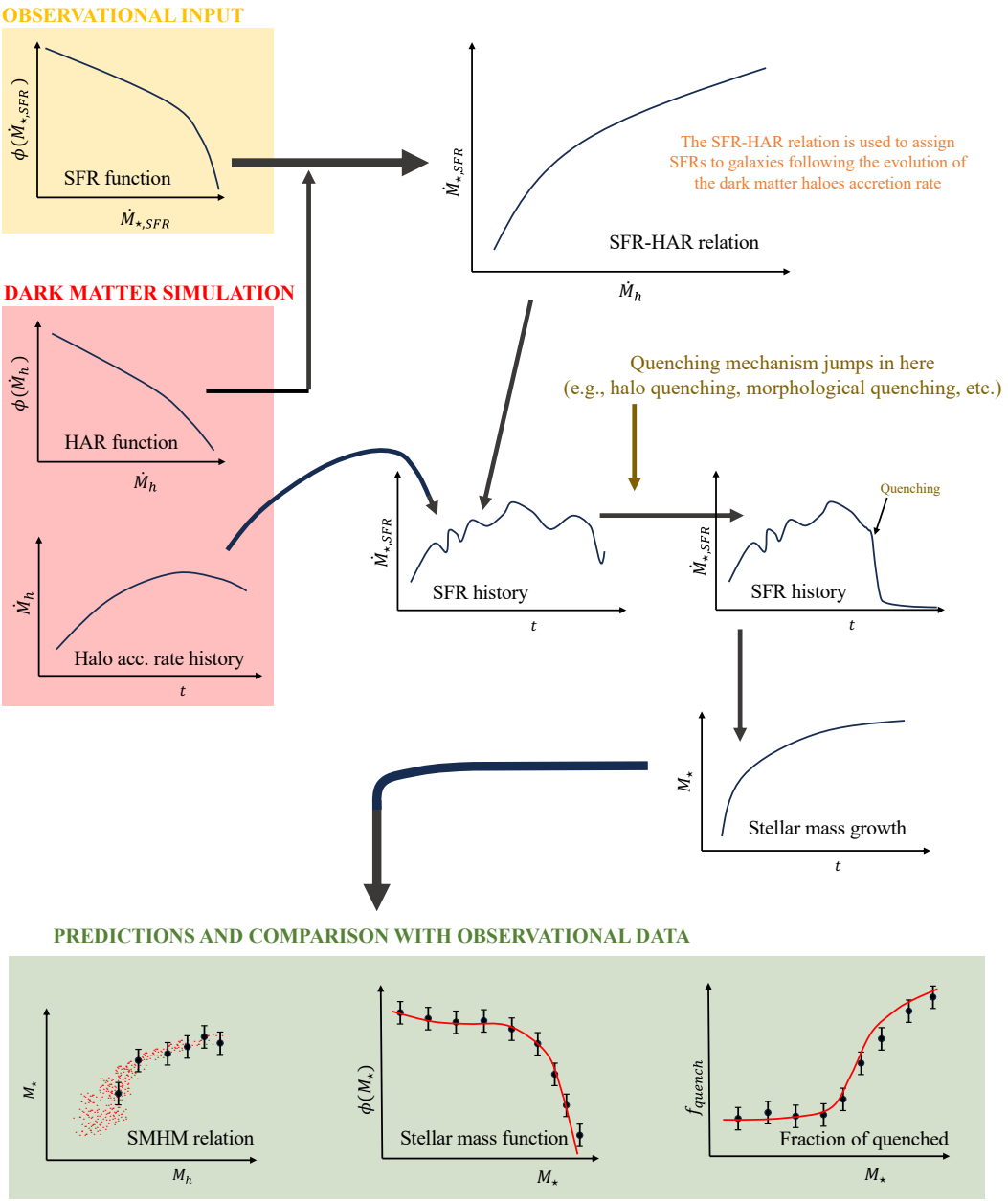

FIGURE 3.6: Cartoon showing the methodology used to form and evolve galaxies in DECODE 2.0. The SFR-HAR relation at each redshift is computed via abundance matching between the observed SFR function and HAR function from simulations. SFRs are assigned to galaxies following the accretion rate history of their dark matter haloes. I drop the SFR instantaneously when the galaxy is quenched. Galaxy stellar mass growths are constructed by integrating the SFR and quenching the star formation via the mechanism that I aim to test. Finally, I make my predictions on the SMHM relation, SMF and quiescent fraction, and compare with observations.

In the build-up of the stellar mass growths, DECODE 2.0 is similar in concept to the semi-empirical model TOPSEM, presented in Boco et al. (2023), although it differs from TOPSEM in some crucial aspects. Indeed, DECODE 2.0 avoids the initialization of galaxies through an input SMF at redshift $z = 0$, because I am able to build up the stellar mass of galaxies forwards in time since I perform the abundance matching between the accretion rates directly, while TOPSEM is based on specific accretion rates. Therefore, an additional pivotal feature, which represents the heart of this work, is the fact that I can directly implement physical quenching mechanisms in the stellar mass build up process and actually predict the fraction of quenched, a quantity that in TOPSEM was an input of the model to trace quiescent galaxies.

In the next subsections, I describe my abundance matching recipe (Section 3.3.1), the way to grow the galaxies stellar mass (Section 3.3.2), the mechanism to grow SMBHs at the centre of galaxies (Section 3.3.3) and the implementation of the quenching mechanisms discussed in this thesis (Section 3.3.4).

3.3.1 Abundance matching

The key element of DECODE 2.0 is the mapping between the galaxy SFR and host halo accretion rate, the SFR-HAR relation. I compute the latter via the abundance matching between observed SFR distributions and the HAR distributions following the same formalism of Equation (3.10), which allows to calculate the mean SFR at given HAR. The only input parameter is the scatter in SFR at fixed HAR, for which I choose the value of 0.3 dex. I have checked that the results do not change significantly by changing the scatter within reasonable values. I will describe the two main ingredients of the abundance matching, the HAR and SFR functions, in Section 7.1.

3.3.2 Growing galaxies stellar mass

The SFR-HAR relation generated via abundance matching is used to assign the SFR to galaxies following the accretion rate of the host dark matter haloes at each redshift. Following the quenching mechanism that I aim to test, i.e., shock heating or feedback processes, I halt the star formation and set the SFR to zero instantaneously. I then simply integrate the SFR forwards across cosmic time and predict the stellar mass growth of each galaxy. Galaxies are initialized at redshift $z \sim 3.5$, since above that redshift the quality of the LF data is poor and the SFR-HAR relation from abundance matching becomes less reliable.

At each redshift, I will have a population of galaxies surviving at redshift $z = 0$, and I correct the missing galaxies at high redshifts following the same formalism of Boco et al.

(2023), as described in Chapter 7. I am able also to compute the relative amount of star-forming and quenched galaxies, which are labelled with the value of their SFR. I stress that the fraction of quenched galaxies is an actual prediction of the model, which makes this work distinguishable and valuable since it allows to directly test the quenching physical mechanisms.

3.3.2.1 The contribution from mergers

An additional important process that cannot be neglected in the galaxy mass assembly, especially in more massive galaxies, is the merger with other galaxies (e.g., Guo and White 2008; Oser et al. 2010; Cattaneo et al. 2011; Lackner et al. 2012; Lee and Yi 2013; Pillepich et al. 2014; Rodriguez-Gomez et al. 2016; Qu et al. 2017; Clauwens et al. 2018; Pillepich et al. 2018a; Monachesi et al. 2019; Davison et al. 2020; Grylls et al. 2020b; Fu et al. 2022). I account for the mergers contribution in each galaxy by assigning to each of them an analytical merger tree generated via SatGen (Jiang et al. 2021; Green et al. 2022b), merging timescale following the recipe described in Section 3.2.2.4 and converting them into cumulative stellar mass merger histories using the SMHM relation predicted by the model itself.

3.3.3 Building up the population of black holes

Since one of the aims of this work is to discuss the SMBH quenching scenario, I need to populate galaxies with central SMBHs. It is now widely accepted that a SMBH is present at the center of each galaxy with a spheroidal component and multiple observational findings have allowed to create a bridge between astrophysics of galaxies and SMBHs. For example, AGN luminosity is seen to correlate with galactic SFR and stellar mass, originating the usually called co-evolution plane, and even the overall cosmic black hole accretion rate density as a function of redshift mirrors the shape of the cosmic SFR density (e.g., Delvecchio et al. 2014). Given this tight link, I grow the SMBHs in my mock catalogue by exploiting the redshift dependent relation between black hole accretion rate (BHAR) and SFR (BHAR-SFR), also computed via abundance matching. I will describe the BHAR distributions, used in the abundance matching, in Section 7.1.

Once the BHAR-SFR relation is computed, I grow black holes in the same way as galaxies, i.e., by integrating their accretion rate across cosmic time. The simultaneous growth of black holes and their host galaxies will give us insights on the role of the black hole feedback on the quenching mechanism.

3.3.4 Treatment of quenching

3.3.4.1 Halo quenching

The main environmental quenching mechanism that I consider is halo quenching (e.g., Birnboim and Dekel 2003; Kereš et al. 2005; Dekel and Birnboim 2006, 2008). The aforementioned works have shown that galaxies living in dark matter haloes above a certain threshold mass stop forming stars because a virial shock propagates across the halo, heating the interstellar medium. On the other hand, below this threshold rapid cooling dominates over the shock gas pressure. Birnboim and Dekel (2003) and Dekel and Birnboim (2006) computed the typical threshold halo mass, being equal to $M_{\rm h,lim} \sim 10^{12}\, M_{\odot}$.

As described in Section 3.3.2, for each galaxy in my catalogue, I assign the SFR via the SFR-HAR relation computed via abundance matching, and I integrate the SFR across cosmic time to build up the stellar mass of each galaxy, assuming that all galaxies are star-forming at high redshifts. Then, I truncate the star formation when the dark matter halo mass exceeds the threshold value $M_{\rm h,lim}$ and I label the galaxy as quenched. Since physically not all galaxies quench when their host halo reach exactly $M_{\rm h,lim} \sim 10^{12}\, M_{\odot}$, I include some dispersion around this quenching halo mass, which I leave as free parameter in the model.

3.3.4.2 Black hole quenching

Many theoretical models also suggest that feedback from the SMBH living at the centre of galaxies can regulate the star formation process (e.g., Silk and Mamon 2012; Vogelsberger et al. 2014; Schaye et al. 2015; Choi et al. 2017; Weinberger et al. 2018; Zinger et al. 2020; Ma et al. 2022; Piotrowska et al. 2022; Bluck et al. 2023a). The energy released from the central black hole to the host galaxy and its surroundings heats or ejects the gas in the galaxy reservoir, obstructing the infall of new cold gas from the halo to feed the star formation.

In order to study the quenching due to black hole, I populate galaxies with black holes following the methodology described in Section 3.3.3. Having assigned black holes with an accretion rate at each redshift, by integrating it across cosmic time one can derive their mass assembly history. Once the black hole mass growths have been computed, black holes can be quenched by using empirically motivated scaling relations, such as the black hole mass-stellar mass ($M_{\rm BH} - M_{\star}$) and the black hole mass-stellar velocity dispersion ($M_{\rm BH} - \sigma_{\star}$) relations (e.g., King and Pounds 2015; Martín-Navarro et al. 2018). I will discuss in Section 7.3 what problems each of these methods bring and how they may affect predictions on the quenching.

3.3.4.3 Morphological quenching

Another interesting mechanism able to quench galaxies in less massive haloes is the morphological quenching (Martig et al. 2009). Such mechanism is due to, instead of the direct removal of cold gas, the existence of a central massive spheroid, whose gravitational potential prevents the disc from collapsing and halts star formation (e.g., Fang et al. 2013; Bluck et al. 2014; Lu et al. 2021).

The morphological quenching can be studied in DECODE by integrating the Sérsic profile (Sérsic 1963) to compute the surface density of each galaxy within the effective radius, assigned via empirical size-mass relations (from, e.g., Suess et al. 2019). Then, the SFR of each galaxy can be quenched by employing a threshold value for the surface density above which morphological quenching is operating (e.g., Brennan et al. 2015; Su et al. 2019; Xu and Peng 2021).

3.4 Data

In this Section, I describe the datasets utilized in this thesis.

3.4.1 The Millennium simulation

I use the Millennium dark matter only simulation (Springel et al. 2005) scaled to the Planck cosmology (Planck Collaboration et al. 2016). All dark matter haloes are identified using the Friends-Of-Friends (FOF) algorithm (Davis et al. 1985), which locates a group of dark matter particles whose mutual distance is less than a linking length $b = 0.2$. Furthermore, all dark matter subhaloes are detected using the SUBFIND algorithm (Springel et al. 2001), based on which each FOF halo has one central subhalo or parent halo (typically the most massive halo), and the rest of the subhaloes are labelled as satellite subhaloes (simply referred to as subhaloes in this thesis). This information is taken from the publicly available L-Galaxies[4] semi-analytical model (Ayromlou et al. 2021a) that runs on top of the Millennium simulation.

I stress that although the halo virial mass M_{200} is defined as the mass within the halo virial radius R_{200}, the FOF halo could extend beyond this scale. Therefore, satellite subhaloes of a FOF halo can exist beyond the R_{200} as well. Nevertheless, this does not constitute a limitation in the comparison of the SHMF with DECODE since I base the subhaloes generation on the unevolved total SHMF from Jiang and van den Bosch (2014, 2016), which has already been shown to be in good agreement with the one from the Millennium simulation as presented in Li and Mo (2009). Furthermore, recently

[4] https://lgalaxiespublicrelease.github.io

Green et al. (2021) presented a more accurate SHMF computed with an updated version of their model SatGen, where they are able to follow subhalo orbits and effects of numerical disruption. The SHMF that I use slightly differs with the one from Green et al. (2021) by a factor of ~ 0.1 dex only at $M_{\rm h,sub}/M_{\rm h,par} \lesssim 10^{-3}$, where their contribution to the galaxy mergers is completely negligible. Nevertheless, I checked that the unevolved total subhalo distribution given by the updated Green et al. (2021) version of SatGen is statistically unchanged with respect to that presented in Jiang and van den Bosch (2016).

I use the data from the Millennium simulation to test the capability of DECODE to predict the dark matter HMF, unevolved SHMF, surviving SHMF and the distribution of infall redshifts. Dr M. Ayromlou (University of Heidelberg) provided the aforementioned quantities.

3.4.2 The TNG simulation

I make use of the public data release[5] from the TNG100 simulation, a component of the IllustrisTNG hydrodynamical simulation suite (TNG hereafter; Nelson et al. 2018; Pillepich et al. 2018a; Springel et al. 2018; Marinacci et al. 2018; Naiman et al. 2018). The TNG simulations are performed utilizing the moving-mesh AREPO code (Springel 2010), which provides solutions for a combination of gravity and magnetohydrodynamical equations (Pakmor et al. 2011; Pakmor and Springel 2013). TNG facilitates the simulation of galaxies via subgrid modelling of critical galaxy formation processes, such as gas cooling, star formation, stellar evolution, feedback from stars, and supermassive black hole associated processes, including seeding, merging, and feedback (refer to Pillepich et al. 2018b and Weinberger et al. 2017 for a comprehensive model description). The TNG simulations encompass different cosmological volumes and mass resolutions. In this thesis, I utilize the TNG100 simulation, executed within an approximately 100 Mpc box, which is the most suitable simulation for the objectives of this thesis.

The TNG simulation also employs the FOF algorithm (Davis et al. 1985) for the identification of haloes and the subhaloes are identified as gravitationally bound groups of particles, by executing the SUBFIND algorithm (Springel et al. 2001). Galaxies are essentially subhaloes with a non-zero stellar mass. FOF haloes generally lack a well-defined shape. However, it is customary to consider R_{200} (R_{500}), the radius within which the mean density is 200 (500) times the critical density of the background, as the halo radius. Given that FOF halos can extend beyond the R_{200}, satellites of a FOF halo can exist and evolve both within and beyond the halo boundary (e.g., see Ayromlou et al. 2021b; Rohr et al. 2023).

[5] https://www.tng-project.org/data

In order to evaluate our mass abundance matching technique against the TNG simulation, the SMHM relation is computed from the simulation. This is done by determining the ratio between the total stellar mass and the total halo mass within the halo boundary, R_{200}, for all haloes in the simulation. Then, subhalo merger trees, created using the SUBLINK algorithm (Rodriguez-Gomez et al. 2015), are employed to trace the evolution of individual galaxies over time. For each galaxy, I start from the present time ($z = 0$, snapshot=99) and trace back the evolution of its main progenitor through the 100 snapshots/redshifts of the TNG100 simulation. This process continues until reaching the first appearance of the galaxy in the simulation. This approach enables us to extract several properties of all individual galaxies across cosmic time, including stellar mass growths and star formation histories. From this, several properties of galaxies, including stellar mass histories, star formation histories, and so on are extracted. The stellar masses of galaxies are also segregated into *in-situ*, formed within the main progenitor branch of a galaxy, and *ex-situ*, originating from minor and major mergers of the galaxy with other objects (see Rodriguez-Gomez et al. 2016).

Furthermore, the galaxy morphologies are calculated as in Genel et al. (2015) and Marinacci et al. (2014). The kinematic decomposition of galaxies is based on the distribution of the circular parameter of individual stellar particles, which is defined as $\epsilon = J_z/J(E)$ (Du et al. 2019). Here, J_z corresponds to the specific angular momentum in the symmetric axis of the galaxy and $J(E)$ the maximum specific angular momentum possible at the specific binding energy (E) of the stellar particle. The bulge component of each galaxy comprises the stellar particles with the circular parameter $\epsilon < 0$ and a fraction of stellar particles with a positive circular parameter that mirrors around zero. The elliptical galaxies are defined as the galaxies with bulge-to-total stellar mass ratio $B/T > 0.7$.

I use the data from the TNG simulation to compare the predictions from DECODE for the fraction of ellipticals and B/T ratios, provided by Dr. Y. Rosas-Guevara (DIPC, San Sebastián). I also use the TNG simulation to test DECODE abundance matching (i.e., the SMHM relation), satellite abundances, star formation and merger histories, provided by Dr M. Ayromlou (University of Heidelberg).

3.4.3 GalICS

I make use of the data from GALICS 2.2 (Koutsouridou and Cattaneo 2022), the latest version of GALICS (Galaxies In Cosmological Simulations; Hatton et al. 2003), a semi-analytic model to follow the evolution of baryons in halo merger trees extracted from cosmological N-body simulations.

In this thesis, I use the GALICS 2.0 framework which includes the information of dark matter substructures within each dark matter halo (Cattaneo et al. 2017). Central galaxies are at the centre of their host haloes. Satellite galaxies are associated with subhaloes.

As soon as a galaxy becomes a satellite, a merging countdown timer starts ticking. The time that a satellite galaxy takes to merge with its central galaxy of its host system is computed using the analytical fit to hydrodynamical simulations from Jiang et al. (2008), similar to the fit from Boylan-Kolchin et al. (2008) used in DECODE.

In GALICS 2.1 (Cattaneo et al. 2020) there was introduced a physical criterion to determine when the gas that accretes onto a halo streams onto the central galaxy in cold flows and when it is shock-heated. In absence of feedback from active galactic nuclei (AGN), the shock-heated gas in a dark matter halo or subhalo can cool onto the associated galaxy. Its cooling provides a second mechanism for gas accretion. Environmental effects, such as ram pressure and tidal stripping, reduce the importance of cooling in satellite galaxies (Koutsouridou and Cattaneo 2019, 2022 for details).

Gas accreted through cold accretion and cooling settles into discs, the sizes of which are determined by the conservation of angular momentum, and form stars on a timescale equal to twenty-five orbital times at one exponential scale-length from the galactic centre (Cattaneo et al. 2017). The conversion of gas into stars is much faster in merger-driven starbursts. Mergers also cause galaxies to grow bulges. The modelling of the effects of galaxy mergers is based on hydrodynamic simulations by Kannan et al. (2015) and described in Koutsouridou and Cattaneo (2022, GALICS 2.2). Since GALICS 2.2, tidal stripping is not the only mechanism for the origin of the intracluster light. At each merger, a stellar mass equal to 20% of the stellar mass transferred to the bulge is scattered into the halo. I note that this assumption is very similar to the one made in DECODE for major mergers, which transfer most of the stars to the bulge component.

The main new features of the GALICS 2.2 version are the presence of feedback from AGNs and the model for morphological transformations in galaxy mergers. AGN feedback's recipe is described with the empirical model of Chen et al. (2020). Black holes grow and deposit feedback energy into the surrounding gas until this feedback energy is larger than a fraction or multiple of its gravitational binding energy, at which point the gas is unbound or, more realistically, heated to high entropy, so that its cooling time becomes long. By doing so, AGN feedback quenches star formation and prevents its reactivation. For mergers, while in GALICS 2.1 major mergers destroy the disc component completely, GALICS 2.2 adopts a more realistic model based on the numerical results of Kannan et al. (2015), described in Section 2.6.2 of Koutsouridou and Cattaneo (2022). There have also been small improvements in the modelling of supernova feedback and disc instabilities with respect to the previous version.

The implementation of the disc instabilities is based on the results of Devergne et al. (2020) who studied the growth of pseudobulges in isolated thin exponential stellar discs embedded in static spherical haloes. They found that discs with $v_d/v_c > 0.6$ are unstable (see also Efstathiou et al. 1982), where v_c is the circular velocity of the galaxy and v_d is the circular velocity considering only the disc's gravity. The following fitting formula

(Devergne et al. 2020) for the B/T mass ratio is adopted

$$B/T = 0.5 f_{\rm d}^{1.8}(3.2 r_{\rm d}) \,, \tag{3.18}$$

where $f_{\rm d} = (v_{\rm d}/v_{\rm c})^2$ is the contribution of the disc to the total gravitational acceleration, and $r_{\rm d} = R_{\rm d}/R_{\rm vir}$ is the dimensionless exponential scale-length in units of the virial radius $R_{\rm vir}$.

I use the data from GALICS to compare DECODE's fraction of ellipticals, B/T ratios and star formation histories. These data were provided by Dr. I. Koutsouridou (Observatory of Arcetri, Florence) and Prof. A. Cattaneo (Observatory of Paris).

3.4.4 Sloan Digital Sky Survey

I use as reference data from the Sloan Digital Sky Survey (SDSS) Data Release 7 (DR7, Abazajian et al. 2009) as presented in Meert et al. (2015, 2016), which has a median redshift of $z \sim 0.1$. Stellar masses are computed from the Meert et al. catalogue using the best-fitting `Sérsic` or `Sérsic-Exponential` photometry of r-band observations, and by adopting the mass-to-light ratios by Mendel et al. (2014). Furthermore, the truncation of the light profile as prescribed in Fischer et al. (2017) is adopted. The Meert et al. catalogues are matched with the Yang et al. (2007, 2012) group catalogues, which allow us to identify central and satellite galaxies and provide an estimate of the group halo mass.

The first observable against which I test our model is the stellar mass function of satellites, which is computed using standard $V_{\rm max}$ weighting and provided by Prof. M. Bernardi (University of Pennsylvania). I further test the model against the fraction of elliptical and lenticular galaxies as a function of stellar mass, computed by Dr. L. Zanisi and myself. Here, I use the neural network-based morphologies from the Domínguez Sánchez et al. (2018) catalogue, which provides estimates of T-Types, as well as the probability for Early Type Galaxies (i.e., T-Type ≤ 0) of being S0, $P_{\rm S0}$. I compute the fraction of ellipticals by considering only Early Type Galaxies for which $P_{\rm S0}$ falls below a certain threshold. I have accurately tested that the dependence of the ellipticals fraction on such threshold is extremely mild, showing variation within 10% even for $P_{\rm S0} \lesssim 0.3$. In this work I adopt $P_{\rm S0} < 0.5$ according to the results from Domínguez Sánchez et al. (2018). I estimate the error bars on the satellite stellar mass functions and on the fraction of ellipticals using the Poisson statistics.

3.4.5 MaNGA

I use the data on the bulge-to-total ratios (B/T) and star formation histories of galaxies from the Mapping Nearby Galaxies at Apache Point Observatory (MaNGA; Bundy

et al. 2015; Drory et al. 2015; Law et al. 2015; Yan et al. 2016a,b). MaNGA is a component of the fourth generation of the Sloan Digital Sky Survey (SDSS IV; Gunn et al. 2006; Smee et al. 2013; Blanton et al. 2017) and uses optical integral field units (IFUs) to measure spectra across nearby galaxies. The MaNGA Data Release 17 (DR17; Abdurro'uf et al. 2021) includes observations of about 10000 galaxies at low redshift. Observations were obtained with the two BOSS (Baryonic Oscillation Spectroscopic Survey) spectrographs on the 2.5 meters Sloan telescope at the Apache Point Observatory, covering wavelengths from 3600 Å to 10300 Å (Smee et al. 2013). The `DR17 MaNGA Morphology Deep Learning` Value Added catalog (DR17-MMDL-VAC) provides morphological classifications and the `DR17 MaNGA PyMorph photometric` Value Added Catalog (DR17-MPP-VAC) provides Sérsic (Ser) and Sérsic + Exponential (SerExp) fits to the 2D surface brightness profiles of these objects, along with a detailed flagging system for using the fits (see Domínguez Sánchez et al. 2022 for details).

Bernardi et al. (2023) describe how to combine the photometric and flagging information to determine reliable B/T values for these objects, and how the B/T correlate with morphology. Because the MaNGA selection function is complicated, and because the MaNGA sample is much smaller than the SDSS, I use SDSS to determine the shape of the stellar mass function and how the fraction of ellipticals varies with stellar mass, but MaNGA to determine how B/T correlates with stellar mass. I test our model against MaNGA's B/T ratios, computed by Prof. M. Bernardi (University of Pennsylvania).

Furthermore, I use the observationally inferred SFHs of MaNGA galaxies (Bertemes and Wuyts in prep.), provided by Dr. Caroline Berthemes (University of Heidelberg), which were derived based on a full spectral fitting procedure following the stellar population synthesis (SPS) method. In more detail, the integrated MaNGA spectra were fit in the optical wavelength range of $3700 - 7400$ Å simultaneously with associated photometry from the NASA-Sloan Atlas (Blanton et al. 2011) using the Bagpipes code (Carnall et al. 2018). I choose piecewise constant SFHs, which consist of 7 segments of constant SFR, and thus leave a significant amount of freedom to the evolution of the SFR in time. The first age bin goes from 0 to 30 Myr in lookback time, and the next one from 30 to 100 Myr. Subsequently, there are 4 segments of equal duration in log time until 85% of the age of the Universe is reached. The last age bin spans the remaining 15% of the age of the Universe. To favour smooth SFHs in the absence of constraining information, the jumps in SFR between the age bins are drawn from a prior corresponding to a student's t-distribution (Leja et al. 2019a). A Calzetti et al. (2000) extinction law was assumed (with the dust attenuation A_V being a free parameter), and all stars were assumed to share a single metallicity, which is left to vary between $0.1Z_\odot$ and $2Z_\odot$. All emission lines were subtracted for the fitting process by using the emission line only (EMLINE) model cube produced by the MaNGA DAP (Westfall et al. 2019). Further, spectra were scaled to a S/N of 30 prior to fitting to allow the procedure to sufficiently explore the parameter space.

3.4.6 GAMA

I use the data from the Galaxy And Mass Assembly (GAMA) survey (Driver et al. 2011; Liske et al. 2015), a spectroscopic survey conducted on the Anglo Australian Telescope, designed to collect redshifts for a highly complete sample of galaxies. The survey consists of redshifts for ∼300,000 galaxies over 5 regions with a total sky area of 230 $\deg^2$. The spectroscopic redshifts of the galaxies are accompanied by 20-band photometry from the ultraviolet to the infrared, providing a vast multi-wavelength dataset by which to study these galaxies. As of the final data release DR4[6] (Driver et al. 2022), which is based on a new derivation of the underlying photometry (Bellstedt et al. 2020) using the source-extracting software ProFound (Robotham et al. 2018), the survey is 95% complete down to an r-band magnitude of 19.65 mag.

In this thesis, I use the observational measurement of the SFHs from GAMA for a complete sample of galaxies, provided by Dr. S. Bellstedt (University of Western Australia). The SFHs used come from Bellstedt et al. (2020), who studied a sample of 6,688 galaxies with $z < 0.06$ and $r < 19.5$ mag in the three equatorial fields. The 20-band photometry was processed with the spectral energy distribution (SED) fitting code ProSpect (Robotham et al. 2020) to derive the SFHs, using the parametric `massfunc_snorm_trunc` function to describe the SFH (corresponding to a skewed Normal function with a truncation in the early Universe), and an evolving metallicity implementation, where the final metallicity is fitted as a free parameter. For further details on the SED fitting implementation, I refer the reader to Bellstedt et al. (2020).

[6] http://www.gama-survey.org/dr4/

Chapter 4

Testing DECODE's performance

Before employing DECODE to predict crucial quantities of galaxy evolution, such as merger rates and stellar mass assembly histories, I assess its performance through validation against numerical simulations. These tests are aimed firstly at ensuring that the statistics of the dark matter haloes and merger trees are consistent with the outputs of N-body simulations at given cosmology, and secondly at checking the self-consistency of DECODE in reproducing the outputs of hydrodynamical simulations when using their SMF as input. The testing involves several steps. Firstly, I evaluate the capability of DECODE in accurately reproducing the abundances of parent haloes, unmerged subhaloes and surviving subhaloes from the Millennium dark matter-only simulation (Section 4.1). Subsequently, I test the abundance matching, the core of DECODE's methodology, against the TNG hydrodynamical simulation (Section 4.2). Additionally, I ensure the self-consistency of DECODE by comparing the stellar mass growths, merger rates and satellite abundances with the TNG simulation. Specifically, the aim is to test whether, by taking the TNG's stellar mass function (SMF) as input, DECODE can predict the aforementioned quantities consistent with those produced by the simulation itself (Section 4.3).

4.1 Validating the dark matter halo population

In this Section, I test the precision of DECODE in matching the number densities and infall redshift distributions of unevolved and unmerged subhaloes of first- and second-order as predicted by N-body simulations. I first verify that the unevolved total subhalo mass function (SHMF) fitted by Jiang and van den Bosch (2016) from the MultiDark simulation (Klypin et al. 2011) is well consistent with the total unevolved SHMF extracted from the Millennium simulation, at least for parent haloes of mass $M_{\rm h} \gtrsim 10^{11}\,M_{\odot}$, above the resolution limit of the simulation. This finding is quite significant as it emphasizes the universality of the SHMF suggested by Jiang et al., which is used

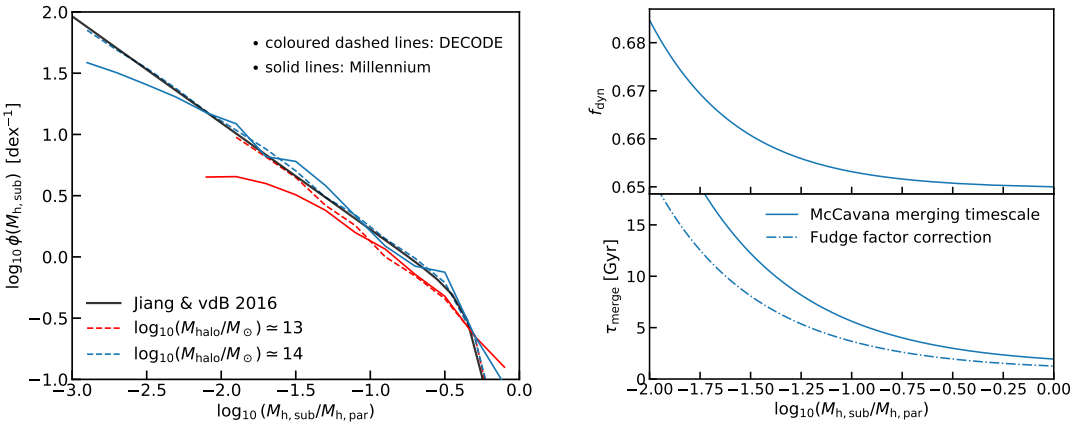

FIGURE 4.1: Left panel: Comparison between the surviving unevolved subhalo mass function for two different parent halo mass bins at redshift $z = 0$. The coloured dashed lines are the results from DECODE, the solid lines are the results extracted from the Millennium simulation (as described in Section 3.4.1) and the solid black line the analytic form taken from Jiang and van den Bosch (2016). Right upper panel: fudge factor as function of the mass ratio according to Equation (4.1). Right lower panel: merging timescale from McCavana et al. (2012) (solid line) compared with that computed by applying the fudge factor correction (dash-dotted line).

as input in DECODE, with respect to the underlying cosmological model and also other aspects of the simulations, such as the halo finder algorithm.

Next, I investigate the population of surviving subhaloes at each redshift, serving as a valuable test for both the merging timescales in DECODE and the subhalo generation algorithm. The left panel of Figure 4.1 shows the unevolved surviving SHMF (i.e., composed by subhaloes not yet merged or completely disrupted) at $z = 0$ for two different values of parent halo masses, $M_{\rm h} \simeq 10^{13}$ and $10^{14}\,M_{\odot}$, as labelled. DECODE's predictions are compared with those from the Millennium simulation and from the fit of Jiang and van den Bosch (2016), which reproduces well the results from the Millennium simulation. The number of surviving unstripped subhaloes predicted by DECODE, represented with dashed lines, becomes indistinguishable from the grey solid line of Jiang and van den Bosch (2016), when a small mass-dependent correction is applied to the merging timescales of McCavana et al. (2012), as described in Section 3.2.2.4. As shown in the right panel of Figure 4.1, the fudge factor $f_{\rm dyn}$ in the dynamical friction timescale is found to be well represented by the following linear relation with the halo-to-subhalo mass ratio $\psi = (M_{\rm h,host}/M_{\rm h,subhalo})$

$$f_{\rm dyn} = a\psi + b\,, \tag{4.1}$$

where the best-fit values for a and b are 0.00035 and 0.65 respectively.

In order to serve as a versatile tool to model, e.g., galaxy merger rates, DECODE must

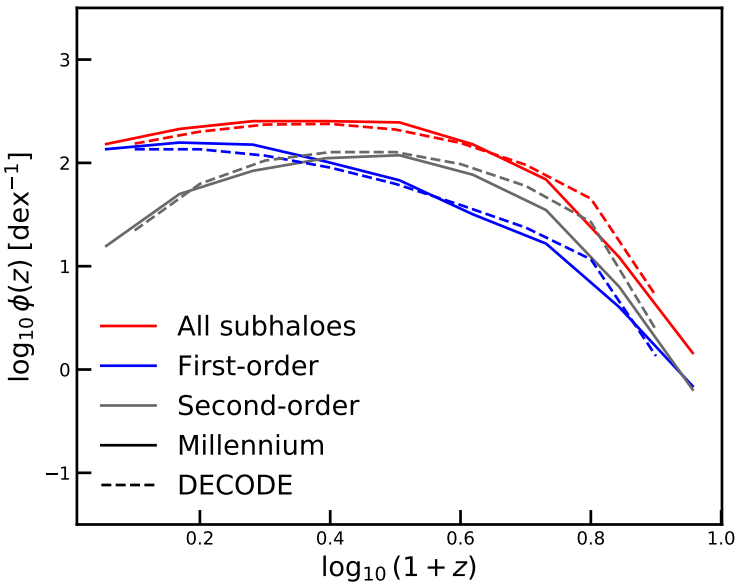

FIGURE 4.2: Comparison between number densities of the infall redshifts from DECODE (dashed lines) and from Millennium simulation (solid lines) for parent haloes of mass selected between $10^{14} M_\odot$ and $10^{14.1} M_\odot$. Results are shown for subhaloes of all orders (red lines), first-order (blue lines) and second-order (grey lines). Similar results are found for other parent halo masses.

not only generate the correct abundances of subhaloes of different orders, but also to reproduce the correct probability distributions of their infall redshifts $z_{\rm inf}$. Figure 4.2 compares the number densities of the infall redshifts of first- and second-order subhaloes accreting onto parent haloes of mass between $10^{14} M_\odot$ and $10^{14.1} M_\odot$ as predicted by DECODE (dashed lines) and the Millennium simulation (solid lines). I performed the same check for several parent halo mass bins, from $M_{\rm h,par} \sim 10^{12.5}\, M_\odot$ to $M_{\rm h,par} \sim 10^{14.5}\, M_\odot$. The agreement found is fairly good, further validating the accuracy of my modelling.

4.2 Abundance matching

After having established the consistency of the dark matter sector, I now test the inner self-consistency of DECODE by comparing it to the outputs of the TNG hydrodynamical simulation, described in Section 3.4.2. The aim here is to test whether, by starting from the SMF of the TNG simulation as input, DECODE is able to accurately match the stellar mass assembly histories, SFHs, merger histories and satellite abundances directly computed from the TNG simulation.

To start, I examine my abundance matching prescription, described in Section 3.2.3, taking as inputs the galaxy SMF and the dark matter HMF extracted from the TNG simulation. My findings reveal that the stellar mass-halo mass (SMHM) relation implied

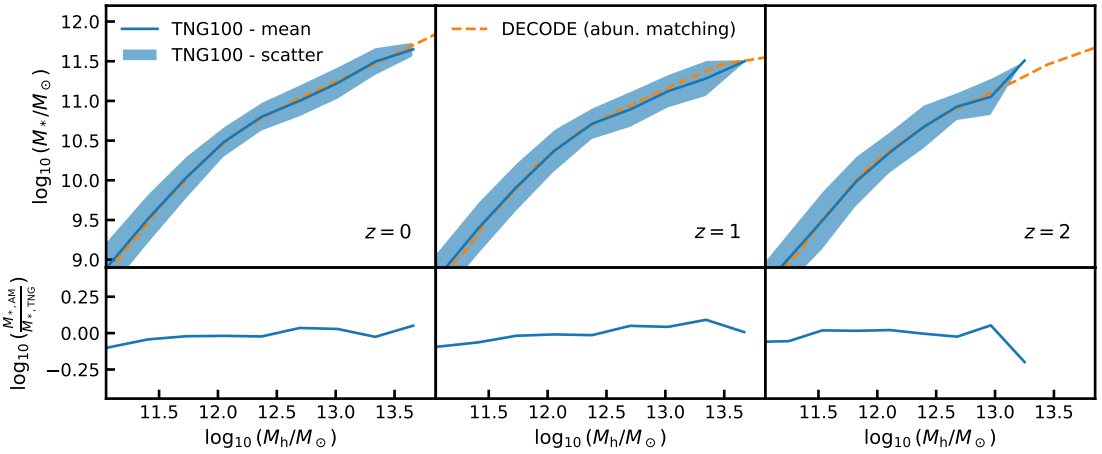

FIGURE 4.3: Upper panels: mean stellar mass-halo mass relation and its variance extracted from the TNG simulation (blue solid lines and shaded areas) at redshifts $z = 0$, 1 and 2, compared to those computed via DECODE's abundance matching taking the TNG's stellar mass function, halo mass function and scatter as input (orange dashed lines). Lower panels: residuals, computed as logarithmic difference, between the stellar mass-halo mass relations shown in the upper panels at the same redshifts.

by Equation (3.10) aligns well with the relation directly computed from the simulation itself at all redshifts, demonstrating the robustness of DECODE's abundance matching procedure in determining the right mapping between galaxy stellar mass and host dark matter halo mass. Figure 4.3 shows the comparison at redshifts $z = 0$, 1 and 2, where the upper panels show the SMHM relation from my abundance matching compared to that from the TNG simulation, and the lower panels show the logarithmic difference between the two of them, detecting a small residual of less than 0.1 dex at all redshifts.

4.3 Stellar mass growth

4.3.1 Satellite galaxies

Once confirmed the strength of the abundance matching prescription, I proceed in testing the self-consistency of DECODE in predicting galaxy stellar mass assemblies. As mentioned in Sections 1.1 and 3.2, central galaxies grow their total stellar mass via both mergers and star formation. The merger history of a central galaxy is directly sensitive to the stellar mass evolution of the merging satellites. Moreover, star formation histories (SFH) in DECODE are computed as difference between the total stellar mass evolution and merger histories, and therefore they are also indirectly highly dependent on the satellites evolution. Hence, it is crucial to have a good understanding and a robust recipe for the evolution of merging satellite galaxies, whose stellar mass increase or loss will lead to different merger and star formation rates in their central galaxies.

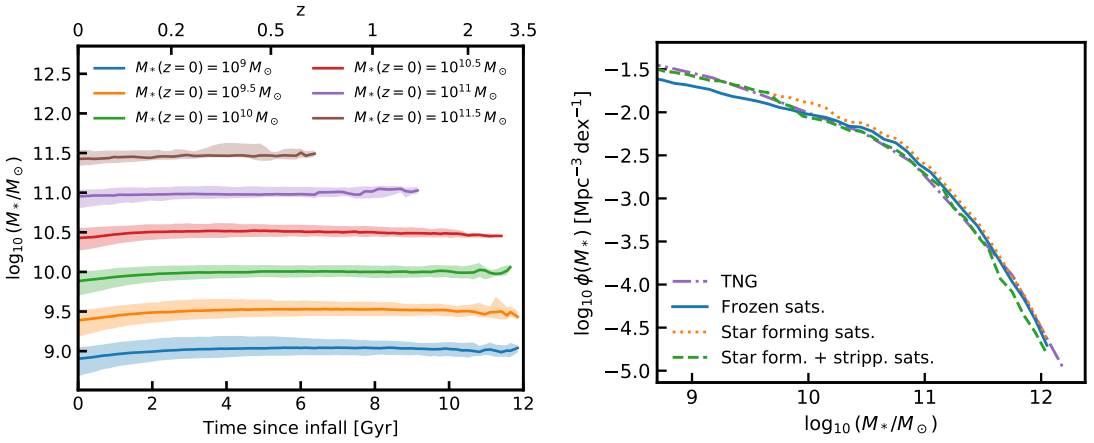

FIGURE 4.4: Left panel: mean stellar mass evolution of satellite galaxies in the TNG simulation as a function of the time elapsed from their infall, for satellite galaxies selected in different stellar mass bins at redshift $z = 0$ as labelled. The solid lines and dashed areas show the mean stellar mass evolution and their variance, respectively. Right panel: satellites stellar mass function at redshift $z = 0$ from the TNG simulation (purple dash-dotted line), compared to that predicted by DECODE using the simulation's stellar mass-halo mass relation as input for the frozen (blue solid line), star-forming (orange dotted line) and stripped satellites (green dashed line) scenarios.

To this purpose, I investigate the satellites' stellar mass evolution in the TNG simulation and test their abundances predicted from DECODE using TNG's inputs against the simulation.

The left panel of Figure 4.4 shows the stellar mass evolution of satellite galaxies from the TNG simulation. The curves show the mean stellar mass evolution of the TNG satellites as a function of their time from the epoch of infall, for satellite galaxies selected in different stellar mass bins at redshift $z = 0$. For satellite stellar masses above $M_\star \gtrsim 10^{10}\,M_\odot$, some galaxies have growing mass due to star formation, some others have decreasing mass due to ram-pressure stripping. However, regardless of the physical mechanism that dominates for each single galaxy, I find that in the TNG simulation most of the satellites have, on average, a roughly constant stellar mass assembly history since their epoch of infall. Therefore, over a large sample, the frozen satellites model statistically is a good approximation for the evolution of satellites in the TNG simulation. Only the very least massive satellites, with $M_\star \lesssim 10^{9.5}\,M_\odot$, continue mostly to form stars after infall before being then rapidly quenched (see, e.g., Shi et al. 2020), resulting in an average growth of their mass of roughly $0.1 - 0.2$ dex from infall after a few Gyr time.

The same findings come also from the test performed against the satellites SMF from the TNG simulation, shown in the right panel of Figure 4.4, which should be reproduced by DECODE at some level of accuracy by design when taking the TNG's SMHM relation as input. I find that, using a frozen satellites scenario, DECODE can relatively

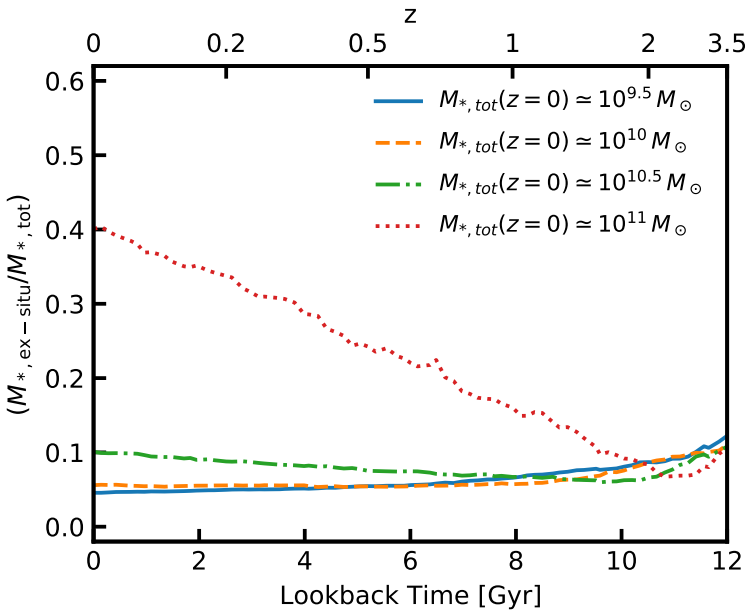

FIGURE 4.5: Mean fraction of *ex-situ* accreted stellar mass as a function of lookback time for galaxies in different stellar mass bins at $z = 0$, as labelled.

well reproduce the simulation's satellite abundances, except for the less massive satellites which continue to form some stellar mass via star formation after their time of infall. When including both stellar stripping and satellite star formation after infall, DECODE is able to reproduce the SMF of satellite galaxies with high accuracy across almost all stellar mass ranges considered in this thesis, further validating DECODE's methodology in successfully, flexibly, and self-consistently reproducing the outputs of a comprehensive galaxy evolution model like the TNG simulation, by only using its SMHM relation as input. It is interesting to note that the detailed evolutionary histories of satellites after infall, within the modelling explored in this thesis, have a relatively minor effect on the resulting satellite SMF at $z = 0$ of less than ~ 0.1 dex, which is comparable or even less than the statistical uncertainties in observational estimates (see, e.g., the SDSS satellites SMF shown in Sections 5.2 and 6.2).

4.3.2 Low- and intermediate-mass central galaxies

Having tested the performance of DECODE in accurately predicting the satellite abundances, I now proceed in checking the self-consistency of DECODE's SFHs for low- and intermediate-mass galaxies, namely those with present-day stellar mass $M_\star(z = 0) \lesssim 10^{11}\,M_\odot$. These galaxies grow primarily via star formation, while mergers becomes increasingly relevant in more massive galaxies with stellar mass $M_\star(z = 0) \gtrsim 10^{11}\,M_\odot$ (e.g., van Dokkum et al. 2010; Leitner 2012; Shankar et al. 2015; Buchan and Shankar 2016; Groenewald et al. 2017; Matharu et al. 2019; Fu et al. 2022; Eisert et al. 2023). Indeed, as shown in Figure 4.5, the fraction of stellar mass that central galaxies with

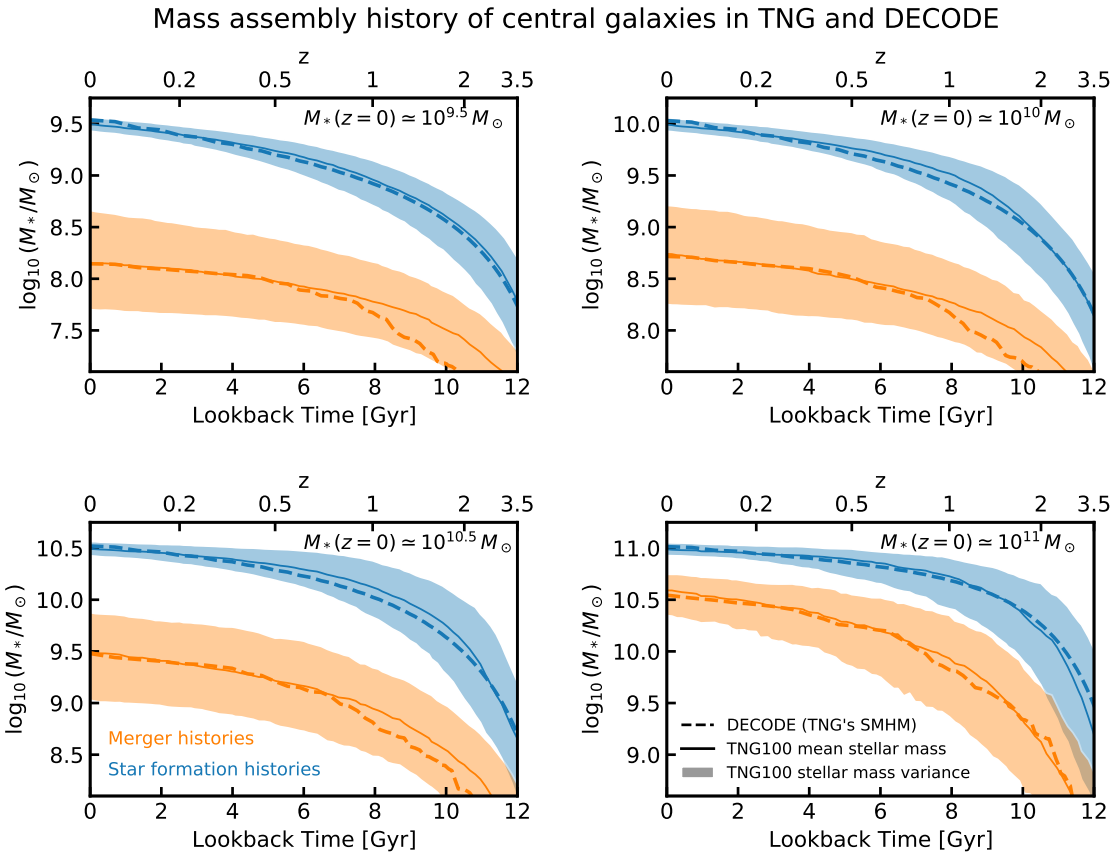

FIGURE 4.6: Stellar mass growths from *in-situ* star formation (blue lines) and *ex-situ* mergers (orange lines) as a function of lookback time for central galaxies of four different mass bins at $z = 0$ ($M_\star \simeq 10^{9.5}$, 10^{10}, $10^{10.5}$ and $10^{11}\,M_\odot$), as labelled. The solid lines and shaded areas show the mean stellar mass growths and variance from the TNG simulation, respectively. The dashed lines show the predictions from DECODE with the TNG's SMHM relation as input.

$M_\star(z=0) \lesssim 10^{10.5}\,M_\odot$ grow *ex-situ* is less than 10% at all redshifts, and reaches 40% at redshift $z = 0$ only for galaxies with $M_\star(z=0) \simeq 10^{11}\,M_\odot$.

In Figure 4.6 I show the mean stellar mass accreted from *in-situ* (blue lines) and *ex-situ* (orange lines) processes for different stellar mass bins ($M_\star \simeq 10^{9.5}$, 10^{10}, $10^{10.5}$ and $10^{11}\,M_\odot$) of central galaxies at redshift $z = 0$, as labelled. Since, the *ex-situ* fraction is small compared to the total stellar mass, as discussed previously, I only show the scenario with frozen satellites, after having checked that by adding star formation and stripping the results do not alter significantly. The SFHs and merger histories predicted from decode using TNG's SMHM relation as input are in good agreement with those extracted from the simulation itself. This test proves the validity of my methodology which I aim to extend to observationally driven SMHM relations in Section 6.3.

The small discrepancy in the merger histories at high redshifts, more evident for galaxies with low present-day stellar mass, may be due to a couple of reasons related to the

SMHM relation. Firstly, satellite galaxies might actually live on a flatter SMHM relation below the knee or higher in normalization, as found in several simulations (e.g., Schaye et al. 2015; Moster et al. 2018; Engler et al. 2021), mapping the subhaloes into more massive satellites. Secondly, such discrepancy may be also related to the lack of data for the SMHM relation. Indeed, the actual SMHM relation from the TNG simulation is retrieved down to $M_\star \sim 10^{7.5}\,M_\odot$ and up to snapshot 30, corresponding to redshift $z = 2.32$. Therefore, the merging satellites of the least massive galaxies are initialized at infall using an extrapolation below $M_\star \lesssim 10^{7.5}\,M_\odot$ and above redshift $z \gtrsim 2.3$ of the available SMHM relation, causing a tiny deviation in the merger histories.

4.3.3 Massive central galaxies

Furthermore, I test DECODE's prediction for the SFHs of massive galaxies, namely those with stellar mass above $M_\star(z = 0) \gtrsim 10^{11}\,M_\odot$. In these galaxies the contribution from mergers becomes more and more important, and it should be accounted carefully when predicting SFHs. Since the total mass assembly history of galaxies in my modelling is given by the SMHM relation and the assembly history of the dark matter haloes, mergers are the only key ingredient in determining the SFH of massive galaxies (as described in Section 3.2.4).

The upper panels of Figure 4.7 show the cumulative stellar mass accreted from mergers for two mass bins of central galaxy ($M_\star(z = 0) \simeq 10^{11.5}$ and $10^{12}\,M_\odot$), as labelled in the figure, computed via DECODE using TNG's SMHM relation as input and compared to the merger histories computed from the simulation directly. I find that DECODE is capable of reproducing fairly well (within ~ 0.1 dex) the merger histories of the TNG simulation when taking as input its SMHM relation and adopting a frozen model for the mass of satellites. In both stellar mass bins, the scenario where satellites lose their mass through stripping tends to slightly underestimate the TNG's merger histories. On the other hand, a model, in which satellites evolve either via star formation only or both star formation and stellar stripping, tends to somewhat overestimate the TNG's merger histories. At the level in which it is modelled in DECODE, the stellar stripping tends to have less impact than the star formation rate in shaping satellites after infall, and thus less influence on the merger histories.

The lower panels of Figure 4.7 show the SFHs for the same galaxy stellar mass bins. As expected, at given stellar mass bin, a satellite evolutionary model that produces a higher merger history predicts lower SFHs and vice versa. Similarly as for the merger histories, the frozen satellites model allows to reproduce the TNG's SFHs fairly in agreement. I note that, for the stellar mass bin of $M_\star(z = 0) = 10^{12}\,M_\odot$, overall DECODE is slightly less performant in reproducing TNG's star formation history for a

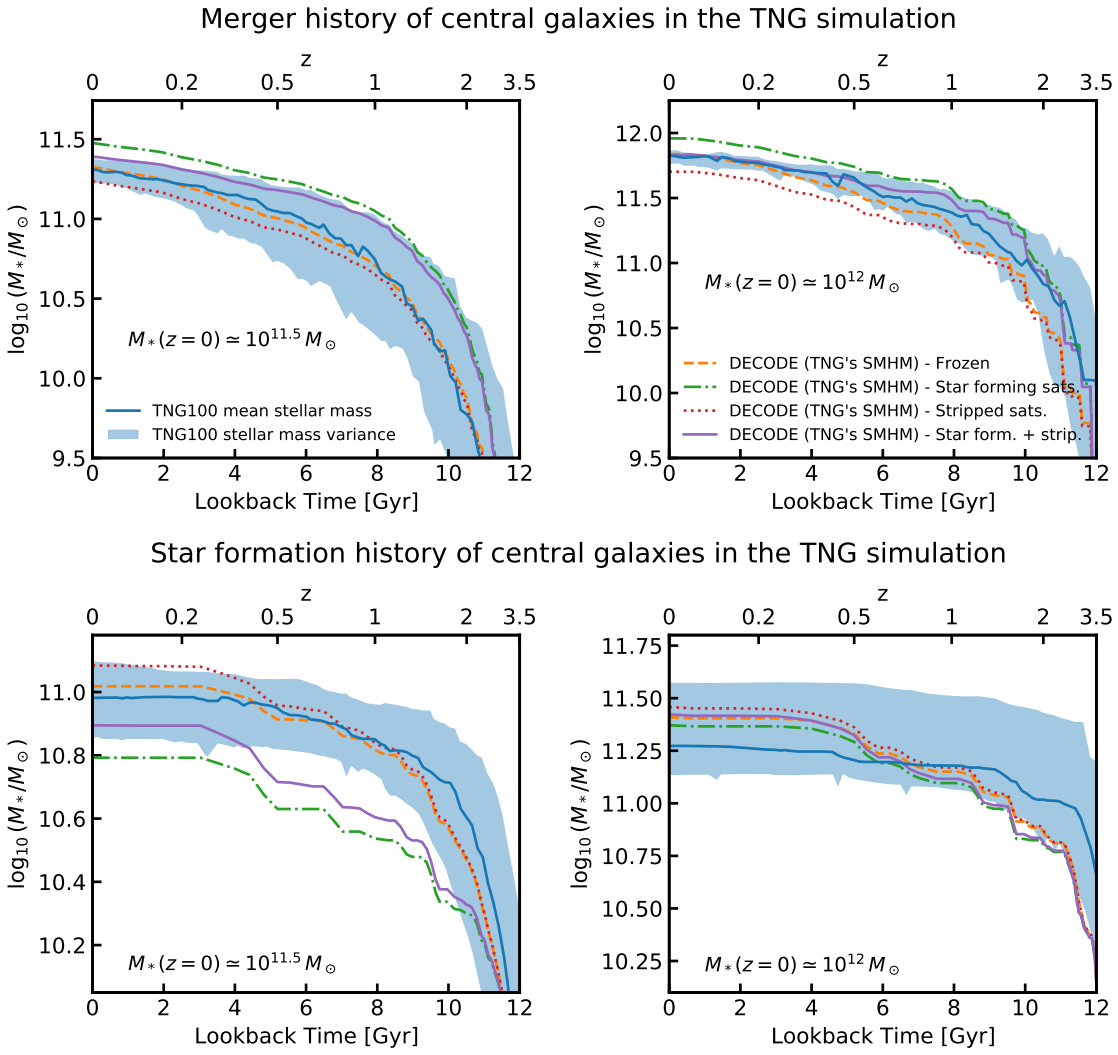

FIGURE 4.7: Upper panels: mean stellar mass accreted from *ex-situ* mergers for two stellar mass bins at $z = 0$ ($M_\star \simeq 10^{11.5}$ and $10^{12}\, M_\odot$). The blue solid lines and shaded areas show the mean and variance from the TNG simulation, respectively. The orange dashed, green dash-dotted, red dotted and purple solid lines show the results from DECODE with TNG's SMHM relation as input for the frozen, star-forming, stripped and star formation+stripping scenarios, respectively. Lower panels: same as upper panels, but for the mean stellar mass accreted via *in-situ* star formation.

couple of reasons. First of all, the limited number of clusters (< 10) in the TNG100 simulation could introduce some bias in the sample. More crucially, the bright end of the SMHM relation computed from the simulation could be affected by a non-negligible numerical uncertainty, with tiny variations in the slope causing large discrepancies in the mass assembly histories in DECODE. Such discrepancy in the most massive stellar mass bin may be improved by investigating the outputs from the TNG300 simulation's volume box.

Chapter 5

Satellite abundances, mergers and morphologies

Having tested the efficacy of DECODE in accurately and self-consistently reproducing the dark matter halo statistics of the Millennium simulation, as well as the mean galaxy assembly histories of the TNG simulation in terms of star formation, mergers, and satellite abundances, by using in input only its stellar mass-halo mass (SMHM) relation, I now turn to real data. In this Chapter, I investigate different SMHM relations as derived from abundance matching using the latest data on the stellar mass function (SMF) at low and high redshifts (Section 5.1). I will then discuss the implied merger rates and the number densities of unmerged satellite galaxies in the local Universe for different SMHM relations (Section 5.2). I will then show the implied fraction of elliptical and lenticular galaxies originating from major mergers (Section 5.3), and the distribution of bulge-to-total stellar mass ratios of galaxies in the local Universe induced by major mergers and some models of disc instabilities (Section 5.4). I will also present the prediction of the growth histories of brightest cluster galaxies (BCG) in Section 5.5.

5.1 Stellar mass functions and SMHM models

5.1.1 Input stellar mass functions

While the dark matter halo mass function (HMF) is well defined in N-body simulations by the cosmology (e.g., Press and Schechter 1974; Jenkins et al. 2001; Sheth et al. 2001; Tinker et al. 2008), determining observationally the galaxy SMF is not trivial due to systematic errors, and the SMHM relation is strongly sensitive to the shape and evolution of the latter (e.g., Wang and Jing 2010; Guo et al. 2011; Moster et al. 2010, 2013; Grylls et al. 2020a; Fu et al. 2022). Unfortunately, the SMF is still not fully well known with

sufficient accuracy, even in the local Universe. Bernardi et al. (2013, 2016, 2017), for example, showed that the SMFs in SDSS and CMASS at $z = 0.1$ and $z = 0.5$, respectively, are highly dependent on the light profile chosen to fit the photometry. When the same methodology is consistently applied to infer stellar masses, no apparent evolution is detected in the high mass end of the SMF up to at least $z = 0.5 - 0.8$ (see also Shankar et al. 2014a). Also Moustakas et al. (2013) and Leja et al. (2020) found that there is no evolution in the SMF in PRIMUS and 3D-HST up to redshift $z \simeq 1$. Kawinwanichakij et al. (2020) suggested that the SMF in the SHELA survey is constant even up to $z = 1.5$. Whilst poor or lack of evolution at all masses has been inferred in several works, others have found a more substantial evolution across cosmic time (e.g., Tomczak et al. 2014; Davidzon et al. 2017; Weaver et al. 2023).

In this thesis, I will explore the role of several toy models of galaxy SMF, guided by different observational data sets, in shaping galaxies. The reasons of using toy models, instead of observationally inferred SMFs, are the following. First of all, the use of toy model will allow to give a direct insight on the impact of each parameter of the SMF on the galaxy stellar mass growths, e.g., by tweaking manually the slope and/or normalization. Secondly, DECODE's method relies on direct abundance matching between the SMF and HMF at any given epoch. However, while for the HMF, accurate analytic fits extracted from N-body simulations are available at all redshifts, this is not the case for the SMF, for which analytic fits are provided only in some predefined redshift bins. In addition, some of the high redshift data of interest to this work lack or have a poor determination of the high-mass end of the SMF (e.g., Tomczak et al. 2014). Therefore, in the stellar mass or redshift ranges not covered by actual data, one would need to rely on extrapolations of the existing data. These are the main reasons why I need to define a full shape for the input SMF at all redshifts, avoiding an unsmooth redshift transition in the SMHM relation.

In what follows, I present four SMHM relations derived from abundance matching, as described in Section 3.2.3, with different toy model SMFs as input. The aim of this exercise is to estimate to what extent observationally informed systematic differences in the input SMHM relation impact the implied galaxy merger rates, star formation histories (SFH) and bulge fractions, a task particularly suited to address with DECODE. The four SMHM models considered for this analysis are summarized as follows:

- Model 1:
  - Bernardi et al. (2017) SMF, assumed to be constant up to $z \approx 1.5$.
  - Tinker et al. (2008) HMF.
  - 0.15 dex constant scatter in stellar mass at fixed halo mass.
- Model 2:

  - evolving SMF guided by Tomczak et al. (2014) at $z > 0$ and Bernardi et al. (2017) at $z = 0$.
  - Tinker et al. (2008) HMF.
  - 0.15 dex constant scatter in stellar mass at fixed halo mass.

- Model 3:
  - equivalent to Model 1 but assuming a linearly increasing scatter in stellar mass at fixed halo mass with redshift up to $z = 2$.

- Model 4:
  - equivalent to Model 2 but with the same z-dependent scatter in stellar mass at fixed halo mass as in Model 3.

The assumption of constant SMF up to $z = 1.5$ in Model 1 is of course extreme, but worth exploring as it is still unclear whether apparent evolution in the SMF at $z > 0$ may be, at least in part, driven by non-ideal/inconsistent estimates of galaxy stellar masses, as mentioned above. Similarly, also Model 2 is also somewhat extreme because, as detailed above, the SMF estimates at redshifts $z > 0$ may be affected by systematic measurement errors and/or incompleteness. Nevertheless, these two models should bracket the range of possible evolutionary patterns of the SMF, at least based on the presently available data and on the assumption of a constant IMF.

All the models listed above start from the same SMF at redshift $z = 0$. The latter is built joining the Bernardi et al. (2017) SMF, which is valid down to $M_\star \sim 10^9 M_\odot$, and the Baldry et al. (2012) SMF which extends down to $M_\star \sim 10^6 M_\odot$ (see also, e.g., Shankar et al. 2006; Kravtsov et al. 2018). In Models 1 and 3, as detailed above, I strictly assume no evolution in the SMF up to $z = 1.5$. Beyond this redshift it becomes unrealistic to assume no further evolution in the SMF and thus I extend the SMF at higher redshift with a toy model that smoothly decreases the normalization of the SMF from $z = 1.5$ using the following log-linear correction, which simultaneously allows to track the Tomczak et al. (2014) SMF data at $z > 1.5$ and to be consistent with the Bernardi et al. (2017) SMF up to $z = 1.5$

$$\log_{10}\phi(M_\star(z)) \simeq (0.99 + 0.13(z - 1.5)) \cdot \log_{10}\phi(M_\star(z = 0.1)) \,. \tag{5.1}$$

In Models 2 and 4 I instead assume the SMF to continuously evolve in normalization at $z > 0$ in a way to be broadly consistent with the Tomczak et al. (2014) SMFs at $0 < z < 3$. When applying the Tomczak et al. (2014) evolution to the SMF, I make use of the following correction to the Bernardi et al. (2017) + Baldry et al. (2012) SMF at $z = 0$

$$\log_{10}\phi(M_\star(z)) \simeq (0.99 + 0.13z) \cdot \log_{10}\phi(M_\star(z = 0.1)) \,. \tag{5.2}$$

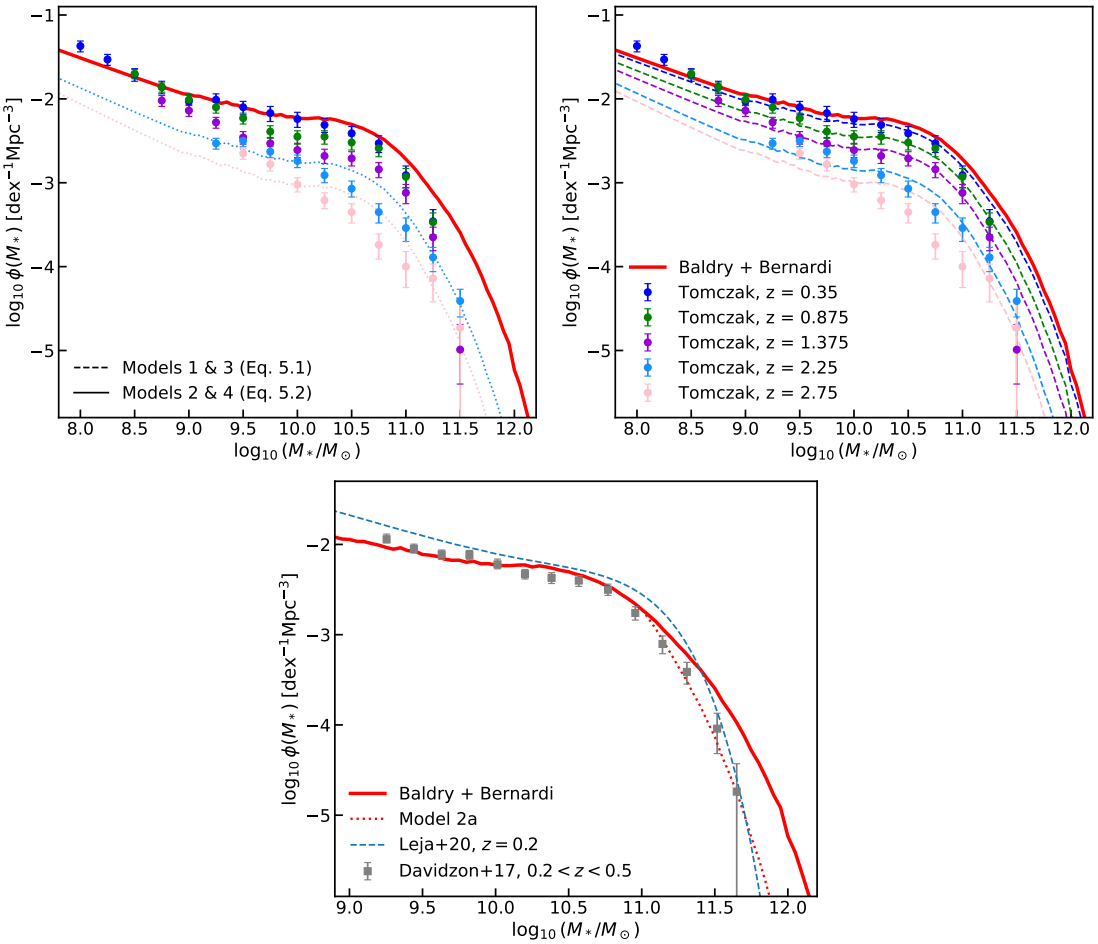

FIGURE 5.1: Stellar mass functions used for the abundance matching for the different toy models described in Section 5.1. In all the panels, the red solid lines represent the combination of the SMF from Baldry et al. (2012) and Bernardi et al. (2017) at $z = 0.1$. In the upper panels, the coloured dots with error bars represent the observational data from Tomczak et al. (2014). The dotted lines in the upper left panel and the dashed lines in the upper right panel shows the redshift-dependent normalization correction from Equations (5.1) and (5.2), respectively applied to the Baldry+Bernardi SMF to be broadly consistent with the Tomczak et al. (2014) data. Lower panel: SMF from Model 2a at $z = 0.1$ (red dotted line), Leja et al. (2020) at $z = 0.2$ (blue dashed line) and Davidzon et al. (2017) at $0.2 < z < 0.5$ (grey squared with error bars).

The scatter in the SMHM relation is an assumption in DECODE, used as input in Equation (3.10) for the abundance matching. Instead, for example, in simulations and some observations it can be directly computed from samples with information on the individual halo and galaxy mass distributions (e.g., Shankar et al. 2014b; Gu et al. 2016; Mitchell et al. 2016; Matthee et al. 2017; Allen et al. 2019; Erfanianfar et al. 2019; Golden-Marx et al. 2022; Shuntov et al. 2022). For Models 3 and 4, I use the following equation for the linearly increasing redshift-dependent scatter in stellar mass at fixed halo mass

$$\begin{cases} \sigma_{\log M_\star} = 0.15 + 0.1z \text{ dex} & \text{for } z < 2 \\ \sigma_{\log M_\star} = 0.25 \text{ dex} & \text{for } z \geq 2 \end{cases} . \tag{5.3}$$

The SMFs considered above are reported in Figure 5.1, where the upper panels show the toy model SMFs described above (coloured dotted and dashed lines), compared to the Bernardi et al. (2017) SDSS (red solid lines) and Tomczak et al. (2014) ZFOURGE/-CANDELS (coloured dots with error bars) SMFs, respectively. Furthermore, I also explore a variant of Model 2, which I refer to as Model 2a, with a SMF matching the SMF calibrated by Davidzon et al. (2017) at $z = 0$ characterised by less massive galaxies (red dotted line in the lower panel of Figure 5.1). I will discuss in the following Sections how the latter SMF will modify the implied SMHM relation and in turn the number of merging pairs and fraction of ellipticals.

Finally, concerning the HMF to use in the abundance matching routine given in Equation 3.10, I choose the Tinker et al. (2008) HMF, which provides the abundances of host parent haloes. I checked that switching to other forms of the HMF yields very similar results throughout. I recall that, as the SMFs at $z > 0$ contain both central and satellite galaxies (though the satellites become progressively negligible in number densities at high redshifts), I correct the Tinker et al. (2008) HMF via the analytic fit, described in Section 3.2.3.2, to account for the abundances of surviving satellites at any epoch of interest.

5.1.2 SMHM relations

The SMHM relations, derived from the abundance matching algorithm for each model, are shown in Figure 5.2 in the redshift range $0 < z < 3$. Models 1 and 3 are characterized by a high-mass slope $\mathrm{d}\log_{10}(M_\star/M_\odot)/\mathrm{d}\log_{10}(M_\mathrm{h}/M_\odot)$ (between $M_\mathrm{h} = 10^{13}M_\odot$ and $M_\mathrm{h} = 10^{14}M_\odot$) of 0.550, and a low-mass one (between $M_\mathrm{h} = 10^{11}M_\odot$ and $M_\mathrm{h} = 10^{11.5}M_\odot$) of 1.30, both with a normalization of 10.509 at $M_\mathrm{h} = 10^{12}M_\odot$, at $z = 1$. Models 2 and 4, instead, have a high-mass slope of 0.588 and 0.508, a low-mass slope of 1.15, and a normalization of 10.138 and 10.163, respectively. As shown in Figure 5.2, Model 2 at $z = 0$ is very close to both Moster et al. (2018) and Behroozi et al. (2019), at least at high stellar masses. The main difference between Model 2a and the others is the significantly flatter slope of 0.414 at the high-mass end. I will show in the following Sections that such apparently small differences in the shape of the SMHM relations, especially the differences in the slopes at the high-mass end of the SMHM relations, are sufficiently large to generate significant systematic differences in the major merger rates and implied elliptical fractions of up to a factor of $2 - 4$ in some stellar mass bins. I notice that by keeping the SMF constant in time (Models 1 and 3) induces a weak evolution at low masses and a more pronounced one at larger masses. On the other hand, the models characterized by an evolving SMF (Models 2 and 4), generate a SMHM relation with evident redshift evolution at low stellar masses and a weak one at higher stellar masses (see also Shankar et al. 2006, Moster et al. 2018 and Grylls et al. 2020a).

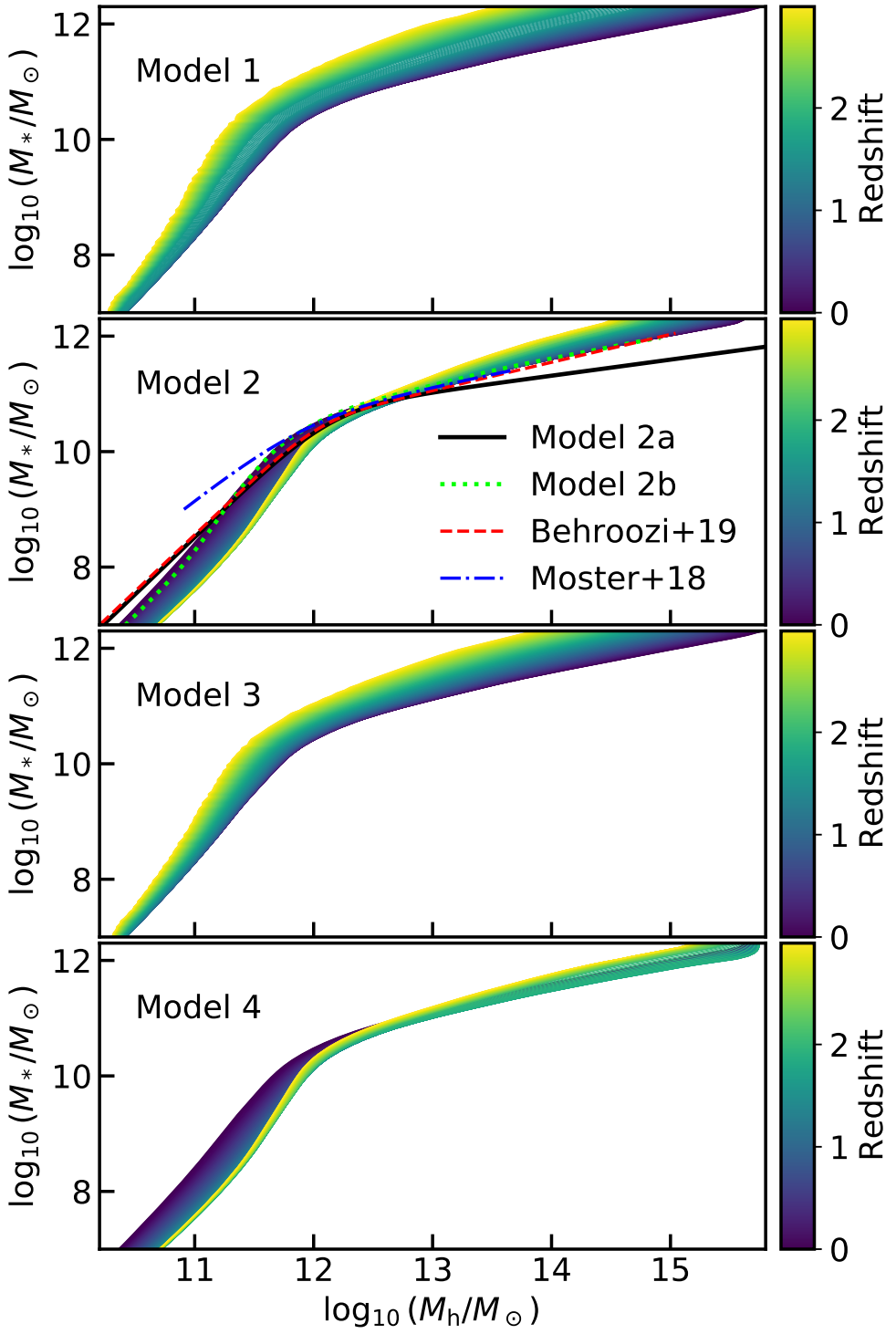

FIGURE 5.2: Stellar mass-halo mass relations computed via abundance matching. The four panels show the relations for the four models described in Section 5.1, respectively, for the range of redshift denoted by the colour code. In the second panel I show also Models 2a and 2b, along with two SMHM relations from other works in the literature (Moster et al. 2018; Behroozi et al. 2019) for comparison (black solid, green dotted, red dashed and blue dash-dotted lines, respectively).

Finally, I also investigated the possibility of a mass-dependent scatter in stellar mass at fixed halo mass as input in the abundance matching. To this purpose, I assume a halo mass-dependent scatter, similarly to what suggested by other semi-empirical models (e.g., Moster et al. 2018; Behroozi et al. 2019), constant at $M_{\rm h} > 10^{12} M_{\odot}$ and increasing linearly with $\log_{10}(M_{\rm h}/M_{\odot})$ below that mass

$$\begin{cases} \sigma_{\log M_\star} = 2.95 - 0.23 \log_{10}(M_{\rm h}/M_{\odot}) \text{ dex} & \text{for } M_{\rm h} < 10^{12} M_{\odot} \\ \sigma_{\log M_\star} = 0.15 \text{ dex} & \text{for } M_{\rm h} \geq 10^{12} M_{\odot} \,. \end{cases} \tag{5.4}$$

The SMHM relation at $z = 0$ implied by the scatter in Equation (5.4) is shown in the second panel of Figure 5.2, labelled as Model 2b. The comparison shows that Model 2b is fully equivalent to Model 2 at high masses and slightly steeper at low masses, and these differences I checked are similar at all redshifts. I have tested that, since Model 2b is equivalent to Model 2 in the mass range where major mergers are significant, i.e., $M_\star \gtrsim 10^{11}\, M_{\odot}$, the predicted amount of major mergers remains unchanged and, hence, also all the other quantities analyzed in this Chapter. Therefore, I do not show the results for Model 2b any further, and concentrate on the two models with redshift-dependent scatter (Models 3 and 4), which alters also the high-mass end of the SMHM relation and consequently the major merger rates.

5.2 Satellite galaxies and merger rates

5.2.1 Satellite abundances

Having defined the mapping between galaxy stellar mass and host dark matter halo mass, I can now start to predict galaxy observables that can be used to validate DECODE and the input SMHM relation. As a very first step, I compute the number density of surviving satellite galaxies in the local Universe and compare it with SDSS data (described in Section 3.4.4). Satellites can be effectively considered as the other side of the same coin with respect to mergers. In fact, surviving satellites in a hierarchical dark matter-dominated Universe, can be interpreted as "failed mergers", i.e., all those infalling satellite galaxies that have not had the time to merge yet with their central galaxies at the time of observation. Therefore satellites, just like mergers, represent a pivotal test of hierarchical models and of the input SMHM relation. I highlight again that, although the total SMF is an input in DECODE, the satellite SMF is an actual prediction of the model, as it depends both on the satellite evolution after infall and on the rate of galaxy mergers, which in turn depend on the high-z SMHM relation and on the dynamical friction timescales.

Figure 5.3 shows the results of the SMF for all galaxies (centrals + satellites) and only satellites (red and blue lines, respectively). The different types of line distinguish the

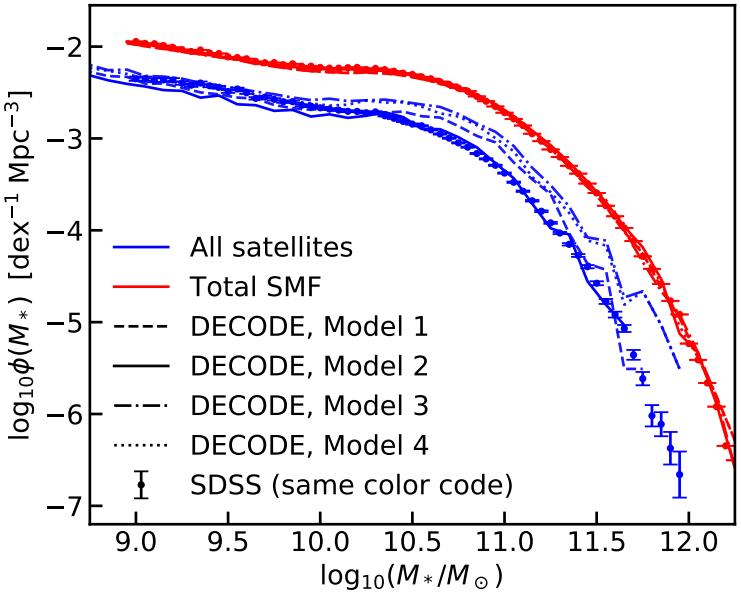

FIGURE 5.3: Total and satellite galaxies stellar mass function predicted by DECODE compared to that inferred by SDSS at $z = 0.1$. The solid, dashed, dash-dotted and dotted lines show the prediction for Model 1, 2, 3 and 4, described in Section 5.1.2, respectively. The dots and error bars represent the data from SDSS.

four SMHM models described in Section 5.1, and the blue and red dots with error bars are, respectively, the satellite and total galaxy SMF as measured in SDSS using, for consistency with the stellar mass calibration of my models, the data from Bernardi et al. (2017). The centrals and satellites classification is taken from Yang et al. (2007), as described in Section 3.4.4. As one can see from the red lines, the total SMF is well reproduced by DECODE regardless of the input SMF model, as expected by construction via the abundance matching relation given in Equation (3.10).

For all SMHM models reported in Figure 5.2, I assume a "frozen" scenario in which satellite galaxies are assumed to retain the same stellar mass after infall with no further growth via star formation or loss via, e.g., stellar stripping. I will further investigate the role of the satellites post-infall evolution in Section 6.2, while here I focus my attention of the role of the SMHM relation on the satellites SMF. Grylls et al. (2019) showed that the frozen model was able to reproduce the bulk of the observed satellite population in their semi-empirical model STEEL. I do find a similar result with DECODE in Figure 5.3, despite using a significantly more accurate distributions of satellites of first- and second-order and dynamical friction timescales. I anticipate here that including standard recipes for stellar stripping as given by, e.g., Smith et al. (2016), and for star formation after infall following the analytic recipes by Grylls et al. (2020a) (and references therein), I obtain very similar results to those shown in Figure 5.3. Figure 5.3 shows that only Model 2, the one characterized by an evolving SMF and constant scatter, better lines up with the observational data of satellites, especially at stellar masses

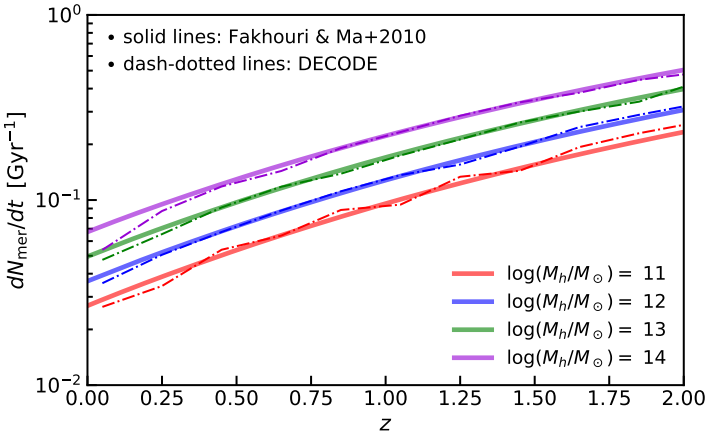

FIGURE 5.4: Dark matter halo merger rates as a function of redshift predicted by DECODE (coloured dash-dotted lines), compared to the results from Fakhouri et al. (2010) (coloured sold lines), for different parent halo mass bins at $z = 0$, as labelled.

$M_\star \gtrsim 3 \cdot 10^{10} M_\odot$. I will see below that Model 2 also performs better against other observational constraints.

5.2.2 Merger rates of central galaxies

I now proceed to study the other side of the coin, i.e., mergers. The input SMHM relation has a direct impact on the merger rate of each galaxy that DECODE produces (see also, e.g., Stewart et al. 2009a; Hopkins et al. 2010a; O'Leary et al. 2021; Grylls et al. 2020b), which in turn influences the implied satellite abundances, fraction of ellipticals, and B/T ratios. In this Section, I focus on both halo and galaxy merger rates, and other predictions will be discussed in the following Sections.

First of all, I check in Figure 5.4 that DECODE's halo-halo merger rates, $\mathrm{d}N_{\rm mer}/\mathrm{d}t$, are consistent with the halo-halo merger rates derived by Fakhouri et al. (2010) from the Millennium simulation at $z \gtrsim 0.35$. Note that DECODE's merger rates drop slightly faster than those of Fakhouri et al. (2010) at $z < 0.35$, as also previously found by Grylls et al. (2020a), which I checked is mostly induced by my adopted halo mass mean accretion histories from van den Bosch et al. (2014) which are somewhat steeper than those presented in Fakhouri et al. (2010) at these redshifts.

Figure 5.5 shows the cumulative number of total and major halo-halo mergers, with mass ratio $M_{\rm h,sub}/M_{\rm h,par} > 0.25$, from DECODE (left and right panels, respectively) below $z < 4$ predicted from DECODE, expected in a hierarchical ΛCDM Universe, as a function of the present-day parent halo mass. I found that the number of mergers, with both first- and second-order subhaloes, is roughly constant with parent halo mass (see also Shankar et al. 2014a). However, such an invariance in halo mass is broken when mapping dark matter halo mergers into galaxy mergers via the double power-law shaped SMHM relation.

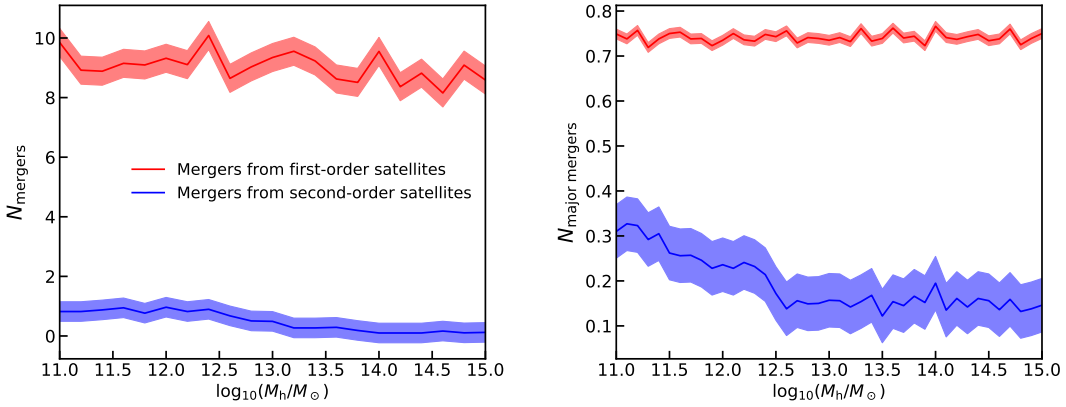

FIGURE 5.5: Left panel: number of dark matter halo mergers from the contribution of first- and second-order subhaloes as function of the final parent halo mass at redshift $z = 0$. The solid lines represent the mean value, while the shaded areas show the 1σ uncertainty. Right panel: same as left panel, but for major mergers, for which I assume a subhalo-to-parent halo mass ratio $M_{\rm h,sub}/M_{\rm h,par} > 0.25$.

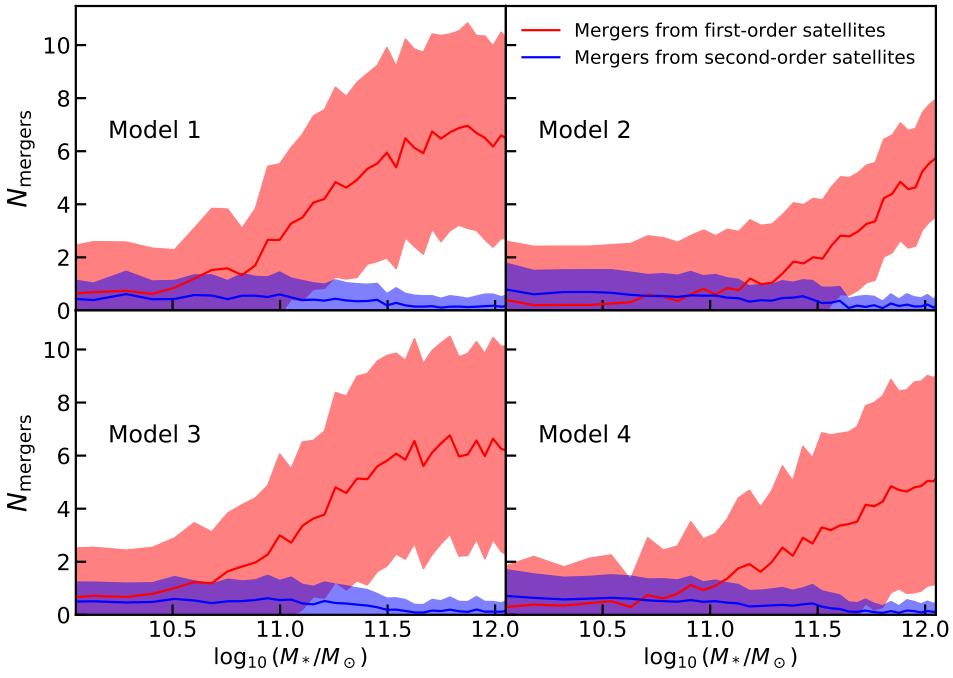

FIGURE 5.6: Number of galaxy major mergers from first- and second-order satellites, with stellar mass ratio $M_{\star,\rm sat}/M_{\star,\rm cen} > 0.25$, as a function of the central galaxy stellar mass at redshift $z = 0$. The solid lines represent the mean value, while the shaded areas show the 1σ uncertainty. Results are shown for the four different models described in Section 5.1, as labelled.

Figure 5.6 shows the average number of galaxy major mergers, along with its 1σ uncertainty, as a function of the (final) present-day central galaxy stellar mass. The red lines represent the contribution of mergers from first-order satellites and the blue lines the contribution of mergers from second-order. The plot clearly shows that, for all the four SMHM models, the contribution from the second-order satellites is in good approximation relatively negligible, at least for massive central galaxies. On the other hand, the number of mergers from the first-order satellites increases significantly when the central galaxy stellar mass increases.

The sharp increase of the number of major mergers with galaxy stellar mass and the fact that major mergers for massive galaxies outnumbers the major mergers of the parent haloes can be both explained from the shape of the SMHM relation. Indeed, while the total number of mergers is roughly the same for the dark matter halo and the hosted galaxy (and it is independent of the halo or stellar mass), the classification as major or minor merger depends on the mass ratio between halo or stellar mass ($M_{h,1}/M_{h,2} > 0.25$ is the major merger threshold for halo mergers and $M_{\star,1}/M_{\star,2} > 0.25$ for galaxy mergers). Since the SMHM relation sets $M_h \propto M_\star^\alpha$, the halo mass ratio is related to the stellar mass ratio as $M_{h,1}/M_{h,2} = (M_{\star,1}/M_{\star,2})^\alpha$. If the SMHM relation was linear (α=1) the halo mass ratio would be equal to the stellar mass ratio and, consequently, a halo major merger would correspond to a galaxy major merger. On the other hand, a steep power law relation with $\alpha > 1$ would decrease the stellar mass ratio with respect to the halo mass ratio, while a flat power law with $\alpha < 1$ would increase it. As a consequence, the number of galaxy major mergers is reduced for a steep power law, while it is enhanced for a flat one. In other words, it is less (more) likely to find similar mass galaxies for similar mass haloes for a steep (flat) SMHM relation.

Since the SMHM relation in all the four considered models is a broken power law with a steep faint end and a flat bright end, the number of galaxy major mergers tends to naturally increase toward higher stellar masses. However, the level of increase is different for the four models since even small variations in the SMHM relation produce strong effects in the merger rates. For example, Model 2 with a high-mass slope of 0.558 predicts less than half of the mergers at $M_\star \sim 1 - 3 \cdot 10^{11} M_\odot$ compared to Model 1 and Model 3 with a high-mass slope of 0.550. On the other hand, Model 4, despite having the lowest high-mass end slope at $z = 0$, produces slightly more mergers than Model 2 but less than Model 1 and Model 3, a trend that can be explained by the lower slope in the SMHM relation at higher redshifts in Model 4 than in Model 2, being for example 0.498 and 0.551 the average slope up to $z = 1.5$, respectively. For more massive galaxies, Models 1 and 3 predict on average a higher number of major mergers compared to Models 2 and 4. This effect is also directly reflected in the fraction of ellipticals and B/T ratios, as I will show in the following Sections. I also note that, although the normalization of the SMHM relation does not directly impact the number of major mergers, it has an important role in determining the total cumulative merger history (in terms of

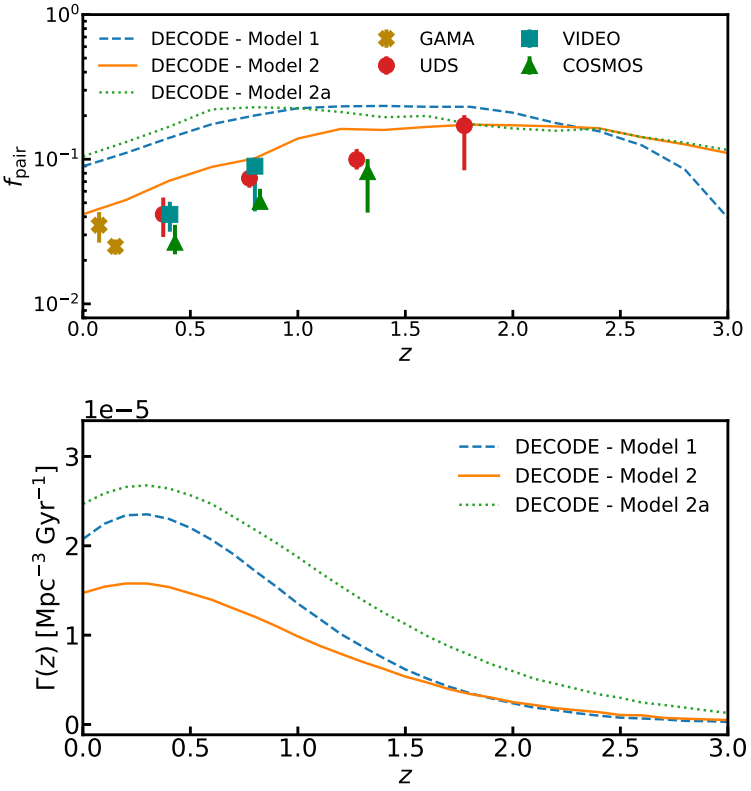

FIGURE 5.7: Upper panel: major merger pair fraction, with mass ratio $M_{\star,\rm sat}/M_{\star,\rm cen} \gtrsim 0.25$, for galaxies with stellar mass $M_\star \gtrsim 10^{11} M_\odot$ at $z = 0$ as predicted by DECODE for Models 1, 2 and 2a (blue dashed, orange solid and green dotted lines, respectively). The points with error bars show the observational data of UDS, VIDEO, COSMOS and GAMA surveys, as presented in Mundy et al. (2017). Lower panel: major merger rates as a function of redshift, as predicted by DECODE's Models 1, 2 and 2a.

cumulative stellar mass growth), which in turns will impact the star formation history. Furthermore, the amount of scatter in the SMHM relation instead seems to play a relatively less significant role in controlling the fraction of major mergers when assuming a constant SMF.

Furthermore, I show in the upper panel of Figure 5.7 the major merger pair fractions as predicted by DECODE for Models 1, 2 and 2a. I compare my results with the data from UKIDSS UDS, VIDEO / CFHT-LS, UltraVISTA / COSMOS and GAMA surveys, presented in Mundy et al. (2017). The pair fraction in DECODE is calculated as the number of infalling satellites with stellar mass ratio above 1/4 living within 5 and 30 kpc from the centre of the central galaxy. I assume that the distance of the satellite galaxies scales proportionally to its dynamical friction timescale (Guo et al. 2011). I make use of the projected two-dimensional distances computed following the recipe in Mundy et al. (2017) and Simons et al. (2019), assigning stochastically a polar angle in spherical coordinates and projecting the three-dimensional distances onto the z axis. Analogously to what inferred for the number of major mergers, Model 1 tends to produce more pair fractions with $M_{\star,\rm sat}/M_{\star,\rm cen} > 0.25$ than Model 2. The available data on pairs is still

sparse, and still subject to systematics in the determination of the stellar masses, but overall Model 2 tends to be more aligned with the data, at least at $z \geq 0.5$. On the other hand, Models 1 and 2a, characterized by a flatter slope in the SMHM relation at the high-mass end, predict a higher pair fraction with respect to the data and to Model 2. This prediction is in line with the fact that a flatter SMHM relation produces a higher number of major mergers, as discussed above.

Finally, in the lower panel of Figure 5.7 I show a prediction of the major merger rates from DECODE's Models 1, 2 and 2a. As one can see, the flatter the SMHM relation (Models 1 and 2a) the higher the rate of implied major mergers, in line with what shown in the upper panel. On the other hand, Model 2, characterized by a steeper SMHM high-mass end, predicts a much lower major merger rate, at least at lower redshifts. I do not show the comparison with observational data or any other model because the merging timescales that I use (McCavana et al. 2012) are different to those adopted in other theoretical and observational works and the comparison would not be fair.

5.3 Morphology of central galaxies

In this Section, I apply DECODE to study another key aspect of galaxy evolution: the role of mergers in shaping galaxies, and in particular in generating elliptical and lenticular type galaxies. Many works have in fact suggested a close link between the number of major mergers and the number of ellipticals (e.g., Bournaud et al. 2007; Hopkins et al. 2009a, 2010b; Shankar et al. 2013a; Fontanot et al. 2015). Major mergers (for which I assume $M_{\star,\rm sat}/M_{\star,\rm cen} \gtrsim 0.25$) may be capable of destroying pre-existing galactic disks and form stellar spheroids, as suggested by hydrodynamical simulations and analytic models (see, e.g., Baugh 2006; Malbon et al. 2007; Bower et al. 2010; Tacchella et al. 2019; Lagos et al. 2022). However, as discussed by Grylls et al. (2020a) and above, as the number of major mergers is strongly dependent on the shape of the input SMHM relation, we expect the fraction of ellipticals to be similarly impacted by the choice of SMHM relation when built via major mergers. I will investigate this possibility in this Section.

For each SMHM model, I follow the merger history of galaxies in the mock from redshift $z = 4$, and I label each galaxy that has undergone a major merger as an "elliptical", and then compute the fraction of ellipticals at different redshifts. I show the results in Figure 5.8. Panels A, B and C show the fraction of ellipticals predicted by DECODE using the four models of SMHM relation described in Section 5.1 for redshifts $z = 0.1$, 1 and 2 respectively, along with the predictions from the TNG simulation and from the semi-analytic model GALICS, as well as with the SDSS data (see Section 3.4.4), only shown in the panels at $z = 0.1$. I note that, as described in Section 3.4, in GalICS and TNG elliptical galaxies are defined in a somewhat different way than a simple cut in

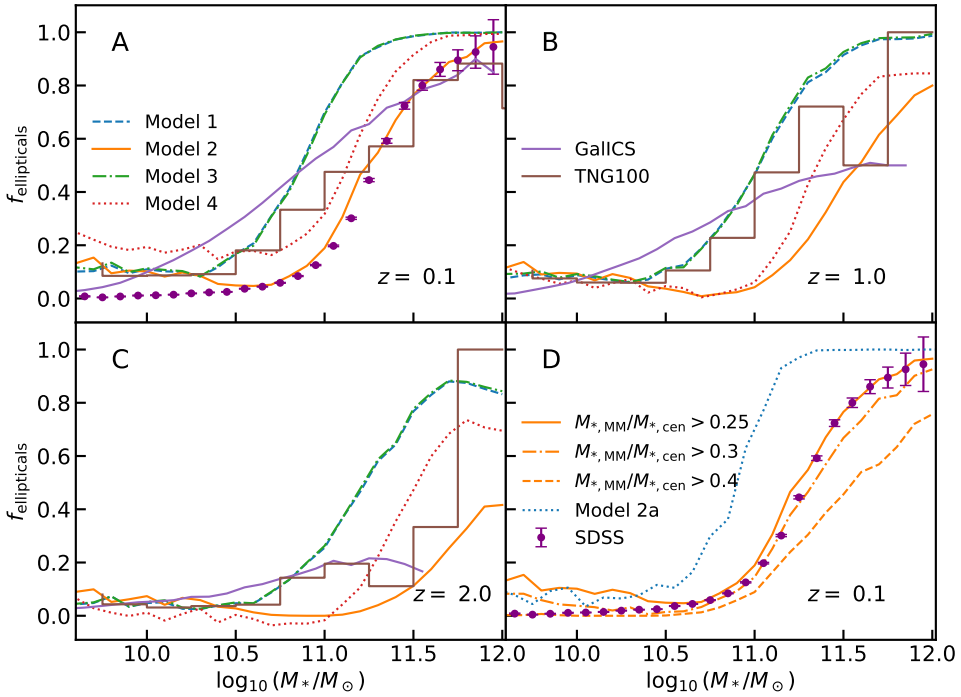

FIGURE 5.8: Fraction of elliptical galaxies as a function of the galaxy stellar mass at different redshifts, as predicted by DECODE. Panels A, B and C show the predictions for the four models described in Section 5.1 at redshifts $z = 0.1$, 1 and 2, respectively. Panel D shows the predictions for Model 2 at redshift $z = 0.1$, along with the impact of assuming different mass ratio for the major mergers (denoted as MM in the legend), as well as the prediction for Model 2a. The data from the SDSS Survey, GALICS semi-analytic model and the TNG100 hydrodynamical simulation are included, as labelled, for comparison.

mergers mass ratio like in DECODE, but it is worth to include their predictions in Figure 5.8 for sake of comparison.

It is immediately clear from Figure 5.8 that Model 2 is the only one among our four chosen models that can faithfully reproduce the SDSS data at $z = 0.1$, on the assumption that ellipticals are strictly formed from major mergers above a mass ratio of $M_{\star,\mathrm{sat}}/M_{\star,\mathrm{cen}} > 0.25$, the standard limit adopted in state-of-the-art semi-analytic models (e.g., Guo et al. 2011; Fontanot et al. 2015; Lacey et al. 2016). Model 4, which only differs from Model 2 on the assumed scatter around the SMHM relation, is moderately close, but still higher than the data for the same cut in merger ratio $M_{\star,\mathrm{sat}}/M_{\star,\mathrm{cen}} > 0.25$, further proving that even a modest variation in the scatter of the SMHM relation can significantly impact galactic outputs. In particular, an increase of the scatter at fixed slope at high stellar masses tends to increase the number of major mergers. On the other hand, Models 1 and 3 produce a significantly higher fraction of ellipticals. The main reason why models including evolution in the SMF predict less elliptical galaxies

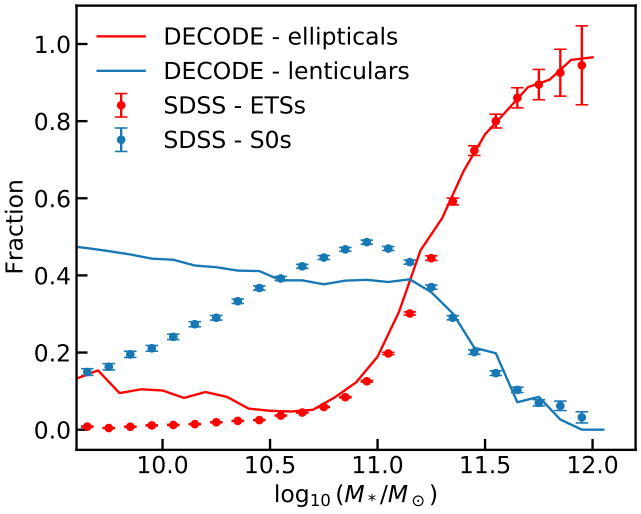

FIGURE 5.9: Fraction of lenticular and elliptical galaxies as a function of stellar mass at redshift $z = 0.1$, as predicted by DECODE for Model 2 compared with the data from the SDSS Survey, as labelled.

than models with constant SMF is a direct consequence of the number of mergers that they predict, as discussed in Section 5.2.2.

Figure 5.8 also shows that the TNG simulation provides a decent match to the SDSS at $z = 0.1$, especially at galaxy stellar masses $M_\star > 2 \cdot 10^{11}\, M_\odot$, although we should caution that some internal self-inconsistencies naturally arise when comparing with the TNG outputs with these data as the TNG simulation does not exactly reproduce the same SMF of Bernardi et al. (2017) at the bright end (see, e.g., Pillepich et al. 2018a), on which the elliptical fractions are based, and thus has a SMHM relation that slightly differs from the one in Model 2. The semi-analytic model GALICS[1] also well matches the SDSS elliptical fractions at high stellar masses, but it overproduces them at lower stellar masses. Lastly, I show in panel D of Figure 5.8 the fraction of ellipticals predicted by Model 2a. This model, characterized by a flatter high-mass end slope, produces a much larger number of mergers, as expected from the discussion in Section 5.2.2, and thus it increases the implied fraction of ellipticals at all stellar masses.

In summary, the question whether major mergers are the triggers for the formation of local ellipticals, is strongly dependent on the input SMHM relation in my semi-empirical framework, and, at fixed SMHM relation, on the exact mass threshold chosen for being classified as a major merger, as shown in panel D.

Finally, I show for completeness the fraction of lenticular type galaxies as a function of stellar mass at $z = 0.1$ in Figure 5.9 predicted from DECODE for Model 2, compared with the observational data from SDSS. Several works have suggested that lenticular

[1] I remind the reader that elliptical galaxies in GALICS are identified as those galaxies with $B/T > 0.7$.

galaxies might be created by mergers as well (e.g., Christlein and Zabludoff 2004; Laurikainen et al. 2005; Blanton and Moustakas 2009). Here, I label the lenticulars as the galaxies that have had at least one merger with mass ratio $0.05 < M_{\star,\rm sat}/M_{\star,\rm cen} < 0.25$, whilst above $M_{\star,\rm sat}/M_{\star,\rm cen} = 0.25$ they would end up as ellipticals. This simple merger recipe is capable of reproducing the data for stellar masses $M_\star \gtrsim 10^{11}\,M_\odot$, but it fails at lower stellar masses, suggesting that additional processes may be at work in forming less massive lenticulars, such as disc instabilities and/or disc regrowth.

5.4 Bulge-to-total ratios

In the previous Sections, I showed that the shape of the SMHM relation drives the number and thus the rate of mergers that galaxies undergo across cosmic time at fixed dynamical friction timescale. Only specific SMHM relations, such as the one defined in Model 2, which is characterized by a larger number density of massive galaxies and a significant evolution in normalization at $z > 0.5 - 1$, are able to simultaneously reproduce the number of local satellites and the number of local ellipticals, on the assumptions that the latter are formed out of mergers between galaxies with a mass ratio $M_{\star,1}/M_{\star,2} > 0.25$. I now move a step forward in my modelling and show how well Models 1 and 2 reproduce the observed B/T ratios of local galaxies, as measured in MaNGA (described in Section 3.4).

To perform a meaningful and instructive comparison between models and data, I make use of two simple but theoretically well-motivated toy models for the formation of bulges in hierarchical models:

- In Model BT1, I assume that when a major merger occurs, with $M_{\star,1}/M_{\star,2} > 0.25$, the descendant galaxy is strictly an elliptical with $B/T = 1$. This is a common assumption made in semi-analytic models of galaxy evolution (e.g., Cole et al. 2000; Hatton et al. 2003; Bower et al. 2006; De Lucia and Blaizot 2007; Guo et al. 2011; Croton et al. 2016; Lacey et al. 2016; Cattaneo et al. 2017). I then assume that in minor mergers the mass of the satellite can be accreted either onto the bulge or onto the disc component.

- In Model BT2, I instead assume that the remnant galaxy has a surviving disc with $B/T = 0.5$. In other words, I assume that the disc is not entirely disrupted in a major merger, irrespective of the gas fraction in the progenitor galaxies, but in fact a significant fraction of it survives and/or is rapidly reaccreted (e.g., Hopkins et al. 2009b; Puech et al. 2012). I then explore the impact on the final B/T of assuming the satellite mass in minor mergers to be added systematically to the disc or to the bulge component. Note that, in what follows, I consider the B/T at fixed galactic stellar mass averaged over *all* central galaxies that enter that bin in stellar mass.

Another popular route to form stellar bulges in galaxies is via disc instabilities, which are usually implemented in semi-analytic models in broadly two ways. A first type envisions that when the circular velocity of the disc becomes larger than a given reference circular velocity, then the disc is considered unstable and a mass is transferred from the disc to the bulge. The amount of mass transferred from the disc to the bulge varies significantly from model to model (e.g., Cole et al. 2000; Bower et al. 2006; Monaco et al. 2007; Guo et al. 2011; Lacey et al. 2016; Henriques et al. 2020; Izquierdo-Villalba et al. 2019). The disc instabilities of the second type are triggered by high redshift cold flows of gas, which favour the formation of (possibly) long-lived gas clumps that migrate towards the centre via dynamical friction in the gaseous disc (e.g., Dekel and Birnboim 2006; Dekel et al. 2009; Bournaud et al. 2011; Di Matteo et al. 2012; Oklopčić et al. 2017; Dekel et al. 2019). I include an example of the second type of disc instabilities in DECODE to generate stellar bulges, for which I adopt the parameterization of the baryonic inflow rate from Bournaud et al. (2011)

$$\dot{M}_{\rm b} = 25 \frac{M_{\rm disc}}{10^{11} M_{\odot}} \left(\frac{1+z}{3} \right)^{3/2} M_{\odot}/{\rm yr} \, , \tag{5.5}$$

with $M_{\rm disc}$ being the mass of the disc at redshift z. Equation (5.5) assumes that most of the mass inflow rate, which is in gaseous form, will form clumps that via dynamical friction will end up forming a stellar bulge at the galaxy centre. I apply this recipe only to galaxies which have a gas fraction $f_{\rm gas} \geq 0.5$ which are more likely to have undergone disc instabilities, since large amount of gas and mass densities inevitably lead to disc fragmentation (Lang et al. 2014). Following other semi-empirical models (e.g., Hopkins et al. 2009b; Shankar et al. 2014a), I assign gas fractions to any galaxy in the mock via the empirical mean relations derived by Stewart et al. (2009b) from a number of galaxy samples out to $z \sim 3$.

I find that Equation (5.5) does not generate enough large stellar bulges at $z = 0$, as expected by simple direct integration of Equation (5.5). Such growth of stellar bulges via clumpy accretion can be further increased by lowering the $f_{\rm gas}$ threshold, though it tends to still be moderate, reaching a value of up to $B/T \sim 0.2$ at low stellar masses, $M_{\star} \lesssim 3 \cdot 10^5 M_{\odot}$. Therefore, some slightly stronger disc instabilities need to be implemented to better match local data. To this purpose, I also consider the recipe from Efstathiou et al. (1982) building on the analytic modelling of many previous works (e.g., Cole et al. 2000; Monaco et al. 2007)

$$\epsilon \sqrt{G M_{\rm disc} / R_{\rm disc}} > V_{\rm ref} \, , \tag{5.6}$$

where $M_{\rm disc}$ is the mass of the disc, $R_{\rm disc}$ is the half mass radius calculated via the redshift-dependent analytic fit by Shen et al. (2003), $V_{\rm ref}$ is the reference velocity calculated assuming an exponential profile (see, e.g., Tonini et al. 2006), and ϵ is a factor

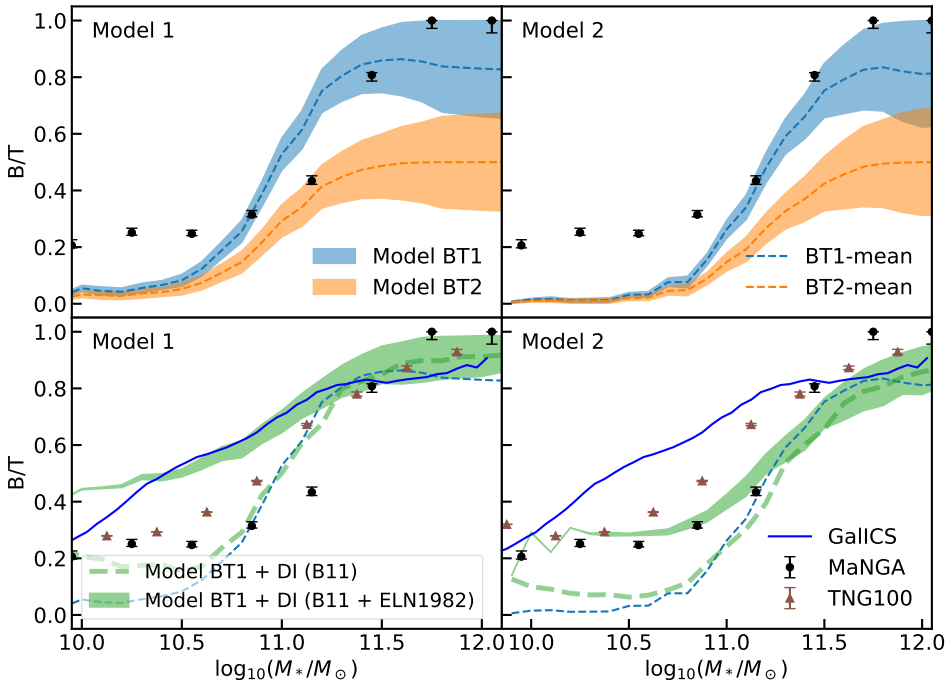

FIGURE 5.10: Bulge-to-total ratios as a function of stellar mass at redshift $z = 0.1$, for the two different toy models described in Section 5.4 and SMHM relationships of Models 1 and 2. The blue and orange shaded areas in the upper panels show the results for Models BT1 and BT2 (for Models 1 and 2 respectively), while the green areas in the lower panels show the results for Model BT1 but by including disc instabilities of Efstathiou et al. (1982) (Equation 5.6). The dashed tick green lines show the B/T ratios for Model BT1 by including only Bournaud et al. (2011) disc instabilities. The shaded areas are constrained by the two limit cases, where all the mass from minor mergers goes into the bulge and disc, respectively, and the thin dashed lines show the mean. The black dots with error bars represent the estimates from the MaNGA survey. Finally the blue solid line shows the prediction from GALICS semi-analytic model and the brown triangles with error bars the results from the TNG simulation. The uncertainties for the MaNGA survey and the TNG simulation are estimated using the standard deviation on the median.

of order unity (see, e.g., Shankar et al. 2014a and references therein). When the condition in Equation (5.6) is verified in galaxies that still have a disc-dominated structure, I assume that the disc transfers a sufficient amount of stellar mass to the bulge until dynamical equilibrium is re-established (e.g., Hatton et al. 2003; Shen et al. 2003).

The top panels of Figure 5.10 report my results for the merger Models BT1 and BT2, for the SMHM relation in Model 1 (left panel) and Model 2 (right panel), shown with cyan and orange shaded areas, respectively, where the upper and lower bounds mark the limiting cases where all the stellar mass of the minor merger is transferred to the bulge and to the disc, respectively, and the dashed lines represent the mean of the two cases. I compare our predictions with data on the mean B/T as a function of galaxy stellar mass

from MaNGA (black dots with error bars), as detailed in Section 3.4.4. The fact that the shaded areas in SMHM Model 2 are slightly broader at high stellar masses than those in Model 1 is an artefact of the number of mergers predicted by these Models, as shown in Figures 5.5 and 5.6. In particular, at fixed number of dark matter halo mergers, Model 2 predicts fewer major mergers, i.e., more minor mergers than Model 1. This leads to a higher bulge/disc mass in the cases where all the mass from minor mergers goes to the bulge/disc, leading, therefore, to a larger bound. Instead, the fact that the bounds are larger at high stellar masses than at low stellar masses is simply due to the higher *ex-situ* stellar mass fraction in more massive galaxies, as discussed in Section 4.3.

The MaNGA data clearly indicate that all local galaxies have a B/T ratio that is confined within $0.2 - 1$, with a mean value slightly rising with increasing stellar mass, from ~ 0.2 reaching an average value of $B/T \sim 1$ only in the most massive galaxies with $M_\star \gtrsim 10^{11}\,M_\odot$. Models that, like our BT1, assume a strict $B/T = 1$ during major mergers, can better reproduce the data at high stellar masses, especially when assuming that all the minor mergers contribute to the bulge component. On the other hand, models that, like BT2, assume that a significant fraction of the disc survives and/or is rapidly reaccreted after the merger, fall short in matching the data at high stellar masses, suggesting that these kinds of model are not extremely suitable to describe the average B/T ratios, at least at high stellar masses.

Irrespectively of what I assume for the B/T ratio in major (or even minor) mergers, both BT1 and BT2 Models drastically fail in reproducing the observed B/T in galaxies with $M_\star \lesssim 2 \times 10^{11} M_\odot$ (top panels of Figure 5.10). An *additional* component/process should be included in DECODE to reproduce the data. Here again one can witness the usefulness of a semi-empirical approach that, as discussed in Sections 2.4 and 3.1, can include additional layers of complexities wherever necessary, as guided by the data, in a transparent and efficient way. The bottom panels of Figure 5.10 show the prediction of Model BT1 by including disc instabilities as discussed above. I do not show Model BT2 as it fails to model the B/T ratios even with the addition of disc instabilities. The main effect of including disc instabilities in our Model BT1 is that it tends to increase the bulge masses at lower, but not at higher, galaxy stellar masses, where the condition in Equation (5.6) is more easily met mainly because lower mass galaxies retain their disc morphologies for a longer time. In particular, I find that, irrespective of the exact input SMHM relation, to broadly match the data I need to assume that a fraction of the disc mass is transferred to the bulge at each disc instability event, in line with some previous cosmological models (e.g., Bower et al. 2006).

In the bottom panels of Figure 5.10, I show both the cases where clumpy accretion (following Bournaud et al. 2011) and "classical" disc instabilities (Efstathiou et al. 1982) are implemented. I note that the narrower shaded areas of the model with disc instabilities are a direct consequence of the transfer of mass from the disc to the bulge and they tend to shrink into single lines in the case where disc instabilities take place at any time

step since the formation epoch of the galaxy, which explains also why the bounds are even thinner at low masses where the condition of Equation 5.6 is more easily satisfied. I find that Model BT1, the one without disc regrowth, with SMHM Model 2 broadly matches the MaNGA local average B/T ratios when some level of disc instabilities is included in the model, while it fails to match the data at low masses with SMHM Model 1. In particular, disc instabilities implemented following Bournaud et al. (2011) appear not to be sufficient to provide enough boost to the average B/T at the low-mass end to match the data, even if the baryonic inflow rate in Equation (5.5) is doubled. On the other hand, disc instabilities as in Efstathiou et al. (1982) allow to broadly reproduce the observational data of MaNGA, when the factor ϵ in Equation (5.6) is roughly 0.5.

Intriguingly, one could argue that strong disc instabilities, and not necessarily major mergers, are responsible for forming most stellar bulges, even at the highest stellar masses. In fact, the strength of a disc instability in forming a bulge closely depends on the disc-to-total ratio, the more disc mass there is, the more potential there is for the bulge to grow in mass after a disc instability. I however checked that even on the assumption of ineffective major mergers preserving a $B/T \sim 0.2$, the disc instabilities would still fall short in boosting the B/T ratio up to unity at high stellar masses.

In the bottom panels of Figure 5.10, for completeness, I compare our predictions with the outputs from the TNG simulation and the GALICS semi-analytic model (brown triangles with error bars and blue solid lines, respectively). Interestingly, both TNG and GALICS predict large mean $B/T \gtrsim 0.9$ at high stellar masses in reasonable agreement with our predictions and the inferred data. In addition, they also include bulge formation via disc instabilities (see, e.g., Tacchella et al. 2019; Cattaneo et al. 2020), predicting indeed $B/T > 0.2$ at low masses in line with the data, though the mean B/T predicted by GALICS tends to be larger than the one measured in MaNGA towards lower stellar masses (I provide in Appendix C a detailed comparison between the B/T ratio found in MaNGA and those from other samples/studies). Our Model 1 is roughly consistent with the predictions of GALICS at all masses but not with the observational data and the TNG simulation at low masses, while Model 2 behaves in nearly the opposite fashion, highlighting once again the dependence of galactic properties, this time the mean B/T ratios, on the input SMHM relation.

Finally, in Figure 5.11 I show the mean stellar mass growth of bulges and discs for four galaxy masses at $z = 0$, using SMHM Model 2 as input, for Model BT1 with and without disc instabilities, as labelled. I note that, when disc instabilities are not included, at low stellar masses (e.g., $M_\star(z = 0) \sim 10^{10.5}\, M_\odot$) the disc dominates the overall mass growth of the galaxies and the bulge component is almost negligible, unless disc instabilities are included (long-dashed orange lines). Moving towards higher stellar masses, the bulge begins to be gradually more dominant, as a direct consequence of the increasing number of mergers, and adding disc instabilities does alter this trend noticeably.

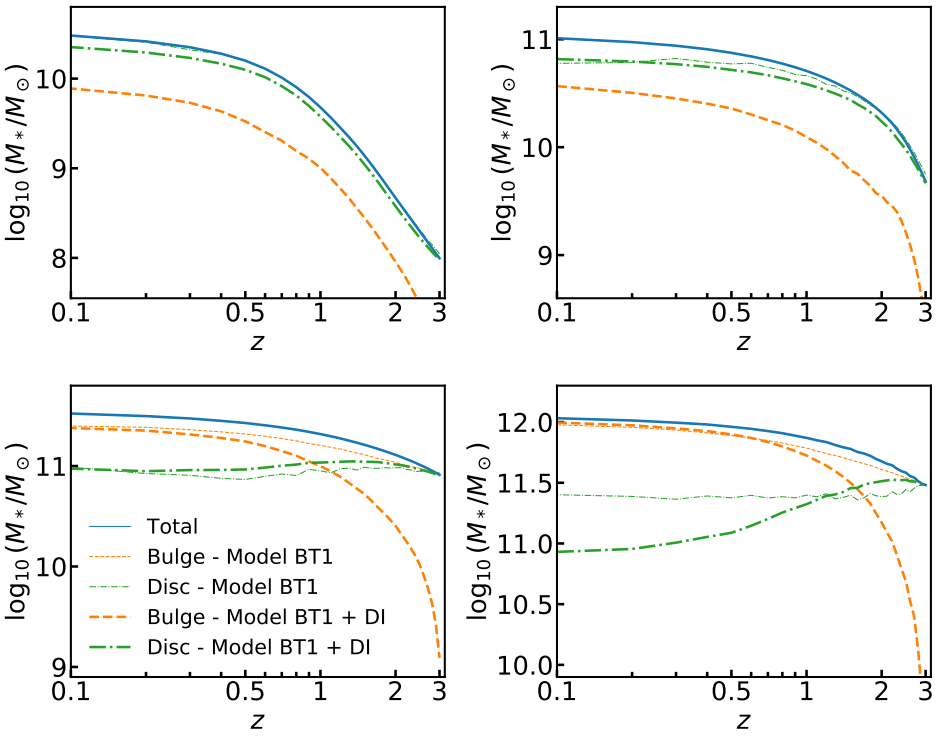

FIGURE 5.11: Average growth of total, bulge and disc stellar mass for four different galaxy mass bins at $z = 0$ for SMHM Model 2. The blue solid lines show the total stellar mass growth. The thin dashed and dash-dotted lines show the mass growth of the bulges and discs, respectively, for Model BT1, while the thick lines show the mass growths for Model BT1 when including disc instabilities.

5.5 Brightest cluster galaxies growth

As a further proof-of-concept application of DECODE, I study the stellar mass growth history of BCGs, which are massive elliptical galaxies that constitutes an additional source of information for understanding the evolution of galaxies and large-scale structure. Several studies have addressed already this issue, both from observations (e.g., Whiley et al. 2008; Collins et al. 2009; Stott et al. 2010; Lidman et al. 2012; Bellstedt et al. 2016; Lin et al. 2017; Zhang et al. 2017) and numerical works, such as semi-analytic models (e.g., De Lucia and Blaizot 2007; Contini et al. 2014), semi-empirical models (Shankar et al. 2015) and hydrodynamical simulations (e.g., Pillepich et al. 2018a; Ragone-Figueroa et al. 2018). Here, I show the predictions of DECODE for the stellar mass assembly of BCGs and how these compare to the results from other works.

The results are shown in Figure 5.12. The red dashed and solid lines show the total stellar mass fractional growth of BCGs, selected in dark matter haloes with present-day mass $M_{\rm h}(z = 0) > 8 \times 10^{14} M_{\odot}$, predicted by DECODE with Models 1 and 2. The

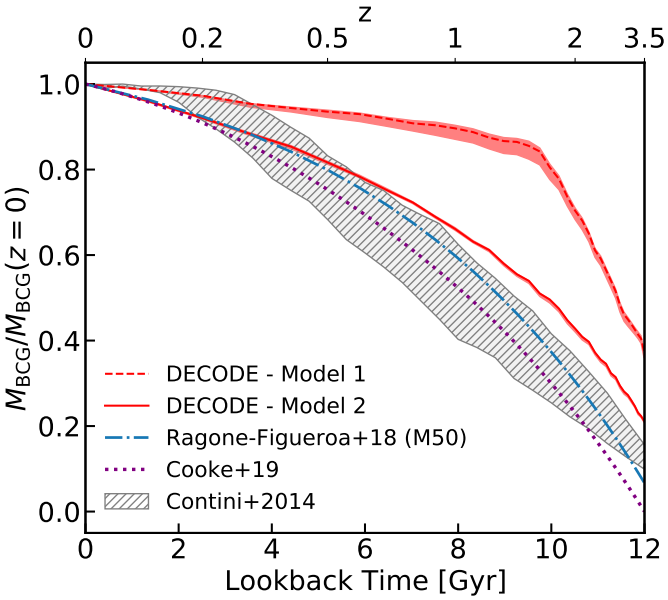

FIGURE 5.12: Fractional stellar mass growth of BCGs predicted by DECODE for Models 1 and 2 as a function of lookback time with their 1σ bounds (red lines and shaded areas). The blue dash-dotted line corresponds to the fit M50 selected BCGs according to Equation (2) in Ragone-Figueroa et al. (2018). The purple dotted line shows the observed median growth from COSMOS as presented in Cooke et al. (2019). The grey dashed area includes the evolutionary histories of the models in the Contini et al. (2014) semi-analytic model.

data are compared with the COSMOS data (Cooke et al. 2019), results from the hydrodynamic simulations of Ragone-Figueroa et al. (2018) and semi-analytic model of Contini et al. (2014, as labelled in the Figure), selected in the same mass region. According to Model 1, BCGs have already formed most of their mass at redshifts $z > 1.5$, because of the assumed constant SMF up to that redshift which maps the dark matter halo mass accretion history into a higher average stellar mass growth. On the other hand, assuming Model 2 BCGs have only formed roughly 50% of their mass by $z = 1.5$ and have grown the remaining mass at later epochs.

The BCG stellar masses in Ragone-Figueroa et al. (2018) are computed with the mass within the spherical radius of 50 kpc (M50). Our Model 2 is in relatively good agreement on the mass formation history of BCGs with M50 selected galaxies, predicting a factor of ~ 1.5 in the mass increase between $z = 1$ and $z = 0$ against the factor 1.4 of Ragone-Figueroa et al. (2018). Figure 5.12 shows that models characterized by a SMHM relation with a significantly evolving underlying SMF as in Model 2, are once again better tuned to reproduce the current data, this time data on BCGs, in line with predictions from hydrodynamic simulations and semi-analytic models.

5.6 Summary of the findings

In this Chapter, I have applied DECODE to predict the galaxy-galaxy merger rates, surviving satellite abundances (which can be considered as failed mergers) and BCG growths. I have also explored how merging pairs can produce the fraction of elliptical/lenticular galaxies and mean B/T ratios in the local Universe, by assuming that the former are formed by major mergers, and the latter are shaped by both major/minor mergers and disc instabilities.

The main results can be summarized as follows:

- I have shown the connection between many galaxy observables and the input SMHM relation, in a semi-empirical framework like DECODE, and thus the input SMF, in particular galaxy merger rates and satellite abundances.
- At fixed mass threshold, the double power law shape of the SMHM relation will break the constant number of halo-halo major mergers, resulting in an increasing number of galaxy-galaxy major mergers with stellar mass, which will highly depend on the slope of the bright end of the SMHM relation.
- A SMHM relation implied by a SMF characterized by a larger number of massive galaxies and a normalization significantly decreasing at high redshift, is more suitable to reproduce the correct observed merging pair fractions (as inferred from GAMA, UDS, VIDEO and COSMOS) and abundances of satellite galaxies (from SDSS) in the local Universe.
- By including residual star formation in satellites after infall improves the match with the low-mass end of the local SDSS satellite SMF, especially in less massive parent haloes.
- The same SMHM relation is also able to reproduce the fraction of local elliptical galaxies of the SDSS galaxies, on the assumption that these are formed from major mergers with mass ratio $M_{\star,\mathrm{sat}}/M_{\star,\mathrm{cen}} > 0.25$, as often assumed in cosmological semi-analytic models. In other words, the validity of the $M_{\star,\mathrm{sat}}/M_{\star,\mathrm{cen}} > 0.25$ threshold also depends on the input SMHM relation.
- This SMHM relation is also able to reproduce the mean B/T ratio distribution of the local MaNGA galaxies, assuming that bulges are formed through minor and major mergers, and with a contribution from disc instabilities at stellar masses below $M_* \lesssim 10^{11}\,M_\odot$.
- Finally, the stellar mass growth of BCGs at $z < 1$ is well described by such SMHM relation as well.

In summary, DECODE is a valuable, complementary tool for probing galaxy evolution and the relevant physical processes involved therein, such as galaxy merger rates, satellites abundances, morphologies, and bulge-to-total ratios for any given input SMHM relation and with minimal input parameters.

Chapter 6

Star formation histories and merger histories

In Chapter 5, I showed that a stellar mass-halo mass (SMHM) relation implied by a stellar mass function (SMF) with flatter and evolving bright end is more suitable to describe the galaxy major merger rates, elliptical fractions and bulge-to-total distributions, compared to a model derived from a constant SMF up to $z = 1.5$, at least for $M_\star \gtrsim 10^{11}\,M_\odot$. On the other hand, these constraints on the shape of the input SMHM relation become gradually significantly less tight at stellar masses below $10^{11}\,M_\odot$, because major mergers are relatively rare at lower stellar masses. In this Chapter, I will underline the role of star formation histories (SFH) and their close link to the shape of the SMF in particular at low stellar masses.

6.1 More stellar mass function models

In Section 5.1, I have discussed the challenges in determining observationally the SMFs and the implications on the galaxy merger rates. Here, I further expand on the SMF and SMHM relation, focusing my attention of their role on the galaxy SFHs. In general, flatter SFHs are on average better mapped into slowly evolving SMFs and vice versa, as expected also from basic continuity equation arguments (e.g., Leja et al. 2015; Grylls et al. 2020a). To highlight the connections between SFHs and SMFs, I consider two models for the SMHM relation that broadly bracket the currently available measurements of the SMF at different redshifts:

- *constant SMF model*: equivalent to Model 1, described in Section 5.1.1.

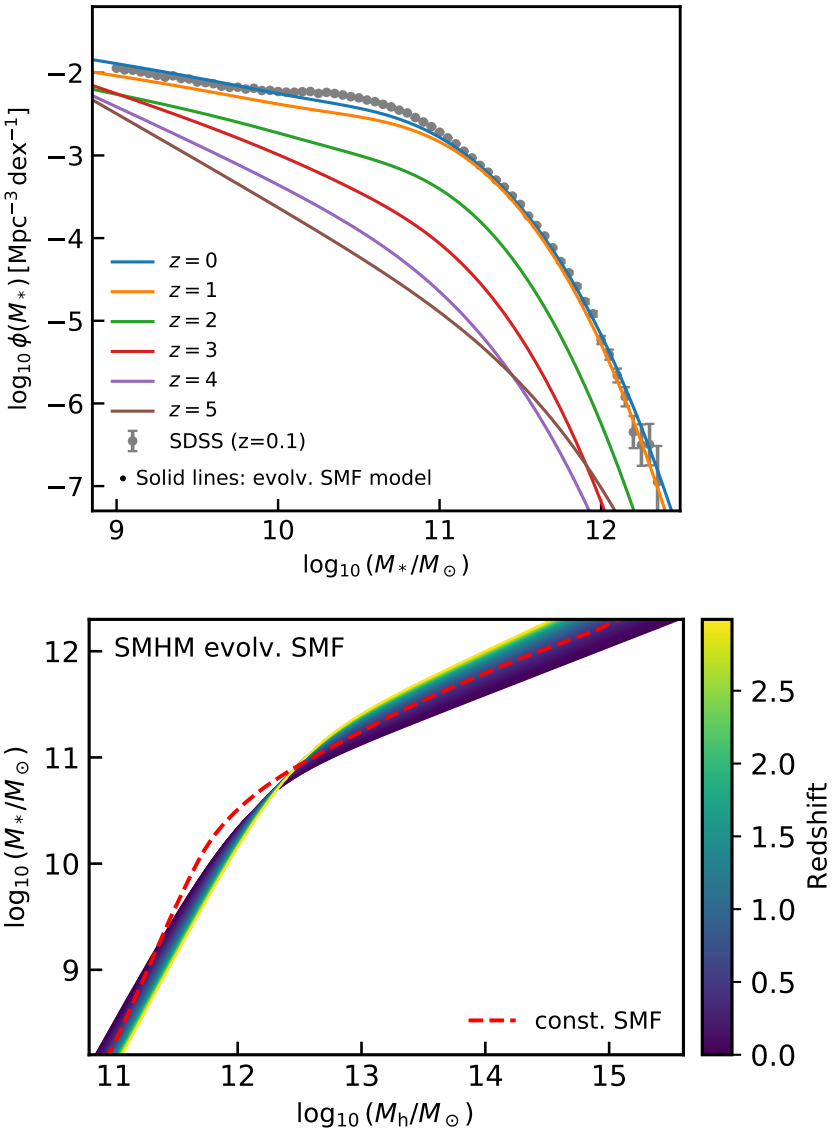

FIGURE 6.1: Upper panel: evolving stellar mass function toy model as described in Section 6.1 (solid lines) at different redshifts, compared to the SDSS SMF (grey dots and error bars) at $z = 0.1$ from Bernardi et al. (2017). Lower panel: stellar mass–halo mass relation computed via abundance matching for the evolving stellar mass function model at redshifts $0 < z < 3$ (denoted by the colour code), compared to the relation at $z = 1$ implied by the constant stellar mass function (red dashed line).

- *evolving SMF model*: SMF characterized by a weakly evolving low-mass end (below the knee $M_\star \lesssim 10^{11}\,M_\odot$) at low redshifts $z \lesssim 1.5$ following Davidzon et al. (2017), and more strongly evolving high-mass end similarly to Model 2.

The evolving SMF model is shown in the upper panel of Figure 6.1 at different redshift bins, as labelled. Davidzon et al. (2017)'s SMF predicts less abundant number of massive galaxies with respect to Bernardi et al. (2017)'s, which could be attributed to the choice of different mass-to-light ratios and/or different photometries. As I am here mainly interested in the differences in the evolution of the SMFs, and their impact in

the SFHs, I have added a scatter of 0.3 dex to the original fit of Davidzon et al. (2017)'s SMF to align their fit to Bernardi et al. (2017)'s SMF, but retaining their original redshift evolution. Furthermore, Davidzon et al. (2017)'s double power-law fit to the SMF also predicts slightly less abundant numbers of galaxies around the knee with respect to Bernardi et al. (2017)'s estimate for the SMF (see solid blue line and data in the upper panel of Figure 6.1), but this relatively small difference has little impact on any of the results presented in this Chapter.

The lower panel of Figure 6.1 shows the redshift evolution of the SMHM relation computed using the evolving SMF model in the redshift range $0 < z < 3$, compared to the constant SMF relation at redshift $z = 1$. The resulting SMHM relation from the evolving model is characterized by an increase in stellar mass at fixed halo mass of 0.29 dex from $z = 0$ to $z = 1$ in the high mass range ($M_{\rm h} \sim 10^{14}\,M_{\odot}$), and by a decrease of 0.24 dex in the low mass range ($M_{\rm h} \sim 10^{11.5}\,M_{\odot}$).

6.2 Further investigation on the satellite abundances

As already discussed in Section 5.2.1 and in other works (see, e.g., Moster et al. 2018; Behroozi et al. 2019; Grylls et al. 2019; Fu et al. 2022), the abundances of surviving satellite galaxies provide a complementary and independent test on the shape of the input SMHM relation, as they can be considered as the other side of the coin with respect to mergers. Indeed, in a dark matter-dominated hierarchical Universe surviving satellites are effectively "failed" mergers at any given epoch, and can thus be used as independent test of the same merger model, and compared against direct observational estimates of the satellite SMF. Any successful cosmological model of galaxy evolution that matches the SFHs and merger histories of galaxies, must also provide the right amount of observed satellites. Any failure in this respect could be, as for any other observable considered so far, attributed to either a shortcoming of the model and/or inconsistencies in the different and independent data sets. I stress once again that the satellite SMF, unlike the total SMF, is a genuine prediction or output of DECODE.

The left panel of Figure 6.2 shows DECODE's predicted satellite SMF (solid blue line) in the evolving SMF model with frozen satellites, compared to the satellite SDSS galaxy data from Bernardi et al. (2017) as labelled in Yang et al. (2007)'s halo catalogue (blue filled circles). The results with the constant SMF as input do not change appreciably, since the satellites SMF is not very sensible to the input SMHM relation, as already shown in Section 5.2.1. It is evident that the model, without any further fine-tuning, nicely matches the data, at least above $M_{\star,\rm sat} \gtrsim 3 \times 10^{10}\,M_{\odot}$, while there is a small shortfall at lower stellar masses. When dividing the observed SDSS sample in satellites hosted in parent haloes above and below a chosen host halo mass of $M_{\rm h,par} = 10^{13}\,M_{\odot}$ (orange triangles and green squares), I see that the major shortfall occurs in the lower

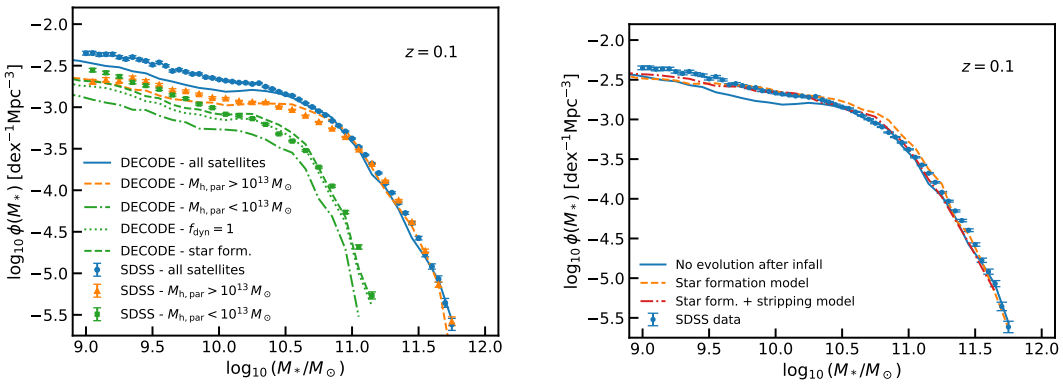

FIGURE 6.2: Left panel: Stellar mass function of surviving satellite galaxies from DECODE's evolving stellar mass function model SMHM relation compared to that observed by SDSS. The blue, orange and green solid lines show the SMF for all satellites and for parent halo mass greater and smaller than $M_{\rm h,par} = 10^{13}\,M_\odot$, respectively. The green dotted line shows the latter case but with fudge factor $f_{\rm dyn} = 1$, i.e., longer dynamical friction timescales with respect to DECODE's default one, and the green dashed line with star-forming satellites. Right panel: Satellites stellar mass function at $z = 0.1$ for star-forming and star formation+stripping models. The orange dashed and the red dash-dotted lines show the mass function for star-forming and stripped merging satellites, respectively.

mass haloes. Allowing for a longer dynamical friction timescale ($f_{\rm dyn} = 1$) with respect to DECODE's reference timescale (Equation 4.1), improves the fit at low stellar masses both in lower mass parent haloes as well as in the total satellite SMF (dotted line). A similar, nearly degenerate, effect of boosting in the number density of satellites is also found by allowing the satellites to continue forming stars after infall as described in Section 3.2.4.1 (dashed lines).

I further show in the right panel of Figure 6.2 the effect on the total satellite mass function of including late, post-infall star formation (orange dashed line) and star formation with stellar stripping (red dash-dotted line), which provide an improved fit to the data with respect to a frozen model at low stellar masses below $M_{\star,\rm sat} \lesssim 3 \times 10^{10}\,M_\odot$. Although the two model renditions discussed above characterized by a lower dynamical friction timescale or by the inclusion of star formation and stripping, provide both a nearly degenerate match to the local stellar mass function of satellites, I note that some stellar stripping in satellites is expected, and indeed observed, in groups and clusters (e.g., Poggianti et al. 2017; Franchetto et al. 2021; Akerman et al. 2023), and can also contribute to the intracluster light level measured in clusters, as discussed in Section 6.4.

6.3 Stellar mass assembly of central galaxies

As already discussed above, the high-mass end slope of the SMHM relation has a profound imprint on the major merger histories of galaxies, and steeper relations would preferentially correspond to less major mergers (e.g., Hopkins et al. 2010a; Grylls et al. 2020a; O'Leary et al. 2021; Fu et al. 2022). On the other hand, at fixed total stellar mass, a larger contribution of (major) mergers will inevitably correspond to less stellar mass growth via star formation, and thus the shape of the input SMHM relation is expected to also have a significant impact on the SFH of a galaxy. In this Section, I show how different SMHM relations and satellite evolution scenarios produce different merger histories and SFHs in central galaxies.

6.3.1 Low- and intermediate-mass galaxies

First of all, I focus only on low- and intermediate-mass galaxies, namely those with stellar mass $M_\star \lesssim 10^{11}\,M_\odot$ at $z = 0$, where the fraction of stellar mass accreted via mergers is negligible. I restrict to this mass limit because I want to isolate the full effect of SMF variations on the SFHs. Most theoretical models indeed support the view that galaxy growth is fully star formation-dominated below $M_\star \lesssim 10^{11}\,M_\odot$ (e.g., Oser et al. 2010; Lackner et al. 2012; Rodriguez-Gomez et al. 2016; Pillepich et al. 2018a; Davison et al. 2020; Cannarozzo et al. 2022; Trujillo-Gomez et al. 2023), and DECODE also predicts the same behaviour (as shown in Section 5.2). Hence, in this stellar mass range, the SMF contains direct information on the SFHs.

In Figure 6.3 I compare DECODE's predictions on the SFHs of galaxies of different stellar masses at $z = 0$, with the SFHs extracted from SED fitting from different surveys and other theoretical models, as labelled. I here focus only on galaxies with stellar mass $M_\star \lesssim 10^{11}\,M_\odot$ at $z = 0$. More specifically, I compare DECODE's outputs for the constant SMF and evolving SMF models (red dash-dotted and brown solid lines) with the TNG hydrodynamical simulation (green dotted lines), GALICS semi-analytic model (blue dotted lines) and the inferred (integrated) SFHs from the MaNGA and GAMA surveys (orange and cyan solid lines and shaded areas).

There are some differences between the MaNGA and GAMA SFHs, especially at stellar masses $M_\star > 10^{10}\,M_\odot$, which are possibly due to the differences between the two data sets themselves. First of all, the two surveys cover different wavelengths, with MaNGA focusing only in the optical regime, while GAMA covers a broad wavelength range from the UV to the IR. Furthermore, due to the smooth truncation of the skewed normal function shape at the beginning of the Universe, the GAMA SFHs might have higher star formation rates (SFR) at high redshifts with respect to MaNGA, where no truncation is used. Additionally, the usage of constant metallicity without modelling

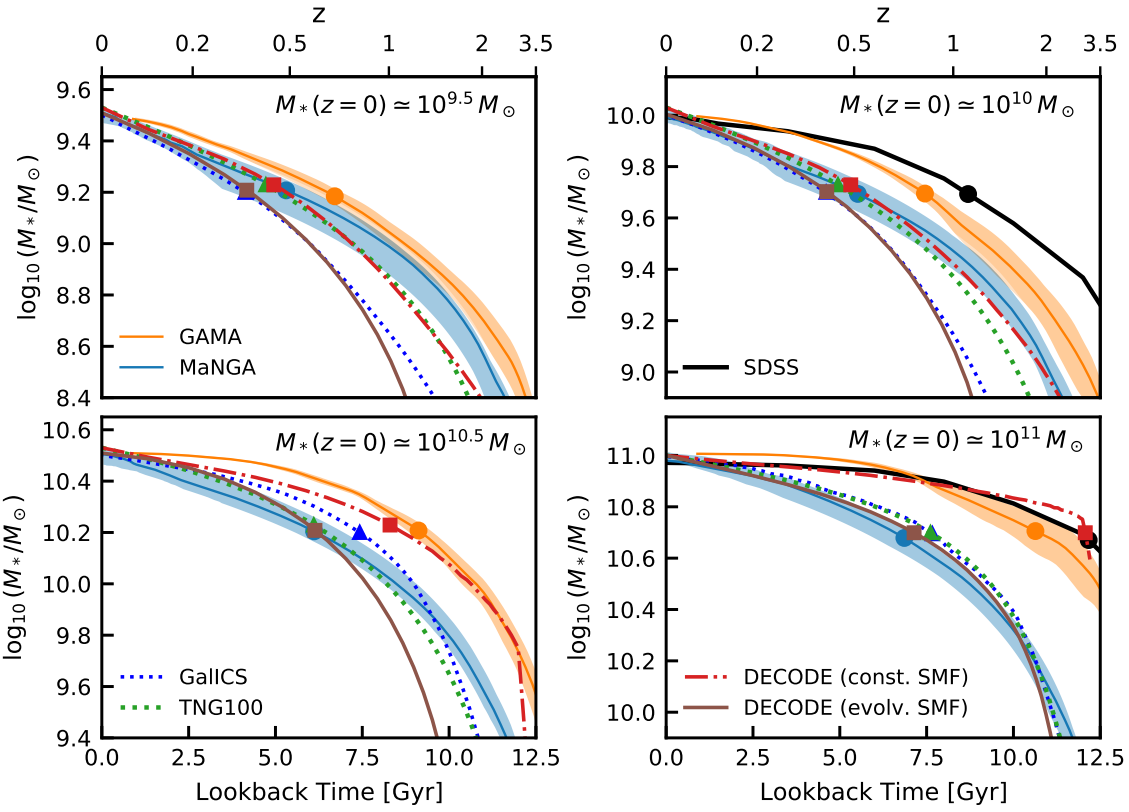

FIGURE 6.3: Mean integrated star formation histories for four stellar mass bins ($M_\star = 10^{9.5}$, 10^{10}, $10^{10.5}$ and $10^{11}\,M_\odot$) at redshift $z = 0$, as predicted by DECODE, compared to the data from the TNG simulation and GALICS, as well as the SDSS, MaNGA and GAMA surveys. The red dash-dotted and brown solid lines show the predictions from models with constant and evolving stellar mass functions, respectively. The blue and green dotted lines show the results from GALICS and the TNG simulation, respectively. The blue and orange lines and shaded areas show the mean SFHs from SEDs and uncertainties of MaNGA and GAMA, respectively. The coloured dots, triangles and squares show the 50% of the stellar mass formed today for the observations (MaNGA and GAMA), theoretical models (TNG and GALICS) and DECODE's SMHM relation models, respectively.

the chemical evolution in the MaNGA fit might introduce some slight bias towards younger galaxies compared to those from GAMA.

The mean SFHs in DECODE are computed by selecting in the stellar bin of interest a relatively large number of galaxies, which are then evolved in mass following the recipe described in Section 3.2.4. The constant input SMF model generates SFHs that are broadly consistent with the SFHs from the TNG simulation, GALICS and MaNGA at $M_\star(z = 0) = 10^{9.5}$ and $10^{10}\,M_\odot$, while it produces flatter SFHs for the other two mass bins, being more consistent with the GAMA and SDSS surveys. On the other hand, the SMHM relation implied by an evolving SMF produces mean SFHs steeper than those predicted by a constant SMF model, as expected, given that there is more stellar mass build up in the former model. The evolving SMF model produces SFHs that are steeper than all the data at $M_\star \lesssim 10^{10}\,M_\odot$ (top panels), while at larger masses

$M_\star \sim 10^{10} - 10^{11}\, M_\odot$ they are consistent with what inferred from MaNGA, but significantly steeper than those from GAMA and SDSS (bottom panels). The SFHs from the evolving SMF model are broadly consistent with those predicted from the TNG simulation at $M_\star \sim 10^{10} - 10^{11}\, M_\odot$, a trend expected as the SMF of the TNG has a weaker evolution below the knee but predicting a stronger evolution at higher stellar masses (see, e.g., Pillepich et al. 2018a).

6.3.2 Massive galaxies

While the total stellar mass growth of less massive galaxies is in good approximation mostly contributed by star formation alone, for more massive galaxies the comparison with observations is less straightforward as mergers can provide a non-negligible contribution to the overall stellar mass assembly histories of galaxies, especially for SMHM relations characterized by a flatter high-mass slope (e.g., Grylls et al. 2020a; Fu et al. 2022), as discussed previously. On the other hand, the SFHs retrieved from SED fitting record the total stellar mass formed in stars but cannot distinguish between the mass formed *ex-situ* or *in-situ*. For this reason, in this Section I do not compare directly with observationally inferred SFHs, but rather show the predicted stellar mass growth histories of massive galaxies predicted by DECODE using my constant and evolving SMF models, distinguishing between the stellar mass growth via *in-situ* star formation and via mergers. In what follows, I will mainly present the results using the evolving SMF model, but highlight the differences in my results when switching to a constant SMF model. In addition, for completeness, I also discuss the predicted stellar mass accretion histories for different types of satellite evolution after infall.

Figure 6.4 shows the mean integrated merger histories (upper panels) and the fraction of stellar mass accreted via mergers (lower panels) for galaxies with stellar masses of $M_\star = 10^{11.5}$ and $10^{12}\, M_\odot$ at $z = 0$. The results in the plot are shown for the evolving SMF as input, and I checked that the stellar mass growths change by less than ~ 0.15 dex in normalization but maintain the same redshift evolution when using the constant SMF as input. I find that, all the merger histories predicted by DECODE are similar to each other, irrespective of the chosen model for the satellite evolution (orange dotted, blue solid, green long dashed lines, as labelled), with only a slight marginal increase of $\sim 10\%$ in stellar mass growth when satellites continue forming stars after infall in the most massive centrals (orange dotted lines, top right panel). In this respect, the shape of the SMHM relation has a larger impact than the satellite evolution in shaping the merger histories of central galaxies. Similarly to the merger histories, the predicted *ex-situ* fraction evolution for the star-forming and stripped satellites is higher and lower, respectively, with respect to the frozen model. Interestingly, DECODE's *ex-situ* fraction are broadly consistent with the TNG simulation for galaxies with stellar

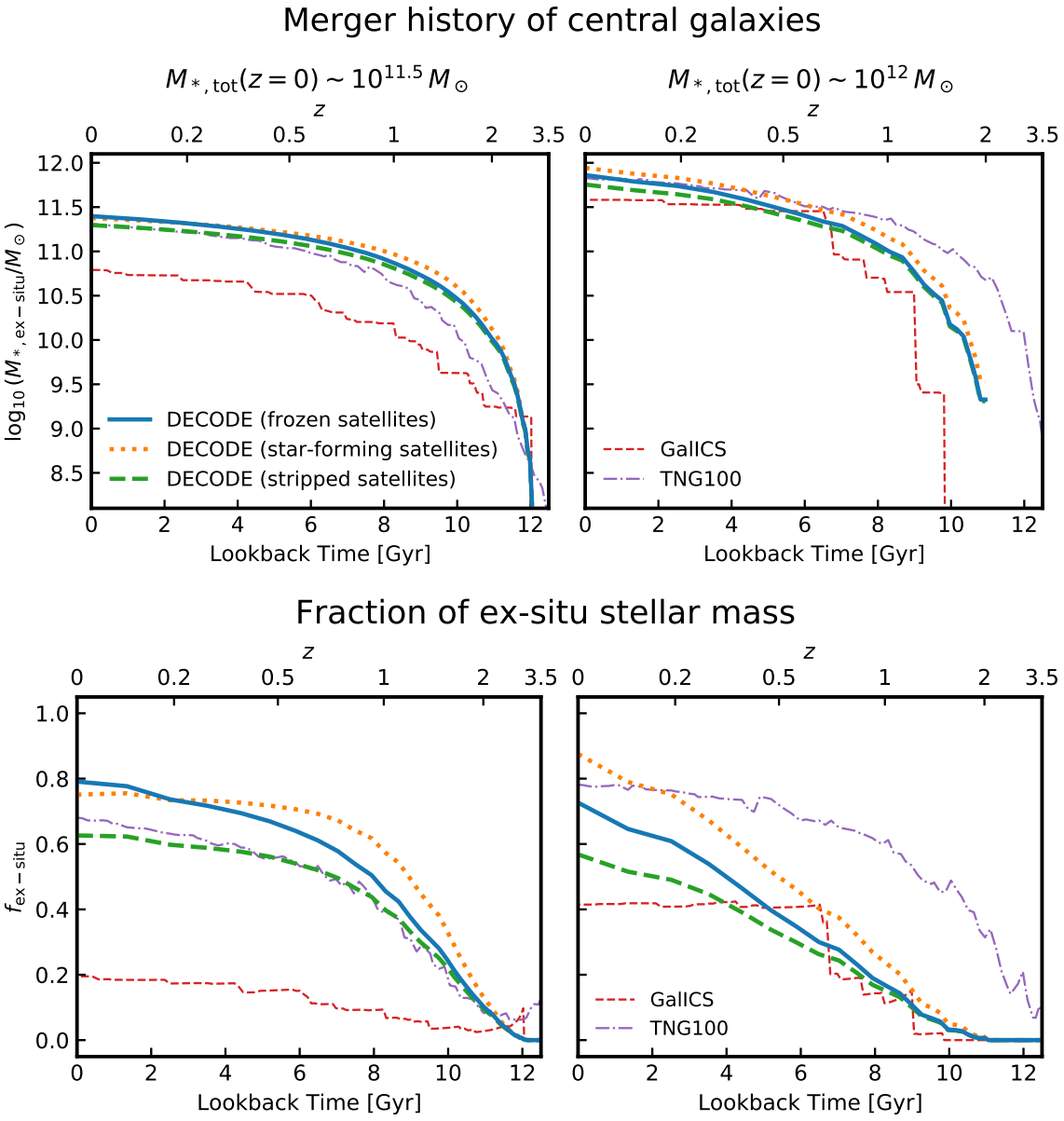

FIGURE 6.4: Upper panels: mean integrated merger history as a function of time for central galaxies of stellar mass $M_\star = 10^{11.5}$ and $10^{12}\,M_\odot$ at redshift $z = 0$, respectively. The blue solid, yellow dotted and green dashed show the predictions from DECODE's evolving SMF model, for the cases where merging satellite galaxies are assumed to not evolve their mass after infall, accrete mass via star formation and lose mass via stellar stripping, respectively. The results are compared with the mean growth histories from GALICS (red dashed lines) and the TNG simulation (purple dash-dotted lines). Lower panels: same as upper panel, but for fraction of *ex-situ* stellar mass.

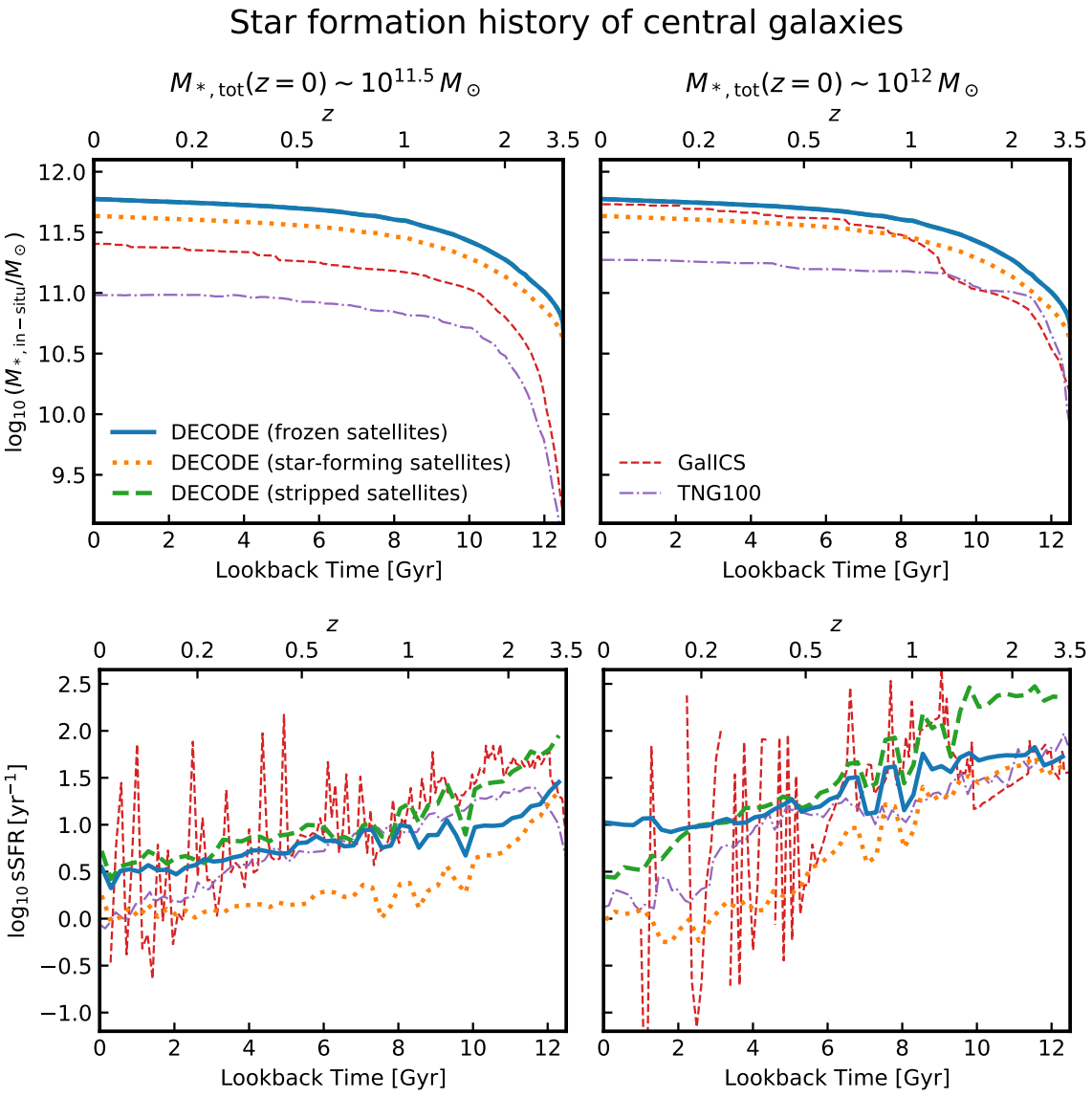

FIGURE 6.5: Same as Figure 6.4, but for mean integrated star formation histories (upper panels) and specific star formation rate evolution (lower panels).

mass $M_\star = 10^{11.5}\,M_\odot$ at $z = 0$ and with GALICS for $M_\star = 10^{12}\,M_\odot$, and are more divergent otherwise.

Figure 6.5 shows the integrated SFHs (upper panels) and the specific star formation rates (sSFR) as a function of time (lower panels) for galaxies in the same stellar mass bins at $z = 0$. The predicted stellar mass growth via *in-situ* star formation is relatively smaller than the one from mergers by a factor of ~ 2 and ~ 3 in the two stellar mass bins, respectively, for both the cases of evolving and constant SMF. It is interesting to note that the SFHs, being overall contributing less to the stellar mass growth in these massive galaxies, are proportionally more dependent on the satellite evolution, in particular the model with star-forming satellites tends to predict a SFH lower by a factor of ~ 2 than that other two models (orange dotted versus blue solid and green long

dashed lines). I stress that the total stellar mass growth remains the same in all models at fixed SMHM relation, i.e., at fixed SMF model, but only the relative proportions of merging and star formation change depending on the satellite evolution. Moreover, the stronger dependence of the *in-situ* stellar mass growth on the satellite evolution with respect to the *ex-situ* growth is an apparent visual effect, due to the high *ex-situ* fraction with respect to the *in-situ* fraction across cosmic time. Indeed, differences of the order of few $\times 10^{-2}$ dex in the *ex-situ* growth will translate into differences of 10 times larger in the *in-situ* growth, causing the apparent more sensible dependence on the satellite evolution.

The sSFRs plotted in the lower panels of Figure 6.5 all show, irrespective of the evolution of satellites, a clear decreasing trend with cosmic time, steepening in more massive galaxies, mimicking the overall gas starvation that all galaxies are expected to undergo given the strong fall off in the cosmic SFR below $z \sim 1-2$ (e.g., Madau and Dickinson 2014). This finding is also in line with what is shown in the lower panels of Figure 6.4, where the *ex-situ* stellar mass fraction steadily takes over towards low redshifts, where mergers dominate the growth of the oldest quenched galaxies. It is interesting to note that in a data-driven model like DECODE, which does not contain any recipe for gas exhaustion or quenching, it is ultimately the shape of the halo accretion rate that drives the stellar mass growth and the sSFR histories, again lending further support to the capital importance of the underlying halo assembly histories in driving the growth of central galaxies (e.g., Wechsler and Tinker 2018; Bose et al. 2019; Boco et al. 2023; Lyu et al. 2023).

6.3.3 Star-forming sequence

Having discussed the mean SFHs of galaxies of different stellar mass along their evolutionary tracks, I now move to the study of the overall SFR-stellar mass relation or main sequence of galaxies as predicted by DECODE using my two reference SMF models with and without redshift evolution. The main sequence represents a complementary self-consistency test between the observed stellar masses and SFRs. As mentioned in Section 2.2, the distribution of galaxies on the SFR-$M_\star$ plane is very spread with a large scatter, with starbursts lying far above the mean relation and quiescent galaxies below. Due to the stochasticity of DECODE (Section 3.2.2.5), I can predict and compare to data only the mean SFR-$M_\star$ relation.

Figure 6.6 shows the main sequence as predicted by DECODE for the evolving SMF model at different redshifts, as labelled. The constant SMF predicts very similar shapes and slopes, but lower in normalization by a factor of $\sim 1.5-2$ at any given redshift up to $z \sim 3$. I show two realisations of the model, the complete model (solid lines) and the model in which I assume galaxies only grow via star formation at all redshifts and stellar masses (dashed lines), or in other words implying that the infalling satellites

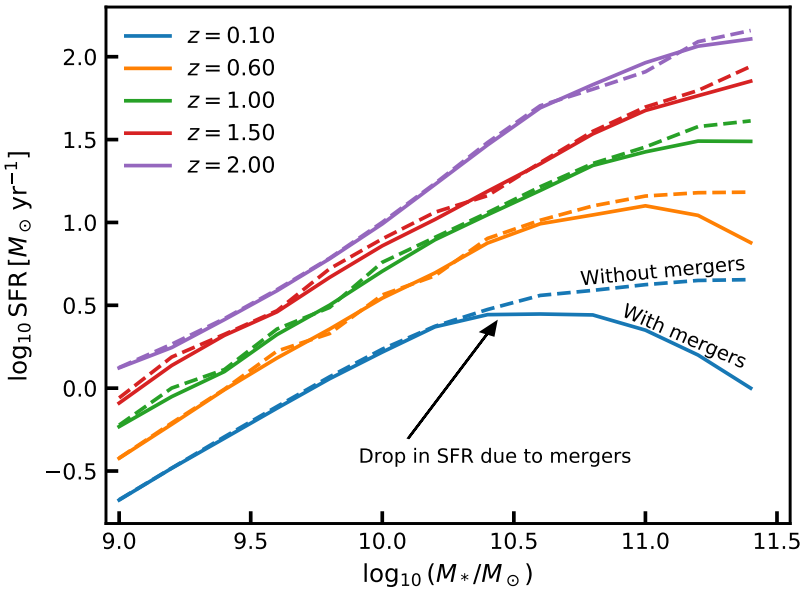

FIGURE 6.6: Comparison of the main sequence SFR-$M_\star$ relation predicted from DECODE for the evolving SMF as input, at redshifts $z = 0, 0.6, 1, 1.5$ and 2 (solid lines). The dashed lines show the extreme case where mergers are absent.

always have very long dynamical timescales. The latter rendition of the model is clearly possibly an oversimplification, and it would predict too many satellites in the local Universe (see Section 6.2), but it is included to provide an overview of the shape of the main sequence in a "maximal" model dominated by star formation, or in other words to isolate the effect of mergers. I first note from Figure 6.6 that all galaxies roughly grow at the same pace in redshift at fixed stellar mass, especially below $M_\star \lesssim 3 \times 10^{10}\, M_\odot$. At larger stellar masses the growth via star formation is actually larger, especially when effective mergers are included, which are the main process that grows the stellar mass in early-type galaxies.

It is also interesting to note that there is no sign of a downturn in the predicted main sequence above $M_\star \gtrsim 3 \times 10^{10}\, M_\odot$. A break or flattening in the main sequence starts appearing only at $z < 1$ (broadly consistent with observation at $z \sim 1 - 2$), and this break is visible even in the extreme model with only SFR. The flattening of the main sequence is a mere consequence of the double power law shape in the input SMHM relation, which implies less stellar mass growth when the central galaxy crosses the knee of the SMHM relation. In the full model inclusive of mergers, the flattening becomes even more pronounced at $z < 1$, creating a down turn in the main sequence, because the majority of massive galaxies is predicted to be quenched with their stellar mass growth being dominated by mergers (see also Section 7.2). The flattening of the main sequence at $z < 1$ is a robust prediction of the model. From the observational point of view, the existence of the break has been widely discussed in the literature with contrasting results, with several works suggesting a single power law shape at all stellar masses and redshifts (e.g., Speagle et al. 2014; Rodighiero et al. 2014; Pearson et al.

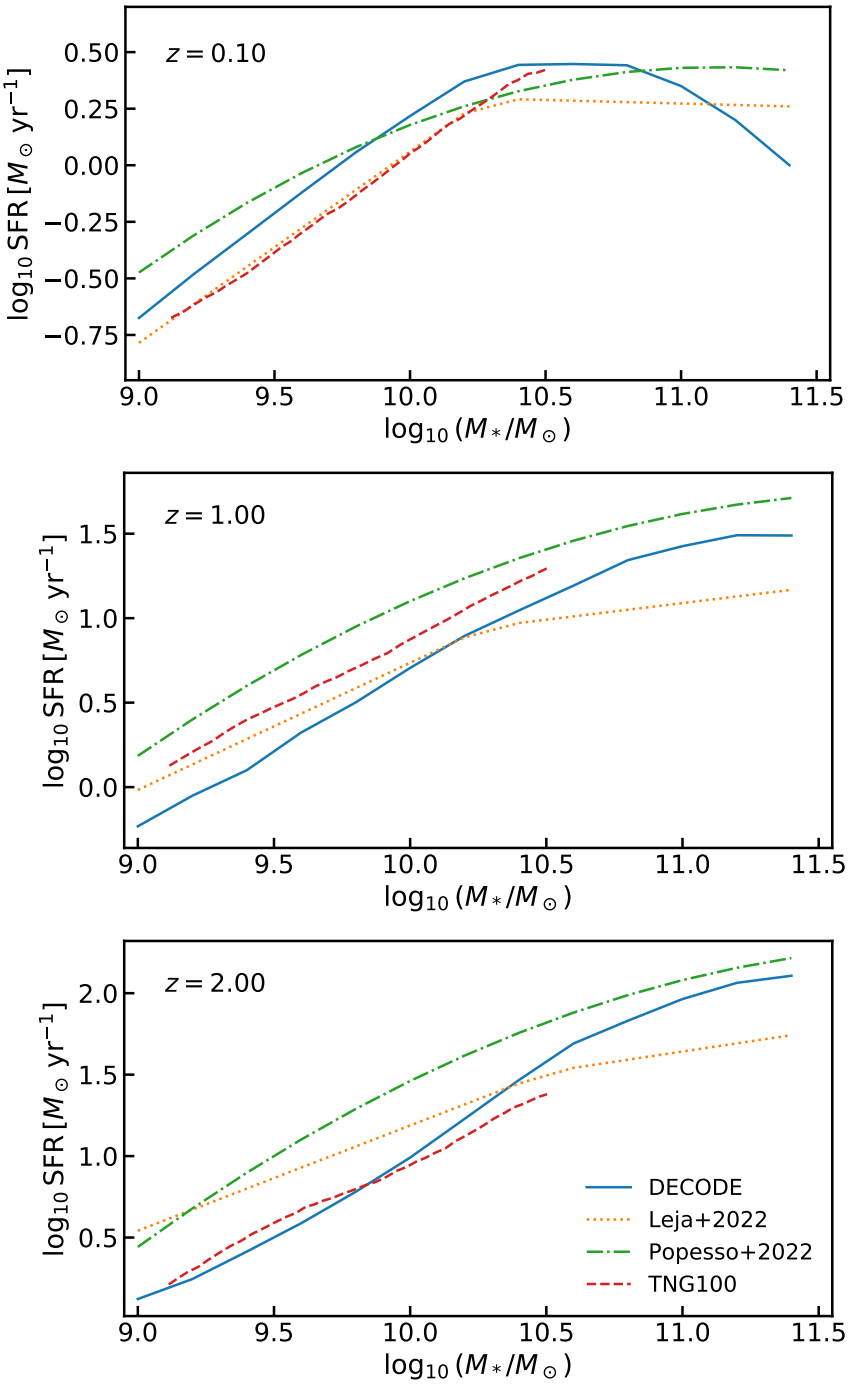

FIGURE 6.7: Upper panel: comparison between the main sequence at redshift $z = 0.1$ from DECODE and those from Leja et al. (2022), Popesso et al. (2023) and the TNG simulation, as labelled. Central and lower panels: same as upper panel but for redshifts $z = 1$ and 2, respectively.

2018), and others suggesting a break towards high stellar masses (e.g., Whitaker et al. 2014; Lee et al. 2015; Tomczak et al. 2016; Thorne et al. 2021; Leja et al. 2022; Popesso et al. 2023).

Figure 6.7 shows a close comparison between the main sequence predicted by the SMF evolving model from DECODE and two reference observational results from Popesso et al. (2023) and Leja et al. (2022), as well as, for completeness, the predictions from the TNG simulation, at different redshifts. First off, it is important to note that this comparison is only at a qualitative level as the definitions of stellar masses, despite a tiny deviation due to the choice of the IMF[1], may still be systematically different in Popesso et al. (2023), Bernardi et al. (2017) and Davidzon et al. (2017), which are the ones on which my reference models are based on. At redshift $z = 0.1$, DECODE predicts a mean SFR-$M_\star$ relation that is well consistent both with the observationally inferred ones and the TNG simulation, despite the down turn at the bright end. At redshift $z \geq 1$, at face value, DECODE tends to generate a mean SFR that is a factor of $\sim 2-3$ systematically lower than in the data even with the evolving SMF as input, and would drop further in normalization with the constant SMF as input.

Leja et al. (2022)'s results are based on neural networks to parameterize the galaxy population density in the main sequence plane. With this method, Leja et al. (2022) finds a mean SFR which is also lower than other direct estimates, in better agreement with my models, at least at $z \sim 1$. Also the TNG simulation tends to predict on average lower SFRs than Popesso et al. (2023) and in better agreement with my predictions. Leja et al. (2022, see Figure 11 therein) also showed that their sSFR time evolution for galaxies of $M_\star = 10^{10}\,M_\odot$ well matches those from numerical simulations, such as EAGLE and IllustrisTNG, even though the main sequence still slightly differs at high redshifts. It has been discussed several times in the literature that some estimates of the SFR-$M_\star$ relations may overproduce the stellar mass density recorded at any given epoch (e.g., Bernardi et al. 2010; Rodríguez-Puebla et al. 2017; Donnari et al. 2019; Hashemizadeh et al. 2021; Leja et al. 2022), which is also what I find here using the evolving SMF model. On the other hand, other groups have found more agreement between the integrated SFR and SMFs (e.g., Bellstedt et al. 2020). My results further show the intimate link between observed SFR densities and measured SMFs, and how each of these observations can provide valuable constraints on the other one.

6.4 Intracluster light

As a further application of DECODE and additional constraint for the assembly history of galaxies, I study the intracluster light (ICL), i.e., the faint diffuse light which freely floats within each cluster's gravitational potential and is not bound to any galaxy

[1]The offset in stellar mass corresponds to 0.03 dex for Kroupa (2001) and Chabrier (2003) IMFs.

within the cluster (e.g., Montes 2022). Many observational works suggested that the origin of the ICL may be due to tidal stripping of satellites and galaxy-galaxy mergers (e.g., Gregg and West 1998; Mihos et al. 2005; Contini et al. 2014, 2018). Implementing the production of ICL in DECODE's modelling is a valuable addition to constrain the viable models. Regardless of the satellites evolution scenario, a constant fraction of stellar mass is always transferred from mergers to the ICL. Furthermore, when including the stellar stripping in the evolution of satellites, which changes simultaneously the stellar masses of merged and surviving satellites, and merger rates and SFHs of central galaxies, the stellar mass stripped from satellites will contribute to the ICL. Indeed, I compute the ICL in DECODE by assuming that it is formed from the stellar mass stripped from the satellite galaxies (Section 3.2.4.1) and/or from the stellar mass lost during a galaxy merger. I assume that a fraction of $\sim$ 20% of the stellar mass during mergers involving the central Brightest Cluster Galaxy (BCG) is lost and transferred to the ICL, similarly to what is assumed in semi-analytic models (see, e.g., Contini et al. 2014; Koutsouridou and Cattaneo 2022). The amount of ICL might correlate with some cluster properties, such as the redshift and cluster halo mass. I will discuss in this Section how the ICL evolves with the latter quantities.

Figure 6.8 shows the redshift evolution of the fraction of ICL. Similarly to semi-analytic models, in each cluster, I define the BCG as the most massive central galaxy that lives in the cluster halo (e.g., Tonini et al. 2012). I define the fraction of ICL as the ratio between the stellar mass of the ICL and the total stellar mass of the cluster (i.e., the sum of the masses of the BCG, surviving satellites and ICL itself). The lines in Figure 6.8 show the predictions from DECODE's evolving SMF model, where the ICL is formed by only stripping mechanisms (green dotted), only galaxy merger processes (orange dashed) and both stripping and mergers (blue solid). The case in which the ICL is formed by stellar stripping only is a scenario where all the stellar mass during mergers goes into the central galaxies without any fraction being transferred to the ICL, while in the default implementation of DECODE such fraction is set equal to $\sim$ 20%, as described above. Even though it is an extreme model, it is still worth to show it in order to isolate the effect of stellar stripping on the ICL. I compare my results with observational data from Rudick et al. (2011), Burke et al. (2012), Burke et al. (2015), Montes and Trujillo (2018) and Furnell et al. (2021). I selected haloes with mass between $10^{14}\,M_{\odot} \lesssim M_{\rm h} \lesssim 10^{15}\,M_{\odot}$, in order to be as most consistent as possible with the data sets of the surveys I compare to. I stress that the ICL data are often derived in heterogeneous ways, using different methods and calibrations, but they are still all included in the same plot to provide a general term of comparison and broad guide to the models. What is evident from the full collection of the data is that despite the ICL fractions being sparse, they tend to point to averages of $\sim$ 20% at all cluster masses, which is a relevant constraint for models.

Consistently with the observations, I find in Figure 6.8 that the ICL gradually builds up

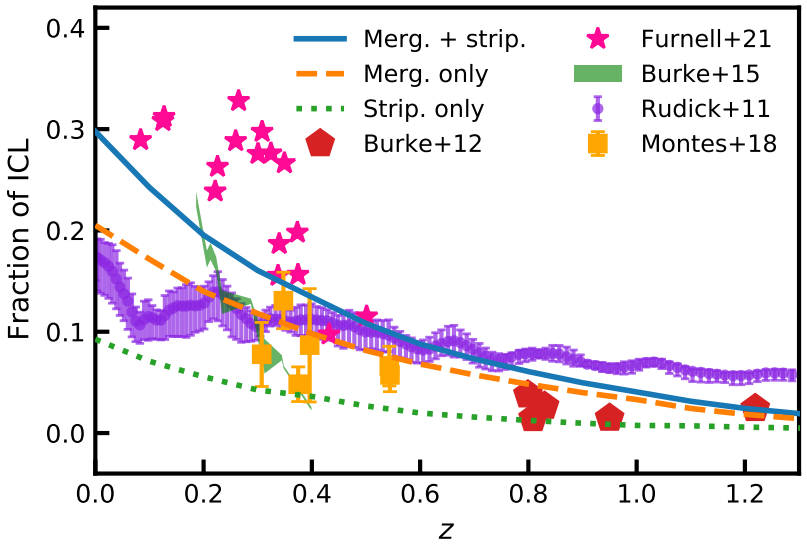

FIGURE 6.8: Fraction of intracluster light as a function of redshift. The blue solid, orange dashed and green dotted lines show the prediction from DECODE's evolving SMF SMHM relation for models with mergers+stripping, mergers only and stripping only, respectively. The points with error bars show the data from different studies in the literature (Rudick et al. 2011; Burke et al. 2012, 2015; Montes and Trujillo 2018; Furnell et al. 2021)

noticeable mass below $z \lesssim 0.7$. If only stellar stripping is considered, then the ICL is only visible at $z < 0.3$. However, the predicted ICL in this model would still be limited to $\sim 10\%$, which lies below the ensemble average of the data, possibly suggesting that the stellar mass stripped from infalling satellites by itself may not account for all the amount of observed ICL. Figure 6.8 shows that the mergers contribution to the ICL is larger with respect to the stripping by a factor of ~ 2. Overall, both the mergers only and stripping + mergers models better align with the general trend found in simulations and observations, i.e., a negligible amount of ICL at redshift $z \gtrsim 1$ and gradually increasing up to $f_{\rm ICL} \sim 20\%$ on average in the local Universe (see also Montes 2022 for a detailed discussion). The predicted ICL will increase/decrease by few percent and the cumulative mass growth from mergers will decrease/increase by a factor of ~ 0.05 dex, by changing the fraction of mass loss in mergers by a factor of 10%. Here, once again one can appreciate the power of a semi-empirical model that can gradually build levels of complexity in a transparent way properly guided by the data.

Figure 6.9 shows the fraction of ICL at redshift $z = 0$ as a function of the cluster total mass, for the same ICL models as in Figure 6.8. The coloured lines show the predictions from DECODE, while the data points show the results from Da Rocha and Mendes de Oliveira (2005), Da Rocha et al. (2008), Kluge et al. (2021) and Poliakov et al. (2021). Exploring the correlation between the ICL and the total halo mass can give an overview on how differently the mass forms in groups and clusters of galaxies. Observations

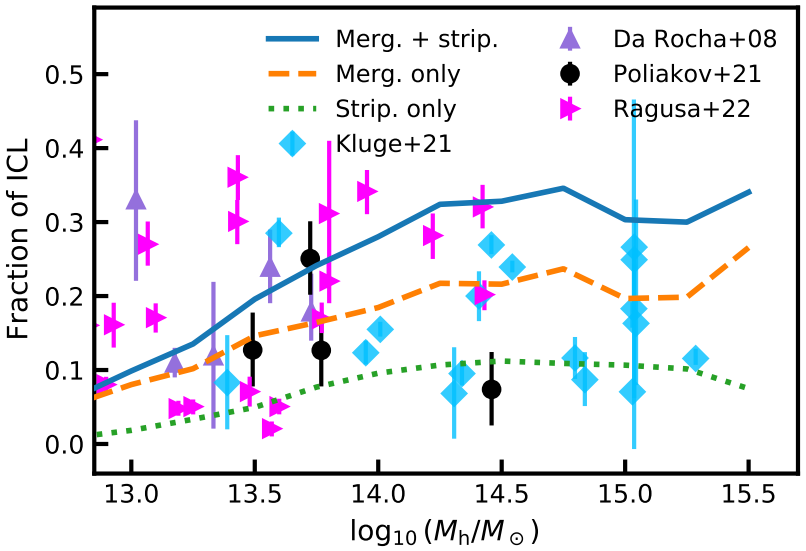

FIGURE 6.9: Same as Figure 6.8, but as a function of the cluster total mass at redshift $z = 0$. The points with error bars show the data from Da Rocha and Mendes de Oliveira (2005), Da Rocha et al. (2008), Kluge et al. (2021) and Poliakov et al. (2021).

suggest that there is no correlation between the ICL and the halo mass, while simulations found contrasting results, i.e., ICL fraction constant, increasing or decreasing with halo mass (e.g., Murante et al. 2004; Lin and Mohr 2004; Purcell et al. 2007; Dolag et al. 2010; Cui et al. 2014; Contini et al. 2018; Brough et al. 2023). Interestingly, my results for all the three models suggest an ICL fraction which is overall in agreement with the data, but slightly increasing from the low mass haloes towards high mass haloes. In DECODE's semi-empirical framework, this increase in ICL is due to the double power-law shape in the SMHM relation, which implies a higher fraction of major mergers in massive galaxies above the knee of the SMF, which are usually hosted in more massive haloes, as also discussed in Section 5.2. Finally, the recent results of Brough et al. (2023), who computed the ICL from the Horizon-AGN, Hydrangea, IllustrisTNG and Magneticum simulations, also suggest a fraction of ICL of $\sim 10 - 20\%$ for haloes with mass $14 < \log_{10}(M_{\rm h}/M_{\odot}) < 14.5$, broadly in line with my findings.

6.5 Further applications of DECODE

In this Section, I show two further applications of DECODE, being the capability in computing the size of galaxies and predicting black hole merger histories.

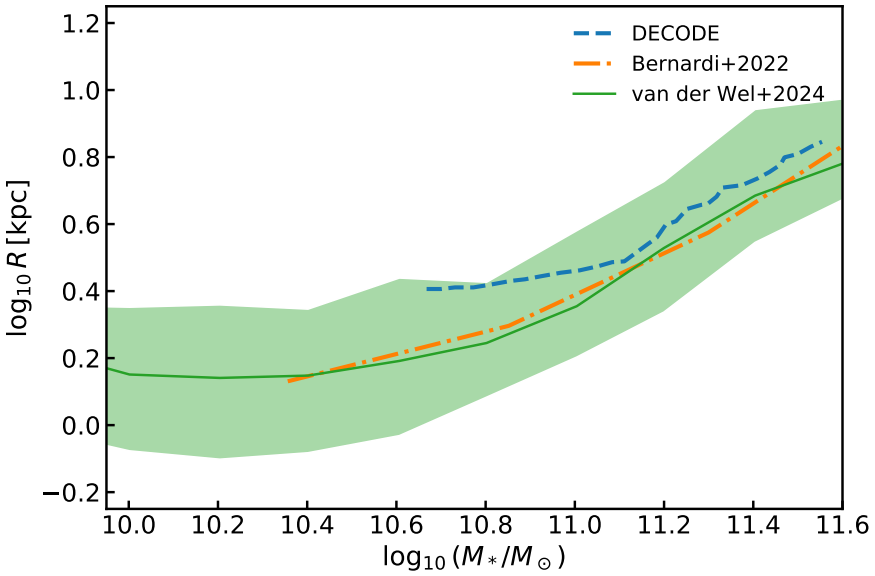

FIGURE 6.10: Mean mass-size relation predicted from DECODE (blue dashed line) at redshift $z = 0$, compared to the observed relation from Bernardi et al. (2022, orange dash-dotted line) and van der Wel et al. (2024, green solid line with shaded area).

6.5.1 Size evolution

Several studies have studied the relation between the galaxy effective radius and stellar mass, the $R_e - M_\star$ relation, showing that galaxies at fixed stellar mass had smaller sizes at higher redshift growing across cosmic time (e.g., van der Wel et al. 2014; van Dokkum et al. 2015; Patel et al. 2017; Mowla et al. 2019; van der Wel et al. 2024). Zanisi et al. (2021) also pointed out that at fixed stellar mass, galaxy sizes are spread following specific distributions across redshifts, the galaxy size function. Here, I focus only on the mean mass-size relation, without accounting for their actual distribution at given stellar mass. The results shown below are part of the Master's research work of K. Brocklebank and are shown here only as a proof-of-concept application of DECODE.

The effective radius, defined as the radius enclosing half of the light, is computed via a simple merger model, similarly to what is done for the B/T ratio evolution in Section 5.4. In particular, the radii of the disc and bulge are assigned via the input scaling relation from Suess et al. (2019) and their stellar masses are evolved following the recipe described in Section 5.4. The total radius of the galaxy is then computed as the weighted average between the sizes of the bulge and disc. Furthermore, when a merger happens, the galaxy size is updated following the equation of conservation of energy (Shankar et al. 2014a)

$$\frac{GM_{\rm fin}^2}{R_{\rm fin}} = \frac{GM_1^2}{R_1} + \frac{GM_2^2}{R_2}\,. \tag{6.1}$$

Figure 6.10 shows the local $R_e - M_\star$ relation predicted from DECODE. Overall, the mass-size relation from DECODE is well consistent in slope with the observed ones

from Bernardi et al. (2022) and van der Wel et al. (2024), especially towards high stellar masses. Instead, the normalization is higher in DECODE's relation with respect to observations, which is possibly due to the lack of gas dissipation in the model.

6.5.2 Super massive black hole mergers

To compute the black hole accretion history, I map the galaxy stellar mass into black hole mass via an input black hole mass-stellar mass ($M_{\rm BH} - M\star$) relation and I use the same relation to assign the masses of merging satellite black holes. I assume a single power law for the $M_{\rm BH} - M\star$ relation, which is the most common shape suggested by several works (e.g., Reines and Volonteri 2015; Shankar et al. 2016; Yang et al. 2018; Davis et al. 2018), as follows

$$\log_{10}(M_{\rm BH}/M_{\odot}) = \alpha \cdot \log_{10}(M_{\star}/M_{\odot}) + \beta\,. \tag{6.2}$$

with the slope $\alpha = 0.9$ and the normalization $\beta = -2.6$, which is broadly consistent with the $M_{\rm BH} - M\star$ relations suggested in the aforementioned works. Here, I show the merger histories for a *maximal* scenario, where all galaxy-galaxy mergers trigger the merger between their host SMBHs. In reality, this is not a realistic scenario, as black hole mergers are extremely complex phenomena and the physics behind is still not fully understood.

Figure 6.11 shows the comparison between the mean merger history and gas accretion history of SMBHs of mass $M_{\rm BH} \sim 10^7\,M_{\odot}$ predicted from DECODE and the results from Shankar et al. (2009) for sake of comparison. First of all, I found that the mass that black holes with present day mass $M_{\rm BH} \lesssim 10^8\,M_{\odot}$ gain via mergers is negligible with respect to the amount of mass acquired via gas accretion, covering a fraction of less than 1%. Furthermore, DECODE predicts a flat accretion history at very low redshifts ($z \lesssim 0.5$) in fair agreement with what found in Shankar et al. (2009). Later on, in the Master's thesis of Cherubini (2022) the author explored the effect of taking a broken power law or redshift-evolving $M_{\rm BH} - M\star$ relation, showing that the latter relations could potentially reproduce better the high-redshift growth histories of SMBHs.

6.6 Summary of the findings

In this Chapter, I have presented a holistic perspective via DECODE among galaxy star formation histories, merger histories, satellite abundances and intracluster light, which are intimately linked quantities in a hierarchical, dark matter-dominated Universe. I have also shown a proof-of-concept application of DECODE in predicting galaxy sizes and black hole merger rates.

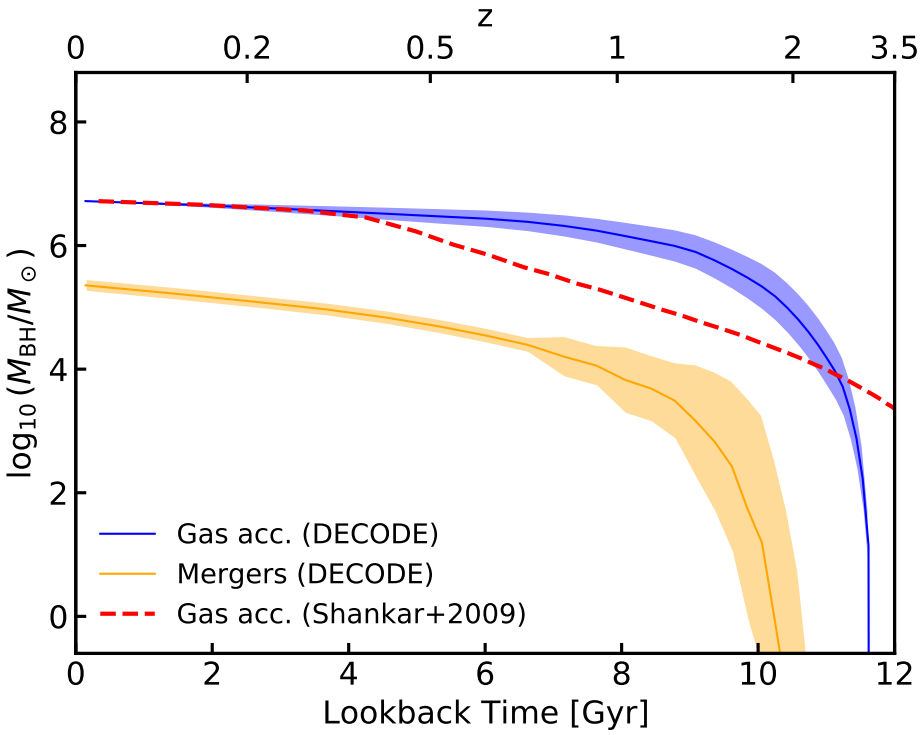

FIGURE 6.11: Mean mass growth histories from gas accretion predicted by DECODE (blue and orange solid lines with errors shown as shaded areas), compared to the results from Shankar et al. (2009, red dashed line), for black holes with mass $M_{BH} \sim 10^7\, M_\odot$ at $z = 0$.

The main results can be summarised as follows:

- A SMHM relation characterized by a weakly evolving low-mass end produces SFHs in relatively good agreement with those inferred from SED fitting in local surveys like MaNGA, GAMA and SDSS. Instead, fast evolving low-mass end of the SMF, suggested by some observational groups, are disfavoured.

- The evolution of satellites stellar mass does not affect the SFHs of central low-mass and intermediate-mass galaxies ($M_\star < 10^{11}\, M_\odot$), since mergers' contribution is relatively small compared to the total stellar mass assembly.

- For more massive galaxies ($M_\star > 3 \times 10^{10}\, M_\odot$) SED-based estimates of the SFHs do not currently agree with each other. Reproducing the approximately flat stellar mass growth histories inferred from GAMA requires a nearly constant SMF at all stellar masses and up to $z \sim 2$, in line with the recent suggestions of an increased star formation efficiency in massive galaxies at $z > 2$ from JWST data (e.g., Atek et al. 2023; Endsley et al. 2023; Labbe et al. 2023; Nelson et al. 2023).

- The merger histories of massive galaxies, with stellar mass above $M_\star > 10^{11}\, M_\odot$, have a relatively weak dependence on the type of post-infall satellite evolution implemented in DECODE, while the integrated SFHs and sSFRs evolution tend to

change by a factor of up to $\sim 2-3$ depending on the assumed satellite evolution after infall.

- The main sequence SFR-$M_\star$ relation implied by DECODE tends to be lower in normalization by a factor $\sim 2-3$ on average with respect to most observations at redshift $z > 0$.
- DECODE's SFR-$M_\star$ relation also shows signs of a flattening at $M_\star > 3 \times 10^{10}\, M_\odot$ but only at $z \lesssim 1$, which is independent of the merger rate but a natural by-product of the break in the SMHM relation. Including mergers in the models tends to further sharpen the drop in the main sequence above $3 \times 10^{10} - 10^{11}\, M_\odot$, as more massive galaxies tend to grow proportionally less via star formation.
- The assumption in DECODE of $\sim 20\%$ of stellar mass loss during mergers as well as stellar stripping in satellites within clusters, provides a good match to current constraints on the ICL at different redshifts and cluster halo masses, irrespective of the input SMHM relation.
- DECODE can relatively well reproduce the shape of the stellar mass-size relation of local galaxies.

In summary, DECODE represents a flexible and efficient data-driven approach to probe the self-consistency within a hierarchical, dark matter-dominated Universe, of the SMF with other key independent observational probes such as the star formation histories, mergers histories, satellite abundances and the ICL.

Chapter 7

Galaxy quenching

In Chapters 5 and 6, I have presented DECODE and how I used it to build a holistic and self-consistent framework, using as input observed stellar mass functions (SMF) in the abundance matching to predict merger rates, star formation histories, satellite abundances, morphologies and intracluster light in a data-driven fashion, which are all intimately connected observables. I now proceed in studying another crucial mechanism in controlling galaxy evolution, the quenching of star formation, via DECODE 2.0 (described in Section 3.3.4). In particular, I will focus my attention mainly on the halo quenching, and will briefly discuss other mechanisms such as black hole quenching, mergers and morphological quenching. In this Chapter, I will describe the data set utilized as input in DECODE 2.0 and will show what are the implications of the quenching mechanisms mentioned above on the stellar mass growth of central galaxies.

7.1 Empirical input scaling relations

In this Section, I describe the input data utilized in DECODE 2.0 modelling to compute the empirical relation that connect galaxies to dark matter haloes. More specifically, the empirical relation employed here connect the dark matter halo accretion rate (HAR) to the galaxy star formation rate (SFR). All the analysis and results shown in this Chapter are strictly based on the assumption that there is a monotonic increasing relationship between these quantities on average.

7.1.1 Input data

7.1.1.1 Dark matter haloes catalogue

I make use of the recipe described in Section 3.2.2 to generate a mock catalogue of $N = 10^5$ dark matter parent haloes at redshift $z = 0$ with mass $M_{\rm h,par} > 10^{11}\,M_{\odot}$,

equivalent to a box of 180 Mpc on a side, following the halo mass function (HMF) from Tinker et al. (2008). This choice represents a good balance between mass resolution, computational efficiency and statistical significance of the sample for massive haloes. I assign the accretion history individually to these dark matter haloes using the DIFFMAH code presented in Hearin et al. (2021), which well reproduces the mean mass accretion and halo mass variance of dark matter haloes in N-body simulations. In such a way, I have created a catalogue of haloes surviving down to redshift $z = 0$, each of them characterized by an individual mass assembly and accretion rate at every redshift, on top of which I perform my analysis.

For the abundance matching between the galaxy SFR and dark matter HAR, I make use of the HAR statistics computed for the parent dark matter haloes in my catalogue. However, since the catalogue is created by evolving backwards in time a sample of haloes in the local Universe, it will only contain the haloes surviving at $z = 0$. Therefore, the number of haloes gets gradually more underestimated towards higher redshifts since the mock catalogue will lack those haloes that have merged and/or disrupted. Such a discrepancy between the number densities of the objects in the catalogue and the one extracted from N-body simulations is corrected using the formalism put forward in Section 2.2 of Boco et al. (2023), who introduced a numerical factor to correct the underestimated halo mass and halo accretion rate functions. Following this recipe, the total HAR function at each redshift can be expressed as follows

$$\phi_{\rm true}(\dot{M}_{\rm h}) = \phi_{\rm cat}(\dot{M}_{\rm h}) \frac{1}{N_{\rm halo}} \sum_{i=0}^{N_{\rm halo}} \delta(\log_{10} \dot{M}_{\rm h} - \log_{10} \dot{M}_{{\rm h},i}) p_i \ , \tag{7.1}$$

where $\phi_{\rm true}(\dot{M}_{\rm h})$ and $\phi_{\rm cat}(\dot{M}_{\rm h})$ are the N-body and analytic HAR functions at given redshift z, respectively, and

$$p_i = p_i(M_{{\rm h},i}, z) = \frac{\phi_{\rm true}(M_{{\rm h},i}, z)}{\phi_{\rm cat}(M_{{\rm h},i}, z)} \tag{7.2}$$

is the weight assigned to each halo of the catalogue of mass $M_{{\rm h},i}$ at redshift z, to reproduce the true number of haloes at that specific mass and redshift. I have checked that the HAR at high redshifts computed from my catalogue with the Boco et al. (2023) correction is well consistent with the one that I computed directly from the MultiDark N-body simulation (Prada et al. 2012; Klypin et al. 2016).

Figure 7.1 shows the HAR function for all the parent haloes in the catalogue at redshifts $z = 0$ and $z = 1$, and I test the performance of the Boco et al. (2023) correction against the MultiDark simulation. The HAR function built from the catalogue at $z = 0$ well matches the reconstructed one by design, whereas the lack of objects at $z = 1$ is clearly visible in the figure (orange solid line). The underestimated number of haloes is well regained via the Boco et al. (2023) correction. The drop at the faint end of my distributions are due to the cut in halo mass at $M_{\rm h} \gtrsim 10^{11}\, M_{\odot}$.

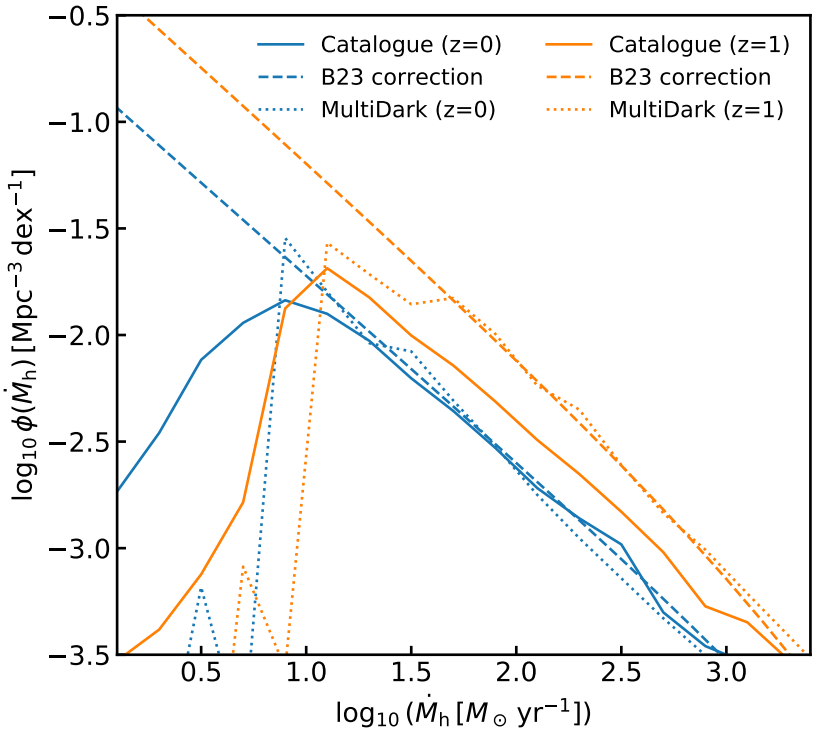

FIGURE 7.1: HAR function at redshifts $z = 0$ and $z = 1$ for the surviving parent haloes in the catalogue (solid lines), the reconstructed ones via the Boco et al. (2023) correction (dashed lines) and from the MultiDark simulation (dotted lines).

In principle, in order to compute the HAR at any redshift z greater than $z = 0$, one could generate a complete catalogue of haloes at redshift z from the HMF and derive the HAR rate from there. However, DIFFMAH allows only to simulate the accretion history of haloes from redshift $z = 0$ and, on the other hand, extracting the HARs at each redshift from an N-body simulation is extremely expensive. Therefore, for reasons of efficiency, I choose to rely on the HAR distributions computed via DIFFMAH and the Boco et al. (2023) correction, without losing any accuracy.

When performing the abundance matching, I make use of the HAR function that contains only haloes hosting star-forming galaxies because the SFR function contains only star-forming galaxies. Such HAR function is computed by manually discarding all haloes that contain quenched galaxies in each quenching model prescription (e.g., haloes with mass above the threshold mass for the halo quenching scenario), as described in Section 3.3.4. Figure 7.2 shows the HAR function for all the parent haloes in the catalogue, as well as those hosting star-forming galaxies for the halo quenching scenario, at redshifts $z = 0$ and $z = 2$. The resulting HAR function is characterized by a net drop in number density at high values due to the cut in halo mass.

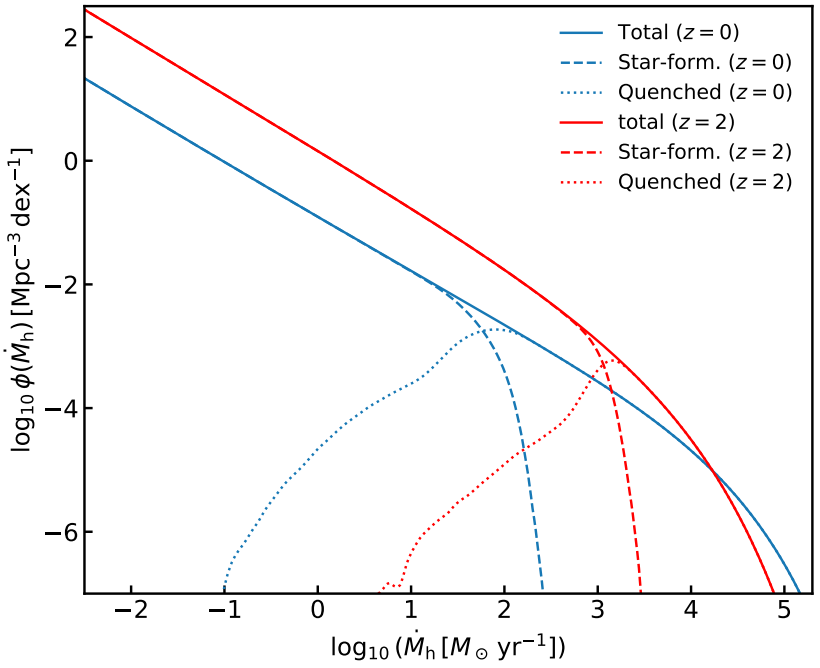

FIGURE 7.2: HAR function at redshifts $z = 0$ (blue lines) and $z = 2$ (red lines), for the halo quenching scenario where haloes hosting star-forming and quenched galaxies are distinguished by the mass threshold $M_\mathrm{h} \sim 10^{12}\,M_\odot$. The solid lines show the HAR functions for all the parent haloes, while the dashed and dotted lines show the distributions for haloes containing star-forming and quenched galaxies, respectively.

7.1.1.2 Observational input galaxy luminosity functions

The other ingredient to compute the SFR-HAR relation is the SFR function. I derive the latter from the observed galaxy luminosity functions (LF), whose determination is affected by several factors, such as observational bands and systematic errors. Depending on the survey, several works suggested different shapes of the LF. For example, Sargent et al. (2012) measured the IR LF and SFR function up to redshift $z \sim 2$ from the COSMOS and GOODS fields (Rodighiero et al. 2011). Other relevant determinations of the IR LF are those from Gruppioni et al. (2013) (*Herschel* PEP and HerMES surveys), Magnelli et al. (2013) (*Herschel*-PACS) and Koprowski et al. (2017) (SCUBA-2 and ALMA) and Gruppioni et al. (2020) (ALPINE-ALMA), covering up to redshift $z \sim 5 - 6$. More recently, Fujimoto et al. (2023) made an estimation of the IR LF by analyzing a large sample of sources from the ALMA Lensing Cluster Survey (Kohno et al. 2023) from redshift $z = 0$ up to $z = 7.5$, and Picouet et al. (2023) estimated the SFR function using the HSC-CLAUDS data (Aihara et al. 2019; Sawicki et al. 2019) up to $z = 2$ pushing the faint end down to SFR $< 10^{-2}\,M_\odot/\mathrm{yr}$.

Precisely measuring the LF is a challenging task, which depends on a number of factors, such as observational SFR estimates (depending on timescales, dust attenuation and selection effects) and the tracers (from the far-UV, IR to the radio). Currently available determinations of the LF have covered a wide range of redshift and luminosities.

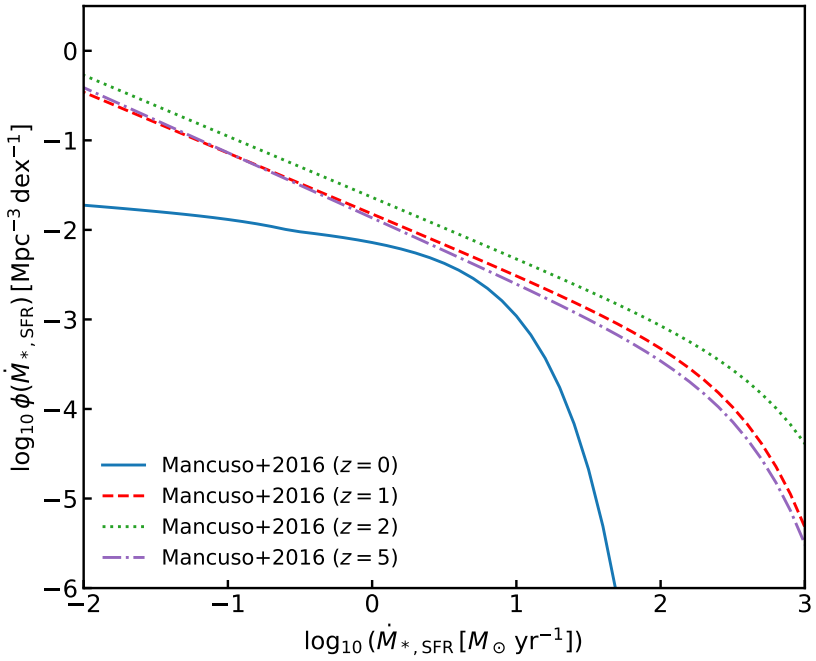

FIGURE 7.3: Star formation rate function from Mancuso et al. (2016) at different redshifts, as labelled.

However, each single data set can be affected by completeness issues depending on the sources. For instance, IR LF observations do not provide a good estimate of the faint end, where the UV component potentially dominates the sources. Indeed, such IR LF typically covers down to luminosities $L_{\mathrm{IR}} \sim 10^{10-10.5}\,L_\odot$ corresponding to a SFR of $\sim 1\,M_\odot/\mathrm{yr}$. Therefore, below that value of SFR the SFR function is just an extrapolation from the fits and should be taken with a grain of salt. Additionally, at the bright end IR inferred LFs tend to be underestimated, due to the presence of dust that dominates sources with SFR $\gtrsim 30\,M_\odot/\mathrm{yr}$ (e.g., Cai et al. 2014; Lapi et al. 2018; Adams et al. 2023).

Given these considerations, in what follows I make use of the SFR function from Mancuso et al. (2016) as input, who developed a robust model to merge the two sets of observations and built a complete LF and its evolution up to redshift $z \sim 3$, based on the UV and far-IR data from a wide range of surveys such as *Herschel*, SCUBA, ALMA and SPT. Figure 7.3 shows the SFR number densities from Mancuso et al. (2016) at different redshifts, that I use in my abundance matching. The SFR function is characterized by a relatively constant behaviour at high redshifts and drops quickly below $z \lesssim 1$, both at the faint and bright ends, possibly due to the formation of quiescent galaxies. In Appendix D, I show how DECODE's predictions change using SFR functions from other data sets (Sargent et al. 2012 and Fujimoto et al. 2023).

7.1.1.3 Empirical input data for black holes

As described in Section 3.3.3, the most straightforward way to grow SMBHs inside galaxies is to make use of several empirical relations connecting the BHAR and galactic properties. In particular, I consider the following three kinds of relation which would allow to assign accretion rates to black holes:

- observed specific BHAR distributions as a function of stellar mass;
- observationally measured BHAR-$M_\star$ relation;
- BHAR-SFR relation from abundance matching between the SFR function and BHAR function.

For the distributions of the specific BHARs, I consider the determination from Aird et al. (2018) based on the NIR galaxies from the CANDELS survey matched with the X-ray detected sources from the *Chandra* data. Using such specific BHAR distributions represents the most fashionable and rigorous approach to populate galaxies with black holes, consisting in assigning a specific accretion rate at each redshift to the black hole living in a galaxy following the measured distribution. However, this approach is affected by two difficulties. Firstly, since these are specific accretion rates, I would need to initialize the mass of the black hole at some high redshift using, for example, the $M_{\rm BH} - M_\star$ relation or any other initial conditional, which will introduce a further assumption to the model. Secondly, such distributions from Aird et al. (2018) are characterized by a very large error, especially at high redshifts, leading to output results that are difficult to be compared to observations.

For the BHAR-$M_\star$ relation, I consider the measurements from Yang et al. (2018) based on the data of the COSMOS and GOODS surveys (see also Carraro et al. 2020). This approach represents an easy way to assign the accretion rates to black holes by simply following the stellar mass of the host galaxies. However, such approach introduces further assumptions in the model, such as the specific X-ray luminosity distributions, and I tested that it does not always reproduce the observed AGN LFs.

Lastly, the BHAR-SFR relation can be computed via abundance matching between the BHAR function and SFR function (described in Section 7.1.1.2). The BHAR function can be derived from the observationally inferred AGN luminosity function (e.g., Shen et al. 2020) based on several optical, UV, IR and X-ray data. Luminosities are converted into accretion rates via the following relation

$$L_{\rm bol} = \epsilon c^2 \dot{M}_{\rm BH}\,, \tag{7.3}$$

where $\epsilon = 0.1$ is the radiative efficiency and c is the speed of light (e.g., Marconi et al. 2004). Once the BHAR-SFR has been computed, one can use it to assign the accretion

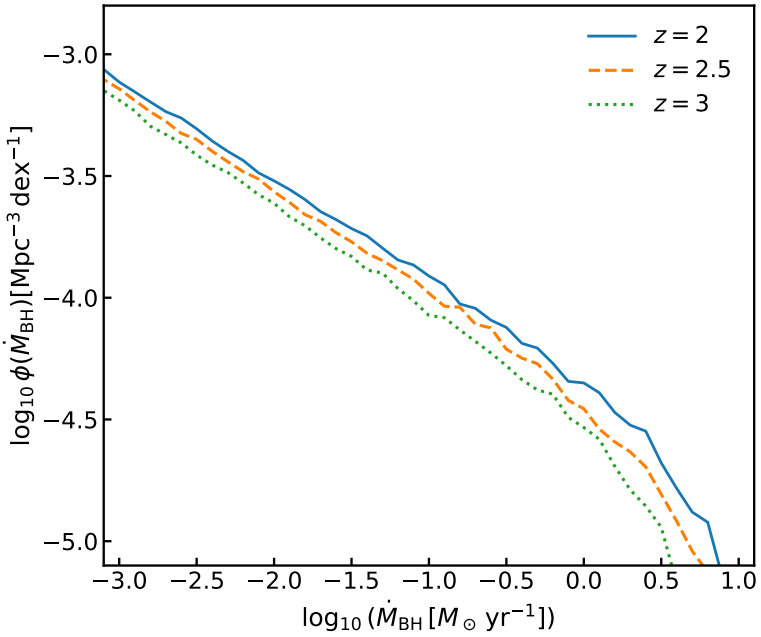

FIGURE 7.4: Black hole accretion rate function computed from Shen et al. (2020) AGN bolometric luminosity function at redshifts $z = 2$, 2.5 and 3, as labelled, using the conversion in Equation (7.3).

rates to black holes and integrate them across cosmic time. Figure 7.4 shows the number densities of the BHAR at redshifts $z = 2$, 2.5 and 3. Interestingly, similarly to the bolometric LFs from which they are computed, the BHAR function is characterized by a weak evolution at high redshifts.

7.1.2 The SFR-HAR relation

Figure 7.5 shows the SFR-HAR relation at $z = 0$ and 2 computed from abundance matching using the Mancuso et al. (2016) SFR function and the HAR function described in Section 7.1.1.1. The relation is shown for the halo quenching scenario, where haloes with mass above $M_{\rm h,lim} \sim 10^{12}\,M_\odot$ are removed. In particular, at redshift $z \sim 2$ the relation is well represented by a log-linear function with constant slope of ~ 1.5. Instead, towards lower redshifts, the SFR-HAR relation is characterized by a bending at high HARs, which already provides a hint on the gradual increase of the number of quenched galaxies, whose SFR drops while the host dark matter halo continues accreting mass.

Such SFR-HAR relations are then used to assign SFRs to galaxies and build up their stellar mass. I recall that, while in the case of halo quenching, the removal of quiescent objects from the dark matter halo statistics is straightforwardly performed by simply discarding haloes above the threshold mass, in the case of SMBH quenching the task is trickier. To remove the passive haloes in the latter case, I adopt an iterative approach,

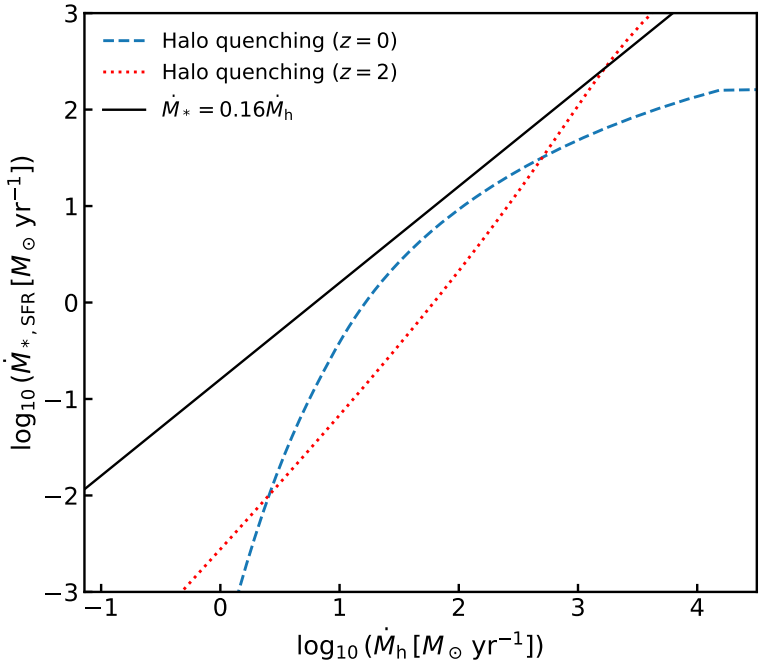

FIGURE 7.5: Star formation rate-halo accretion rate relation at redshifts $z = 0$ and 2 from the abundance matching using as input the star formation rate function from Mancuso et al. (2016) for the halo quenching scenario. The black solid line shows the limit $\dot{M}_\star = 0.16\dot{M}_\mathrm{h}$ relation.

by initially assuming that all haloes host star-forming galaxies at every redshift in the abundance matching and, then, remove passive objects gradually when galaxies are being quenched by their SMBHs.

7.1.3 The BHAR-SFR relation

Figure 7.6 shows the BHAR-SFR relation from the abundance matching using the Mancuso et al. (2016) SFR function and Shen et al. (2020) BHAR function described in Section 7.1.1.3. The BHAR-SFR is characterized by a power law relationship with roughly constant slope of ~ 1.55 across all redshifts.

In this Chapter, I will show only the results predicted by the abundance matching approach, which is safer compared to the former two described in Section 7.1.1.3. Once the BHAR-SFR relation is computed, I grow black holes in the same way as galaxies, i.e., by assigning them an accretion rate at each redshift following the SFHs of their host galaxies and integrating it across cosmic time. The simultaneous growth of black holes and their host galaxies will give us insights on the role of the black hole feedback on the quenching mechanism.

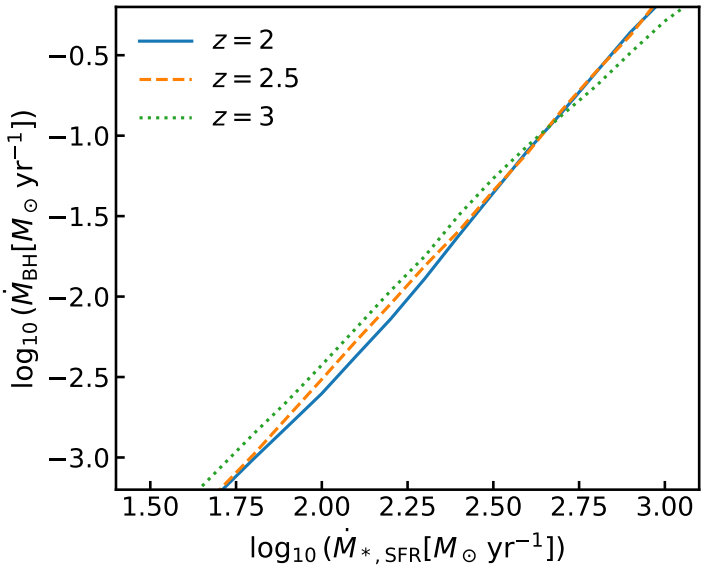

FIGURE 7.6: Black hole accretion rate-star formation rate relation from abundance matching at redshifts $z = 2$, 2.5 and 3, using as input the star formation rate function from Mancuso et al. (2016) and the black hole accretion rate function computed from Shen et al. (2020).

7.2 Halo quenching

In this Section, I show the predictions from DECODE 2.0 for the galaxy stellar mass assemblies for the halo quenching. In particular, I will show the output stellar mass-halo mass (SMHM) relations, SMF and fraction of quenched galaxies as predicted by DECODE 2.0 for the halo quenching scenario, and discuss how they compare to the latest observational determinations.

7.2.1 Examples of mass growth tracks

First of all, I show a schematic view of how I grow and quench galaxies following their host dark matter halo accretion histories. As described in Section 3.3, stellar mass assembly histories are computed by assigning SFRs following the HAR histories and by subsequently integrating the SFRs across cosmic time. On top of this, the stellar mass accreted by mergers with other galaxies is added using the methodology described in Section 3.3.2.1.

As mentioned in Section 3.3.4, to allow for some flexibility in DECODE 2.0 to fit the observed output quantities, I leave the threshold quenching halo mass and the dispersion around it as free parameters. To define their best-fitting values, I make use of a predefined grid for the two parameters and look for the best combination that minimizes the χ^2. The χ^2 is computed over the SMF and fraction of quenched galaxies from the COSMOS survey (Davidzon et al. 2017; Weaver et al. 2023). For the halo quenching

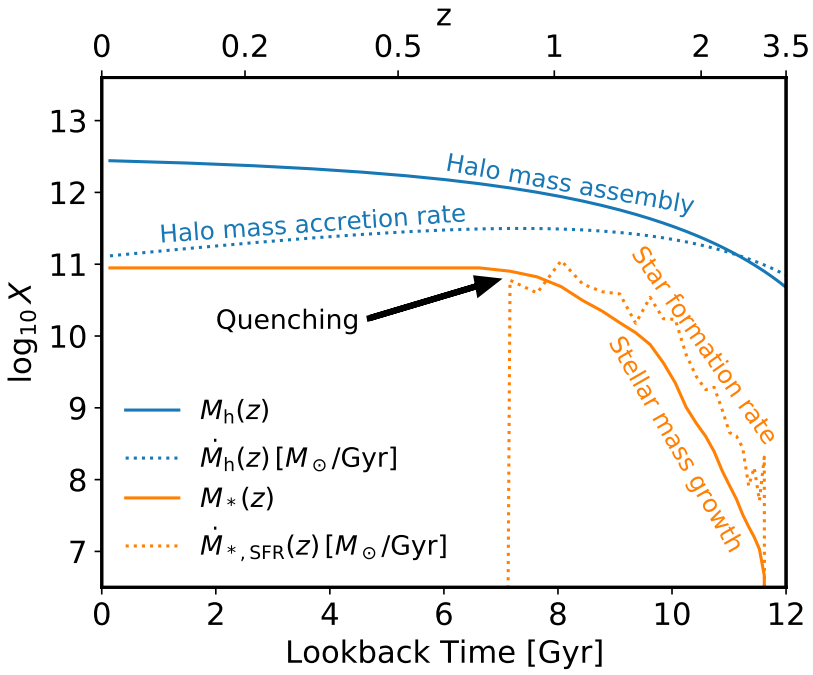

FIGURE 7.7: Example of evolution of one galaxy from the catalogue, for the case of halo quenching. The blue solid and blue dotted lines show the halo mass assembly and accretion rate history, respectively. The orange solid and orange dotted lines show the stellar mass growth and star formation rate, respectively. At redshift $z \sim 0.8$, when the halo mass reaches the threshold value, the star formation rate drops and the galaxy is quenched.

parameters, I predefine the following grid within reasonable values

$$\begin{aligned} &\log_{10}(M_{\mathrm{h,lim}}/M_\odot) \in \{11.8, 11.85, 11.9, ..., 12.5\} \\ &\sigma_{\log_{10} M_{\mathrm{h,lim}}} \in \{0.1, 0.15, 0.2, ...0.5\}\,, \end{aligned} \tag{7.4}$$

finding that the values that best fit the observed SMHM relation, SMFs and quenched fractions are $(\log_{10}(M_{\mathrm{h,lim}}/M_\odot), \sigma_{\log_{10} M_{\mathrm{h,lim}}}) = (12.25, 0.4)$. In what follows, I will show the results for this set of parameters.

Figure 7.7 shows an example of evolution of a quenched galaxy and its host dark matter halo in DECODE's catalogue, for the case of halo quenching. The galaxy initially forms stars at a rate given by the SFR-HAR relation following the dark matter HAR evolution. Then, at $z \sim 0.8$, when the halo reaches the critical mass of quenching, the SFR drops instantaneously and the galaxy is labelled as quenched in the catalogue. After being quenched the galaxy can still continue to grow in stellar mass *ex-situ* via mergers.

7.2.2 The stellar mass-halo mass relation

Having built up the mass assembly tracks of the galaxies in the catalogue, a first quantity that DECODE 2.0 can naturally predict is the SMHM relation at any redshift. I stress

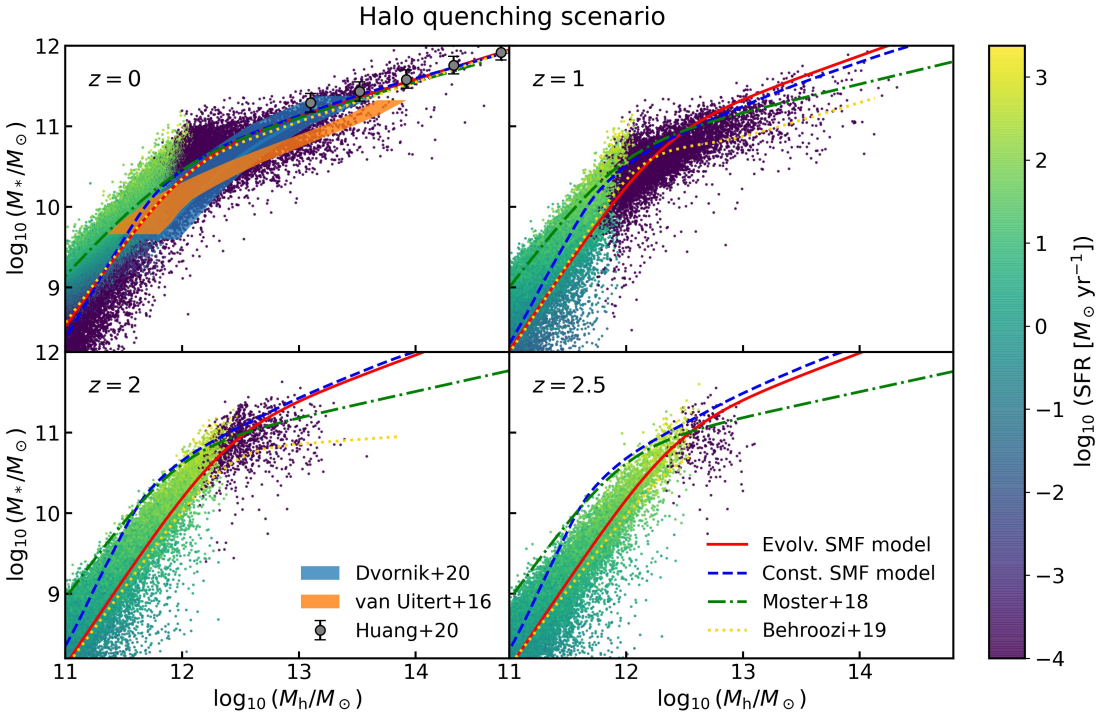

FIGURE 7.8: Distribution of the galaxies in DECODE's catalogue on the $M_\star - M_\mathrm{h}$ plane at redshifts $z = 0, 1, 2$ and 2.5, for the halo quenching scenario. The colour bar represents the star formation rate of the galaxies. The predictions of DECODE 2.0 are compared to the stellar mass-halo mass relation from weak lensing determinations at low redshifts from van Uitert et al. (2016) (orange shaded area), Dvornik et al. (2020) (blue shaded are) and Huang et al. (2020) (grey dots with error bars). I also show the stellar mass-halo mass relation for the evolving and constant stellar mass function models from the abundance matching in the first version of DECODE (red solid and blue dashed lines), as well as the relations from Moster et al. (2018) (green dash-dotted lines) and Behroozi et al. (2019) (yellow dotted lines), at the same redshifts.

again that, unlike in the first version of DECODE, the SMHM relation and its scatter are both predictions of DECODE 2.0. Figure 7.8 shows how the galaxies in DECODE's mock catalogue are distributed on the stellar mass-halo mass plane at different redshifts ($z = 0$, 1, 2 and 2.5) depending on their SFRs. I compare my predictions to the SMHM relations inferred by weak lensing determinations from the KiDS and GAMA surveys (van Uitert et al. 2016; Dvornik et al. 2020) and the Hyper Suprime-Cam survey (Huang et al. 2020). I also show, for comparison, the SMHM relations from abundance matching between the masses for the evolving and constant SMF models (described in Section 6.1), as well as those from UniverseMachine (Behroozi et al. 2019) and EMERGE (Moster et al. 2018). The SFRs of galaxies are shown via the colour bar.

I find that at high redshifts most galaxies are small and forming stars at higher rates, due to the higher accretion rate of their dark matter haloes. When moving towards lower redshifts, more massive galaxies are being formed and the number of quenched galaxies increases gradually. One can also note the role of the quenching threshold mass at $M_\mathrm{h} \sim 10^{12.25}\,M_\odot$, above which galaxies are mostly all quenched. Moreover,

at all redshifts the distribution of DECODE's galaxies in the $M_\star - M_\mathrm{h}$ plane is broadly consistent with the SMHM relations from mass abundance matching and from other theoretical models, especially at $z = 0$ both at the faint end and bright end. At $z = 0$, DECODE's SMHM relation is also in relatively good consistency with the relations observationally determined from weak lensing, further showing the quality of DECODE 2.0's predictions on the galaxy stellar mass assemblies. I also find that the scatter in stellar mass at fixed halo mass increases with redshift and decreases with halo mass, as also suggested by other works (e.g., Matthee et al. 2017; Allen et al. 2019; Erfanianfar et al. 2019).

7.2.3 The stellar mass function

I now show the ability of DECODE 2.0 to predict the statistical abundances of galaxies, described by the SMF, for the halo quenching scenario. While in the first version of DECODE the galaxy SMF is an input for the abundance matching, here it is an actual output of the model. Following the recipe from Section 3.3.2, I grow the galaxies in my catalogue and estimate the SMF for star-forming and quiescent galaxies at each redshift. Figure 7.9 shows the SMF for my galaxies for the halo quenching scenario, for redshifts $z = 0.35$, 1.75 and 2.75. I compare DECODE's predictions with the latest data sets on the SMF at the same redshifts from COSMOS2015 (purple triangles with error bars; Davidzon et al. 2017) and COSMOS2020 (red squares with error bars; Weaver et al. 2023), as well as that of SDSS at $z = 0.1$ (grey dots with error bars; Bernardi et al. 2017). The blue, orange and green solid lines show the SMF of all, quiescent and star-forming central galaxies in the catalogue, respectively. Similarly to the dark matter haloes, these are only the central galaxies surviving at $z = 0$ and such SMF towards high redshifts tends to be underestimated with respect to the *real* one due to the presence of missing galaxies that have merged or have been tidally stripped early on. I account for this discrepancy via the same correction from Boco et al. (2023) used for the dark matter, as described in Section 7.1.1.1. The red solid lines show the SMF of all galaxies including such correction for missing galaxies and also the addition of satellite galaxies (see Section 7.2.3.1 below). The red dashed lines show the extreme case where galaxies grow their stellar mass only via star formation and mergers do not take place.

I find that in the halo quenching scenario the predicted SMF is broadly in agreement with the COSMOS2015 and COSMOS2020 observed SMFs at all redshifts, except at $z \sim 1.75$ where it is slightly overestimated, as well as with SDSS. In particular, the high-mass end of the SMF produced by DECODE 2.0 is in excellent agreement with the observed ones, showing the efficacy of such quenching mechanism. Such a good consistency with the data in the brightest part of the SMF also witnesses the necessity of including mergers' contribution in the galaxy mass growth. Indeed, the plots show that

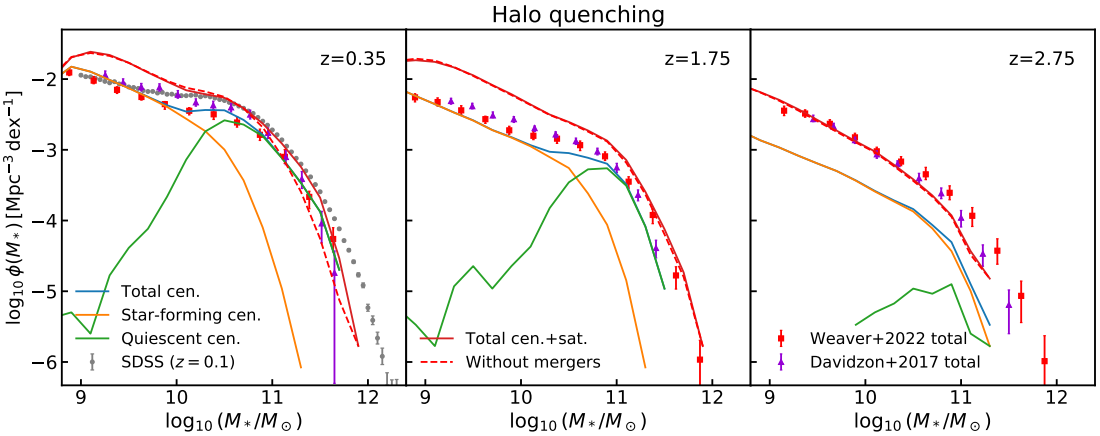

FIGURE 7.9: Stellar mass function predicted by DECODE 2.0 at redshifts $z = 0.35$, 1.75 and 2.75, for the scenario of halo quenching. The blue, orange and green solid lines show the stellar mass function for all, star-forming and quenched central galaxies surviving at redshift $z = 0$ in DECODE's catalogue. The red solid lines show the stellar mass function with the inclusion of non-surviving or merged galaxies at $z > 0$ and satellites, and the red dashed lines show the same case but without the contribution of mergers. The grey dots, red squares and purple triangles with error bars show the observational total stellar mass functions from the SDSS at $z = 0.1$ (Bernardi et al. 2017), COSMOS2020 (Weaver et al. 2023) and COSMOS2015 (Davidzon et al. 2017) surveys.

without the accretion from mergers the model does not produce enough massive galaxies, underestimating the massive part by a factor of up to ~ 0.3 dex at low redshifts, where the mergers become the most dominant mechanism for growing mass (see, e.g., Hopkins et al. 2010b; Grylls et al. 2020a; O'Leary et al. 2021; Fu et al. 2022).

7.2.3.1 Satellite galaxies

The total galaxy SMF, shown in Section 7.2.3, takes into account the satellite galaxies. While in the massive part of the SMF satellites are approximately negligible, in the fainter part below the knee they start to be more and more significant (e.g., Grylls et al. 2019; Fu et al. 2022). Therefore, it is important to have a good recipe to account for their contribution to the total galaxy abundance.

The satellites SMF is computed starting from the dark matter subhalo mass function (SHMF). I compute the SHMF according to the analytical correction to the parent HMF described in Section 3.2.3.2 (Equations 3.11 to 3.14), and I use it to generate the population of subhaloes in the same cosmological volume of the catalogue. Subsequently, I use the SMHM relation and scatter predicted by the model, shown in Section 7.2.2, to assign the satellite galaxies to the subhaloes and compute the satellites SMF from there. I then add the satellites SMF to the centrals SMF to estimate the total galaxy abundances.

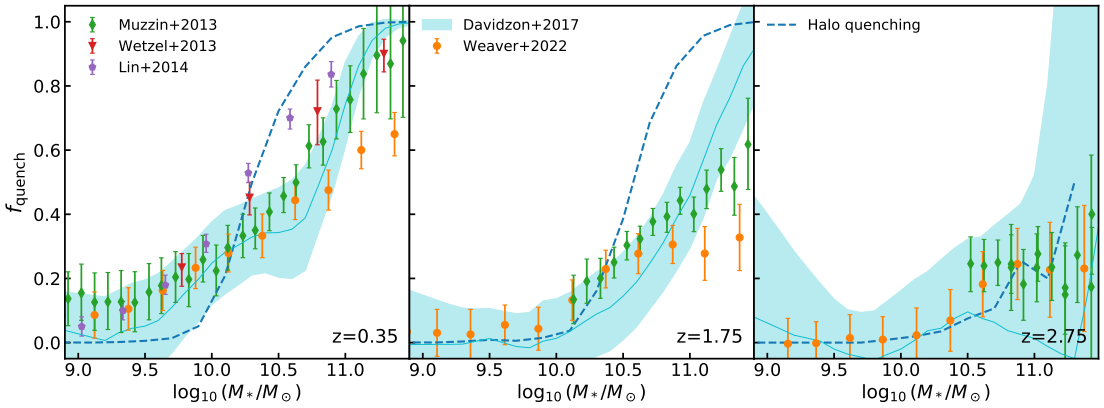

FIGURE 7.10: Fraction of quenched galaxies as a function of stellar mass at redshifts $z = 0.35$ (left panel), $z = 1.75$ (central panel) and $z = 2.75$ (right panel). The predictions from DECODE 2.0 are shown for the halo quenching as blue dashed lines. I compare DECODE's predictions with the observed quenched fractions from the COSMOS2015 (shown as cyan solid lines and shaded areas; Davidzon et al. 2017) and COSMOS2020 (shown as green dots with error bars; Weaver et al. 2023) surveys. Further data from Muzzin et al. (2013) (red dots with error bars), Wetzel et al. (2013) (purple triangles with error bars) and Lin et al. (2014) (brown pentagons with error bars) are shown for comparison.

7.2.4 Fraction of quenched galaxies

The comparison of the SMF is aimed at checking that DECODE's predicted galaxy abundances are reasonable with respect to observations. However, the optimal reproduction of the observed SMF is neither a self-consistency requirement since it is not an input of the model, nor the aim of this analysis since the study of the quenching is the main purpose of this part of the thesis. Indeed, the relative amount of star-forming and quiescent galaxies is the quantity of real interest that can provide information on the role of the two quenching scenarios investigated here.

Figure 7.10 shows the fraction of quenched galaxies as a function of stellar mass predicted by DECODE 2.0 at redshifts $z = 0.35$, 1.75 and 2.75, for the case of halo quenching, compared to those observationally inferred from the COSMOS/UltraVISTA (red dots; Muzzin et al. 2013), SDSS (purple triangles; Wetzel et al. 2013), Pan-STARRS1 Medium-Deep (brown pentagons; Lin et al. 2014), COSMOS2015 (cyan shaded areas; Davidzon et al. 2017) and COSMOS2020 (green dots; Weaver et al. 2023) surveys. The general behaviour of the quenched fraction is broadly reproduced. I note that towards higher stellar masses above the halo mass threshold, all galaxies are quenched, overestimating the quiescent fraction with respect to observations, while towards low stellar masses all galaxies in our catalogue are star-forming, which is clearly because they are galaxies that live in dark matter haloes below the critical quenching mass. Moreover, the implementation of the quenching mechanism depends on a small number of parameters, as discussed in Section 7.2.1, being the value of the critical halo mass and the scatter around the halo mass threshold. These parameters have a determining role in shaping

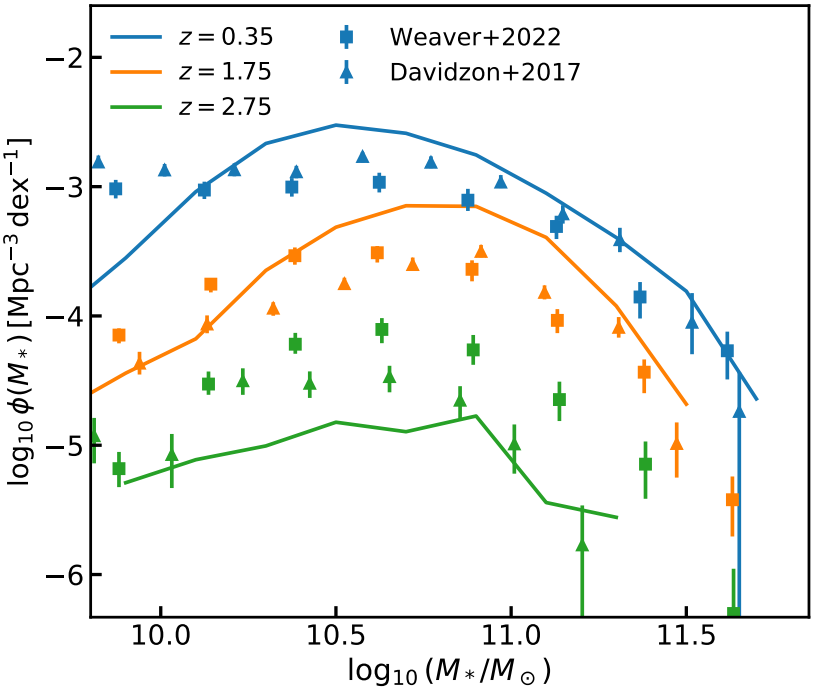

FIGURE 7.11: Stellar mass function of quenched galaxies for the halo quenching scenario (coloured solid lines) at different redshifts (represented by the colours), compared to those inferred by COSMOS2015 (Davidzon et al. 2017, coloured triangles with error bars) and COSMOS2020 (Weaver et al. 2023, coloured squares with error bars).

the abundances of quenched galaxies, with the fraction of quenched being shifted in stellar mass when varying the halo mass threshold and becoming steeper when using a smaller scatter.

The quenched fractions are calculated over the galaxies of my catalogue (surviving at $z = 0$). The universal validity of this prediction is based on the assumption of the Boco et al. (2023), which is equivalent to say that the missing galaxies in the catalogue at given stellar mass followed the same evolutionary history of the existing galaxies in the same stellar mass bin. This hypothesis is tested in Figure 7.11, where I show the SMF of quenched galaxies for the halo quenching scenario computed using the Boco et al. (2023), compared to the observationally determined SMFs from Davidzon et al. (2017) and Weaver et al. (2023). The comparison shows that at redshift $z \lesssim 2$ there is broad agreement between DECODE's prediction and the observed SMF. Instead, the underestimation of the quenched SMF at high redshifts may be due to fact that the value of redshift $z = 2.75$ is too close to the starting point of my simulation ($z \sim 3.5$) or, additionally, due to the need of other physical mechanisms to quench early-formed galaxies.

Moreover, interestingly, the very recent determinations from JWST (e.g., Nanayakkara et al. 2022; Carnall et al. 2023; Valentino et al. 2023; Dome et al. 2024) showed a relatively high fraction of quenched galaxies at high redshifts ($z \gtrsim 5$). A possible way to address

quenching at high redshifts with DECODE could be to start the simulation at a higher redshift z, instead of $z = 0$. However, unfortunately, with the presently available data on the SFRs at high redshifts, it is extremely difficult to test the quenching activity in galaxies with a fully data-driven semi-empirical model like DECODE. A possible solution could be to assume a parametric formula for the SFR-HAR relation, but risking in being trapped in the degeneracy between the parameters of the latter and of the quenching.

7.3 Black hole quenching

In this Section, I show the predictions from DECODE 2.0 for the scenario of quenching from black hole feedback. When exploring the quenching from feedback of the central SMBH, I first need to form and grow the latter in the catalogue. To do so, I assign the accretion rate to black holes following the BHAR-SFR relation computed via abundance matching, as shown in Section 7.1.3. Then the BHARs are integrated across cosmic time and truncated via empirical scaling relation. However, when performing the abundance matching between the galaxy SFR function and black hole LF, one is automatically assuming that the duty cycle, i.e., the probability of a black hole to be active ($P_{\rm AGN}$), is equal to ~ 1 at any redshift. This hypothesis is inconsistent with what other observational and theoretical works suggest, i.e., $P_{\rm AGN} \lesssim 0.1$ in the local Universe and $P_{\rm AGN} \sim 1$ at redshifts $z \gtrsim 2$ (e.g., Schulze and Wisotzki 2010; Goulding et al. 2010; Shankar et al. 2013b; Georgakakis et al. 2017; Aird et al. 2018; Man et al. 2019). Therefore, without accounting for the duty cycle, the resulting BHAR-SFR would be significantly altered at $z \lesssim 2$, making the abundance matching methodology not robust in modelling the growth of SMBHs. For this reason, in what follows, I will show the predictions for the black hole quenching only down to redshift $z = 2$.

In order to quench galaxies following the central SMBHs, a first attempt could be to use the $M_{\rm BH} - \sigma_\star$ relation, as mentioned in Section 3.3.4.2. However, using such relation is not trivial because one would need to make additional assumptions for assigning the stellar velocity dispersion to galaxies, following either galactic properties or halo properties (e.g., Ferrarese and Merritt 2000; Marsden et al. 2021; Zhang et al. 2024). Instead, a much safer and more straightforward way is to employ the $M_{\rm BH} - M_\star$ relation, and quench SMBHs and galaxies when their masses go beyond the mean relation. I assume a single power law for the $M_{\rm BH} - M_\star$ relation, following Equation (6.2), with the slope α and the normalization β being free parameters. Similarly to the halo quenching scenario, I also use the following predefined grid to search for the best-fitting parameters

$$\begin{aligned} \alpha &\in \{0.8, 0.85, ...1.1\} \\ \beta &\in \{-3, -2.9, ...0\}\,, \end{aligned} \tag{7.5}$$

where I left α varying around 1 and β in a reasonable range of values following the data from the works mentioned above. I find the best-fitting values to be $(\alpha, \beta) = (0.9, -2.6)$. In what follows, I will show the results for this set of parameters for the case of black hole quenching scenario only. Furthermore, in order to account for some dispersion around the mean $M_{\rm BH} - M_\star$ relation, I include a fixed scatter of 0.2 dex in black hole mass at fixed stellar mass, although the results do not alter significantly by employ other values within reasonable ranges. Such scatter is implemented by assigning a random Gaussian number $\log M_{\rm scatter}$ centered in 0 with standard deviation $\sigma = 0.2$ to each galaxy in the catalogue, which will be quenched when it reaches $\langle \log(M_{\rm BH}(M_\star) \rangle + \log M_{\rm scatter}$.

7.3.1 Examples of mass growth

Figure 7.12 shows two examples of evolution of galaxy and black hole from DECODE's catalogue, one steadily star-forming galaxy (upper panel) and one quenched galaxy (lower panel), in the assumption of black hole quenching only. For the star-forming galaxy, I note that, since the mass of the black hole is always below the $M_{\rm BH} - M_\star$ threshold relation, the galaxy continues to form stars throughout its life (down to $z = 2$). Instead, for the quiescent galaxy, I see that at $z \sim 2.25$ when the black hole overcomes the $M_{\rm BH} - M_\star$ relation, the galaxy immediately quenches its star formation rate and it continues to grow its stellar mass *ex-situ* only via the contribution of incoming mergers. I stress that here I assume a relationship between the galaxy SFR and black hole accretion rate from infalling gas. However, similarly to galaxies and dark matter haloes, another route where SMBHs grow their mass is via mergers (e.g., Hopkins et al. 2006; Shankar et al. 2009; Chen et al. 2019; Volonteri et al. 2020; Zhang et al. 2021).

7.3.2 The stellar mass-halo mass relation and fraction of quenched

Figure 7.13 shows the distribution of the galaxies in the catalogue on the SMHM plane (left panel) and the fraction of quenched (right panel) at $z = 2$, compared to the same data sets and theoretical models as in Figures 7.8 and 7.10, respectively. Similarly to the halo quenching scenario, also here the distribution of the galaxies in the mock is broadly consistent with the SMHM relation from mass abundance matching and other models. The general behaviour of the observed quenched fraction at $z = 2$ is also broadly reproduced when employing the black hole quenching. Instead, the SMF of quenched galaxies is slightly underestimated at high stellar masses when employing this quenching mechanism, supporting the idea that black hole quenching alone is not sufficient to quench massive galaxies, but still has a non-negligible role.

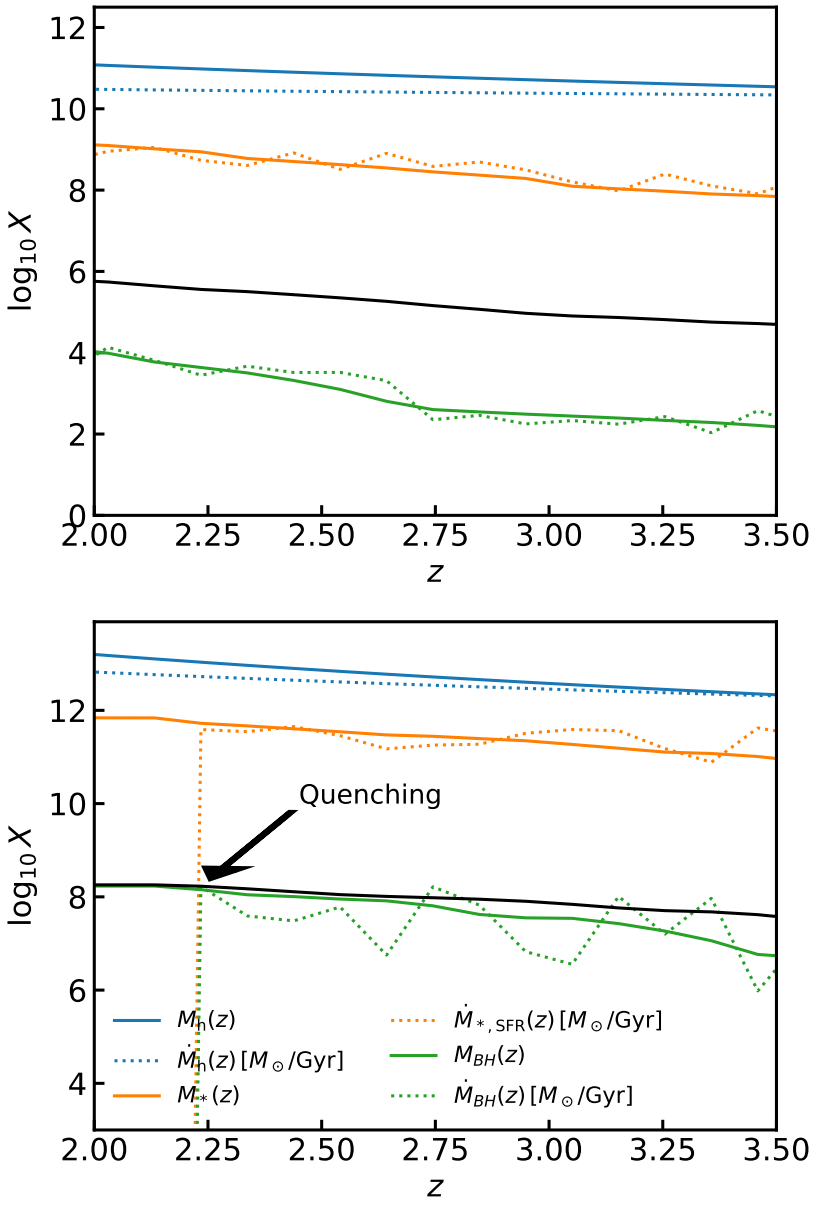

FIGURE 7.12: Upper panel: example of evolution of one steadily star-forming galaxy and its central black hole from the catalogue, for the case of black hole quenching. Lower panel: same as upper panel but for a quenched galaxy. The blue solid and blue dotted lines show the halo mass assembly and accretion rate history, respectively. The orange solid and orange dotted lines show the stellar mass growth and star formation rate, respectively. The green solid and green dotted lines show the black hole mass growth and accretion rate, respectively. The black solid lines show the $M_{\mathrm{BH}} - M_\star$ threshold used to quench the galaxy. At redshift $z \sim 2.25$, when the black hole mass reaches the threshold, both the black hole and the galaxy are quenched.

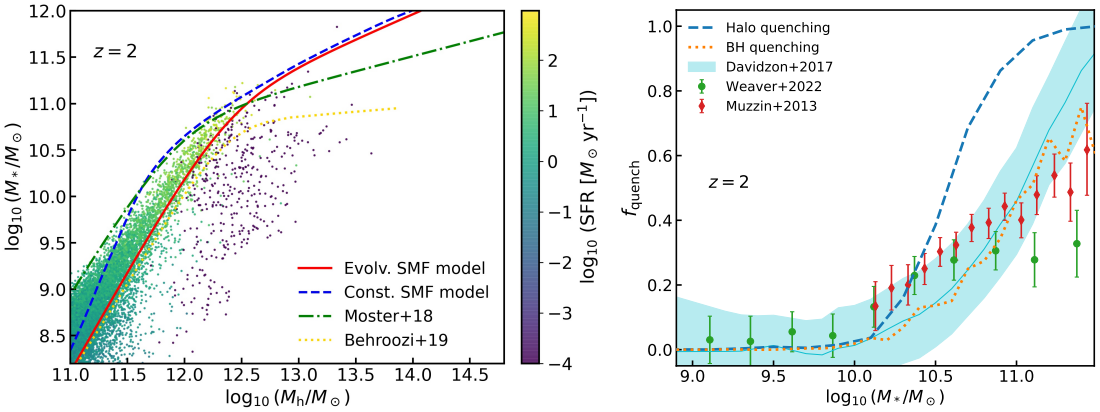

FIGURE 7.13: Left panel: distribution of the galaxies in DECODE's catalogue on the $M_\star - M_\mathrm{h}$ plane at redshift $z = 2$, for the black hole quenching scenario, compared to the SMHM relation from the same models as in Figure 7.8. The colour bar represents the star formation rate of the galaxies. Right panel: fraction of quenched galaxies as a function of stellar mass at redshift $z = 2$ for the black hole quenching scenario (orange dotted line), compared to the halo quenching scenario (blue dashed line) and the same other data sets as in Figure 7.10.

7.4 Further quenching mechanisms

In this Section, I study two additional quenching mechanisms, the role of mergers and the morphological quenching, and discuss what information DECODE can bring in this respect.

7.4.1 The role of major mergers in galaxy quenching

As discussed in Section 5.3, major mergers are found to be strictly linked to the formation of early-type quiescent galaxies. Indeed, when a major merger occurs, the interaction between the two merging galaxies causes a strong starburst due to the inflow of cold gas, which can extinguish the gas reservoir and quench the remnant galaxy (e.g., Mihos and Hernquist 1996; Hopkins et al. 2006, 2008; Sparre and Springel 2016). Major mergers are also thought to be connected to the triggering of AGN events, since the cold gas inflow from mergers can fuel the accretion of the central SMBHs (e.g., Di Matteo et al. 2005; Hopkins and Hernquist 2009; Treister et al. 2010, 2012). I have discussed in the previous Sections that feedback from the AGN of central SMBHs can heat or remove the available gas, halting the star formation. Below, I investigate whether there can be a direct link between major mergers and quenching events.

First of all, I attempt to directly model a quenching event through major mergers. To do so, to each central galaxy I assign an analytical merger tree via SatGen, as described in Section 3.3.2.1. Galaxies are assigned with a SFR and their stellar masses are built up in the same way, as done above. Then, each central galaxy that has undergone a major merger with mass ratio $M_{\star,\mathrm{sat}}/M_{\star,\mathrm{cen}} > 0.25$ will be labelled as quenched.

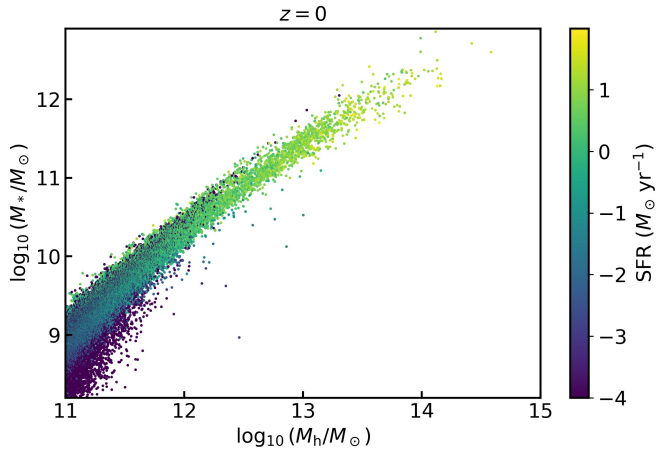

FIGURE 7.14: Same as Figure 7.8, but for quenching from major mergers model, at redshift $z = 0$.

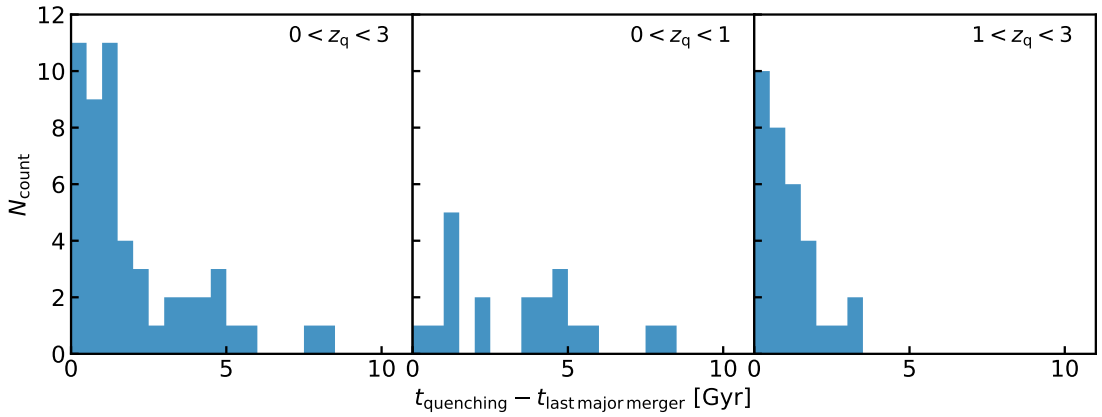

FIGURE 7.15: Distribution of the times elapsed from the last major merger until the time of quenching, for the complete model for different redshift at quenching bins, as labelled, and for galaxies with stellar mass above $M_\star > 10^{11}\,M_\odot$.

When converting SatGen's subhalo structures into merging satellite galaxies, I make use of the SMHM relation predicted by the model itself, which is initially computed assuming that all galaxies are star-forming and then updated iteratively while they are being gradually quenched by major mergers.

Figure 7.14 shows the resulting SMHM relation at $z = 0$ for the merger quenching model described above. As one can see, the DECODE 2.0 methodology cannot produce any quenched galaxy because, since initially all galaxy are assumed to be star-forming, all galaxies will be distributed on a SMHM relation characterized by a single power law with slope ≥ 1, as shown in Figure 7.14. However, if the SMHM relation does not show a break at high stellar masses with slope < 1, the predicted output major merger rate will be zero (as extensively discussed in Chapter 5) and therefore also the quenched fraction will be constantly zero at all stellar masses and all redshifts, in the assumption of quenching by major mergers.

Furthermore, I also check whether there are some connections between major mergers and quenching mechanisms. To do so, I reconsider the halo quenching model and compute the distribution of the time between the quenching and the previous last major merger, which is shown in Figure 7.15 for galaxies with stellar mass above $M_\star > 10^{11}\,M_\odot$ that covers the vast majority of quenched galaxies. The Figure shows that most of the values for the elapsed time are distribution below ~ 2 Gyr, supporting the idea that major mergers could potentially trigger quenching mechanisms in galaxies. Furthermore, interestingly, such dependency is mostly generated during quenching mechanisms happened at $z > 1$, while at lower redshifts I record fewer quenching events overall.

7.4.2 Morphological quenching

Finally, I discuss here the role of morphological quenching, which is another powerful mechanism that can halt star formation in galaxies living in less massive haloes, as described in Section 3.3.4.3.

To study the morphological quenching, I assign an effective radius R_e to each galaxy using the star-forming mass-size relation from Suess et al. (2019), and compute the surface density within this radius by integrating the Sérsic profile

$$I(R) = I_\mathrm{e} \exp\left\{ -b_n \left[\left(\frac{R}{R_\mathrm{e}} \right)^{1/n} - 1 \right] \right\}, \tag{7.6}$$

where b_n is approximated using Equation (18) from Ciotti and Bertin (1999). The Sérsic index n is assigned to galaxies following the empirical analytic fits from Huertas-Company et al. (2013, see also Marsden et al. 2021). Then, I halt the SFR instantaneously as soon as the surface density value goes above the threshold value of $\Sigma \sim 9\,M_\odot/\mathrm{kpc}^2$ (e.g., Xu and Peng 2021).

I find that, following this recipe, the morphological quenching is able to quench lower mass galaxies allowing to reproduce much better the observed SMF below the knee, at least down to $M_\star \gtrsim 5 \cdot 10^9\,M_\odot$. Also the fraction of quenched as a function of stellar mass increases to roughly 0.1, improving much the fit.

7.5 Summary of the findings

In this Chapter, I have studied the quenching processes in galaxy evolution via DECODE 2.0, investigating the role of the halo quenching mechanism. I have also discussed the role of other quenching mechanisms such as morphological quenching and major mergers.

The main results can be summarised as follows:

- When assuming the halo quenching scenario, DECODE's population of galaxies is able to well reproduce the mean SMHM relation measured by weak lensing observations such as van Uitert et al. (2016), Dvornik et al. (2020) and Huang et al. (2020) in the local Universe, as well as those from other theoretical works (EMERGE and UniverseMachine) up to $z \lesssim 3$.
- The same model can also well reproduce the bright end of the COSMOS SMF (Davidzon et al. 2017; Weaver et al. 2023) at all redshifts, but slightly overestimates the faint end of the SMF.
- The excess of objects at the faint end of the SMF may be due to the need of some other quenching mechanisms, e.g. morphological quenching, which is able to halt the star formation in galaxies with moderate stellar mass.
- Similar results are found for the black hole quenching scenario at redshifts $z \gtrsim 2$, which is able to relatively well reproduce the quenched fractions but is not enough alone to quench the most massive galaxies.
- The results of DECODE suggests a possible correlation between the quenching event and major mergers happened in each galaxy, supporting the theory that major mergers are involved in galaxy quenching by fueling the accretion of the central SMBH.
- Galaxies living in less massive haloes, below the golden mass, can quench their star formation via morphological quenching thanks to the existence of massive central bulges.

In summary, DECODE 2.0 constitutes a powerful tool to model galaxy evolution, especially allowing to directly test quenching mechanism recipes and their impact on the stellar mass assembly histories of galaxies.

Chapter 8

Conclusions

In this thesis, I have used DECODE, the Discrete statistical sEmi-empiriCal mODEl, to study galaxy formation and stellar mass growth, addressing particular attention to the interplay between mergers, star formation and quenching mechanisms. Using DECODE, I have provided a holistic perspective encompassing galaxy star formation histories (SFH), merger histories, satellite abundances, morphologies and intracluster light (ICL).

DECODE relies on discrete statistical populations of dark matter haloes and generates their merger trees via an input subhalo distribution function, and assigns to each subhalo the infall redshift and dynamical friction timescale using statistical density functions, that I fit and accurately test against N-body simulations. Then, dark matter assemblies and merger trees are converted into galaxy mass growths and merger histories via the input stellar mass-halo mass (SMHM) relation, computed via numerical abundance matching techniques which are very sensitive to the shape of the input stellar mass function (SMF). In the updated version of DECODE (2.0), dark matter assembly histories are converted into galaxy star formation histories via the input star formation rate-halo accretion rate (SFR-HAR) relation, computed via abundance matching as well. In both versions, thanks to the statistical nature, DECODE is flexible, rapid, and not affected by limitation in volume or mass resolution.

Firstly, I have extensively tested DECODE's self-consistency and performance against the Millennium dark matter-only simulation and the TNG hydrodynamical simulation in Chapter 4. Secondly, I have tested the role of several input photometries, SMFs, on several galactic properties such as satellite abundances and merger rates in Chapter 5. Then, I have presented DECODE's self-consistent predictions for the galaxy SFHs comparing with the latest data sets in Chapter 6. Lastly, I have investigated the role of quenching due to halo shock heating using DECODE 2.0, and have discussed the role of other quenching mechanisms in Chapter 7.

In this Chapter, I will summarize and discuss the main findings of this thesis (Section 8.1), and draw the final conclusions (Section 8.3).

8.1 Summary and discussion

8.1.1 The role of the stellar mass-halo mass relation in galaxy evolution

In this thesis, I have highlighted the intimate connection that exists in a hierarchical dark matter-dominated Universe among distinct observables, namely the SMFs, the SFHs, the merger rates, the abundances of satellites, and the amount of ICL. All of these probes are all sides of the same coin, and a comprehensive model of galaxy evolution should aim at simultaneously predicting these observations. However, the challenge arises when these independent data sets may suffer from underlying inconsistencies which would prevent a safe comparison between models and data. I have shown here that a semi-empirical, data-driven approach is the most suited to shed light on such possible discrepancies in the data, by using a subset of the data in input and others in output. DECODE, in particular, uses the SMF as input to predict the SMHM relation, and from there predicts the SFHs, merger rates, and ICL fractions using very minimal additional input assumptions and parameters.

Preferred stellar mass function, merger rates, satellites, morphologies and B/Ts

As discussed in Sections 5.1 and 6.1, the galaxy SMF is far from being well known, especially at high redshifts, and many works suggested different (and sometimes contrasting) results, in terms of shape and/or evolution in time (e.g., Tomczak et al. 2014; Bernardi et al. 2013, 2016, 2017; Davidzon et al. 2017; Huang et al. 2018; Kawinwanichakij et al. 2020; Leja et al. 2020; Weaver et al. 2023). The fact that DECODE starts from the SMF to compute the SMHM relation, makes DECODE a powerful tool to set more stringent constraints on the SMF. The tests conducted in this thesis show a preference for SMFs characterised by a larger number of massive galaxies and a significant evolution in time at the bright end ($M_\star \gtrsim 10^{11}\,M_\odot$). These SMFs generate SMHM relations that, in turn, produce a sufficient number of mergers to match the local fraction of ellipticals, satellite abundances, and BCG growths. This work highlights the fact that, for a fixed dark matter merger tree, the major merger rates and other quantities strongly depend on the mapping between stellar mass and halo mass, which in turn depends on the systematics, shape and evolution of the SMF (see also, e.g., Stewart et al. 2009a; Hopkins et al. 2010a; Grylls et al. 2020a). In this thesis, I also found evidence for the need of disc instabilities to boost the formation of bulges at lower stellar masses. This result is in line with the general notion of fast and slow rotators (e.g., Bernardi et al. 2019; Domínguez Sánchez et al. 2020), which suggests that the former dominates at $M_* \lesssim 10^{11.5} M_\odot$ and

the latter at $M_* \gtrsim 10^{11.5} M_\odot$, or also with the distinction between pseudo and classical bulges (see discussions in Gadotti 2009; Fisher and Drory 2010; Shankar et al. 2012, 2013a and references therein). Similar findings are retrieved in semi-analytic models. Guo et al. (2011) found that at stellar masses $M_* \gtrsim 10^{11}\, M_\odot$ mostly all galaxies have a $B/T > 0.7$, and mostly $B/T < 0.7$ below the same stellar mass threshold, in line with the results of this thesis. Similar conclusions are derived from GALICS and the TNG simulation, as well as from other works in the literature (e.g., Rodriguez-Gomez et al. 2015; Tacchella et al. 2019; Kannan et al. 2015; Fontanot et al. 2015).

The stellar mass function and star formation histories

Furthermore, to study the galaxy SFHs, I explored two additional SMF models, one with an evolving and another extreme one with a constant SMF up to $z \sim 1.5$. A slowly evolving SMF at low masses predicts SFHs in good agreement with those retrieved from SED fitting from local data. For galaxies above the knee of the SMF instead, data suggest quite flat SFHs up to $z \sim 3$, which would align with the SFHs from a constant SMF at low masses. I found a preference for a SMF characterized by a weak evolution in time at the faint end and by a bright end with flatter slope and significantly evolving. These features allow to predict SFHs for central galaxies with stellar mass today $M_\star \lesssim 10^{11}\, M_\odot$ that well match the observed ones (Section 6.3) and to produce enough major mergers to simultaneously reproduce the fraction of ellipticals, satellite abundances and B/T distributions in models in which ellipticals are predominantly originating from major mergers (Chapter 5).

Moreover, a SMF with a flatter and evolving high-mass end would be in agreement with the findings of significantly high volume densities of massive star-forming galaxies at $z > 3$ from deep ALMA and radio surveys, likely to provide a conspicuous contribution to the high-z SFR density (HST-dark galaxies, e.g., Franco et al. 2018; Wang 2019; Gruppioni et al. 2020; Talia et al. 2021). The existence of similar numbers of high-z massive star-forming systems is a real challenge for the existing semi-analytical models (e.g., Henriques et al. 2015) and hydrodynamical simulations (e.g., Pillepich et al. 2018a), which underestimate their number density by one to two orders of magnitude (see also Wang 2019). Recent observations with JWST extended these results to even higher redshifts, i.e., $z = 8$, finding heavily dust-obscured, massive ($M_\star \sim 10^{10}\, M_\odot$), star-forming sources at $z \sim 2 - 8$ with a surface densities of $\sim 0.8\,\mathrm{arcmin}^{-2}$ (Barrufet et al. 2023; Nelson et al. 2023). This suggests that an important fraction of massive galaxies may have been missing from my cosmic census at $z > 3$ all the way to the Epoch of Reionization.

The shape and evolution of the main sequence

I have also found that the main sequence as observed by several surveys is higher in normalization or flatter in slope at low masses than DECODE's predictions, and are not always in line with their observed stellar masses (e.g., Whitaker et al. 2014; Speagle

et al. 2014; Tomczak et al. 2016; Pearson et al. 2018; Popesso et al. 2023; Pearson et al. 2023). Leja et al. (2015) extensively discussed this problem and, following a continuity equation approach to evolve galaxy stellar mass growths forwards in time, also found that a main sequence with steeper low-mass end is more suitable to fit the observed SMFs. Similar results are put forward by Leja et al. (2019b), where they evolved the galaxy SMF backwards in time with the SFRs from the 3D-HST catalogues. Similarly, by deriving the SFRs directly from the stellar mass assemblies, which by design fit the mass function, I have also found a main sequence which is lower in normalization and steeper in slope than those suggested by some observations cited above, whilst consistent with those from simulations (see, e.g., Donnari et al. 2019). Moreover, I have found that the main sequence presents a break and drops towards high stellar masses, especially at lower redshifts. In my semi-empirical modelling, the shape of the SFR-$M_\star$ relation is a direct by-product of the SMHM relation. As the latter is a double power law, also the main sequence tends to present a similar shape. However, the break in the SFR-$M_\star$ relation changes significantly with redshift, moving from $2 \times 10^{11}\ M_\odot$ at $z \geq 2$, to $3 \times 10^{10}\ M_\odot$ at $z < 1$. Therefore, the main sequence does not present any significant break or flattening up to high stellar masses of a few $10^{11}\ M_\odot$ at high redshifts, with a flattening appearing only below $z < 1$, more or less pronounced depending on the shape of the input SMHM relation. This behaviour in the predicted main sequence is visible even in the extreme case where mergers are not included in the model (see Figure 6.6). When mergers are self-consistently included, they become the dominant process in the stellar mass assembly of massive galaxies at low redshifts leading to a further, more marked drop in the SFR, irrespective of the input SMF model. On the other hand, towards higher redshifts galaxies are still in an active star-forming phase where merger's contribution is less with respect to lower redshifts, and the flattening in the main sequence is barely visible. My results are in line with the recent works that found a flattening in the slope of the main sequence at high stellar masses, e.g., Leja et al. (2022) and Popesso et al. (2023), who suggested that such a curvature in the SFR-$M_\star$ relation is most likely due to the suppression of the SFR in galaxies.

The intracluster light

Finally, in this work, I also found evidence for the need of both mergers in addition to the stellar stripping to form the ICL at all stellar masses. This finding is in line with what is found by several observational and theoretical works (see, e.g., Puchwein et al. 2010; Rudick et al. 2011; Burke et al. 2012; Contini et al. 2014, 2018; Contini 2021; Montes and Trujillo 2018, 2019). Indeed, for example, Contini et al. (2014) showed in their semi-analytic model that mergers can form up to $\sim$ 20% of the mass of the ICL in massive clusters. Furthermore, many works, such as Montes and Trujillo (2018) and Contini and Gu (2020), suggested that the stellar stripping forms gradually more mass in the ICL during redshift evolution. The very recent work of Contini et al. (2023) showed that the fraction of ICL also slightly depends on the halo mass, increasing with the latter and

then staying steady at ~ 0.35, similarly to what I found. These findings are based on the assumption that 20% of the mass of the merging satellites is lost during mergers, which is the value assumed in most of the semi-analytical models in the literature and allows a good compromise between mergers, SFHs and ICL.

8.1.2 The role of quenching in galaxy growths

In this thesis, I have underlined the importance of having good quality and complete data on the galaxy SFR distributions for building up galaxies in a semi-empirical model such as DECODE 2.0. I have chosen to use the analytic fit from Mancuso et al. (2016) which covers a wide range of SFR values and redshift. Such SFR function is also in relatively good agreement with the most recent observationally inferred SFR function (e.g., Katsianis et al. 2017; Picouet et al. 2023) across a wide range of redshifts and luminosities. The choice of this SFR function implies a SFR-HAR that produces galaxy abundances in agreement with the observed SMFs, when assuming the quenching mechanisms studied in Chapter 7.

I found that the halo quenching mechanism is efficient alone in halting star formation in massive galaxies ($M_\star \gtrsim 10^{10.5}\,M_\odot$), being able to well match the observed quenched fractions up to $z \sim 2$. However, at redshifts $z \gtrsim 2$ DECODE's predictions for the quenched abundances are not in agreement with those data sets, and not even with the data from JWST at $2 < z < 4$ (Bluck et al. 2023b). Such inconsistency may be due to the presence of galaxies that have merged at $z > 0$ whose stellar masses formed at very early stages with a huge star burst (e.g., Cole et al. 2023) before being rapidly quenched, while in DECODE I considered only galaxies surviving at $z = 0$ and the statistics might be biased when gradually moving towards higher redshifts. Moreover, I found that morphological quenching is helpful in producing less massive quenched galaxies, in haloes with more moderate mass, further improving DECODE's fit of the quenched fraction over a wider stellar mass range.

Finally, I explored various possibilities of modelling the growth of SMBHs in DECODE 2.0 to study the quenching due to the central SMBH feedback. Such analysis is extremely challenging due to the problems discussed in Section 7.3, which may be improved by making further assumptions in the model. For example, growing black holes via the distributions of their specific accretion rates can be performed by initializing the black hole mass via an input scaling relation or black hole mass function. On the other hand, the abundance matching could be performed by assuming an input duty cycle as a function of mass and redshift. All these inputs will add layer of complexity and assumptions to the model, getting farther from the initial idea of simplicity of DECODE and potentially leading to a multi-parametric model. From the preliminary analysis of this thesis, SMBH feedback is a crucial, but not only, mechanism able to quench

intermediate-mass and massive galaxies. I found that the SMBH feedback is an important quenching mechanism to quench intermediate-mass and massive galaxies, at least down to redshift $z = 2$, where the accuracy of the abundance matching is still not affected by the duty cycle.

8.2 Future plans

In a future perspective, the work presented in this thesis, especially the work presented in Chapter 7, could be further expanded in order to be consolidated. I will discuss below the further tests on DECODE 2.0 and some of possible future enrichment that I plan to perform. These include the test on the abundance matching and the implementation of several other physical processes and features such as the morphological quenching, size evolution, bulge and disc growths, black hole growth and quenching due to feedback processes.

First of all, the existence of a monotonic relationship between the galaxy SFR and dark matter HAR is a mere assumption of DECODE 2.0. In order to test the trustworthiness of this hypothesis, I plan to make use of the data from a comprehensive hydrodynamical simulation, such as the TNG simulation, which is by definition self-consistent. In particular, I would extract the SFR-HAR relation from the simulation directly, along with their statistical distributions, and perform the abundance matching between the latter to test if the empirical relation could be reconstructed at some level of preciseness. Moreover, additional secondary tests are the impact of different values of the scatter in SFR at fixed HAR and the binning in cosmic time, although some works have found that these features do not alter significantly the stellar mass assemblies of galaxies (e.g., Boco et al. 2023).

Once DECODE 2.0 is fully tested, I would like to enrich the model as follows:

- further investigate on the role of the morphological quenching by making use of the recipe described in Section 7.4.2;
- implement other features in DECODE 2.0, such as the size, bulge and disc evolution, which will make the model more complete;
- implement the formation and growth of central supermassive black holes, by employing observationally inferred accretion rate distributions and duty cycles;
- implement and test the quenching due to SMBH (or AGN) feedback, by employing empirical relations between, e.g., black hole mass and galaxy stellar velocity dispersion.

Finally, by performing a simultaneous comparison with the latest observational determinations of the galaxy stellar mass function, relative amounts of star-forming and quenched galaxies, stellar mass-halo mass distributions, black hole mass-stellar mass relation, AGN luminosity function, etc., one could fully test the robustness of the model and make considerations on the relative role of each physical mechanism involved.

8.3 Closing

In conclusion, I have presented my semi-empirical model DECODE in both its versions. DECODE constitutes a complementary tool to existing models for probing galaxy evolution and the relevant physical processes involved therein in a flexible and efficient data-driven approach. More particularly, I have used the first version of DECODE to probe the self-consistency within a hierarchical, dark matter-dominated Universe, of the SMF with other key independent observational probes such as the merger rates, star formation rates, the satellite abundance, morphologies, structural properties and the ICL, comparing to the latest data sets, by using minimal input parameters, namely the SMHM relation and the scatter in stellar mass at fixed halo mass. My study suggests that a SMF characterized by more massive galaxies, a fastly evolving bright end in normalization and slowly evolving faint end, is the most suitable to predict the aforementioned quantities simultaneously and self-consistently, despite the observational heterogeneity between the data sets. Both the analyses from DECODE and with the TNG hydrodynamical simulation suggest that the less massive galaxies ($M_\star \lesssim 10^{11}\,M_\odot$) grow their stellar mass mainly via star formation, while more massive ones ($M_\star \gtrsim 10^{11}\,M_\odot$) formed stellar mass via star formation at earlier time and continue to grow via mergers after having been quenched. Furthermore, I have used the last version of DECODE, which grows galaxies by using an input SFR-HAR relation, to test the role of diverse quenching scenarios, such as quenching due to halo, SMBH feedback, major mergers and morphological quenching. The analysis suggests that each quenching mechanism is relevant at different stellar masses and redshifts, and that the accretion and feedback from central SMBHs are strictly connected to the growth of the host galaxies.

Finally, DECODE will also constitute a very precious instrument for generating robust galaxy mock catalogues for the upcoming large-scale extra-galactic surveys such as LSST (Ptak and LSST Galaxies Collaboration 2011). The advent of new high-quality data from ongoing surveys, such as JWST (Gardner et al. 2006) and Euclid (Amiaux et al. 2012), which will provide self-consistent determinations of the galaxy SMF and SFRs, will be extremely beneficial for building a more comprehensive and complete theoretical model of galaxy evolution.

Appendix A

Testing the self-consistency of DECODE's stochasticity

In this Appendix, I check the self-consistency of my approach in DECODE (referred to as *discrete* method) in reproducing the average properties of dark matter haloes and galaxy evolution. To do so, I develop a variant of DECODE, which I refer to as *weighted* method. I here describe the details of the weighted method. I reiterate that the weighted method is more difficult to generalise to all model variants, for example when multiple galaxy properties are included in the evolution, which makes the discrete method more flexible to grow each single galaxy. Therefore, in the main body of this thesis I make use of the discrete method only, whilst here I make use of the weighted method to test some simple scenarios in the discrete method.

First of all, I focus the attention on the merger history of dark matter haloes. To compute the latter, in the weighted method I employ the recipe from Section 3.1.3 of Grylls et al. (2019). Such approach is based on statistical weights, which are defined as the

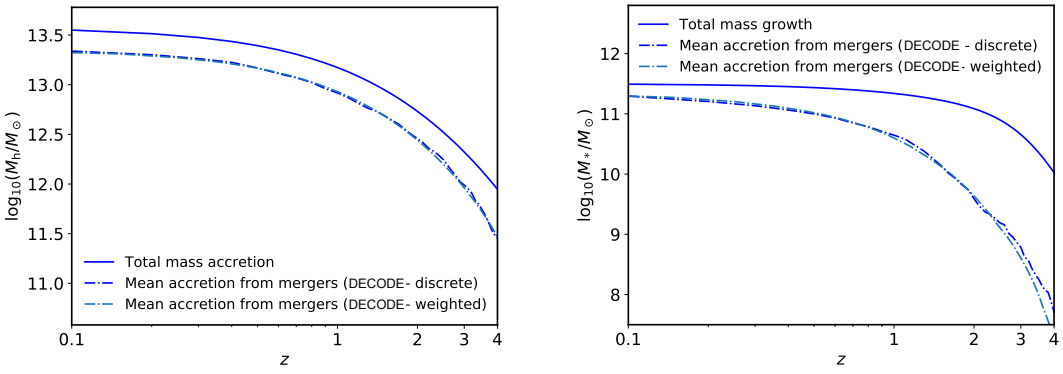

FIGURE A.1: Left panel: total halo mass accretion history (solid line) along with the comparison between the merger history of from the discrete and weighted methods (dashed lines). Right panel: same as upper panel but for galaxy stellar mass.

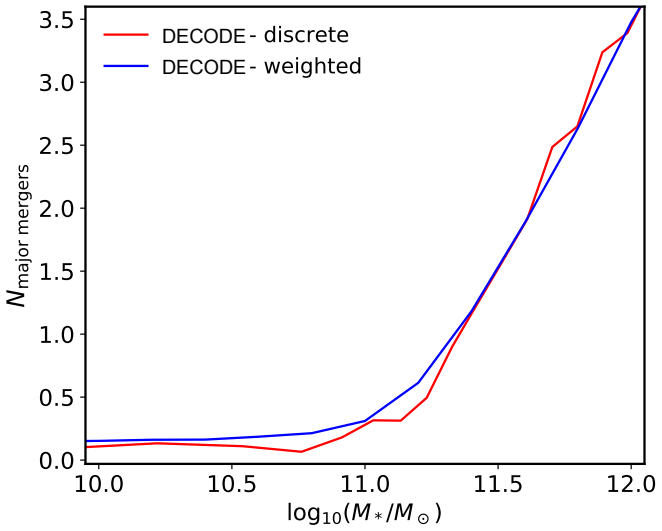

FIGURE A.2: Number of major mergers predicted by the discrete version of DECODE compared to that computed with the weighted method.

difference of the SHMF between redshifts z and $z + \mathrm{d}z$ at given subhalo mass and interpreted as the probability of the infalling subhaloes in the given mass bin. In simpler words, the weight, at given redshift step and mass bin, is the fractional average number ($\in \mathbb{R}^+$) of subhaloes of that mass which cross the virial radius of the parent halo at that redshift. The comparison between the weighted and discrete methods for one parent halo mass bin is shown in the left panel of Figure A.1, where the total mass assembly history of van den Bosch et al. (2014) is also shown for completeness. Despite the fact that in the discrete method I perform my analysis on the assumption of identical mean accretion for all haloes competing to the same bin of host halo mass at $z = 0$, the resulting mean contribution from subhalo mergers in the discrete method appears to be in very good agreement with the one computed from the weighted method, further supporting the validity of DECODE's discrete approach.

Similarly to the host dark matter haloes, the right panel of Figure A.1 compares the merger contributions to the central galaxy stellar mass growth computed via the discrete and weighted methods, as labelled, showing again very good agreement between the two methods. I note that this agreement is, as expected, independent of the choice of the input SMHM relation or dynamical friction timescales, as long as the same parameters are adopted in both methods.

I also provide the number of major mergers, implied fraction of ellipticals and mean B/T ratios as predicted from the two methods in Figures A.2, A.3 and A.4, respectively. The selection of the major mergers and the ellipticals in the discrete method is already described in Section 5.3. In the weighted method the number of major mergers is computed by directly integrating the merging satellites SMF at each redshift over the range

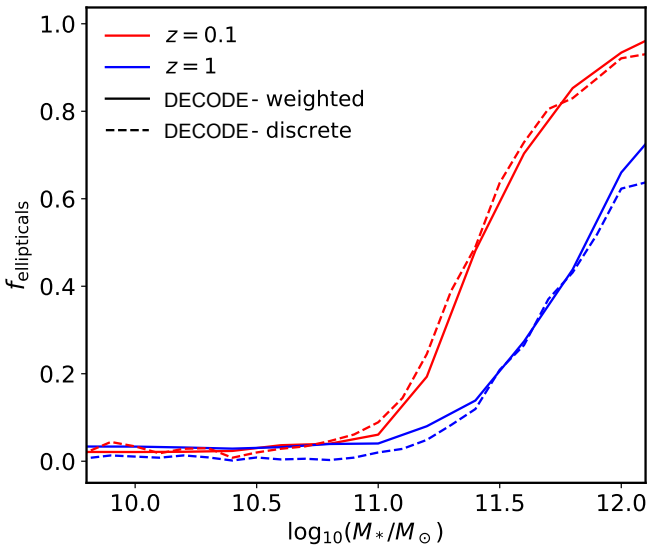

FIGURE A.3: Fraction of ellipticals predicted by the discrete version of DECODE compared to those computed with the weighted method, for redshifts 0.1 and 1.

of mass $M_{*,\rm sat}/M_{*,\rm cen} > \mu$, with μ being the major mergers mass ratio threshold. Concerning the fraction of ellipticals, I also label the galaxies that had at least one major merger as ellipticals, similarly as I do in the discrete method. To this purpose, I initialize the fraction of ellipticals at redshift $z_{\rm ini} = 4$ equal to 0, assuming that all galaxies are disc-like at high redshifts. From that epoch, I proceed forwards in time and at each redshift I analytically compute the probability of a galaxy to have had at least one major merger, which I interpret as the fraction of ellipticals itself, according to the following formula

$$\mathcal{P}_{\rm 1MM} = 1 - \mathcal{P}_{\rm MM}^{W} \,, \tag{A.1}$$

where $\mathcal{P}_{\rm 1MM}$ is the probability of having at least one major merger, $\mathcal{P}_{\rm MM}$ is the probability of a generic merger to be a major one, and the exponent W is the weight integrated over the major mergers stellar mass range. At each time step, I update the fraction of spirals and ellipticals according to Equation (A.1). Finally, I also provide the comparison of the B/T ratio for Model BT2 (Section 5.4), which I compute in the weighted model as the cumulative sum of the probabilities of having at least one major merger in each time bin. It is clear from the results reported in Figures A.2-A.4 that the both methods provide extremely consistent predictions on the aforementioned quantities, further validating the use of the discrete method to predict mean galactic properties.

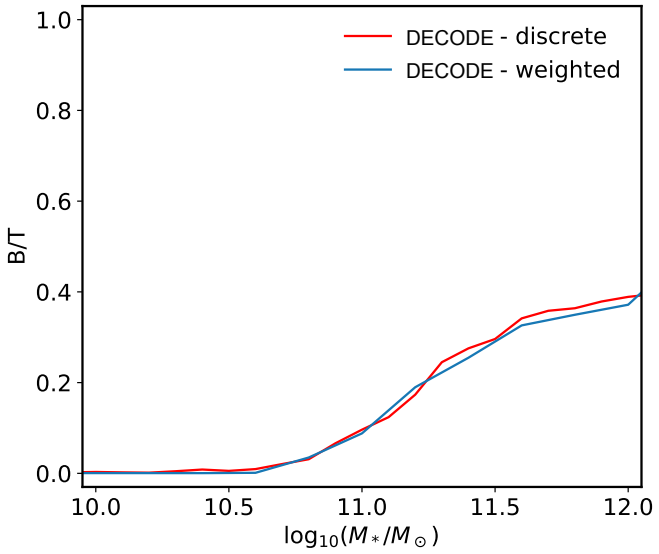

FIGURE A.4: Bulge-to-total ratio predicted by the discrete version of DECODE compared to that computed with the weighted method for Model BT2.

Appendix B

Completeness of the halo mass function

Figure B.1 shows a comparison of the SHMF for all unevolved surviving subhaloes between DECODE and the MultiDark N-body simulation. As one can see, the low-mass end of the MultiDark SHMF may be affected by incompleteness (compared to DECODE) due to resolution issues, resulting in smaller subhaloes to be destroyed in the simulation.

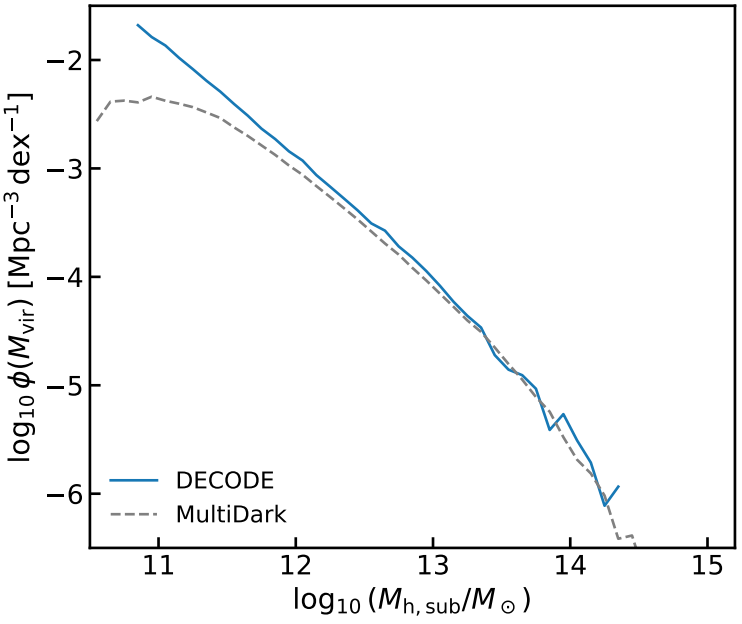

FIGURE B.1: Subhalo mass function of unevolved surviving subhaloes at $z = 0$ from DECODE compared to that from the MultiDark simulation.

Appendix C

Bulge-to-total ratios modelling

I show in Figure C.1 a comparison of the B/T ratios from different observational data sets. In particular, I compare the MaNGA data (black error bars), described in Section 3.4.4 and used as a reference for the models in this work, with the SDSS data from Mendel et al. (2014) who selected a subsample of the Simard et al. (2011) catalogue. I also show the B/T ratio of SDSS that I have computed directly from the Simard et al. (2011) catalogue (grey error bars), as well as the predictions of Models 2 from this work (green dotted and blue dashed lines). Interestingly, our results for SDSS are not consistent with those from Mendel et al. (2014). Nevertheless, our results discussed in the main text are still valid, irrespective of the exact data set chosen for computing mean B/T ratios. All the three observational B/T ratios show in fact that models based only on mergers, such as our BT1 and BT2 described in Section 5.4, are not sufficient to reproduce the measure B/T ratios, at least at low stellar masses. On the other hand, models that include also disc instabilities perform much better in reproducing the observational data. In summary, all observational B/T data suggest that at low stellar masses some level of disc instabilities is still expected in addition to mergers in order to well describe the evolution of galactic bulges.

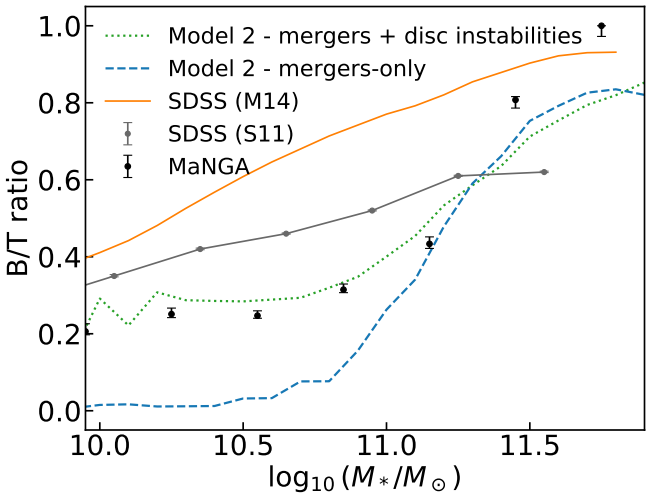

FIGURE C.1: Bulge-to-total ratios as a function of stellar mass at redshift $z = 0.1$ presented in Section 5.4 compared to different observational samples. The green dotted and blue dashed lines show the Model 2 predictions for the mergers+disc instabilities and mergers-only toy models, respectively. The orange line shows the mean B/T of SDSS using the sample of Mendel et al. (2014), as shown in Devergne et al. (2020). The grey dots with error bars show the SDSS B/T computed using the Simard et al. (2011) catalogue and the black dots with error bars the MaNGA data.

Appendix D

Additional SFR functions

In this Appendix, I show the results on the galaxy stellar mass growths by employing different data sets for the SFR function. Figure D.1 shows the SFR function from Sargent et al. (2012) and Fujimoto et al. (2023) (upper panels), in addition to that from Mancuso

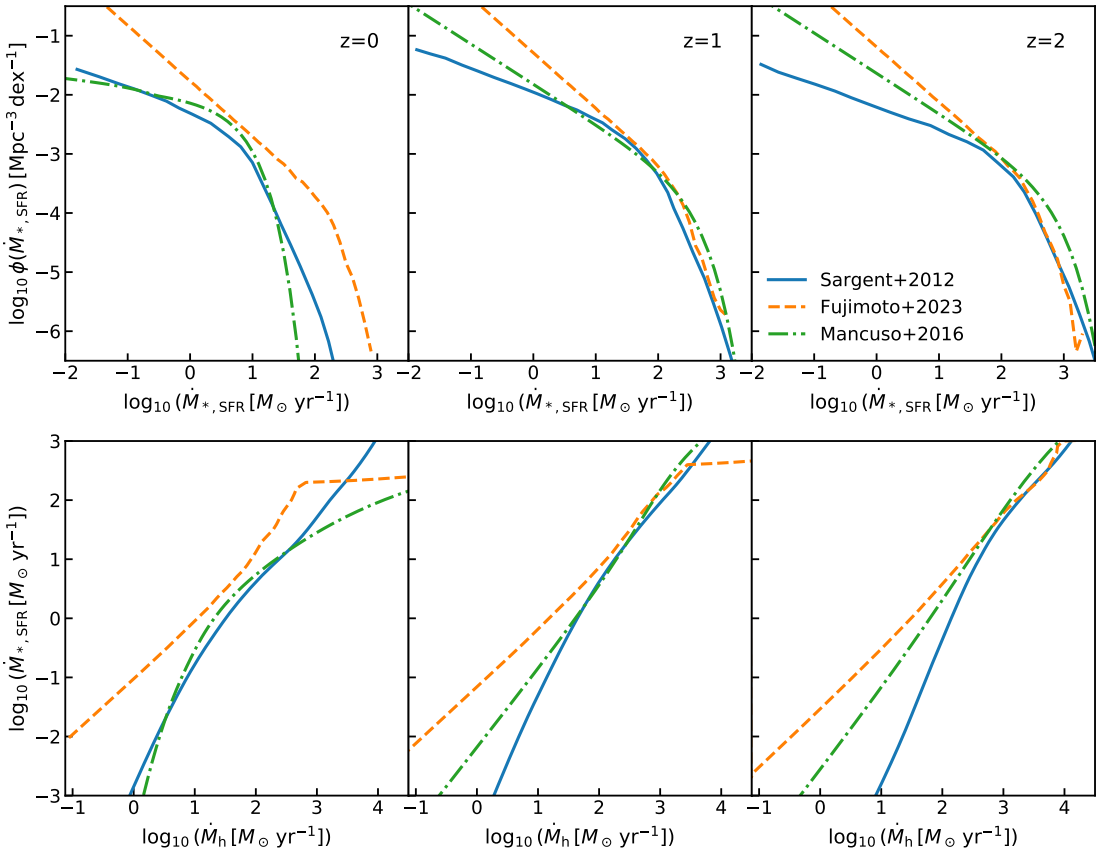

FIGURE D.1: Upper panels: Star formation rate function from Sargent et al. (2012, blue solid lines), Fujimoto et al. (2023, orange dashed lines) and Mancuso et al. (2016, green dash-dotted lines) at different redshifts, as labelled. Lower panels: Star formation rate-halo accretion rate relation from abundance matching for the same data sets of the upper panels at the same redshifts.

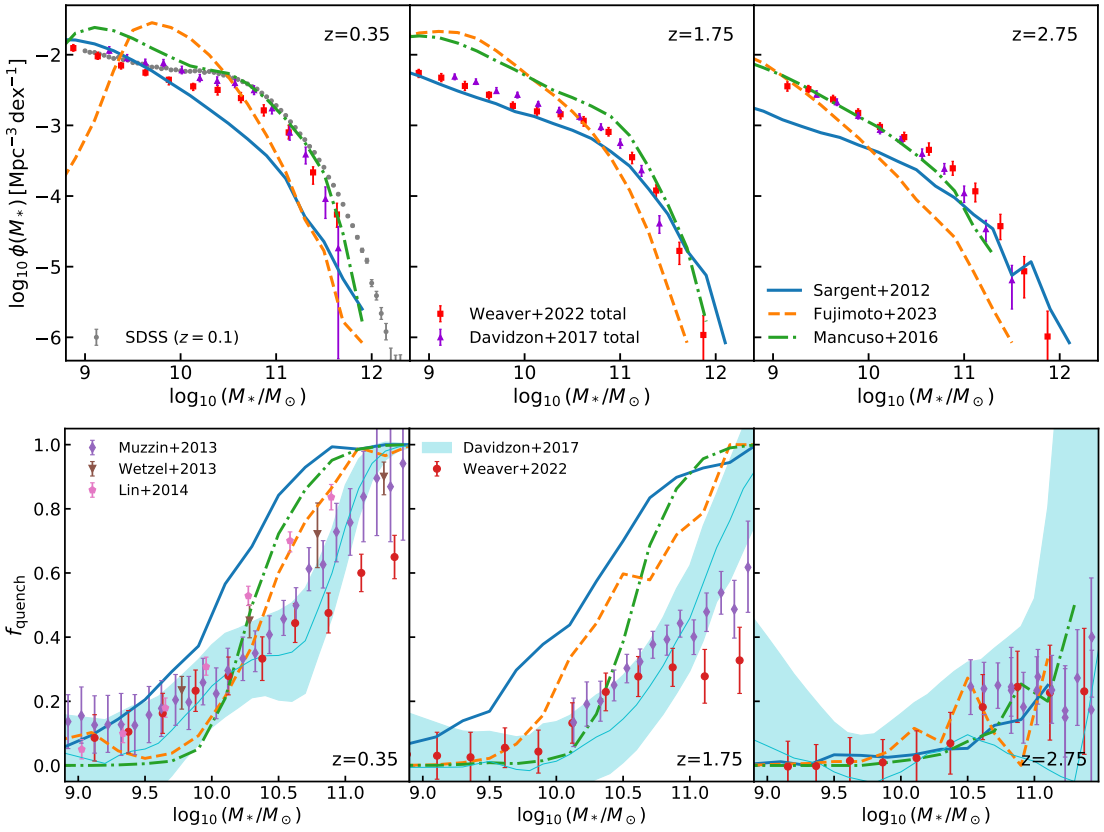

FIGURE D.2: Upper panels: Stellar mass function for the same data sets of Figure D.1 in the case of halo quenching scenario at different redshifts. Lower panels: same as upper panels but for fraction of quenched galaxies as a function of stellar mass.

et al. (2016) already presented in Section 7.1.1.2, and the resulting SFR-HAR relation from abundance matching (lower panels). The Fujimoto et al. (2023) fit is much steeper at the faint end compared to the others at all redshifts and at the bright end contains a higher number of bright objects. Instead, the SFR function of Sargent et al. (2012) has a flatter faint end with respect to the others at $z > 0$. The corresponding SFR-HAR is consequently characterized by a flatter slope for a steeper SFR function and vice versa.

Figure D.2 shows the output SMFs (upper panels) and fraction of quenched galaxies (lower panels) for the input SFR functions mentioned above in the case of halo quenching scenario. The flatter SFR-HAR relation from the Fujimoto et al. (2023) inputs produces a SMF with a high excess of low-mass galaxies due to the high SFR, and results into lower quenched fractions. On the other hand, the Sargent et al. (2012) input SFR function predicts opposite results.

Appendix E

Comparison of DECODE to other semi-empirical models

The discrete statistical and semi-empirical model, DECODE, presented in this thesis constitutes an invaluable complementary tool to the existing cosmological models for modelling galaxy evolution. These models, either analytic or numerical, are affected by significant volume/mass resolution limitations and/or a large amount of input assumptions and parameters. Also other existing multi-parameter semi-empirical models, such as Behroozi et al. (2019) and Moster et al. (2018), based on abundance matching between galaxy-halo properties, still need large computational resources to run. Instead DECODE, based on statistical input distributions, allows to rapidly simulate a large volume box and investigate the mean properties of galaxies without relying on ab-initio analytic models or simulations.

In the last decade, several semi-empirical models have been developed. Several examples have been mentioned already in Section 2.4.3. I discuss here how DECODE differs from and complements them. Moster et al. (2018) showed an empirical relation between the mass growth of dark matter haloes and the galaxy SFR, from which they retrieve the mergers history and other properties. Moster et al. (2013) and Behroozi et al. (2019) proposed semi-empirical models where they populate dark matter haloes via SMHM relations with galaxies in vast catalogues. These models connect galaxy to dark matter halo properties via several analytic relations, which could involve a non-negligible number of free parameters to fit various observational quantities. DECODE, instead, although more restricted in scope as it only focuses on mean galaxy assembly histories, essentially relies on only one input parameter (similarly to, e.g., Grylls et al. 2019 and Boco et al. 2023), the scatter in the SMHM relation. From this single parameter and abundance matching, DECODE can then generate robust predictions on mean galaxy growth histories, merger rates, satellite abundances, and star formation histories, thus providing a flexible and transparent tool to probe galaxy evolution in a full

cosmological context. The semi-empirical model developed by Grylls et al. (2019) applies abundance matching to statistical distributions of dark matter haloes and galaxies, which is limited by the non-discreteness since it is based on statistical weights over continuous probability densities. DECODE instead applies the SMHM relation from abundance matching directly to the mock universe generated stochastically by making a realization of the distributions themselves. These features make DECODE an extremely valuable novel tool in galaxy modelling.

The semi-empirical model TOPSEM, very recently developed by Boco et al. (2023), exploits the abundance matching between the dark matter specific HAR and galaxy sSFR, using only the sSFR distribution at each redshift and the scatter in sSFR as input parameters, and with minimal dependence on the latter. Such model, based on specific accretion rates, relies on input SMF at $z = 0$ to initialize the galaxy stellar masses and fraction of quenched to retrieve the passive galaxies. Inspired by Boco et al. (2023), I developed DECODE 2.0, which applies the abundance matching directly to the HAR and SFR, without the need to add an input SMF to initialize my galaxies, allowing at the same time to study the evolution of galaxies individually, instead of being limited to mean quantities. Moreover, the fact that DECODE 2.0 strongly depends on the employed quenching mechanism, makes it an extremely suitable tool to study galaxy stellar mass formation and evolution histories.

Appendix F

Euclid mission mocks

During my PhD I have also worked on the AGN mocks within the Euclid Consortium WP9, in collaboration with Dr. Viola Allevato (Observatory of Naples) and my supervisor.

The methodology followed to build the AGN population can be summarized as follows:

- populate dark matter haloes with galaxies via the SMHM relation;
- populate galaxies with SMBHs via the $M_{\rm BH} - M_{\star}$ relation;
- assign SMBHs a duty cycle and Eddington ratio;
- assign AGNs, galaxy SEDs and magnitude in the Euclid filters.

Within this project, I have worked on the computation of the galaxy SEDs and magnitudes in the Euclid filters. Figure F.1 shows an example of SED of a Type II AGN.

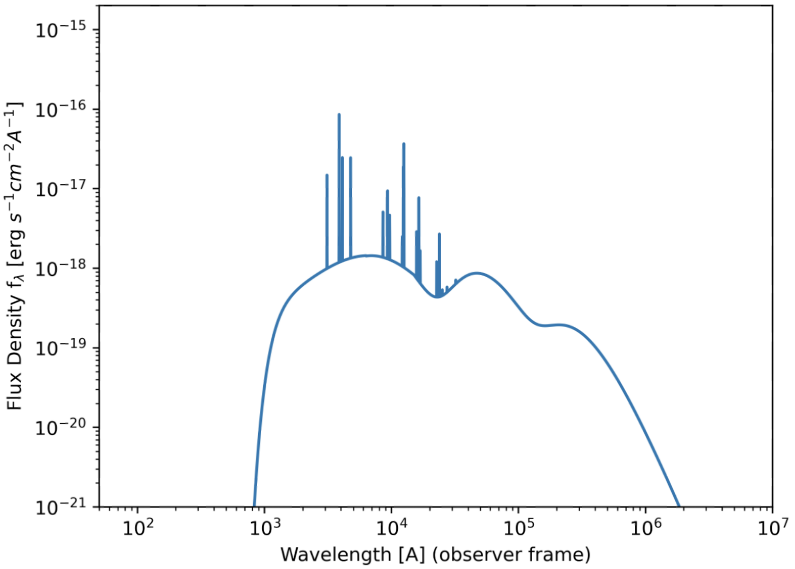

FIGURE F.1: Spectral energy distribution of a Type II AGN.

Appendix G

Industrial secondment

As part of the Marie Curie-Innovative Training Network (ITN) programme, I have completed an industrial secondment at OmegaLambdaTec in Munich. There I have worked with the Automatic Identification System (AIS) data, an automatic tracking system for vessels. Such data set provides several information of each vessel such as identification number, position, speed, direction, time etc. The main goal was to predict the time of arrival of cargo ships, that carry goods from Asia into European ports, by analyzing the available AIS data.

The main tasks of the secondment can be summarized as follows:

- get familiar with the data set;
- data cleaning and building the database;
- identify the ships with the itineraries of interest;
- explore the trajectories (i.e., port of loading, intermediate stops, port of arrival, time of departure and arrival etc);
- extract any useful information.

References

Jeremy Tinker, Andrey V. Kravtsov, Anatoly Klypin, Kevork Abazajian, Michael Warren, Gustavo Yepes, Stefan Gottlöber, and Daniel E. Holz. Toward a Halo Mass Function for Precision Cosmology: The Limits of Universality. *ApJ*, 688(2):709–728, December 2008. . URL https://ui.adsabs.harvard.edu/abs/2008ApJ...688..709T.

Volker Springel, Simon D. M. White, Giuseppe Tormen, and Guinevere Kauffmann. Populating a cluster of galaxies - I. Results at [formmu2]z=0. *MNRAS*, 328(3):726–750, December 2001. .

Fangzhou Jiang and Frank C. van den Bosch. Statistics of dark matter substructure - I. Model and universal fitting functions. *MNRAS*, 458(3):2848–2869, May 2016. .

I. Davidzon, O. Ilbert, C. Laigle, J. Coupon, H. J. McCracken, I. Delvecchio, D. Masters, P. Capak, B. C. Hsieh, O. Le Fèvre, L. Tresse, M. Bethermin, Y. Y. Chang, A. L. Faisst, E. Le Floc'h, C. Steinhardt, S. Toft, H. Aussel, C. Dubois, G. Hasinger, M. Salvato, D. B. Sanders, N. Scoville, and J. D. Silverman. The COSMOS2015 galaxy stellar mass function . Thirteen billion years of stellar mass assembly in ten snapshots. *A&A*, 605: A70, September 2017. .

J. R. Weaver, I. Davidzon, S. Toft, O. Ilbert, H. J. McCracken, K. M. L. Gould, C. K. Jespersen, C. Steinhardt, C. D. P. Lagos, P. L. Capak, C. M. Casey, N. Chartab, A. L. Faisst, C. C. Hayward, J. S. Kartaltepe, O. B. Kauffmann, A. M. Koekemoer, V. Kokorev, C. Laigle, D. Liu, A. Long, G. E. Magdis, C. J. R. McPartland, B. Milvang-Jensen, B. Mobasher, A. Moneti, Y. Peng, D. B. Sanders, M. Shuntov, A. Sneppen, F. Valentino, L. Zalesky, and G. Zamorani. COSMOS2020: The galaxy stellar mass function. The assembly and star formation cessation of galaxies at $0.2< z \leq 7.5$. *A&A*, 677:A184, September 2023. .

P. Popesso, A. Concas, G. Cresci, S. Belli, G. Rodighiero, H. Inami, M. Dickinson, O. Ilbert, M. Pannella, and D. Elbaz. The main sequence of star-forming galaxies across cosmic times. *MNRAS*, 519(1):1526–1544, February 2023. .

John Kormendy and Luis C. Ho. Coevolution (Or Not) of Supermassive Black Holes and Host Galaxies. *ARA&A*, 51(1):511–653, August 2013. .

Amy E. Reines and Marta Volonteri. Relations between Central Black Hole Mass and Total Galaxy Stellar Mass in the Local Universe. *ApJ*, 813(2):82, November 2015. .

Dalya Baron and Brice Ménard. Black hole mass estimation for active galactic nuclei from a new angle. *MNRAS*, 487(3):3404–3418, August 2019. .

Francesco Shankar, Mariangela Bernardi, Ravi K. Sheth, Laura Ferrarese, Alister W. Graham, Giulia Savorgnan, Viola Allevato, Alessandro Marconi, Ronald Läsker, and Andrea Lapi. Selection bias in dynamically measured supermassive black hole samples: its consequences and the quest for the most fundamental relation. *MNRAS*, 460 (3):3119–3142, August 2016. .

Giulia A. D. Savorgnan, Alister W. Graham, Alessandro Marconi, and Eleonora Sani. Supermassive Black Holes and Their Host Spheroids. II. The Red and Blue Sequence in the M_{BH}-$M_{*,sph}$ Diagram. *ApJ*, 817(1):21, January 2016. .

Laura Ferrarese and David Merritt. A Fundamental Relation between Supermassive Black Holes and Their Host Galaxies. *ApJ*, 539(1):L9–L12, August 2000. .

Karl Gebhardt, Ralf Bender, Gary Bower, Alan Dressler, S. M. Faber, Alexei V. Filippenko, Richard Green, Carl Grillmair, Luis C. Ho, John Kormendy, Tod R. Lauer, John Magorrian, Jason Pinkney, Douglas Richstone, and Scott Tremaine. A Relationship between Nuclear Black Hole Mass and Galaxy Velocity Dispersion. *ApJ*, 539(1): L13–L16, August 2000. .

Ignacio Martín-Navarro, Jean P. Brodie, Aaron J. Romanowsky, Tomás Ruiz-Lara, and Glenn van de Ven. Black-hole-regulated star formation in massive galaxies. *Nature*, 553(7688):307–309, January 2018. .

Nandini Sahu, Alister W. Graham, and Benjamin L. Davis. Black Hole Mass Scaling Relations for Early-type Galaxies. I. M_{BH}-$M_{*,sph}$ and M_{BH}-$M_{*,gal}$. *ApJ*, 876(2):155, May 2019. .

Peter S. Behroozi, Risa H. Wechsler, and Charlie Conroy. The Average Star Formation Histories of Galaxies in Dark Matter Halos from z = 0-8. *ApJ*, 770(1):57, June 2013. . URL https://ui.adsabs.harvard.edu/abs/2013ApJ...770...57B.

Benjamin P. Moster, Thorsten Naab, and Simon D. M. White. Galactic star formation and accretion histories from matching galaxies to dark matter haloes. *MNRAS*, 428(4):3121–3138, February 2013. . URL https://ui.adsabs.harvard.edu/abs/2013MNRAS.428.3121M.

Aldo Rodríguez-Puebla, Joel R. Primack, Vladimir Avila-Reese, and S. M. Faber. Constraining the galaxy-halo connection over the last 13.3 Gyr: star formation histories, galaxy mergers and structural properties. *MNRAS*, 470(1):651–687, September 2017. .

Philip J. Grylls, F. Shankar, L. Zanisi, and M. Bernardi. A statistical semi-empirical model: satellite galaxies in groups and clusters. *MNRAS*, 483(2):2506–2523, February 2019. . URL https://ui.adsabs.harvard.edu/abs/2019MNRAS.483.2506G.

Lumen Boco, Andrea Lapi, Francesco Shankar, Hao Fu, Francesco Gabrielli, and Alex Sicilia. TOPSEM, TwO Parameters Semi Empirical Model: Galaxy Evolution and Bulge/Disk Dicothomy from Two-Stage Halo Accretion. *arXiv e-prints*, art. arXiv:2307.13036, July 2023.

Frank C. van den Bosch, Fangzhou Jiang, Andrew Hearin, Duncan Campbell, Douglas Watson, and Nikhil Padmanabhan. Coming of age in the dark sector: how dark matter haloes grow their gravitational potential wells. *MNRAS*, 445(2):1713–1730, December 2014. .

Tom McCavana, Miroslav Micic, Geraint F. Lewis, Manodeep Sinha, Sanjib Sharma, Kelly Holley-Bockelmann, and Joss Bland-Hawthorn. The lives of high-redshift mergers. *MNRAS*, 424(1):361–371, July 2012. .

I. K. Baldry, S. P. Driver, J. Loveday, E. N. Taylor, L. S. Kelvin, J. Liske, P. Norberg, A. S. G. Robotham, S. Brough, A. M. Hopkins, S. P. Bamford, J. A. Peacock, J. Bland-Hawthorn, C. J. Conselice, S. M. Croom, D. H. Jones, H. R. Parkinson, C. C. Popescu, M. Prescott, R. G. Sharp, and R. J. Tuffs. Galaxy And Mass Assembly (GAMA): the galaxy stellar mass function at z < 0.06. *MNRAS*, 421(1):621–634, March 2012. .

M. Bernardi, A. Meert, R. K. Sheth, J. L. Fischer, M. Huertas-Company, C. Maraston, F. Shankar, and V. Vikram. The high mass end of the stellar mass function: Dependence on stellar population models and agreement between fits to the light profile. *MNRAS*, 467(2):2217–2233, May 2017. .

Adam R. Tomczak, Ryan F. Quadri, Kim-Vy H. Tran, Ivo Labbé, Caroline M. S. Straatman, Casey Papovich, Karl Glazebrook, Rebecca Allen, Gabriel B. Brammer, Glenn G. Kacprzak, Lalitwadee Kawinwanichakij, Daniel D. Kelson, Patrick J. McCarthy, Nicola Mehrtens, Andrew J. Monson, S. Eric Persson, Lee R. Spitler, Vithal Tilvi, and Pieter van Dokkum. Galaxy Stellar Mass Functions from ZFOURGE/CANDELS: An Excess of Low-mass Galaxies since z = 2 and the Rapid Buildup of Quiescent Galaxies. *ApJ*, 783(2):85, March 2014. .

Joel Leja, Joshua S. Speagle, Benjamin D. Johnson, Charlie Conroy, Pieter van Dokkum, and Marijn Franx. A New Census of the 0.2 < z < 3.0 Universe. I. The Stellar Mass Function. *ApJ*, 893(2):111, April 2020. .

Benjamin P. Moster, Thorsten Naab, and Simon D. M. White. EMERGE - an empirical model for the formation of galaxies since z $\sim$ 10. *MNRAS*, 477(2):1822–1852, June 2018. .

Peter Behroozi, Risa H. Wechsler, Andrew P. Hearin, and Charlie Conroy. UNIVERSEMACHINE: The correlation between galaxy growth and dark matter halo assembly from z = 0-10. *MNRAS*, 488(3):3143–3194, September 2019. .

Onsi Fakhouri, Chung-Pei Ma, and Michael Boylan-Kolchin. The merger rates and mass assembly histories of dark matter haloes in the two Millennium simulations. *MNRAS*, 406(4):2267–2278, August 2010. .

Carl J. Mundy, Christopher J. Conselice, Kenneth J. Duncan, Omar Almaini, Boris Häußler, and William G. Hartley. A consistent measure of the merger histories of massive galaxies using close-pair statistics - I. Major mergers at z < 3.5. *MNRAS*, 470 (3):3507–3531, September 2017. .

G. Efstathiou, G. Lake, and J. Negroponte. The stability and masses of disc galaxies. *MNRAS*, 199:1069–1088, June 1982. .

Frédéric Bournaud, Avishai Dekel, Romain Teyssier, Marcello Cacciato, Emanuele Daddi, Stéphanie Juneau, and Francesco Shankar. Black Hole Growth and Active Galactic Nuclei Obscuration by Instability-driven Inflows in High-redshift Disk Galaxies Fed by Cold Streams. *ApJ*, 741(2):L33, November 2011. .

C. Ragone-Figueroa, G. L. Granato, M. E. Ferraro, G. Murante, V. Biffi, S. Borgani, S. Planelles, and E. Rasia. BCG mass evolution in cosmological hydro-simulations. *MNRAS*, 479(1):1125–1136, September 2018. .

Kevin C. Cooke, Jeyhan S. Kartaltepe, K. D. Tyler, Behnam Darvish, Caitlin M. Casey, Olivier Le Fèvre, Mara Salvato, and Nicholas Scoville. Stellar Mass Growth of Brightest Cluster Galaxy Progenitors in COSMOS Since z $\sim$ 3. *ApJ*, 881(2):150, August 2019. .

E. Contini, G. De Lucia, Á. Villalobos, and S. Borgani. On the formation and physical properties of the intracluster light in hierarchical galaxy formation models. *MNRAS*, 437(4):3787–3802, February 2014. .

Joel Leja, Joshua S. Speagle, Yuan-Sen Ting, Benjamin D. Johnson, Charlie Conroy, Katherine E. Whitaker, Erica J. Nelson, Pieter van Dokkum, and Marijn Franx. A New Census of the 0.2 < z < 3.0 Universe. II. The Star-forming Sequence. *ApJ*, 936(2): 165, September 2022. .

Craig S. Rudick, J. Christopher Mihos, and Cameron K. McBride. The Quantity of Intracluster Light: Comparing Theoretical and Observational Measurement Techniques using Simulated Clusters. *ApJ*, 732(1):48, May 2011. .

Claire Burke, Chris A. Collins, John P. Stott, and Matt Hilton. Measurement of the intracluster light at z $\sim$ 1. *MNRAS*, 425(3):2058–2068, September 2012. .

Claire Burke, Matt Hilton, and Chris Collins. Coevolution of brightest cluster galaxies and intracluster light using CLASH. *MNRAS*, 449(3):2353–2367, May 2015. .

Mireia Montes and Ignacio Trujillo. Intracluster light at the Frontier - II. The Frontier Fields Clusters. *MNRAS*, 474(1):917–932, February 2018. .

Kate E. Furnell, Chris A. Collins, Lee S. Kelvin, Ivan K. Baldry, Phil A. James, Maria Manolopoulou, Robert G. Mann, Paul A. Giles, Alberto Bermeo, Matthew Hilton, Reese Wilkinson, A. Kathy Romer, Carlos Vergara, Sunayana Bhargava, John P. Stott, Julian Mayers, and Pedro Viana. The growth of intracluster light in XCS-HSC galaxy clusters from 0.1 < z < 0.5. *MNRAS*, 502(2):2419–2437, April 2021. .

C. Da Rocha and C. Mendes de Oliveira. Intragroup diffuse light in compact groups of galaxies: HCG 79, 88 and 95. *MNRAS*, 364(3):1069–1081, December 2005. .

C. Da Rocha, B. L. Ziegler, and C. Mendes de Oliveira. Intragroup diffuse light in compact groups of galaxies - II. HCG 15, 35 and 51. *MNRAS*, 388(3):1433–1443, August 2008. .

M. Kluge, R. Bender, A. Riffeser, C. Goessl, U. Hopp, M. Schmidt, and C. Ries. Photometric Dissection of Intracluster Light and Its Correlations with Host Cluster Properties. *ApJS*, 252(2):27, February 2021. .

Denis Poliakov, Aleksandr V. Mosenkov, Noah Brosch, Shuki Koriski, and R. Michael Rich. Quantified diffuse light in compact groups of galaxies. *MNRAS*, 503(4):6059–6077, June 2021. .

M. Bernardi, R. K. Sheth, H. Dominguez Sanchez, B. Margalef-Bentabol, D. Bizyaev, and R. R. Lane. The half mass radius of MaNGA galaxies. I. Effect of IMF gradients. *arXiv e-prints*, art. arXiv:2201.07810, January 2022.

Arjen van der Wel, Marco Martorano, Boris Häußler, Kalina V. Nedkova, Tim B. Miller, Gabriel B. Brammer, Glenn van de Ven, Joel Leja, Rachel S. Bezanson, Adam Muzzin, Danilo Marchesini, Anna de Graaff, Erica J. Nelson, Mariska Kriek, Eric F. Bell, and Marijn Franx. Stellar Half-mass Radii of 0.5 z < 2.3 Galaxies: Comparison with JWST/NIRCam Half-light Radii. *ApJ*, 960(1):53, January 2024. .

Francesco Shankar, David H. Weinberg, and Jordi Miralda-Escudé. Self-Consistent Models of the AGN and Black Hole Populations: Duty Cycles, Accretion Rates, and the Mean Radiative Efficiency. *ApJ*, 690(1):20–41, January 2009. .

C. Mancuso, A. Lapi, J. Shi, Z. Y. Cai, J. Gonzalez-Nuevo, M. Béthermin, and L. Danese. The Main Sequences of Star-forming Galaxies and Active Galactic Nuclei at High Redshift. *ApJ*, 833(2):152, December 2016. .

Xuejian Shen, Philip F. Hopkins, Claude-André Faucher-Giguère, D. M. Alexander, Gordon T. Richards, Nicholas P. Ross, and R. C. Hickox. The bolometric quasar luminosity function at z = 0-7. *MNRAS*, 495(3):3252–3275, January 2020. .

Edo van Uitert, Marcello Cacciato, Henk Hoekstra, Margot Brouwer, Cristóbal Sifón, Massimo Viola, Ivan Baldry, Joss Bland-Hawthorn, Sarah Brough, M. J. I. Brown, Ami Choi, Simon P. Driver, Thomas Erben, Catherine Heymans, Hendrik Hildebrandt, Benjamin Joachimi, Konrad Kuijken, Jochen Liske, Jon Loveday, John McFarland, Lance Miller, Reiko Nakajima, John Peacock, Mario Radovich, A. S. G. Robotham, Peter Schneider, Gert Sikkema, Edward N. Taylor, and Gijs Verdoes Kleijn. The stellar-to-halo mass relation of GAMA galaxies from 100 deg^2 of KiDS weak lensing data. *MNRAS*, 459(3):3251–3270, July 2016. .

Andrej Dvornik, Henk Hoekstra, Konrad Kuijken, Angus H. Wright, Marika Asgari, Maciej Bilicki, Thomas Erben, Benjamin Giblin, Alister W. Graham, Catherine Heymans, Hendrik Hildebrandt, Andrew M. Hopkins, Arun Kannawadi, Chieh-An Lin, Edward N. Taylor, and Tilman Tröster. KiDS+GAMA: The weak lensing calibrated stellar-to-halo mass relation of central and satellite galaxies. *A&A*, 642:A83, October 2020. .

Song Huang, Alexie Leauthaud, Andrew Hearin, Peter Behroozi, Christopher Bradshaw, Felipe Ardila, Joshua Speagle, Ananth Tenneti, Kevin Bundy, Jenny Greene, Cristóbal Sifón, and Neta Bahcall. Weak lensing reveals a tight connection between dark matter halo mass and the distribution of stellar mass in massive galaxies. *MNRAS*, 492(3):3685–3707, March 2020. .

Adam Muzzin, Danilo Marchesini, Mauro Stefanon, Marijn Franx, Henry J. McCracken, Bo Milvang-Jensen, James S. Dunlop, J. P. U. Fynbo, Gabriel Brammer, Ivo Labbé, and Pieter G. van Dokkum. The Evolution of the Stellar Mass Functions of Star-forming and Quiescent Galaxies to z = 4 from the COSMOS/UltraVISTA Survey. *ApJ*, 777(1): 18, November 2013. .

Andrew R. Wetzel, Jeremy L. Tinker, Charlie Conroy, and Frank C. van den Bosch. Galaxy evolution in groups and clusters: satellite star formation histories and quenching time-scales in a hierarchical Universe. *MNRAS*, 432(1):336–358, June 2013. .

Lihwai Lin, Hung-Yu Jian, Sebastien Foucaud, Peder Norberg, R. G. Bower, Shaun Cole, Pablo Arnalte-Mur, Chin-Wei Chen, Jean Coupon, Bau-Ching Hsieh, Sebastien Heinis, Stefanie Phleps, Wen-Ping Chen, Chien-Hsiu Lee, William Burgett, K. C. Chambers, L. Denneau, P. Draper, H. Flewelling, K. W. Hodapp, M. E. Huber, N. Kaiser, R. P. Kudritzki, E. A. Magnier, N. Metcalfe, Paul A. Price, J. L. Tonry, R. J. Wainscoat, and C. Waters. The Pan-STARRS1 Medium-Deep Survey: The Role of Galaxy Group Environment in the Star Formation Rate versus Stellar Mass Relation and Quiescent Fraction out to z $\sim$0.8. *ApJ*, 782(1):33, February 2014. .

J. T. Mendel, L. Simard, M. Palmer, S. L. Ellison, and D. R. Patton. A Catalog of Bulge, Disk, and Total Stellar Mass Estimates for the Sloan Digital Sky Survey. *ApJS*, 210:3, January 2014. .

T. Devergne, A. Cattaneo, F. Bournaud, I. Koutsouridou, A. Winter, P. Dimauro, G. A. Mamon, W. Vacher, and M. Varin. Bulge formation through disc instability. I. Stellar discs. *A&A*, 644:A56, December 2020. .

L. Simard, J. Trevor Mendel, D. R. Patton, S. L. Ellison, and A. W. McConnachie. VizieR Online Data Catalog: Bulge+disk decompositions of SDSS galaxies (Simard+, 2011). *VizieR Online Data Catalog*, art. J/ApJS/196/11, November 2011.

M. T. Sargent, M. Béthermin, E. Daddi, and D. Elbaz. The Contribution of Starbursts and Normal Galaxies to Infrared Luminosity Functions at z < 2. *ApJ*, 747(2):L31, March 2012. .

Seiji Fujimoto, Kotaro Kohno, Masami Ouchi, Masamune Oguri, Vasily Kokorev, Gabriel Brammer, Fengwu Sun, Jorge Gonzalez-Lopez, Franz E. Bauer, Gabriel B. Caminha, Bunyo Hatsukade, Johan Richard, Ian Smail, Akiyoshi Tsujita, Yoshihiro Ueda, Ryosuke Uematsu, Adi Zitrin, Dan Coe, Jean-Paul Kneib, Marc Postman, Keiichi Umetsu, Claudia del P. Lagos, Gergo Popping, Yiping Ao, Larry Bradley, Karina Caputi, Miroslava Dessauges-Zavadsky, Eiichi Egami, Daniel Espada, R. J. Ivison, Mathilde Jauzac, Kirsten K. Knudsen, Anton M. Koekemoer, Georgios E. Magdis, Guillaume Mahler, A. M. Munoz Arancibia, Timothy Rawle, Kazuhiro Shimasaku, Sune Toft, Hideki Umehata, Francesco Valentino, Tao Wang, and Wei-Halo Wang. ALMA Lensing Cluster Survey: Deep 1.2 mm Number Counts and Infrared Luminosity Functions at $z \simeq 1 - 8$. *arXiv e-prints*, art. arXiv:2303.01658, March 2023. .

Hao Fu, Francesco Shankar, Mohammadreza Ayromlou, Max Dickson, Ioanna Koutsouridou, Yetli Rosas-Guevara, Christopher Marsden, Kristina Brocklebank, Mariangela Bernardi, Nikolaos Shiamtanis, Joseph Williams, Lorenzo Zanisi, Viola Allevato, Lumen Boco, Silvia Bonoli, Andrea Cattaneo, Paola Dimauro, Fangzhou Jiang, Andrea Lapi, Nicola Menci, Stefani Petropoulou, and Carolin Villforth. Testing the key role of the stellar mass-halo mass relation in galaxy merger rates and morphologies via DECODE, a novel Discrete statistical sEmi-empiriCal mODEl. *MNRAS*, 516(3):3206–3233, November 2022. . URL https://ui.adsabs.harvard.edu/abs/2022MNRAS.516.3206F.

Hao Fu, Francesco Shankar, Mohammadreza Ayromlou, Ioanna Koutsouridou, Andrea Cattaneo, Caroline Bertemes, Sabine Bellstedt, Ignacio Martín-Navarro, Joel Leja, Viola Allevato, Mariangela Bernardi, Lumen Boco, Paola Dimauro, Carlotta Gruppioni, Andrea Lapi, Nicola Menci, Annagrazia Puglisi, and Alba V. Alonso-Tetilla. Unveiling the (in)consistencies among the galaxy stellar mass function, star formation histories, satellite abundances and intracluster light from a semi-empirical perspective. *Submitted to MNRAS*, 2024.

Rachel S. Somerville, Gergö Popping, and Scott C. Trager. Star formation in semi-analytic galaxy formation models with multiphase gas. *MNRAS*, 453(4):4337–4367, November 2015. .

Andrew King and Ken Pounds. Powerful Outflows and Feedback from Active Galactic Nuclei. *ARA&A*, 53:115–154, August 2015. .

Risa H. Wechsler and Jeremy L. Tinker. The Connection Between Galaxies and Their Dark Matter Halos. *ARA&A*, 56:435–487, September 2018. .

M. White. The mass of a halo. *A&A*, 367:27–32, February 2001. .

G. Mark Voit. Tracing cosmic evolution with clusters of galaxies. *Reviews of Modern Physics*, 77(1):207–258, April 2005. .

William H. Press and Paul Schechter. Formation of Galaxies and Clusters of Galaxies by Self-Similar Gravitational Condensation. *ApJ*, 187:425–438, February 1974. . URL https://ui.adsabs.harvard.edu/abs/1974ApJ...187..425P.

A. Jenkins, C. S. Frenk, S. D. M. White, J. M. Colberg, S. Cole, A. E. Evrard, H. M. P. Couchman, and N. Yoshida. The mass function of dark matter haloes. *MNRAS*, 321(2):372–384, February 2001. . URL https://ui.adsabs.harvard.edu/abs/2001MNRAS.321..372J.

Ravi K. Sheth, H. J. Mo, and Giuseppe Tormen. Ellipsoidal collapse and an improved model for the number and spatial distribution of dark matter haloes. *MNRAS*, 323 (1):1–12, May 2001. . URL https://ui.adsabs.harvard.edu/abs/2001MNRAS.323....1S.

M. Davis, G. Efstathiou, C. S. Frenk, and S. D. M. White. The evolution of large-scale structure in a universe dominated by cold dark matter. *ApJ*, 292:371–394, May 1985. .

Carlo Giocoli, Giuseppe Tormen, and Frank C. van den Bosch. The population of dark matter subhaloes: mass functions and average mass-loss rates. *MNRAS*, 386(4):2135–2144, June 2008. .

Fangzhou Jiang and Frank C. van den Bosch. Generating merger trees for dark matter haloes: a comparison of methods. *MNRAS*, 440(1):193–207, May 2014. .

Anatoly A. Klypin, Sebastian Trujillo-Gomez, and Joel Primack. Dark Matter Halos in the Standard Cosmological Model: Results from the Bolshoi Simulation. *ApJ*, 740(2): 102, October 2011. .

S. Khochfar and A. Burkert. Orbital parameters of merging dark matter halos. *A&A*, 445(2):403–412, January 2006. .

Q. Guo and S. D. M. White. Galaxy growth in the concordance ΛCDM cosmology. *MNRAS*, 384(1):2–10, February 2008. .

Ludwig Oser, Jeremiah P. Ostriker, Thorsten Naab, Peter H. Johansson, and Andreas Burkert. The Two Phases of Galaxy Formation. *ApJ*, 725(2):2312–2323, December 2010. .

A. Cattaneo, G. A. Mamon, K. Warnick, and A. Knebe. How do galaxies acquire their mass? *A&A*, 533:A5, September 2011. .

C. N. Lackner, R. Cen, J. P. Ostriker, and M. R. Joung. Building galaxies by accretion and in situ star formation. *MNRAS*, 425(1):641–656, September 2012. .

Vicente Rodriguez-Gomez, Annalisa Pillepich, Laura V. Sales, Shy Genel, Mark Vogelsberger, Qirong Zhu, Sarah Wellons, Dylan Nelson, Paul Torrey, Volker Springel, Chung-Pei Ma, and Lars Hernquist. The stellar mass assembly of galaxies in the Illustris simulation: growth by mergers and the spatial distribution of accreted stars. *MNRAS*, 458(3):2371–2390, May 2016. .

Annalisa Pillepich, Dylan Nelson, Lars Hernquist, Volker Springel, Rüdiger Pakmor, Paul Torrey, Rainer Weinberger, Shy Genel, Jill P. Naiman, Federico Marinacci, and Mark Vogelsberger. First results from the IllustrisTNG simulations: the stellar mass content of groups and clusters of galaxies. *MNRAS*, 475(1):648–675, March 2018a. .

Antonela Monachesi, Facundo A. Gómez, Robert J. J. Grand, Christine M. Simpson, Guinevere Kauffmann, Sebastián Bustamante, Federico Marinacci, Rüdiger Pakmor, Volker Springel, Carlos S. Frenk, Simon D. M. White, and Patricia B. Tissera. The Auriga stellar haloes: connecting stellar population properties with accretion and merging history. *MNRAS*, 485(2):2589–2616, May 2019. .

Philip J. Grylls, F. Shankar, J. Leja, N. Menci, B. Moster, P. Behroozi, and L. Zanisi. Predicting fully self-consistent satellite richness, galaxy growth, and star formation rates from the STatistical sEmi-Empirical modeL STEEL. *MNRAS*, 491(1):634–654, January 2020a. . URL https://ui.adsabs.harvard.edu/abs/2020MNRAS.491..634G.

R. Thomas, O. Le Fèvre, G. Zamorani, B. C. Lemaux, P. Hibon, A. Koekemoer, N. Hathi, D. Maccagni, P. Cassata, L. P. Cassarà, S. Bardelli, M. Talia, and E. Zucca. The most massive, passive, and oldest galaxies at $0.5 < z < 2.1$: Downsizing signature from galaxies selected from Mg_{UV} index. *A&A*, 630:A145, October 2019. .

S. F. Sánchez, V. Avila-Reese, A. Rodríguez-Puebla, H. Ibarra-Medel, R. Calette, M. Bershady, H. Hernández-Toledo, K. Pan, and D. Bizyaev. SDSS-IV MaNGA - an archaeological view of the cosmic star formation history. *MNRAS*, 482(2):1557–1586, January 2019. .

Sabine Bellstedt, Aaron S. G. Robotham, Simon P. Driver, Jessica E. Thorne, Luke J. M. Davies, Claudia del P. Lagos, Adam R. H. Stevens, Edward N. Taylor, Ivan K. Baldry, Amanda J. Moffett, Andrew M. Hopkins, and Steven Phillipps. Galaxy And Mass

Assembly (GAMA): a forensic SED reconstruction of the cosmic star formation history and metallicity evolution by galaxy type. *MNRAS*, 498(4):5581–5603, November 2020. .

R. B. Larson, B. M. Tinsley, and C. N. Caldwell. The evolution of disk galaxies and the origin of S0 galaxies. *ApJ*, 237:692–707, May 1980. .

James E. Gunn and III Gott, J. Richard. On the Infall of Matter Into Clusters of Galaxies and Some Effects on Their Evolution. *ApJ*, 176:1, August 1972. .

L. L. Cowie and A. Songaila. Thermal evaporation of gas within galaxies by a hot intergalactic medium. *Nature*, 266:501–503, April 1977. .

Gian Luigi Granato, Gianfranco De Zotti, Laura Silva, Alessandro Bressan, and Luigi Danese. A Physical Model for the Coevolution of QSOs and Their Spheroidal Hosts. *ApJ*, 600(2):580–594, January 2004. .

Avishai Dekel and Yuval Birnboim. Galaxy bimodality due to cold flows and shock heating. *MNRAS*, 368(1):2–20, May 2006. .

F. Shankar, A. Lapi, P. Salucci, G. De Zotti, and L. Danese. New Relationships between Galaxy Properties and Host Halo Mass, and the Role of Feedbacks in Galaxy Formation. *ApJ*, 643(1):14–25, May 2006. .

Avishai Dekel and Yuval Birnboim. Gravitational quenching in massive galaxies and clusters by clumpy accretion. *MNRAS*, 383(1):119–138, January 2008. .

Marie Martig, Frédéric Bournaud, Romain Teyssier, and Avishai Dekel. Morphological Quenching of Star Formation: Making Early-Type Galaxies Red. *ApJ*, 707(1):250–267, December 2009. .

Simon J. Lilly, C. Marcella Carollo, Antonio Pipino, Alvio Renzini, and Yingjie Peng. Gas Regulation of Galaxies: The Evolution of the Cosmic Specific Star Formation Rate, the Metallicity-Mass-Star-formation Rate Relation, and the Stellar Content of Halos. *ApJ*, 772(2):119, August 2013. .

Kevin Schawinski, C. Megan Urry, Brooke D. Simmons, Lucy Fortson, Sugata Kaviraj, William C. Keel, Chris J. Lintott, Karen L. Masters, Robert C. Nichol, Marc Sarzi, Ramin Skibba, Ezequiel Treister, Kyle W. Willett, O. Ivy Wong, and Sukyoung K. Yi. The green valley is a red herring: Galaxy Zoo reveals two evolutionary pathways towards quenching of star formation in early- and late-type galaxies. *MNRAS*, 440 (1):889–907, May 2014. .

A. Lapi, L. Pantoni, L. Zanisi, J. Shi, C. Mancuso, M. Massardi, F. Shankar, A. Bressan, and L. Danese. The Dramatic Size and Kinematic Evolution of Massive Early-type Galaxies. *ApJ*, 857(1):22, April 2018. .

Bingxiao Xu and Yingjie Peng. Critical Stellar Central Densities Drive Galaxy Quenching in the Nearby Universe. *ApJ*, 923(2):L29, December 2021. .

Lalitwadee Kawinwanichakij, Casey Papovich, Robin Ciardullo, Steven L. Finkelstein, Matthew L. Stevans, Isak G. B. Wold, Shardha Jogee, Sydney Sherman, Jonathan Florez, and Caryl Gronwall. On the (Lack of) Evolution of the Stellar Mass Function of Massive Galaxies from z = 1.5 to 0.4. *ApJ*, 892(1):7, March 2020. .

Jr. Kennicutt, Robert C. The Global Schmidt Law in Star-forming Galaxies. *ApJ*, 498(2): 541–552, May 1998. .

Katherine E. Whitaker, Marijn Franx, Joel Leja, Pieter G. van Dokkum, Alaina Henry, Rosalind E. Skelton, Mattia Fumagalli, Ivelina G. Momcheva, Gabriel B. Brammer, Ivo Labbé, Erica J. Nelson, and Jane R. Rigby. Constraining the Low-mass Slope of the Star Formation Sequence at 0.5 < z < 2.5. *ApJ*, 795(2):104, November 2014. .

J. S. Speagle, C. L. Steinhardt, P. L. Capak, and J. D. Silverman. A Highly Consistent Framework for the Evolution of the Star-Forming "Main Sequence" from z ∼0-6. *ApJS*, 214(2):15, October 2014. .

O. Ilbert, S. Arnouts, E. Le Floc'h, H. Aussel, M. Bethermin, P. Capak, B. C. Hsieh, M. Kajisawa, A. Karim, O. Le Fèvre, N. Lee, S. Lilly, H. J. McCracken, L. Michel-Dansac, T. Moutard, M. A. Renzini, M. Salvato, D. B. Sanders, N. Scoville, K. Sheth, J. D. Silverman, V. Smolčić, Y. Taniguchi, and L. Tresse. Evolution of the specific star formation rate function at z< 1.4 Dissecting the mass-SFR plane in COSMOS and GOODS. *A&A*, 579:A2, July 2015. .

Yuval Birnboim and Avishai Dekel. Virial shocks in galactic haloes? *MNRAS*, 345(1): 349–364, October 2003. .

Avishai Dekel, Re'em Sari, and Daniel Ceverino. Formation of Massive Galaxies at High Redshift: Cold Streams, Clumpy Disks, and Compact Spheroids. *ApJ*, 703(1): 785–801, September 2009. .

Alan Meert, Vinu Vikram, and Mariangela Bernardi. Simulations of single- and two-component galaxy decompositions for spectroscopically selected galaxies from the Sloan Digital Sky Survey. *MNRAS*, 433(2):1344–1361, August 2013. .

M. Bernardi, A. Meert, R. K. Sheth, V. Vikram, M. Huertas-Company, S. Mei, and F. Shankar. The massive end of the luminosity and stellar mass functions: dependence on the fit to the light profile. *MNRAS*, 436(1):697–704, November 2013. .

A. V. Kravtsov, A. A. Vikhlinin, and A. V. Meshcheryakov. Stellar Mass—Halo Mass Relation and Star Formation Efficiency in High-Mass Halos. *Astronomy Letters*, 44(1): 8–34, January 2018. . URL https://ui.adsabs.harvard.edu/abs/2018AstL...44...8K.

Edwin E. Salpeter. The Luminosity Function and Stellar Evolution. *ApJ*, 121:161, January 1955. .

Pavel Kroupa. On the variation of the initial mass function. *MNRAS*, 322(2):231–246, April 2001. .

Gilles Chabrier. Galactic Stellar and Substellar Initial Mass Function. *PASP*, 115(809): 763–795, July 2003. .

Alessandro Sonnenfeld, Carlo Nipoti, and Tommaso Treu. Merger-driven evolution of the effective stellar initial mass function of massive early-type galaxies. *MNRAS*, 465 (2):2397–2410, February 2017. .

H. Domínguez Sánchez, M. Bernardi, J. R. Brownstein, N. Drory, and R. K. Sheth. Galaxy properties as revealed by MaNGA - I. Constraints on IMF and M_*/L gradients in ellipticals. *MNRAS*, 489(4):5612–5632, November 2019. .

M. Bernardi, R. K. Sheth, J. L. Fischer, A. Meert, K. H. Chae, H. Dominguez-Sanchez, M. Huertas-Company, F. Shankar, and V. Vikram. Stellar mass functions and implications for a variable IMF. *MNRAS*, 475(1):757–771, March 2018a. .

M. Bernardi, R. K. Sheth, H. Dominguez-Sanchez, J. L. Fischer, K. H. Chae, M. Huertas-Company, and F. Shankar. M_*/L gradients driven by IMF variation: large impact on dynamical stellar mass estimates. *MNRAS*, 477(2):2560–2571, June 2018b. .

Sidney Lower, Desika Narayanan, Joel Leja, Benjamin D. Johnson, Charlie Conroy, and Romeel Davé. How Well Can We Measure the Stellar Mass of a Galaxy: The Impact of the Assumed Star Formation History Model in SED Fitting. *ApJ*, 904(1):33, November 2020. .

Donald G. York, J. Adelman, Jr. Anderson, John E., Scott F. Anderson, James Annis, Neta A. Bahcall, J. A. Bakken, Robert Barkhouser, Steven Bastian, Eileen Berman, William N. Boroski, Steve Bracker, Charlie Briegel, John W. Briggs, J. Brinkmann, Robert Brunner, Scott Burles, Larry Carey, Michael A. Carr, Francisco J. Castander, Bing Chen, Patrick L. Colestock, A. J. Connolly, J. H. Crocker, István Csabai, Paul C. Czarapata, John Eric Davis, Mamoru Doi, Tom Dombeck, Daniel Eisenstein, Nancy Ellman, Brian R. Elms, Michael L. Evans, Xiaohui Fan, Glenn R. Federwitz, Larry Fiscelli, Scott Friedman, Joshua A. Frieman, Masataka Fukugita, Bruce Gillespie, James E. Gunn, Vijay K. Gurbani, Ernst de Haas, Merle Haldeman, Frederick H. Harris, J. Hayes, Timothy M. Heckman, G. S. Hennessy, Robert B. Hindsley, Scott Holm, Donald J. Holmgren, Chi-hao Huang, Charles Hull, Don Husby, Shin-Ichi Ichikawa, Takashi Ichikawa, Željko Ivezić, Stephen Kent, Rita S. J. Kim, E. Kinney, Mark Klaene, A. N. Kleinman, S. Kleinman, G. R. Knapp, John Korienek, Richard G. Kron, Peter Z. Kunszt, D. Q. Lamb, B. Lee, R. French Leger, Siriluk Limmongkol, Carl Lindenmeyer, Daniel C. Long, Craig Loomis, Jon Loveday, Rich Lucinio, Robert H. Lupton, Bryan

MacKinnon, Edward J. Mannery, P. M. Mantsch, Bruce Margon, Peregrine McGehee, Timothy A. McKay, Avery Meiksin, Aronne Merelli, David G. Monet, Jeffrey A. Munn, Vijay K. Narayanan, Thomas Nash, Eric Neilsen, Rich Neswold, Heidi Jo Newberg, R. C. Nichol, Tom Nicinski, Mario Nonino, Norio Okada, Sadanori Okamura, Jeremiah P. Ostriker, Russell Owen, A. George Pauls, John Peoples, R. L. Peterson, Donald Petravick, Jeffrey R. Pier, Adrian Pope, Ruth Pordes, Angela Prosapio, Ron Rechenmacher, Thomas R. Quinn, Gordon T. Richards, Michael W. Richmond, Claudio H. Rivetta, Constance M. Rockosi, Kurt Ruthmansdorfer, Dale Sandford, David J. Schlegel, Donald P. Schneider, Maki Sekiguchi, Gary Sergey, Kazuhiro Shimasaku, Walter A. Siegmund, Stephen Smee, J. Allyn Smith, S. Snedden, R. Stone, Chris Stoughton, Michael A. Strauss, Christopher Stubbs, Mark SubbaRao, Alexander S. Szalay, Istvan Szapudi, Gyula P. Szokoly, Anirudda R. Thakar, Christy Tremonti, Douglas L. Tucker, Alan Uomoto, Dan Vanden Berk, Michael S. Vogeley, Patrick Waddell, Shu-i. Wang, Masaru Watanabe, David H. Weinberg, Brian Yanny, Naoki Yasuda, and SDSS Collaboration. The Sloan Digital Sky Survey: Technical Summary. *AJ*, 120(3):1579–1587, September 2000. .

Andrés Almeida, Scott F. Anderson, Maria Argudo-Fernández, Carles Badenes, Kat Barger, Jorge K. Barrera-Ballesteros, Chad F. Bender, Erika Benitez, Felipe Besser, Jonathan C. Bird, Dmitry Bizyaev, Michael R. Blanton, John Bochanski, Jo Bovy, William Nielsen Brandt, Joel R. Brownstein, Johannes Buchner, Esra Bulbul, Joseph N. Burchett, Mariana Cano Díaz, Joleen K. Carlberg, Andrew R. Casey, Vedant Chandra, Brian Cherinka, Cristina Chiappini, Abigail A. Coker, Johan Comparat, Charlie Conroy, Gabriella Contardo, Arlin Cortes, Kevin Covey, Jeffrey D. Crane, Katia Cunha, Collin Dabbieri, James W. Davidson, Megan C. Davis, Anna Barbara de Andrade Queiroz, Nathan De Lee, José Eduardo Méndez Delgado, Sebastian Demasi, Francesco Di Mille, John Donor, Peter Dow, Tom Dwelly, Mike Eracleous, Jamey Eriksen, Xiaohui Fan, Emily Farr, Sara Frederick, Logan Fries, Peter Frinchaboy, Boris T. Gänsicke, Junqiang Ge, Consuelo González Ávila, Katie Grabowski, Catherine Grier, Guillaume Guiglion, Pramod Gupta, Patrick Hall, Keith Hawkins, Christian R. Hayes, J. J. Hermes, Lorena Hernández-García, David W. Hogg, Jon A. Holtzman, Hector Javier Ibarra-Medel, Alexander Ji, Paula Jofre, Jennifer A. Johnson, Amy M. Jones, Karen Kinemuchi, Matthias Kluge, Anton Koekemoer, Juna A. Kollmeier, Marina Kounkel, Dhanesh Krishnarao, Mirko Krumpe, Ivan Lacerna, Paulo Jakson Assuncao Lago, Chervin Laporte, Chao Liu, Ang Liu, Xin Liu, Alexandre Roman Lopes, Matin Macktoobian, Steven R. Majewski, Viktor Malanushenko, Dan Maoz, Thomas Masseron, Karen L. Masters, Gal Matijevic, Aidan McBride, Ilija Medan, Andrea Merloni, Sean Morrison, Natalie Myers, Szabolcs Mészáros, C. Alenka Negrete, David L. Nidever, Christian Nitschelm, Daniel Oravetz, Audrey Oravetz, Kaike Pan, Yingjie Peng, Marc H. Pinsonneault, Rick Pogge, Dan Qiu, Solange V. Ramirez, Hans-Walter Rix, Daniela Fernández Rosso,

Jessie Runnoe, Mara Salvato, Sebastian F. Sanchez, Felipe A. Santana, Andrew Saydjari, Conor Sayres, Kevin C. Schlaufman, Donald P. Schneider, Axel Schwope, Javier Serna, Yue Shen, Jennifer Sobeck, Ying-Yi Song, Diogo Souto, Taylor Spoo, Keivan G. Stassun, Matthias Steinmetz, Ilya Straumit, Guy Stringfellow, José Sánchez-Gallego, Manuchehr Taghizadeh-Popp, Jamie Tayar, Ani Thakar, Patricia B. Tissera, Andrew Tkachenko, Hector Hernandez Toledo, Benny Trakhtenbrot, José G. Fernández-Trincado, Nicholas Troup, Jonathan R. Trump, Sarah Tuttle, Natalie Ulloa, Jose Antonio Vazquez-Mata, Pablo Vera Alfaro, Sandro Villanova, Stefanie Wachter, Anne-Marie Weijmans, Adam Wheeler, John Wilson, Leigh Wojno, Julien Wolf, Xiang-Xiang Xue, Jason E. Ybarra, Eleonora Zari, and Gail Zasowski. The Eighteenth Data Release of the Sloan Digital Sky Surveys: Targeting and First Spectra from SDSS-V. *ApJS*, 267(2):44, August 2023. .

Norman A. Grogin, Dale D. Kocevski, S. M. Faber, Henry C. Ferguson, Anton M. Koekemoer, Adam G. Riess, Viviana Acquaviva, David M. Alexander, Omar Almaini, Matthew L. N. Ashby, Marco Barden, Eric F. Bell, Frédéric Bournaud, Thomas M. Brown, Karina I. Caputi, Stefano Casertano, Paolo Cassata, Marco Castellano, Peter Challis, Ranga-Ram Chary, Edmond Cheung, Michele Cirasuolo, Christopher J. Conselice, Asantha Roshan Cooray, Darren J. Croton, Emanuele Daddi, Tomas Dahlen, Romeel Davé, Duília F. de Mello, Avishai Dekel, Mark Dickinson, Timothy Dolch, Jennifer L. Donley, James S. Dunlop, Aaron A. Dutton, David Elbaz, Giovanni G. Fazio, Alexei V. Filippenko, Steven L. Finkelstein, Adriano Fontana, Jonathan P. Gardner, Peter M. Garnavich, Eric Gawiser, Mauro Giavalisco, Andrea Grazian, Yicheng Guo, Nimish P. Hathi, Boris Häussler, Philip F. Hopkins, Jia-Sheng Huang, Kuang-Han Huang, Saurabh W. Jha, Jeyhan S. Kartaltepe, Robert P. Kirshner, David C. Koo, Kamson Lai, Kyoung-Soo Lee, Weidong Li, Jennifer M. Lotz, Ray A. Lucas, Piero Madau, Patrick J. McCarthy, Elizabeth J. McGrath, Daniel H. McIntosh, Ross J. McLure, Bahram Mobasher, Leonidas A. Moustakas, Mark Mozena, Kirpal Nandra, Jeffrey A. Newman, Sami-Matias Niemi, Kai G. Noeske, Casey J. Papovich, Laura Pentericci, Alexandra Pope, Joel R. Primack, Abhijith Rajan, Swara Ravindranath, Naveen A. Reddy, Alvio Renzini, Hans-Walter Rix, Aday R. Robaina, Steven A. Rodney, David J. Rosario, Piero Rosati, Sara Salimbeni, Claudia Scarlata, Brian Siana, Luc Simard, Joseph Smidt, Rachel S. Somerville, Hyron Spinrad, Amber N. Straughn, Louis-Gregory Strolger, Olivia Telford, Harry I. Teplitz, Jonathan R. Trump, Arjen van der Wel, Carolin Villforth, Risa H. Wechsler, Benjamin J. Weiner, Tommy Wiklind, Vivienne Wild, Grant Wilson, Stijn Wuyts, Hao-Jing Yan, and Min S. Yun. CANDELS: The Cosmic Assembly Near-infrared Deep Extragalactic Legacy Survey. *ApJS*, 197(2):35, December 2011. .

Gabriel B. Brammer, Pieter G. van Dokkum, Marijn Franx, Mattia Fumagalli, Shannon Patel, Hans-Walter Rix, Rosalind E. Skelton, Mariska Kriek, Erica Nelson, Kasper B. Schmidt, Rachel Bezanson, Elisabete da Cunha, Dawn K. Erb, Xiaohui Fan, Natascha

Förster Schreiber, Garth D. Illingworth, Ivo Labbé, Joel Leja, Britt Lundgren, Dan Magee, Danilo Marchesini, Patrick McCarthy, Ivelina Momcheva, Adam Muzzin, Ryan Quadri, Charles C. Steidel, Tomer Tal, David Wake, Katherine E. Whitaker, and Anna Williams. 3D-HST: A Wide-field Grism Spectroscopic Survey with the Hubble Space Telescope. *ApJS*, 200(2):13, June 2012. .

S. P. Driver, D. T. Hill, L. S. Kelvin, A. S. G. Robotham, J. Liske, P. Norberg, I. K. Baldry, S. P. Bamford, A. M. Hopkins, J. Loveday, J. A. Peacock, E. Andrae, J. Bland-Hawthorn, S. Brough, M. J. I. Brown, E. Cameron, J. H. Y. Ching, M. Colless, C. J. Conselice, S. M. Croom, N. J. G. Cross, R. de Propris, S. Dye, M. J. Drinkwater, S. Ellis, Alister W. Graham, M. W. Grootes, M. Gunawardhana, D. H. Jones, E. van Kampen, C. Maraston, R. C. Nichol, H. R. Parkinson, S. Phillipps, K. Pimbblet, C. C. Popescu, M. Prescott, I. G. Roseboom, E. M. Sadler, A. E. Sansom, R. G. Sharp, D. J. B. Smith, E. Taylor, D. Thomas, R. J. Tuffs, D. Wijesinghe, L. Dunne, C. S. Frenk, M. J. Jarvis, B. F. Madore, M. J. Meyer, M. Seibert, L. Staveley-Smith, W. J. Sutherland, and S. J. Warren. Galaxy and Mass Assembly (GAMA): Survey diagnostics and core data release. *MNRAS*, 413:971–995, May 2011. ISSN 0035-8711. .

Kayhan Gültekin, Douglas O. Richstone, Karl Gebhardt, Tod R. Lauer, Scott Tremaine, M. C. Aller, Ralf Bender, Alan Dressler, S. M. Faber, Alexei V. Filippenko, Richard Green, Luis C. Ho, John Kormendy, John Magorrian, Jason Pinkney, and Christos Siopis. The M-σ and M-L Relations in Galactic Bulges, and Determinations of Their Intrinsic Scatter. *ApJ*, 698(1):198–221, June 2009. .

Alan Dressler and Douglas O. Richstone. Stellar Dynamics in the Nuclei of M31 and M32: Evidence for Massive Black Holes. *ApJ*, 324:701, January 1988. .

John Kormendy and Douglas Richstone. Inward Bound—The Search For Supermassive Black Holes In Galactic Nuclei. *ARA&A*, 33:581, January 1995. .

John Magorrian, Scott Tremaine, Douglas Richstone, Ralf Bender, Gary Bower, Alan Dressler, S. M. Faber, Karl Gebhardt, Richard Green, Carl Grillmair, John Kormendy, and Tod Lauer. The Demography of Massive Dark Objects in Galaxy Centers. *AJ*, 115(6):2285–2305, June 1998. .

Luis Ho. Supermassive Black Holes in Galactic Nuclei: Observational Evidence and Astrophysical Consequences. In Sandip K. Chakrabarti, editor, *Observational Evidence for the Black Holes in the Universe*, volume 234 of *Astrophysics and Space Science Library*, page 157, January 1999. .

Nadine Häring and Hans-Walter Rix. On the Black Hole Mass-Bulge Mass Relation. *ApJ*, 604(2):L89–L92, April 2004. .

Laura Ferrarese and Holland Ford. Supermassive Black Holes in Galactic Nuclei: Past, Present and Future Research. *Space Science Reviews*, 116(3-4):523–624, February 2005. .

Alister W. Graham, Simon P. Driver, Paul D. Allen, and Jochen Liske. The Millennium Galaxy Catalogue: the local supermassive black hole mass function in early- and late-type galaxies. *MNRAS*, 378(1):198–210, June 2007. .

E. Sani, A. Marconi, L. K. Hunt, and G. Risaliti. The Spitzer/IRAC view of black hole-bulge scaling relations. *MNRAS*, 413(2):1479–1494, May 2011a. .

E. Sani, A. Marconi, L. K. Hunt, and G. Risaliti. The Spitzer/IRAC view of black hole-bulge scaling relations. *MNRAS*, 413(2):1479–1494, May 2011b. .

Alessandro Marconi, David J. Axon, Roberto Maiolino, Tohru Nagao, Guia Pastorini, Paola Pietrini, Andrew Robinson, and Guidetta Torricelli. The Effect of Radiation Pressure on Virial Black Hole Mass Estimates and the Case of Narrow-Line Seyfert 1 Galaxies. *ApJ*, 678(2):693–700, May 2008. .

Marta Volonteri and Luca Ciotti. Massive Black Holes in Central Cluster Galaxies. *ApJ*, 768(1):29, May 2013. .

Timothy M. Heckman and Philip N. Best. The Coevolution of Galaxies and Supermassive Black Holes: Insights from Surveys of the Contemporary Universe. *ARA&A*, 52: 589–660, August 2014. .

R. Calvi, B. Vulcani, B. M. Poggianti, A. Moretti, J. Fritz, and G. Fasano. Morphology rather than environment drives the SFR-mass relation in the local universe. *MNRAS*, 481(3):3456–3469, December 2018. .

Andrew King. Supermassive Black Hole Accretion and Feedback. *Saas-Fee Advanced Course*, 48:95, January 2019. .

Vardha N. Bennert, Matthew W. Auger, Tommaso Treu, Jong-Hak Woo, and Matthew A. Malkan. The Relation between Black Hole Mass and Host Spheroid Stellar Mass Out to z $\sim$2. *ApJ*, 742(2):107, December 2011. .

Remington O. Sexton, Gabriela Canalizo, Kyle D. Hiner, Stefanie Komossa, Jong-Hak Woo, Ezequiel Treister, and Sabrina Lyn Hiner Dimassimo. Stronger Constraints on the Evolution of the M $_{BH} - \sigma_\star$ Relation up to z $\sim$ 0.6. *ApJ*, 878(2):101, June 2019. .

S. P. Driver, J. Liske, and A. W. Graham. The Millennium Galaxy Catalogue: Science Highlights. In A. Vallenari, R. Tantalo, L. Portinari, and A. Moretti, editors, *From Stars to Galaxies: Building the Pieces to Build Up the Universe*, volume 374 of *Astronomical Society of the Pacific Conference Series*, page 481, December 2007. .

Nadia Biava, Monica Colpi, Pedro R. Capelo, Matteo Bonetti, Marta Volonteri, Tomas Tamfal, Lucio Mayer, and Alberto Sesana. The lifetime of binary black holes in Sérsic galaxy models. *MNRAS*, 487(4):4985–4994, August 2019. .

Siyuan Chen, Alberto Sesana, and Christopher J. Conselice. Constraining astrophysical observables of galaxy and supermassive black hole binary mergers using pulsar timing arrays. *MNRAS*, 488(1):401–418, September 2019. .

Ronald Läsker, Laura Ferrarese, Glenn van de Ven, and Francesco Shankar. Supermassive Black Holes and Their Host Galaxies. II. The Correlation with Near-infrared Luminosity Revisited. *ApJ*, 780(1):70, January 2014. .

Amy E. Reines, Gregory R. Sivakoff, Kelsey E. Johnson, and Crystal L. Brogan. An actively accreting massive black hole in the dwarf starburst galaxy Henize2-10. *Nature*, 470(7332):66–68, February 2011. .

N. J. Secrest, S. Satyapal, M. Gliozzi, C. C. Cheung, A. C. Seth, and T. Böker. The Chandra View of NGC 4178: The Lowest Mass Black Hole in a Bulgeless Disk Galaxy? *ApJ*, 753(1):38, July 2012. .

Brooke D. Simmons, Chris Lintott, Kevin Schawinski, Edward C. Moran, Anna Han, Sugata Kaviraj, Karen L. Masters, C. Megan Urry, Kyle W. Willett, Steven P. Bamford, and Robert C. Nichol. Galaxy Zoo: bulgeless galaxies with growing black holes. *MNRAS*, 429(3):2199–2211, March 2013. .

M. Schramm, J. D. Silverman, J. E. Greene, W. N. Brandt, B. Luo, Y. Q. Xue, P. Capak, Y. Kakazu, J. Kartaltepe, and V. Mainieri. Unveiling a Population of Galaxies Harboring Low-mass Black Holes with X-Rays. *ApJ*, 773(2):150, August 2013. .

S. Satyapal, N. J. Secrest, W. McAlpine, S. L. Ellison, J. Fischer, and J. L. Rosenberg. Discovery of a Population of Bulgeless Galaxies with Extremely Red Mid-IR Colors: Obscured AGN Activity in the Low-mass Regime? *ApJ*, 784(2):113, April 2014. .

G. A. D. Savorgnan and A. W. Graham. Supermassive Black Holes and Their Host Spheroids. I. Disassembling Galaxies. *ApJS*, 222(1):10, January 2016a. .

Giulia A. D. Savorgnan and Alister W. Graham. Explaining the reportedly overmassive black holes in early-type galaxies with intermediate-scale discs. *MNRAS*, 457(1):320–327, March 2016b. .

G. Busarello, G. Longo, and A. Feoli. The role played by rotation and random motions in elliptical galaxies. *A&A*, 262:52–62, August 1992.

Simon D. M. White and Carlos S. Frenk. Galaxy Formation through Hierarchical Clustering. *ApJ*, 379:52, September 1991. .

Shaun Cole. Modeling Galaxy Formation in Evolving Dark Matter Halos. *ApJ*, 367:45, January 1991. .

Cedric Lacey and Joseph Silk. Tidally Triggered Galaxy Formation. I. Evolution of the Galaxy Luminosity Function. *ApJ*, 381:14, November 1991. .

Shaun Cole, Cedric G. Lacey, Carlton M. Baugh, and Carlos S. Frenk. Hierarchical galaxy formation. *MNRAS*, 319(1):168–204, November 2000. .

Darren J. Croton, Volker Springel, Simon D. M. White, G. De Lucia, C. S. Frenk, L. Gao, A. Jenkins, G. Kauffmann, J. F. Navarro, and N. Yoshida. The many lives of active galactic nuclei: cooling flows, black holes and the luminosities and colours of galaxies. *MNRAS*, 365(1):11–28, January 2006. .

Gabriella De Lucia and Jérémy Blaizot. The hierarchical formation of the brightest cluster galaxies. *MNRAS*, 375(1):2–14, February 2007. .

Rachel S. Somerville, Philip F. Hopkins, Thomas J. Cox, Brant E. Robertson, and Lars Hernquist. A semi-analytic model for the co-evolution of galaxies, black holes and active galactic nuclei. *MNRAS*, 391(2):481–506, December 2008. .

Pierluigi Monaco, Fabio Fontanot, and Giuliano Taffoni. The MORGANA model for the rise of galaxies and active nuclei. *MNRAS*, 375(4):1189–1219, March 2007. .

Steve Hatton, Julien E. G. Devriendt, Stéphane Ninin, François R. Bouchet, Bruno Guiderdoni, and Didier Vibert. GALICS- I. A hybrid N-body/semi-analytic model of hierarchical galaxy formation. *MNRAS*, 343(1):75–106, July 2003. .

A. Cattaneo, J. Blaizot, J. E. G. Devriendt, G. A. Mamon, E. Tollet, A. Dekel, B. Guiderdoni, M. Kucukbas, and A. C. R. Thob. The new semi-analytic code GalICS 2.0 - reproducing the galaxy stellar mass function and the Tully-Fisher relation simultaneously. *MNRAS*, 471(2):1401–1427, October 2017. .

A. Cattaneo, I. Koutsouridou, E. Tollet, J. Devriendt, and Y. Dubois. GalICS 2.1: a new semianalytic model for cold accretion, cooling, feedback, and their roles in galaxy formation. *MNRAS*, 497(1):279–301, September 2020. .

I. Koutsouridou and A. Cattaneo. Probing the link between quenching and morphological evolution. *MNRAS*, 516(3):4194–4211, November 2022. .

Bruno M. B. Henriques, Simon D. M. White, Peter A. Thomas, Raul Angulo, Qi Guo, Gerard Lemson, Volker Springel, and Roderik Overzier. Galaxy formation in the Planck cosmology - I. Matching the observed evolution of star formation rates, colours and stellar masses. *MNRAS*, 451(3):2663–2680, August 2015. .

Bruno M. B. Henriques, Robert M. Yates, Jian Fu, Qi Guo, Guinevere Kauffmann, Chaichalit Srisawat, Peter A. Thomas, and Simon D. M. White. L-GALAXIES 2020: Spatially resolved cold gas phases, star formation, and chemical enrichment in galactic discs. *MNRAS*, 491(4):5795–5814, February 2020. .

Mohammadreza Ayromlou, Guinevere Kauffmann, Robert M. Yates, Dylan Nelson, and Simon D. M. White. Galaxy formation with L-GALAXIES: modelling the environmental dependency of galaxy evolution and comparing with observations. *MNRAS*, 505(1):492–514, July 2021a. .

Claudia del P. Lagos, Rodrigo J. Tobar, Aaron S. G. Robotham, Danail Obreschkow, Peter D. Mitchell, Chris Power, and Pascal J. Elahi. Shark: introducing an open source, free, and flexible semi-analytic model of galaxy formation. *MNRAS*, 481(3):3573–3603, December 2018. .

Claudia del P. Lagos, Eric Emsellem, Jesse van de Sande, Katherine E. Harborne, Luca Cortese, Thomas Davison, Caroline Foster, and Ruby J. Wright. The diverse nature and formation paths of slow rotator galaxies in the EAGLE simulations. *MNRAS*, 509(3):4372–4391, January 2022. .

Fangzhou Jiang, Avishai Dekel, Jonathan Freundlich, Frank C. van den Bosch, Sheridan B. Green, Philip F. Hopkins, Andrew Benson, and Xiaolong Du. SatGen: a semi-analytical satellite galaxy generator - I. The model and its application to Local-Group satellite statistics. *MNRAS*, 502(1):621–641, March 2021. .

Sheridan B. Green, Frank C. van den Bosch, and Fangzhou Jiang. SatGen - II. Assessing the impact of a disc potential on subhalo populations. *MNRAS*, 509(2):2624–2636, January 2022a. .

Philip F. Hopkins, Rachel S. Somerville, Thomas J. Cox, Lars Hernquist, Shardha Jogee, Dusan Kereš, Chung-Pei Ma, Brant Robertson, and Kyle Stewart. The effects of gas on morphological transformation in mergers: implications for bulge and disc demographics. *MNRAS*, 397(2):802–814, August 2009a. .

Charlie Conroy and Risa H. Wechsler. Connecting Galaxies, Halos, and Star Formation Rates Across Cosmic Time. *ApJ*, 696(1):620–635, May 2009. .

Peter S. Behroozi, Charlie Conroy, and Risa H. Wechsler. A Comprehensive Analysis of Uncertainties Affecting the Stellar Mass-Halo Mass Relation for $0 < z < 4$. *ApJ*, 717 (1):379–403, July 2010. .

Benjamin P. Moster, Rachel S. Somerville, Christian Maulbetsch, Frank C. van den Bosch, Andrea V. Macciò, Thorsten Naab, and Ludwig Oser. Constraints on the Relationship between Stellar Mass and Halo Mass at Low and High Redshift. *ApJ*, 710 (2):903–923, February 2010. . URL https://ui.adsabs.harvard.edu/abs/2010ApJ...710..903M.

Xiaohu Yang, H. J. Mo, Frank C. van den Bosch, Youcai Zhang, and Jiaxin Han. Evolution of the Galaxy-Dark Matter Connection and the Assembly of Galaxies in Dark Matter Halos. *ApJ*, 752(1):41, June 2012. .

Jesus Zavala, Vladimir Avila-Reese, Claudio Firmani, and Michael Boylan-Kolchin. The growth of galactic bulges through mergers in Λ CDM haloes revisited - I. Present-day properties. *MNRAS*, 427(2):1503–1516, December 2012. .

Francesco Shankar, Simona Mei, Marc Huertas-Company, Jorge Moreno, Fabio Fontanot, Pierluigi Monaco, Mariangela Bernardi, Andrea Cattaneo, Ravi Sheth, Rossella Licitra, Lauriane Delaye, and Anand Raichoor. Environmental dependence of bulge-dominated galaxy sizes in hierarchical models of galaxy formation. Comparison with the local Universe. *MNRAS*, 439(4):3189–3212, April 2014a. .

Édouard Tollet, Andrea Cattaneo, Gary A. Mamon, Thibaud Moutard, and Frank C. van den Bosch. On stellar mass loss from galaxies in groups and clusters. *MNRAS*, 471(4):4170–4193, November 2017. .

S. Contreras, R. E. Angulo, and M. Zennaro. A flexible subhalo abundance matching model for galaxy clustering in redshift space. *MNRAS*, 508(1):175–189, November 2021. .

Andrew P. Hearin, Jonás Chaves-Montero, Mathew R. Becker, and Alex Alarcon. A Differentiable Model of the Assembly of Individual and Populations of Dark Matter Halos. *The Open Journal of Astrophysics*, 4(1):7, July 2021. .

Benedikt Diemer. COLOSSUS: A Python Toolkit for Cosmology, Large-scale Structure, and Dark Matter Halos. *ApJS*, 239(2):35, December 2018. .

Eric Hayashi, Julio F. Navarro, James E. Taylor, Joachim Stadel, and Thomas Quinn. The Structural Evolution of Substructure. *ApJ*, 584(2):541–558, February 2003. .

Giuliano Taffoni, Lucio Mayer, Monica Colpi, and Fabio Governato. On the life and death of satellite haloes. *MNRAS*, 341(2):434–448, May 2003. .

James E. Taylor and Arif Babul. The evolution of substructure in galaxy, group and cluster haloes - I. Basic dynamics. *MNRAS*, 348(3):811–830, March 2004. .

Jorge Peñarrubia and Andrew J. Benson. Effects of dynamical evolution on the distribution of substructures. *MNRAS*, 364(3):977–989, December 2005. .

Frank C. van den Bosch, Giuseppe Tormen, and Carlo Giocoli. The mass function and average mass-loss rate of dark matter subhaloes. *MNRAS*, 359(3):1029–1040, May 2005. .

Andrew R. Zentner, Andreas A. Berlind, James S. Bullock, Andrey V. Kravtsov, and Risa H. Wechsler. The Physics of Galaxy Clustering. I. A Model for Subhalo Populations. *ApJ*, 624(2):505–525, May 2005. .

R. E. Angulo, C. G. Lacey, C. M. Baugh, and C. S. Frenk. The fate of substructures in cold dark matter haloes. *MNRAS*, 399(2):983–995, October 2009. .

Jianling Gan, Xi Kang, Frank C. van den Bosch, and Jinliang Hou. An improved model for the dynamical evolution of dark matter subhaloes. *MNRAS*, 408(4):2201–2212, November 2010. .

Anatoly Klypin, Francisco Prada, Gustavo Yepes, Steffen Heß, and Stefan Gottlöber. Halo abundance matching: accuracy and conditions for numerical convergence. *MNRAS*, 447(4):3693–3707, March 2015. .

Frank C. van den Bosch, Fangzhou Jiang, Duncan Campbell, and Peter Behroozi. On the segregation of dark matter substructure. *MNRAS*, 455(1):158–177, January 2016. .

Frank C. van den Bosch. Dissecting the evolution of dark matter subhaloes in the Bolshoi simulation. *MNRAS*, 468(1):885–909, June 2017. .

Sheridan B. Green and Frank C. van den Bosch. The tidal evolution of dark matter substructure - I. subhalo density profiles. *MNRAS*, 490(2):2091–2101, December 2019. .

Greg L. Bryan and Michael L. Norman. Statistical Properties of X-Ray Clusters: Analytic and Numerical Comparisons. *ApJ*, 495(1):80–99, March 1998. .

Michael Boylan-Kolchin, Chung-Pei Ma, and Eliot Quataert. Dynamical friction and galaxy merging time-scales. *MNRAS*, 383(1):93–101, January 2008. .

R. Aversa, A. Lapi, G. de Zotti, F. Shankar, and L. Danese. Black Hole and Galaxy Coevolution from Continuity Equation and Abundance Matching. *ApJ*, 810(1):74, September 2015. . URL https://ui.adsabs.harvard.edu/abs/2015ApJ...810...74A.

Samuel N. Leitner and Andrey V. Kravtsov. Fuel Efficient Galaxies: Sustaining Star Formation with Stellar Mass Loss. *ApJ*, 734(1):48, June 2011. .

Sean P. Fillingham, Michael C. Cooper, Andrew B. Pace, Michael Boylan-Kolchin, James S. Bullock, Shea Garrison-Kimmel, and Coral Wheeler. Under pressure: quenching star formation in low-mass satellite galaxies via stripping. *MNRAS*, 463 (2):1916–1928, December 2016. .

Rory Smith, Hoseung Choi, Jaehyun Lee, Jinsu Rhee, Ruben Sanchez-Janssen, and Sukyoung K. Yi. The Preferential Tidal Stripping of Dark Matter versus Stars in Galaxies. *ApJ*, 833(1):109, December 2016. .

Jingjing Shi, Huiyuan Wang, Houjun Mo, Mark Vogelsberger, Luis C. Ho, Min Du, Dylan Nelson, Annalisa Pillepich, and Lars Hernquist. The Formation History of Subhalos and the Evolution of Satellite Galaxies. *ApJ*, 893(2):139, April 2020. .

Ruby J. Wright, Claudia del P. Lagos, Chris Power, Adam R. H. Stevens, Luca Cortese, and Rhys J. J. Poulton. An orbital perspective on the starvation, stripping, and quenching of satellite galaxies in the EAGLE simulations. *MNRAS*, 516(2):2891–2912, October 2022. .

Christoph Engler, Annalisa Pillepich, Gandhali D. Joshi, Anna Pasquali, Dylan Nelson, and Eva K. Grebel. Satellites of Milky Way- and M31-like galaxies with TNG50: Quenched fractions, gas content, and star formation histories. *MNRAS*, May 2023. .

Michael R. Blanton, David W. Hogg, Neta A. Bahcall, Ivan K. Baldry, J. Brinkmann, István Csabai, Daniel Eisenstein, Masataka Fukugita, James E. Gunn, Željko Ivezić, D. Q. Lamb, Robert H. Lupton, Jon Loveday, Jeffrey A. Munn, R. C. Nichol, Sadanori Okamura, David J. Schlegel, Kazuhiro Shimasaku, Michael A. Strauss, Michael S. Vogeley, and David H. Weinberg. The Broadband Optical Properties of Galaxies with Redshifts 0.02<z<0.22. *ApJ*, 594(1):186–207, September 2003. .

Ivan K. Baldry, Karl Glazebrook, Jon Brinkmann, Željko Ivezić, Robert H. Lupton, Robert C. Nichol, and Alexander S. Szalay. Quantifying the Bimodal Color-Magnitude Distribution of Galaxies. *ApJ*, 600(2):681–694, January 2004. .

J. Brinchmann, S. Charlot, S. D. M. White, C. Tremonti, G. Kauffmann, T. Heckman, and J. Brinkmann. The physical properties of star-forming galaxies in the low-redshift Universe. *MNRAS*, 351(4):1151–1179, July 2004. .

Guinevere Kauffmann, Simon D. M. White, Timothy M. Heckman, Brice Ménard, Jarle Brinchmann, Stéphane Charlot, Christy Tremonti, and Jon Brinkmann. The environmental dependence of the relations between stellar mass, structure, star formation and nuclear activity in galaxies. *MNRAS*, 353(3):713–731, September 2004. .

L. J. M. Davies, A. S. G. Robotham, C. del P. Lagos, S. P. Driver, A. R. H. Stevens, Y. M. Bahé, M. Alpaslan, M. N. Bremer, M. J. I. Brown, S. Brough, J. Bland-Hawthorn, L. Cortese, P. Elahi, M. W. Grootes, B. W. Holwerda, A. D. Ludlow, S. McGee, M. Owers, and S. Phillipps. Galaxy and Mass Assembly (GAMA): environmental quenching of centrals and satellites in groups. *MNRAS*, 483(4):5444–5458, March 2019. .

Ying-jie Peng, Simon J. Lilly, Katarina Kovač, Micol Bolzonella, Lucia Pozzetti, Alvio Renzini, Gianni Zamorani, Olivier Ilbert, Christian Knobel, Angela Iovino, Christian Maier, Olga Cucciati, Lidia Tasca, C. Marcella Carollo, John Silverman, Pawel Kampczyk, Loic de Ravel, David Sanders, Nicholas Scoville, Thierry Contini, Vincenzo Mainieri, Marco Scodeggio, Jean-Paul Kneib, Olivier Le Fèvre, Sandro Bardelli, Angela Bongiorno, Karina Caputi, Graziano Coppa, Sylvain de la Torre, Paolo Franzetti, Bianca Garilli, Fabrice Lamareille, Jean-Francois Le Borgne, Vincent Le Brun, Marco Mignoli, Enrique Perez Montero, Roser Pello, Elena Ricciardelli, Masayuki Tanaka, Laurence Tresse, Daniela Vergani, Niraj Welikala, Elena Zucca, Pascal Oesch, Ummi Abbas, Luke Barnes, Rongmon Bordoloi, Dario Bottini, Alberto Cappi, Paolo Cassata, Andrea Cimatti, Marco Fumana, Gunther Hasinger, Anton Koekemoer, Alexei Leauthaud, Dario Maccagni, Christian Marinoni, Henry McCracken, Pierdomenico Memeo, Baptiste Meneux, Preethi Nair, Cristiano Porciani, Valentina Presotto, and Roberto Scaramella. Mass and Environment as Drivers of Galaxy Evolution in

SDSS and zCOSMOS and the Origin of the Schechter Function. *ApJ*, 721(1):193–221, September 2010. .

Ying-jie Peng, Simon J. Lilly, Alvio Renzini, and Marcella Carollo. Mass and Environment as Drivers of Galaxy Evolution. II. The Quenching of Satellite Galaxies as the Origin of Environmental Effects. *ApJ*, 757(1):4, September 2012. .

Richard B. Larson. Effects of supernovae on the early evolution of galaxies. *MNRAS*, 169:229–246, November 1974. .

A. Dekel and J. Silk. The Origin of Dwarf Galaxies, Cold Dark Matter, and Biased Galaxy Formation. *ApJ*, 303:39, April 1986. .

Joseph Silk and Martin J. Rees. Quasars and galaxy formation. *A&A*, 331:L1–L4, March 1998. .

R. G. Bower, A. J. Benson, R. Malbon, J. C. Helly, C. S. Frenk, C. M. Baugh, S. Cole, and C. G. Lacey. Breaking the hierarchy of galaxy formation. *MNRAS*, 370(2):645–655, August 2006. .

A. C. Fabian. Observational Evidence of Active Galactic Nuclei Feedback. *ARA&A*, 50: 455–489, September 2012. .

Jerome J. Fang, S. M. Faber, David C. Koo, and Avishai Dekel. A Link between Star Formation Quenching and Inner Stellar Mass Density in Sloan Digital Sky Survey Central Galaxies. *ApJ*, 776(1):63, October 2013. .

C. Cicone, R. Maiolino, E. Sturm, J. Graciá-Carpio, C. Feruglio, R. Neri, S. Aalto, R. Davies, F. Fiore, J. Fischer, S. García-Burillo, E. González-Alfonso, S. Hailey-Dunsheath, E. Piconcelli, and S. Veilleux. Massive molecular outflows and evidence for AGN feedback from CO observations. *A&A*, 562:A21, February 2014. .

Fu, Boco et al. "". ″″, in prep.

Jaehyun Lee and Sukyoung K. Yi. On the Assembly History of Stellar Components in Massive Galaxies. *ApJ*, 766(1):38, March 2013. .

Annalisa Pillepich, Mark Vogelsberger, Alis Deason, Vicente Rodriguez-Gomez, Shy Genel, Dylan Nelson, Paul Torrey, Laura V. Sales, Federico Marinacci, Volker Springel, Debora Sijacki, and Lars Hernquist. Halo mass and assembly history exposed in the faint outskirts: the stellar and dark matter haloes of Illustris galaxies. *MNRAS*, 444(1):237–249, October 2014. .

Yan Qu, John C. Helly, Richard G. Bower, Tom Theuns, Robert A. Crain, Carlos S. Frenk, Michelle Furlong, Stuart McAlpine, Matthieu Schaller, Joop Schaye, and Simon D. M. White. A chronicle of galaxy mass assembly in the EAGLE simulation. *MNRAS*, 464(2):1659–1675, January 2017. .

Bart Clauwens, Joop Schaye, Marijn Franx, and Richard G. Bower. The three phases of galaxy formation. *MNRAS*, 478(3):3994–4009, August 2018. .

Thomas A. Davison, Mark A. Norris, Joel L. Pfeffer, Jonathan J. Davies, and Robert A. Crain. An EAGLE's view of ex situ galaxy growth. *MNRAS*, 497(1):81–93, September 2020. .

Philip J. Grylls, F. Shankar, and C. J. Conselice. The significant effects of stellar mass estimation on galaxy pair fractions. *MNRAS*, 499(2):2265–2275, December 2020b. .

Sheridan B. Green, Frank C. van den Bosch, and Fangzhou Jiang. SatGen - II. Assessing the impact of a disc potential on subhalo populations. *MNRAS*, 509(2):2624–2636, January 2022b. .

I. Delvecchio, C. Gruppioni, F. Pozzi, S. Berta, G. Zamorani, A. Cimatti, D. Lutz, D. Scott, C. Vignali, G. Cresci, A. Feltre, A. Cooray, M. Vaccari, J. Fritz, E. Le Floc'h, B. Magnelli, P. Popesso, S. Oliver, J. Bock, M. Carollo, T. Contini, O. Le Févre, S. Lilly, V. Mainieri, A. Renzini, and M. Scodeggio. Tracing the cosmic growth of supermassive black holes to z $\sim$ 3 with Herschel. *MNRAS*, 439(3):2736–2754, April 2014. .

Dušan Kereš, Neal Katz, David H. Weinberg, and Romeel Davé. How do galaxies get their gas? *MNRAS*, 363(1):2–28, October 2005. .

Joseph Silk and Gary A. Mamon. The current status of galaxy formation. *Research in Astronomy and Astrophysics*, 12(8):917–946, August 2012. .

Mark Vogelsberger, Shy Genel, Volker Springel, Paul Torrey, Debora Sijacki, Dandan Xu, Greg Snyder, Dylan Nelson, and Lars Hernquist. Introducing the Illustris Project: simulating the coevolution of dark and visible matter in the Universe. *MNRAS*, 444 (2):1518–1547, October 2014. .

Joop Schaye, Robert A. Crain, Richard G. Bower, Michelle Furlong, Matthieu Schaller, Tom Theuns, Claudio Dalla Vecchia, Carlos S. Frenk, I. G. McCarthy, John C. Helly, Adrian Jenkins, Y. M. Rosas-Guevara, Simon D. M. White, Maarten Baes, C. M. Booth, Peter Camps, Julio F. Navarro, Yan Qu, Alireza Rahmati, Till Sawala, Peter A. Thomas, and James Trayford. The EAGLE project: simulating the evolution and assembly of galaxies and their environments. *MNRAS*, 446(1):521–554, January 2015. .

Ena Choi, Jeremiah P. Ostriker, Thorsten Naab, Rachel S. Somerville, Michaela Hirschmann, Alejandro Núñez, Chia-Yu Hu, and Ludwig Oser. Physics of Galactic Metals: Evolutionary Effects due to Production, Distribution, Feedback, and Interaction with Black Holes. *ApJ*, 844(1):31, July 2017. .

Rainer Weinberger, Volker Springel, Rüdiger Pakmor, Dylan Nelson, Shy Genel, Annalisa Pillepich, Mark Vogelsberger, Federico Marinacci, Jill Naiman, Paul Torrey, and Lars Hernquist. Supermassive black holes and their feedback effects in the IllustrisTNG simulation. *MNRAS*, 479(3):4056–4072, September 2018. .

Elad Zinger, Annalisa Pillepich, Dylan Nelson, Rainer Weinberger, Rüdiger Pakmor, Volker Springel, Lars Hernquist, Federico Marinacci, and Mark Vogelsberger. Ejective and preventative: the IllustrisTNG black hole feedback and its effects on the thermodynamics of the gas within and around galaxies. *MNRAS*, 499(1):768–792, November 2020. .

Wenlin Ma, Kexin Liu, Hong Guo, Weiguang Cui, Michael G. Jones, Jing Wang, Le Zhang, and Romeel Davé. Effects of Active Galactic Nucleus Feedback on Cold Gas Depletion and Quenching of Central Galaxies. *ApJ*, 941(2):205, December 2022. .

Joanna M. Piotrowska, Asa F. L. Bluck, Roberto Maiolino, and Yingjie Peng. On the quenching of star formation in observed and simulated central galaxies: evidence for the role of integrated AGN feedback. *MNRAS*, 512(1):1052–1090, May 2022. .

Asa F. L. Bluck, Joanna M. Piotrowska, and Roberto Maiolino. The Fundamental Signature of Star Formation Quenching from AGN Feedback: A Critical Dependence of Quiescence on Supermassive Black Hole Mass, Not Accretion Rate. *ApJ*, 944(1):108, February 2023a. .

Asa F. L. Bluck, J. Trevor Mendel, Sara L. Ellison, Jorge Moreno, Luc Simard, David R. Patton, and Else Starkenburg. Bulge mass is king: the dominant role of the bulge in determining the fraction of passive galaxies in the Sloan Digital Sky Survey. *MNRAS*, 441(1):599–629, June 2014. .

Shiying Lu, Guanwen Fang, Yizhou Gu, Qirong Yuan, Zhen-Yi Cai, and Xu Kong. The Effect of the Morphological Quenching Mechanism on Star Formation Activity at 0.5 $<$ z $<$ 1.5 in 3D-HST/CANDELS. *ApJ*, 913(2):81, June 2021. .

J. L. Sérsic. Influence of the atmospheric and instrumental dispersion on the brightness distribution in a galaxy. *Boletin de la Asociacion Argentina de Astronomia La Plata Argentina*, 6:41–43, February 1963.

Katherine A. Suess, Mariska Kriek, Sedona H. Price, and Guillermo Barro. Half-mass Radii of Quiescent and Star-forming Galaxies Evolve Slowly from $0 \lesssim z \leq 2.5$: Implications for Galaxy Assembly Histories. *ApJ*, 885(1):L22, November 2019. .

Ryan Brennan, Viraj Pandya, Rachel S. Somerville, Guillermo Barro, Edward N. Taylor, Stijn Wuyts, Eric F. Bell, Avishai Dekel, Henry C. Ferguson, Daniel H. McIntosh, Casey Papovich, and Joel Primack. Quenching and morphological transformation in semi-analytic models and CANDELS. *MNRAS*, 451(3):2933–2956, August 2015. .

Kung-Yi Su, Philip F. Hopkins, Christopher C. Hayward, Xiangcheng Ma, Claude-André Faucher-Giguère, Dušan Kereš, Matthew E. Orr, T. K. Chan, and Victor H. Robles. The failure of stellar feedback, magnetic fields, conduction, and morphological quenching in maintaining red galaxies. *MNRAS*, 487(3):4393–4408, August 2019. .

Volker Springel, Simon D. M. White, Adrian Jenkins, Carlos S. Frenk, Naoki Yoshida, Liang Gao, Julio Navarro, Robert Thacker, Darren Croton, John Helly, John A. Peacock, Shaun Cole, Peter Thomas, Hugh Couchman, August Evrard, Jörg Colberg, and Frazer Pearce. Simulations of the formation, evolution and clustering of galaxies and quasars. *Nature*, 435(7042):629–636, June 2005. .

Planck Collaboration, P. A. R. Ade, N. Aghanim, M. Arnaud, M. Ashdown, J. Aumont, C. Baccigalupi, A. J. Banday, R. B. Barreiro, J. G. Bartlett, N. Bartolo, E. Battaner, R. Battye, K. Benabed, A. Benoît, A. Benoit-Lévy, J. P. Bernard, M. Bersanelli, P. Bielewicz, J. J. Bock, A. Bonaldi, L. Bonavera, J. R. Bond, J. Borrill, F. R. Bouchet, F. Boulanger, M. Bucher, C. Burigana, R. C. Butler, E. Calabrese, J. F. Cardoso, A. Catalano, A. Challinor, A. Chamballu, R. R. Chary, H. C. Chiang, J. Chluba, P. R. Christensen, S. Church, D. L. Clements, S. Colombi, L. P. L. Colombo, C. Combet, A. Coulais, B. P. Crill, A. Curto, F. Cuttaia, L. Danese, R. D. Davies, R. J. Davis, P. de Bernardis, A. de Rosa, G. de Zotti, J. Delabrouille, F. X. Désert, E. Di Valentino, C. Dickinson, J. M. Diego, K. Dolag, H. Dole, S. Donzelli, O. Doré, M. Douspis, A. Ducout, J. Dunkley, X. Dupac, G. Efstathiou, F. Elsner, T. A. Enßlin, H. K. Eriksen, M. Farhang, J. Fergusson, F. Finelli, O. Forni, M. Frailis, A. A. Fraisse, E. Franceschi, A. Frejsel, S. Galeotta, S. Galli, K. Ganga, C. Gauthier, M. Gerbino, T. Ghosh, M. Giard, Y. Giraud-Héraud, E. Giusarma, E. Gjerløw, J. González-Nuevo, K. M. Górski, S. Gratton, A. Gregorio, A. Gruppuso, J. E. Gudmundsson, J. Hamann, F. K. Hansen, D. Hanson, D. L. Harrison, G. Helou, S. Henrot-Versillé, C. Hernández-Monteagudo, D. Herranz, S. R. Hildebrandt, E. Hivon, M. Hobson, W. A. Holmes, A. Hornstrup, W. Hovest, Z. Huang, K. M. Huffenberger, G. Hurier, A. H. Jaffe, T. R. Jaffe, W. C. Jones, M. Juvela, E. Keihänen, R. Keskitalo, T. S. Kisner, R. Kneissl, J. Knoche, L. Knox, M. Kunz, H. Kurki-Suonio, G. Lagache, A. Lähteenmäki, J. M. Lamarre, A. Lasenby, M. Lattanzi, C. R. Lawrence, J. P. Leahy, R. Leonardi, J. Lesgourgues, F. Levrier, A. Lewis, M. Liguori, P. B. Lilje, M. Linden-Vørnle, M. López-Caniego, P. M. Lubin, J. F. Macías-Pérez, G. Maggio, D. Maino, N. Mandolesi, A. Mangilli, A. Marchini, M. Maris, P. G. Martin, M. Martinelli, E. Martínez-González, S. Masi, S. Matarrese, P. McGehee, P. R. Meinhold, A. Melchiorri, J. B. Melin, L. Mendes, A. Mennella, M. Migliaccio, M. Millea, S. Mitra, M. A. Miville-Deschênes, A. Moneti, L. Montier, G. Morgante, D. Mortlock, A. Moss, D. Munshi, J. A. Murphy, P. Naselsky, F. Nati, P. Natoli, C. B. Netterfield, H. U. Nørgaard-Nielsen, F. Noviello, D. Novikov, I. Novikov, C. A. Oxborrow, F. Paci, L. Pagano, F. Pajot, R. Paladini, D. Paoletti, B. Partridge, F. Pasian, G. Patanchon, T. J. Pearson, O. Perdereau, L. Perotto, F. Perrotta, V. Pettorino, F. Piacentini, M. Piat, E. Pierpaoli, D. Pietrobon, S. Plaszczynski, E. Pointecouteau, G. Polenta, L. Popa, G. W. Pratt, G. Prézeau, S. Prunet, J. L. Puget, J. P. Rachen, W. T. Reach, R. Rebolo, M. Reinecke, M. Remazeilles, C. Renault, A. Renzi, I. Ristorcelli, G. Rocha, C. Rosset, M. Rossetti, G. Roudier, B. Rouillé d'Orfeuil, M. Rowan-Robinson, J. A. Rubiño-Martín, B. Rusholme, N. Said, V. Salvatelli, L. Salvati, M. Sandri, D. Santos, M. Savelainen, G. Savini, D. Scott, M. D.

Seiffert, P. Serra, E. P. S. Shellard, L. D. Spencer, M. Spinelli, V. Stolyarov, R. Stompor, R. Sudiwala, R. Sunyaev, D. Sutton, A. S. Suur-Uski, J. F. Sygnet, J. A. Tauber, L. Terenzi, L. Toffolatti, M. Tomasi, M. Tristram, T. Trombetti, M. Tucci, J. Tuovinen, M. Türler, G. Umana, L. Valenziano, J. Valiviita, F. Van Tent, P. Vielva, F. Villa, L. A. Wade, B. D. Wandelt, I. K. Wehus, M. White, S. D. M. White, A. Wilkinson, D. Yvon, A. Zacchei, and A. Zonca. Planck 2015 results. XIII. Cosmological parameters. *A&A*, 594:A13, September 2016. .

Yun Li and Houjun Mo. Mass distribution and accretion of sub-halos. *arXiv e-prints*, art. arXiv:0908.0301, August 2009.

Sheridan B. Green, Frank C. van den Bosch, and Fangzhou Jiang. The tidal evolution of dark matter substructure - II. The impact of artificial disruption on subhalo mass functions and radial profiles. *MNRAS*, 503(3):4075–4091, May 2021. .

D. Nelson, A. Pillepich, V. Springel, R. Weinberger, L. Hernquist, R. Pakmor, S. Genel, P. Torrey, M. Vogelsberger, G. Kauffmann, F. Marinacci, and J. Naiman. First results from the IllustrisTNG simulations: the galaxy colour bimodality. *MNRAS*, 475:624–647, March 2018. .

Volker Springel, Rüdiger Pakmor, Annalisa Pillepich, Rainer Weinberger, Dylan Nelson, Lars Hernquist, Mark Vogelsberger, Shy Genel, Paul Torrey, Federico Marinacci, and Jill Naiman. First results from the IllustrisTNG simulations: matter and galaxy clustering. *MNRAS*, 475(1):676–698, March 2018. .

Federico Marinacci, Mark Vogelsberger, Rüdiger Pakmor, Paul Torrey, Volker Springel, Lars Hernquist, Dylan Nelson, Rainer Weinberger, Annalisa Pillepich, Jill Naiman, and Shy Genel. First results from the IllustrisTNG simulations: radio haloes and magnetic fields. *MNRAS*, 480(4):5113–5139, November 2018. .

Jill P. Naiman, Annalisa Pillepich, Volker Springel, Enrico Ramirez-Ruiz, Paul Torrey, Mark Vogelsberger, Rüdiger Pakmor, Dylan Nelson, Federico Marinacci, Lars Hernquist, Rainer Weinberger, and Shy Genel. First results from the IllustrisTNG simulations: a tale of two elements - chemical evolution of magnesium and europium. *MNRAS*, 477(1):1206–1224, June 2018. .

Volker Springel. E pur si muove: Galilean-invariant cosmological hydrodynamical simulations on a moving mesh. *MNRAS*, 401(2):791–851, January 2010. .

Ruediger Pakmor, Andreas Bauer, and Volker Springel. Magnetohydrodynamics on an unstructured moving grid. *MNRAS*, 418(2):1392–1401, December 2011. .

Rüdiger Pakmor and Volker Springel. Simulations of magnetic fields in isolated disc galaxies. *MNRAS*, 432(1):176–193, June 2013. .

Annalisa Pillepich, Volker Springel, Dylan Nelson, Shy Genel, Jill Naiman, Rüdiger Pakmor, Lars Hernquist, Paul Torrey, Mark Vogelsberger, Rainer Weinberger, and Federico Marinacci. Simulating galaxy formation with the IllustrisTNG model. *MNRAS*, 473(3):4077–4106, January 2018b. .

Rainer Weinberger, Volker Springel, Lars Hernquist, Annalisa Pillepich, Federico Marinacci, Rüdiger Pakmor, Dylan Nelson, Shy Genel, Mark Vogelsberger, Jill Naiman, and Paul Torrey. Simulating galaxy formation with black hole driven thermal and kinetic feedback. *MNRAS*, 465(3):3291–3308, March 2017. .

Mohammadreza Ayromlou, Dylan Nelson, Robert M. Yates, Guinevere Kauffmann, Malin Renneby, and Simon D. M. White. Comparing galaxy formation in the L-GALAXIES semi-analytical model and the IllustrisTNG simulations. *MNRAS*, 502 (1):1051–1069, March 2021b. .

Eric Rohr, Annalisa Pillepich, Dylan Nelson, Elad Zinger, Gandhali Joshi, and Mohommadreza Ayromlou. Jellyfish galaxies with the IllustrisTNG simulations – When, where, and for how long does ram pressure stripping of cold gas occur? *arXiv e-prints*, art. arXiv:2304.09196, April 2023. .

Vicente Rodriguez-Gomez, Shy Genel, Mark Vogelsberger, Debora Sijacki, Annalisa Pillepich, Laura V. Sales, Paul Torrey, Greg Snyder, Dylan Nelson, Volker Springel, Chung-Pei Ma, and Lars Hernquist. The merger rate of galaxies in the Illustris simulation: a comparison with observations and semi-empirical models. *MNRAS*, 449(1): 49–64, May 2015. .

Shy Genel, S. Michael Fall, Lars Hernquist, Mark Vogelsberger, Gregory F. Snyder, Vicente Rodriguez-Gomez, Debora Sijacki, and Volker Springel. Galactic Angular Momentum in the Illustris Simulation: Feedback and the Hubble Sequence. *ApJ*, 804(2): L40, May 2015. .

Federico Marinacci, Rüdiger Pakmor, and Volker Springel. The formation of disc galaxies in high-resolution moving-mesh cosmological simulations. *MNRAS*, 437(2):1750–1775, January 2014. .

Min Du, Luis C. Ho, Dongyao Zhao, Jingjing Shi, Victor P. Debattista, Lars Hernquist, and Dylan Nelson. Identifying Kinematic Structures in Simulated Galaxies Using Unsupervised Machine Learning. *ApJ*, 884(2):129, October 2019. .

C. Y. Jiang, Y. P. Jing, A. Faltenbacher, W. P. Lin, and Cheng Li. A Fitting Formula for the Merger Timescale of Galaxies in Hierarchical Clustering. *ApJ*, 675(2):1095–1105, March 2008. .

I. Koutsouridou and A. Cattaneo. Bursting and quenching in satellite galaxies. *MNRAS*, 490(4):5375–5389, December 2019. .

Rahul Kannan, Andrea V. Macciò, Fabio Fontanot, Benjamin P. Moster, Wouter Karman, and Rachel S. Somerville. From discs to bulges: effect of mergers on the morphology of galaxies. *MNRAS*, 452(4):4347–4360, October 2015. .

Zhu Chen, S. M. Faber, David C. Koo, Rachel S. Somerville, Joel R. Primack, Avishai Dekel, Aldo Rodríguez-Puebla, Yicheng Guo, Guillermo Barro, Dale D. Kocevski, A. van der Wel, Joanna Woo, Eric F. Bell, Jerome J. Fang, Henry C. Ferguson, Mauro Giavalisco, Marc Huertas-Company, Fangzhou Jiang, Susan Kassin, Lin Lin, F. S. Liu, Yifei Luo, Zhijian Luo, Camilla Pacifici, Viraj Pandya, Samir Salim, Chenggang Shu, Sandro Tacchella, Bryan A. Terrazas, and Hassen M. Yesuf. Quenching as a Contest between Galaxy Halos and Their Central Black Holes. *ApJ*, 897(1):102, July 2020. .

K. N. Abazajian, J. K. Adelman-McCarthy, M. A. Agüeros, S. S. Allam, C. Allende Prieto, D. An, K. S. J. Anderson, S. F. Anderson, J. Annis, N. A. Bahcall, and et al. The Seventh Data Release of the Sloan Digital Sky Survey. *ApJS*, 182:543–558, June 2009. .

A. Meert, V. Vikram, and M. Bernardi. A catalogue of 2D photometric decompositions in the SDSS-DR7 spectroscopic main galaxy sample: preferred models and systematics. *MNRAS*, 446:3943–3974, February 2015. .

A. Meert, V. Vikram, and M. Bernardi. A catalogue of two-dimensional photometric decompositions in the SDSS-DR7 spectroscopic main galaxy sample: extension to g and I bands. *MNRAS*, 455:2440–2452, January 2016. .

J. L. Fischer, M. Bernardi, and A. Meert. Comparing pymorph and SDSS photometry - I. Background sky and model fitting effects. *MNRAS*, 467(1):490–500, May 2017. .

X. Yang, H. J. Mo, F. C. van den Bosch, A. Pasquali, C. Li, and M. Barden. Galaxy Groups in the SDSS DR4. I. The Catalog and Basic Properties. *ApJ*, 671:153–170, December 2007. .

H. Domínguez Sánchez, M. Huertas-Company, M. Bernardi, D. Tuccillo, and J. L. Fischer. Improving galaxy morphologies for SDSS with Deep Learning. *MNRAS*, 476: 3661–3676, May 2018. .

Kevin Bundy, Matthew A. Bershady, David R. Law, Renbin Yan, Niv Drory, Nicholas MacDonald, David A. Wake, Brian Cherinka, José R. Sánchez-Gallego, Anne-Marie Weijmans, Daniel Thomas, Christy Tremonti, Karen Masters, Lodovico Coccato, Aleksandar M. Diamond-Stanic, Alfonso Aragón-Salamanca, Vladimir Avila-Reese, Carles Badenes, Jésus Falcón-Barroso, Francesco Belfiore, Dmitry Bizyaev, Guillermo A. Blanc, Joss Bland-Hawthorn, Michael R. Blanton, Joel R. Brownstein, Nell Byler, Michele Cappellari, Charlie Conroy, Aaron A. Dutton, Eric Emsellem, James Etherington, Peter M. Frinchaboy, Hai Fu, James E. Gunn, Paul Harding, Evelyn J. Johnston, Guinevere Kauffmann, Karen Kinemuchi, Mark A. Klaene, Johan H. Knapen, Alexie Leauthaud, Cheng Li, Lihwai Lin, Roberto Maiolino, Viktor

Malanushenko, Elena Malanushenko, Shude Mao, Claudia Maraston, Richard M. McDermid, Michael R. Merrifield, Robert C. Nichol, Daniel Oravetz, Kaike Pan, John K. Parejko, Sebastian F. Sanchez, David Schlegel, Audrey Simmons, Oliver Steele, Matthias Steinmetz, Karun Thanjavur, Benjamin A. Thompson, Jeremy L. Tinker, Remco C. E. van den Bosch, Kyle B. Westfall, David Wilkinson, Shelley Wright, Ting Xiao, and Kai Zhang. Overview of the SDSS-IV MaNGA Survey: Mapping nearby Galaxies at Apache Point Observatory. *ApJ*, 798(1):7, January 2015. .

N. Drory, N. MacDonald, M. A. Bershady, K. Bundy, J. Gunn, D. R. Law, M. Smith, R. Stoll, C. A. Tremonti, D. A. Wake, R. Yan, A. M. Weijmans, N. Byler, B. Cherinka, F. Cope, A. Eigenbrot, P. Harding, D. Holder, J. Huehnerhoff, K. Jaehnig, T. C. Jansen, M. Klaene, A. M. Paat, J. Percival, and C. Sayres. The MaNGA Integral Field Unit Fiber Feed System for the Sloan 2.5 m Telescope. *AJ*, 149:77, February 2015. .

David R. Law, Renbin Yan, Matthew A. Bershady, Kevin Bundy, Brian Cherinka, Niv Drory, Nicholas MacDonald, José R. Sánchez-Gallego, David A. Wake, Anne-Marie Weijmans, Michael R. Blanton, Mark A. Klaene, Sean M. Moran, Sebastian F. Sanchez, and Kai Zhang. Observing Strategy for the SDSS-IV/MaNGA IFU Galaxy Survey. *AJ*, 150(1):19, Jul 2015. .

Renbin Yan, Christy Tremonti, Matthew A. Bershady, David R. Law, David J. Schlegel, Kevin Bundy, Niv Drory, Nicholas MacDonald, Dmitry Bizyaev, Guillermo A. Blanc, Michael R. Blanton, Brian Cherinka, Arthur Eigenbrot, James E. Gunn, Paul Harding, David W. Hogg, José R. Sánchez-Gallego, Sebastian F. Sánchez, David A. Wake, Anne-Marie Weijmans, Ting Xiao, and Kai Zhang. SDSS-IV/MaNGA: Spectrophotometric Calibration Technique. *The Astrophysical Journal*, 151(1):8, January 2016a. .

Renbin Yan, Kevin Bundy, David R. Law, Matthew A. Bershady, Brett Andrews, Brian Cherinka, Aleksandar M. Diamond-Stanic, Niv Drory, Nicholas MacDonald, José R. Sánchez-Gallego, Daniel Thomas, David A. Wake, Anne-Marie Weijmans, Kyle B. Westfall, Kai Zhang, Alfonso Aragón-Salamanca, Francesco Belfiore, Dmitry Bizyaev, Guillermo A. Blanc, Michael R. Blanton, Joel Brownstein, Michele Cappellari, Richard D'Souza, Eric Emsellem, Hai Fu, Patrick Gaulme, Mark T. Graham, Daniel Goddard, James E. Gunn, Paul Harding, Amy Jones, Karen Kinemuchi, Cheng Li, Hongyu Li, Roberto Maiolino, Shude Mao, Claudia Maraston, Karen Masters, Michael R. Merrifield, Daniel Oravetz, Kaike Pan, John K. Parejko, Sebastian F. Sanchez, David Schlegel, Audrey Simmons, Karun Thanjavur, Jeremy Tinker, Christy Tremonti, Remco van den Bosch, and Zheng Zheng. SDSS-IV MaNGA IFS Galaxy Survey—Survey Design, Execution, and Initial Data Quality. *The Astrophysical Journal*, 152(6):197, December 2016b. .

James E. Gunn, Walter A. Siegmund, Edward J. Mannery, Russell E. Owen, Charles L. Hull, R. French Leger, Larry N. Carey, Gillian R. Knapp, Donald G. York, William N. Boroski, Stephen M. Kent, Robert H. Lupton, Constance M. Rockosi, Michael L.

Evans, Patrick Waddell, John E. Anderson, James Annis, John C. Barentine, Larry M. Bartoszek, Steven Bastian, Stephen B. Bracker, Howard J. Brewington, Charles I. Briegel, Jon Brinkmann, Yorke J. Brown, Michael A. Carr, Paul C. Czarapata, Craig C. Drennan, Thomas Dombeck, Glenn R. Federwitz, Bruce A. Gillespie, Carlos Gonzales, Sten U. Hansen, Michael Harvanek, Jeffrey Hayes, Wendell Jordan, Ellyne Kinney, Mark Klaene, S. J. Kleinman, Richard G. Kron, Jurek Kresinski, Glenn Lee, Siriluk Limmongkol, Carl W. Lindenmeyer, Daniel C. Long, Craig L. Loomis, Peregrine M. McGehee, Paul M. Mantsch, Jr. Neilsen, Eric H., Richard M. Neswold, Peter R. Newman, Atsuko Nitta, Jr. Peoples, John, Jeffrey R. Pier, Peter S. Prieto, Angela Prosapio, Claudio Rivetta, Donald P. Schneider, Stephanie Snedden, and Shu-i. Wang. The 2.5 m Telescope of the Sloan Digital Sky Survey. *AJ*, 131(4):2332–2359, Apr 2006. .

Stephen A. Smee, James E. Gunn, Alan Uomoto, Natalie Roe, David Schlegel, Constance M. Rockosi, Michael A. Carr, French Leger, Kyle S. Dawson, Matthew D. Olmstead, Jon Brinkmann, Russell Owen, Robert H. Barkhouser, Klaus Honscheid, Paul Harding, Dan Long, Robert H. Lupton, Craig Loomis, Lauren Anderson, James Annis, Mariangela Bernardi, Vaishali Bhardwaj, Dmitry Bizyaev, Adam S. Bolton, Howard Brewington, John W. Briggs, Scott Burles, James G. Burns, Francisco Javier Castander, Andrew Connolly, James R. A. Davenport, Garrett Ebelke, Harland Epps, Paul D. Feldman, Scott D. Friedman, Joshua Frieman, Timothy Heckman, Charles L. Hull, Gillian R. Knapp, David M. Lawrence, Jon Loveday, Edward J. Mannery, Elena Malanushenko, Viktor Malanushenko, Aronne James Merrelli, Demitri Muna, Peter R. Newman, Robert C. Nichol, Daniel Oravetz, Kaike Pan, Adrian C. Pope, Paul G. Ricketts, Alaina Shelden, Dale Sandford, Walter Siegmund, Audrey Simmons, D. Shane Smith, Stephanie Snedden, Donald P. Schneider, Mark SubbaRao, Christy Tremonti, Patrick Waddell, and Donald G. York. The Multi-object, Fiber-fed Spectrographs for the Sloan Digital Sky Survey and the Baryon Oscillation Spectroscopic Survey. *AJ*, 146(2):32, Aug 2013. .

M. R. Blanton, M. A. Bershady, B. Abolfathi, F. D. Albareti, C. Allende Prieto, A. Almeida, J. Alonso-García, F. Anders, S. F. Anderson, B. Andrews, and et al. Sloan Digital Sky Survey IV: Mapping the Milky Way, Nearby Galaxies, and the Distant Universe. *AJ*, 154:28, July 2017. .

Abdurro'uf, Katherine Accetta, Conny Aerts, Victor Silva Aguirre, Romina Ahumada, Nikhil Ajgaonkar, N. Filiz Ak, Shadab Alam, Carlos Allende Prieto, Andres Almeida, Friedrich Anders, Scott F. Anderson, Brett H. Andrews, Borja Anguiano, Erik Aquino-Ortiz, Alfonso Aragon-Salamanca, Maria Argudo-Fernandez, Metin Ata, Marie Aubert, Vladimir Avila-Reese, Carles Badenes, Rodolfo H. Barba, Kat Barger, Jorge K. Barrera-Ballesteros, Rachael L. Beaton, Timothy C. Beers, Francesco Belfiore, Chad F. Bender, Mariangela Bernardi, Matthew A. Bershady, Florian Beutler, Christian Moni Bidin, Jonathan C. Bird, Dmitry Bizyaev, Guillermo A. Blanc,

Michael R. Blanton, Nicholas Fraser Boardman, Adam S. Bolton, Mederic Boquien, Jura Borissova, Jo Bovy, W. N. Brandt, Jordan Brown, Joel R. Brownstein, Marcella Brusa, Johannes Buchner, Kevin Bundy, Joseph N. Burchett, Martin Bureau, Adam Burgasser, Tuesday K. Cabang, Stephanie Campbell, Michele Cappellari, Joleen K. Carlberg, Fabio Carneiro Wanderley, Ricardo Carrera, Jennifer Cash, Yan-Ping Chen, Wei-Huai Chen, Brian Cherinka, Cristina Chiappini, Peter Doohyun Choi, S. Drew Chojnowski, Haeun Chung, Nicolas Clerc, Roger E. Cohen, Julia M. Comerford, Johan Comparat, Luiz da Costa, Kevin Covey, Jeffrey D. Crane, Irene Cruz-Gonzalez, Connor Culhane, Katia Cunha, Y. Sophia Dai, Guillermo Damke, Jeremy Darling, Jr. Davidson, James W., Roger Davies, Kyle Dawson, Nathan De Lee, Aleksandar M. Diamond-Stanic, Mariana Cano-Diaz, Helena Dominguez Sanchez, John Donor, Chris Duckworth, Tom Dwelly, Daniel J. Eisenstein, Yvonne P. Elsworth, Eric Emsellem, Mike Eracleous, Stephanie Escoffier, Xiaohui Fan, Emily Farr, Shuai Feng, Jose G. Fernandez-Trincado, Diane Feuillet, Andreas Filipp, Sean P Fillingham, Peter M. Frinchaboy, Sebastien Fromenteau, Lluis Galbany, Rafael A. Garcia, D. A. Garcia-Hernandez, Junqiang Ge, Doug Geisler, Joseph Gelfand, Tobias Geron, Benjamin J. Gibson, Julian Goddy, Diego Godoy-Rivera, Kathleen Grabowski, Paul J. Green, Michael Greener, Catherine J. Grier, Emily Griffith, Hong Guo, Julien Guy, Massinissa Hadjara, Paul Harding, Sten Hasselquist, Christian R. Hayes, Fred Hearty, Jess Hernndez, Lewis Hill, David W. Hogg, Jon A. Holtzman, Danny Horta, Bau-Ching Hsieh, Chin-Hao Hsu, Yun-Hsin Hsu, Daniel Huber, Marc Huertas-Company, Brian Hutchinson, Ho Seong Hwang, Hector J. Ibarra-Medel, Jacob Ider Chitham, Gabriele S. Ilha, Julie Imig, Will Jaekle, Tharindu Jayasinghe, Xihan Ji, Jennifer A. Johnson, Amy Jones, Henrik Jonsson, Ivan Katkov, Dr. Khalatyan, Arman, Karen Kinemuchi, Shobhit Kisku, Johan H. Knapen, Jean-Paul Kneib, Juna A. Kollmeier, Miranda Kong, Marina Kounkel, Kathryn Kreckel, Dhanesh Krishnarao, Ivan Lacerna, Richard R. Lane, Rachel Langgin, Ramon Lavender, David R. Law, Daniel Lazarz, Henry W. Leung, Ho-Hin Leung, Hannah M. Lewis, Cheng Li, Ran Li, Jianhui Lian, Fu-Heng Liang, Lihwai Lin, Yen-Ting Lin, Sicheng Lin, Chris Lintott, Dan Long, Penelope Longa-Pena, Carlos Lopez-Coba, Shengdong Lu, Britt F. Lundgren, Yuanze Luo, J. Ted Mackereth, Axel de la Macorra, Suvrath Mahadevan, Steven R. Majewski, Arturo Manchado, Travis Mandeville, Claudia Maraston, Berta Margalef-Bentabol, Thomas Masseron, Karen L. Masters, Savita Mathur, Richard M. McDermid, Myles Mckay, Andrea Merloni, Michael Merrifield, Szabolcs Meszaros, Andrea Miglio, Francesco Di Mille, Dante Minniti, Rebecca Minsley, Antonela Monachesi, Jeongin Moon, Benoit Mosser, John Mulchaey, Demitri Muna, Ricardo R. Munoz, Adam D. Myers, Natalie Myers, Seshadri Nadathur, Preethi Nair, Kirpal Nandra, Justus Neumann, Jeffrey A. Newman, David L. Nidever, Farnik Nikakhtar, Christian Nitschelm, Julia E. O'Connell, Luis Garma-Oehmichen, Gabriel Luan Souza de Oliveira, Richard Olney, Daniel Oravetz, Mario Ortigoza-Urdaneta, Yeisson Osorio, Justin Otter, Zachary J. Pace, Nelson Padilla, Kaike Pan, Hsi-An

Pan, Taniya Parikh, James Parker, Sebastien Peirani, Karla Pena Ramirez, Samantha Penny, Will J. Percival, Ismael Perez-Fournon, Marc Pinsonneault, Frederick Poidevin, Vijith Jacob Poovelil, Adrian M. Price-Whelan, Anna Barbara de Andrade Queiroz, M. Jordan Raddick, Amy Ray, Sandro Barboza Rembold, Nicole Riddle, Rogemar A. Riffel, Rogerio Riffel, Hans-Walter Rix, Annie C. Robin, Aldo Rodriguez-Puebla, Felipe Antonio Santana Rojas, Alexandre Roman-Lopes, Carlos Roman-Zuniga, Benjamin Rose, Ashley J. Ross, Graziano Rossi, Kate H. R. Rubin, Mara Salvato, Jose R. Sanchez-Gallego, Robyn Sanderson, Edgar Sarceno, Regina Sarmiento, Conor Sayres, Elizaveta Sazonova, Adam L. Schaefer, David J Schlegel, Donald P. Schneider, Mathias Schultheis, Axel Schwope, Aldo Serenelli, Javier Serna, Zhengyi Shao, Griffin Shapiro, Anubhav Sharma, Yue Shen, Matthew Shetrone, Yiping Shu, Joshua D. Simon, M. F. Skrutskie, Rebecca Smethurst, Verne Smith, Jennifer Sobeck, Taylor Spoo, Dani Sprague, David V. Stark, Keivan G. Stassun, Matthias Steinmetz, Dennis Stello, Alexander Stone-Martinez, Thaisa Storchi-Bergmann, Guy S. Stringfellow, Amelia Stutz, Yung-Chau Su, Manuchehr Taghizadeh-Popp, Michael S. Talbot, Jamie Tayar, Eduardo Telles, Johanna Teske, Ani Thakar, Christopher Theissen, Daniel Thomas, Andrew Tkachenko, Rita Tojeiro, Hector Hernandez Toledo, Nicholas W. Troup, Jonathan R. Trump, James Trussler, Jacqueline Turner, Sarah Tuttle, Eduardo Unda-Sanzana, Jose Antonio Vazquez-Mata, Marica Valentini, Octavio Valenzuela, Jaime Vargas-Gonzalez, Mariana Vargas-Magana, Pablo Vera Alfaro, Sandro Villanova, Fiorenzo Vincenzo, David Wake, Jack T. Warfield, Jessica Diane Washington, Benjamin Alan Weaver, Anne-Marie Weijmans, David H. Weinberg, Achim Weiss, Kyle B. Westfall, Vivienne Wild, Matthew C. Wilde, John C. Wilson, Robert F. Wilson, Mikayla Wilson, Julien Wolf, W. M. Wood-Vasey, Renbin Yan, Olga Zamora, Gail Zasowski, Kai Zhang, Cheng Zhao, Zheng Zheng, Zheng Zheng, and Kai Zhu. The Seventeenth Data Release of the Sloan Digital Sky Surveys: Complete Release of MaNGA, MaStar and APOGEE-2 Data. *arXiv e-prints*, art. arXiv:2112.02026, December 2021.

H. Domínguez Sánchez, B. Margalef, M. Bernardi, and M. Huertas-Company. SDSS-IV DR17: final release of MaNGA PyMorph photometric and deep-learning morphological catalogues. *MNRAS*, 509(3):4024–4036, January 2022. .

M. Bernardi, R. K. Sheth, H. Domínguez Sánchez, B. Margalef-Bentabol, D. Bizyaev, and R. R. Lane. The half-mass radius of MaNGA galaxies: effect of IMF gradients. *MNRAS*, 518(3):3494–3508, January 2023. .

C. Bertemes and S. Wuyts. "". ””, in prep.

Michael R. Blanton, Eyal Kazin, Demitri Muna, Benjamin A. Weaver, and Adrian Price-Whelan. Improved Background Subtraction for the Sloan Digital Sky Survey Images. *The Astrophysical Journal*, 142(1):31, July 2011. .

A. C. Carnall, R. J. McLure, J. S. Dunlop, and R. Davé. Inferring the star formation histories of massive quiescent galaxies with BAGPIPES: Evidence for multiple quenching mechanisms. *Monthly Notices of the Royal Astronomical Society*, 480(4):4379–4401, 2018. ISSN 13652966. .

Joel Leja, Adam C. Carnall, Benjamin D. Johnson, Charlie Conroy, and Joshua S. Speagle. How to Measure Galaxy Star Formation Histories. II. Nonparametric Models. *ApJ*, 876(1):3, May 2019a. .

Daniela Calzetti, Lee Armus, Ralph C. Bohlin, Anne L. Kinney, Jan Koornneef, and Thaisa Storchi-Bergmann. The Dust Content and Opacity of Actively Star-forming Galaxies. *The Astrophysical Journal*, 533(2):682–695, April 2000. .

Kyle B. Westfall, Michele Cappellari, Matthew A. Bershady, Kevin Bundy, Francesco Belfiore, Xihan Ji, David R. Law, Adam Schaefer, Shravan Shetty, Christy A. Tremonti, Renbin Yan, Brett H. Andrews, Joel R. Brownstein, Brian Cherinka, Lodovico Coccato, Niv Drory, Claudia Maraston, Taniya Parikh, José R. Sánchez-Gallego, Daniel Thomas, Anne-Marie Weijmans, Jorge Barrera-Ballesteros, Cheng Du, Daniel Goddard, Niu Li, Karen Masters, Héctor Javier Ibarra Medel, Sebastián F. Sánchez, Meng Yang, Zheng Zheng, and Shuang Zhou. The Data Analysis Pipeline for the SDSS-IV MaNGA IFU Galaxy Survey: Overview. *AJ*, 158(6):231, December 2019. .

J. Liske, I. K. Baldry, S. P. Driver, R. J. Tuffs, M. Alpaslan, E. Andrae, S. Brough, M. E. Cluver, M. W. Grootes, M. L. P. Gunawardhana, L. S. Kelvin, J. Loveday, A. S. G. Robotham, E. N. Taylor, S. P. Bamford, J. Bland-Hawthorn, M. J. I. Brown, M. J. Drinkwater, A. M. Hopkins, M. J. Meyer, P. Norberg, J. A. Peacock, N. K. Agius, S. K. Andrews, A. E. Bauer, J. H. Y. Ching, M. Colless, C. J. Conselice, S. M. Croom, L. J. M. Davies, R. De Propris, L. Dunne, E. M. Eardley, S. Ellis, C. Foster, C. S. Frenk, B. Häußler, B. W. Holwerda, C. Howlett, H. Ibarra, M. J. Jarvis, D. H. Jones, P. R. Kafle, C. G. Lacey, R. Lange, M. A. Lara-López, Á. R. López-Sánchez, S. Maddox, B. F. Madore, T. McNaught-Roberts, A. J. Moffett, R. C. Nichol, M. S. Owers, D. Palamara, S. J. Penny, S. Phillipps, K. A. Pimbblet, C. C. Popescu, M. Prescott, R. Proctor, E. M. Sadler, A. E. Sansom, M. Seibert, R. Sharp, W. Sutherland, J. A. Vázquez-Mata, E. van Kampen, S. M. Wilkins, R. Williams, and A. H. Wright. Galaxy And Mass Assembly (GAMA): End of survey report and data release 2. *MNRAS*, 452:2087–2126, September 2015. ISSN 0035-8711. .

Simon P. Driver, Sabine Bellstedt, Aaron S. G. Robotham, Ivan K. Baldry, Luke J. Davies, Jochen Liske, Danail Obreschkow, Edward N. Taylor, Angus H. Wright, Mehmet Alpaslan, Steven P. Bamford, Amanda E. Bauer, Joss Bland-Hawthorn, Maciej Bilicki, Matías Bravo, Sarah Brough, Sarah Casura, Michelle E. Cluver, Matthew Colless, Christopher J. Conselice, Scott M. Croom, Jelte de Jong, Franceso D'Eugenio, Roberto De Propris, Burak Dogruel, Michael J. Drinkwater, Andrej Dvornik, Daniel J. Farrow,

Carlos S. Frenk, Benjamin Giblin, Alister W. Graham, Meiert W. Grootes, Madusha L. P. Gunawardhana, Abdolhosein Hashemizadeh, Boris Häußler, Catherine Heymans, Hendrik Hildebrandt, Benne W. Holwerda, Andrew M. Hopkins, Tom H. Jarrett, D. Heath Jones, Lee S. Kelvin, Soheil Koushan, Konrad Kuijken, Maritza A. Lara-López, Rebecca Lange, Ángel R. López-Sánchez, Jon Loveday, Smriti Mahajan, Martin Meyer, Amanda J. Moffett, Nicola R. Napolitano, Peder Norberg, Matt S. Owers, Mario Radovich, Mojtaba Raouf, John A. Peacock, Steven Phillipps, Kevin A. Pimbblet, Cristina Popescu, Khaled Said, Anne E. Sansom, Mark Seibert, Will J. Sutherland, Jessica E. Thorne, Richard J. Tuffs, Ryan Turner, Arjen van der Wel, Eelco van Kampen, and Steve M. Wilkins. Galaxy And Mass Assembly (GAMA): Data Release 4 and the z $<$ 0.1 total and z $<$ 0.08 morphological galaxy stellar mass functions. *MNRAS*, 513:439–467, June 2022. ISSN 0035-8711. .

Sabine Bellstedt, Simon P. Driver, Aaron S. G. Robotham, Luke J. M. Davies, Cameron R. J. Bogue, Robin H. W. Cook, Abdolhosein Hashemizadeh, Soheil Koushan, Edward N. Taylor, Jessica E. Thorne, Ryan J. Turner, and Angus H. Wright. Galaxy And Mass Assembly (GAMA): Assimilation of KiDS into the GAMA database. *MNRAS*, 496:3235–3256, August 2020. ISSN 0035-8711. .

A. S. G. Robotham, L. J. M. Davies, S. P. Driver, S. Koushan, D. S. Taranu, S. Casura, and J. Liske. ProFound: Source Extraction and Application to Modern Survey Data. *MNRAS*, 476:3137–3159, May 2018. ISSN 0035-8711. .

A. S. G. Robotham, S. Bellstedt, C. del P. Lagos, J. E. Thorne, L. J. Davies, S. P. Driver, and M. Bravo. ProSpect: Generating spectral energy distributions with complex star formation and metallicity histories. *MNRAS*, 495:905–931, June 2020. ISSN 0035-8711. .

Pieter G. van Dokkum, Katherine E. Whitaker, Gabriel Brammer, Marijn Franx, Mariska Kriek, Ivo Labbé, Danilo Marchesini, Ryan Quadri, Rachel Bezanson, Garth D. Illingworth, Adam Muzzin, Gregory Rudnick, Tomer Tal, and David Wake. The Growth of Massive Galaxies Since z = 2. *ApJ*, 709(2):1018–1041, February 2010. .

Samuel N. Leitner. On the Last 10 Billion Years of Stellar Mass Growth in Star-forming Galaxies. *ApJ*, 745(2):149, February 2012. .

Francesco Shankar, Stewart Buchan, Alessandro Rettura, Vincent R. Bouillot, Jorge Moreno, Rossella Licitra, Mariangela Bernardi, Marc Huertas-Company, Simona Mei, Begoña Ascaso, Ravi Sheth, Lauriane Delaye, and Anand Raichoor. Avoiding Progenitor Bias: The Structural and Mass Evolution of Brightest Group and Cluster Galaxies in Hierarchical Models since z $<_\sim$1. *ApJ*, 802(2):73, April 2015. .

Stewart Buchan and Francesco Shankar. Setting firmer constraints on the evolution of the most massive, central galaxies from their local abundances and ages. *MNRAS*, 462(2):2001–2010, October 2016. .

Danièl N. Groenewald, Rosalind E. Skelton, David G. Gilbank, and S. Ilani Loubser. The close pair fraction of BCGs since z = 0.5: major mergers dominate recent BCG stellar mass growth. *MNRAS*, 467(4):4101–4117, June 2017. .

J. Matharu, A. Muzzin, G. B. Brammer, R. F. J. van der Burg, M. W. Auger, P. C. Hewett, A. van der Wel, P. van Dokkum, M. Balogh, J. C. C. Chan, R. Demarco, D. Marchesini, E. J. Nelson, A. Noble, G. Wilson, and H. K. C. Yee. HST/WFC3 grism observations of $z \sim 1$ clusters: the cluster versus field stellar mass-size relation and evidence for size growth of quiescent galaxies from minor mergers. *MNRAS*, 484(1):595–617, March 2019. .

Lukas Eisert, Annalisa Pillepich, Dylan Nelson, Ralf S. Klessen, Marc Huertas-Company, and Vicente Rodriguez-Gomez. ERGO-ML I: inferring the assembly histories of IllustrisTNG galaxies from integral observable properties via invertible neural networks. *MNRAS*, 519(2):2199–2223, February 2023. .

Christoph Engler, Annalisa Pillepich, Gandhali D. Joshi, Dylan Nelson, Anna Pasquali, Eva K. Grebel, Thorsten Lisker, Elad Zinger, Martina Donnari, Federico Marinacci, Mark Vogelsberger, and Lars Hernquist. The distinct stellar-to-halo mass relations of satellite and central galaxies: insights from the IllustrisTNG simulations. *MNRAS*, 500(3):3957–3975, January 2021. .

Lan Wang and Y. P. Jing. Modelling galaxy stellar mass evolution from z $\sim$0.8 to today. *MNRAS*, 402(3):1796–1806, March 2010. . URL https://ui.adsabs.harvard.edu/abs/2010MNRAS.402.1796W.

Qi Guo, Simon White, Michael Boylan-Kolchin, Gabriella De Lucia, Guinevere Kauffmann, Gerard Lemson, Cheng Li, Volker Springel, and Simone Weinmann. From dwarf spheroidals to cD galaxies: simulating the galaxy population in a ΛCDM cosmology. *MNRAS*, 413(1):101–131, May 2011. . URL https://ui.adsabs.harvard.edu/abs/2011MNRAS.413..101G.

M. Bernardi, A. Meert, R. K. Sheth, M. Huertas-Company, C. Maraston, F. Shankar, and V. Vikram. The massive end of the luminosity and stellar mass functions and clustering from CMASS to SDSS: evidence for and against passive evolution. *MNRAS*, 455 (4):4122–4135, February 2016. .

John Moustakas, Alison L. Coil, James Aird, Michael R. Blanton, Richard J. Cool, Daniel J. Eisenstein, Alexander J. Mendez, Kenneth C. Wong, Guangtun Zhu, and Stéphane Arnouts. PRIMUS: Constraints on Star Formation Quenching and Galaxy Merging, and the Evolution of the Stellar Mass Function from z = 0-1. *ApJ*, 767(1):50, April 2013. .

Francesco Shankar, Hong Guo, Vincent Bouillot, Alessandro Rettura, Alan Meert, Stewart Buchan, Andrey Kravtsov, Mariangela Bernardi, Ravi Sheth, Vinu Vikram,

Danilo Marchesini, Peter Behroozi, Zheng Zheng, Claudia Maraston, Begoña Ascaso, Brian C. Lemaux, Diego Capozzi, Marc Huertas-Company, Roy R. Gal, Lori M. Lubin, Christopher J. Conselice, Marcella Carollo, and Andrea Cattaneo. On the Intermediate-redshift Central Stellar Mass-Halo Mass Relation, and Implications for the Evolution of the Most Massive Galaxies Since z $\sim$1. *ApJ*, 797(2):L27, December 2014b. .

Meng Gu, Charlie Conroy, and Peter Behroozi. Hierarchical Galaxy Growth and Scatter in the Stellar Mass-Halo Mass Relation. *ApJ*, 833(1):2, December 2016. .

Peter D. Mitchell, Cedric G. Lacey, Carlton M. Baugh, and Shaun Cole. The evolution of the stellar mass versus halo mass relationship. *MNRAS*, 456(2):1459–1483, February 2016. .

Jorryt Matthee, Joop Schaye, Robert A. Crain, Matthieu Schaller, Richard Bower, and Tom Theuns. The origin of scatter in the stellar mass-halo mass relation of central galaxies in the EAGLE simulation. *MNRAS*, 465(2):2381–2396, February 2017. .

Magdelena Allen, Peter Behroozi, and Chung-Pei Ma. Constraining scatter in the stellar mass-halo mass relation for haloes less massive than the Milky Way. *MNRAS*, 488 (4):4916–4925, October 2019. .

G. Erfanianfar, A. Finoguenov, K. Furnell, P. Popesso, A. Biviano, S. Wuyts, C. A. Collins, M. Mirkazemi, J. Comparat, H. Khosroshahi, K. Nandra, R. Capasso, E. Rykoff, D. Wilman, A. Merloni, N. Clerc, M. Salvato, J. I. Chitham, L. S. Kelvin, G. Gozaliasl, A. Weijmans, J. Brownstein, E. Egami, M. J. Pereira, D. P. Schneider, C. Kirkpatrick, S. Damsted, and A. Kukkola. Stellar mass-halo mass relation for the brightest central galaxies of X-ray clusters since z $\sim$ 0.65. *A&A*, 631:A175, November 2019. .

Jesse B. Golden-Marx, C. J. Miller, Y. Zhang, R. L. C. Ogando, A. Palmese, T. M. C. Abbott, M. Aguena, S. Allam, F. Andrade-Oliveira, J. Annis, D. Bacon, E. Bertin, D. Brooks, E. Buckley-Geer, A. Carnero Rosell, M. Carrasco Kind, F. J. Castander, M. Costanzi, M. Crocce, L. N. da Costa, M. E. S. Pereira, J. De Vicente, S. Desai, H. T. Diehl, P. Doel, A. Drlica-Wagner, S. Everett, A. E. Evrard, I. Ferrero, B. Flaugher, P. Fosalba, J. Frieman, J. García-Bellido, E. Gaztanaga, D. W. Gerdes, D. Gruen, R. A. Gruendl, J. Gschwend, G. Gutierrez, W. G. Hartley, S. R. Hinton, D. L. Hollowood, K. Honscheid, B. Hoyle, D. J. James, T. Jeltema, A. G. Kim, E. Krause, K. Kuehn, N. Kuropatkin, O. Lahav, M. Lima, M. A. G. Maia, J. L. Marshall, P. Melchior, F. Menanteau, R. Miquel, J. J. Mohr, R. Morgan, F. Paz-Chinchón, D. Petravick, A. Pieres, A. A. Plazas Malagón, J. Prat, A. K. Romer, E. Sanchez, B. Santiago, V. Scarpine, M. Schubnell, S. Serrano, I. Sevilla-Noarbe, M. Smith, M. Soares-Santos, E. Suchyta, G. Tarle, and T. N. Varga. The Observed Evolution of the Stellar Mass-Halo Mass Relation for Brightest Central Galaxies. *ApJ*, 928(1):28, March 2022. .

M. Shuntov, H. J. McCracken, R. Gavazzi, C. Laigle, J. R. Weaver, I. Davidzon, O. Ilbert, O. B. Kauffmann, A. Faisst, Y. Dubois, A. M. Koekemoer, A. Moneti, B. Milvang-Jensen, B. Mobasher, D. B. Sanders, and S. Toft. COSMOS2020: Cosmic evolution of the stellar-to-halo mass relation for central and satellite galaxies up to z $\sim$ 5. *A&A*, 664:A61, August 2022. .

Kyle R. Stewart, James S. Bullock, Elizabeth J. Barton, and Risa H. Wechsler. Galaxy Mergers and Dark Matter Halo Mergers in ΛCDM: Mass, Redshift, and Mass-Ratio Dependence. *ApJ*, 702(2):1005–1015, September 2009a. .

Philip F. Hopkins, Kevin Bundy, Darren Croton, Lars Hernquist, Dusan Keres, Sadegh Khochfar, Kyle Stewart, Andrew Wetzel, and Joshua D. Younger. Mergers and Bulge Formation in ΛCDM: Which Mergers Matter? *ApJ*, 715(1):202–229, May 2010a. .

Joseph A. O'Leary, Benjamin P. Moster, Thorsten Naab, and Rachel S. Somerville. EMERGE: empirical predictions of galaxy merger rates since z $\sim$ 6. *MNRAS*, 501 (3):3215–3237, March 2021. .

Raymond C. Simons, Susan A. Kassin, Gregory F. Snyder, Joel R. Primack, Daniel Ceverino, Avishai Dekel, Christopher C. Hayward, Nir Mandelker, Kameswara Bharadwaj Mantha, Camilla Pacifici, Alexander de la Vega, and Weichen Wang. Distinguishing Mergers and Disks in High-redshift Observations of Galaxy Kinematics. *ApJ*, 874 (1):59, March 2019. .

F. Bournaud, C. J. Jog, and F. Combes. Multiple minor mergers: formation of elliptical galaxies and constraints for the growth of spiral disks. *A&A*, 476(3):1179–1190, December 2007. .

Philip F. Hopkins, Joshua D. Younger, Christopher C. Hayward, Desika Narayanan, and Lars Hernquist. Mergers, active galactic nuclei and 'normal' galaxies: contributions to the distribution of star formation rates and infrared luminosity functions. *MNRAS*, 402(3):1693–1713, March 2010b. .

Francesco Shankar, Federico Marulli, Mariangela Bernardi, Simona Mei, Alan Meert, and Vinu Vikram. Size evolution of spheroids in a hierarchical Universe. *MNRAS*, 428(1):109–128, January 2013a. .

Fabio Fontanot, Andrea V. Macciò, Michaela Hirschmann, Gabriella De Lucia, Rahul Kannan, Rachel S. Somerville, and Dave Wilman. On the dependence of galaxy morphologies on galaxy mergers. *MNRAS*, 451(3):2968–2977, August 2015. .

C. M. Baugh. A primer on hierarchical galaxy formation: the semi-analytical approach. *Reports on Progress in Physics*, 69(12):3101–3156, December 2006. .

Rowena K. Malbon, C. M. Baugh, C. S. Frenk, and C. G. Lacey. Black hole growth in hierarchical galaxy formation. *MNRAS*, 382(4):1394–1414, December 2007. .

R. G. Bower, I. Vernon, M. Goldstein, A. J. Benson, C. G. Lacey, C. M. Baugh, S. Cole, and C. S. Frenk. The parameter space of galaxy formation. *MNRAS*, 407(4):2017–2045, October 2010. .

Sandro Tacchella, Benedikt Diemer, Lars Hernquist, Shy Genel, Federico Marinacci, Dylan Nelson, Annalisa Pillepich, Vicente Rodriguez-Gomez, Laura V. Sales, Volker Springel, and Mark Vogelsberger. Morphology and star formation in IllustrisTNG: the build-up of spheroids and discs. *MNRAS*, 487(4):5416–5440, August 2019. .

Cedric G. Lacey, Carlton M. Baugh, Carlos S. Frenk, Andrew J. Benson, Richard G. Bower, Shaun Cole, Violeta Gonzalez-Perez, John C. Helly, Claudia D. P. Lagos, and Peter D. Mitchell. A unified multiwavelength model of galaxy formation. *MNRAS*, 462(4):3854–3911, November 2016. .

Daniel Christlein and Ann I. Zabludoff. Can Early-Type Galaxies Evolve from the Fading of the Disks of Late-Type Galaxies? *ApJ*, 616(1):192–198, November 2004. .

Eija Laurikainen, Heikki Salo, and Ronald Buta. Multicomponent decompositions for a sample of S0 galaxies. *MNRAS*, 362(4):1319–1347, October 2005. .

Michael R. Blanton and John Moustakas. Physical Properties and Environments of Nearby Galaxies. *ARA&A*, 47(1):159–210, September 2009. .

Darren J. Croton, Adam R. H. Stevens, Chiara Tonini, Thibault Garel, Maksym Bernyk, Antonio Bibiano, Luke Hodkinson, Simon J. Mutch, Gregory B. Poole, and Genevieve M. Shattow. Semi-Analytic Galaxy Evolution (SAGE): Model Calibration and Basic Results. *ApJS*, 222(2):22, February 2016. .

Philip F. Hopkins, Thomas J. Cox, Joshua D. Younger, and Lars Hernquist. How do Disks Survive Mergers? *ApJ*, 691(2):1168–1201, February 2009b. .

M. Puech, F. Hammer, P. F. Hopkins, E. Athanassoula, H. Flores, M. Rodrigues, J. L. Wang, and Y. B. Yang. Galaxy Disks Do Not Need to Survive in the ΛCDM Paradigm: The Galaxy Merger Rate Out to z ∼1.5 from Morpho-kinematic Data. *ApJ*, 753(2):128, July 2012. .

David Izquierdo-Villalba, Silvia Bonoli, Daniele Spinoso, Yetli Rosas-Guevara, Bruno M. B. Henriques, and Carlos Hernández-Monteagudo. The build-up of pseudo-bulges in a hierarchical universe. *MNRAS*, 488(1):609–632, September 2019. .

T. Di Matteo, N. Khandai, C. DeGraf, Y. Feng, R. A. C. Croft, J. Lopez, and V. Springel. Cold Flows and the First Quasars. *ApJ*, 745(2):L29, February 2012. .

Antonija Oklopčić, Philip F. Hopkins, Robert Feldmann, Dušan Kereš, Claude-André Faucher-Giguère, and Norman Murray. Giant clumps in the FIRE simulations: a case study of a massive high-redshift galaxy. *MNRAS*, 465(1):952–969, February 2017. .

Avishai Dekel, Sharon Lapiner, and Yohan Dubois. Origin of the Golden Mass of Galaxies and Black Holes. *arXiv e-prints*, art. arXiv:1904.08431, April 2019.

Philipp Lang, Stijn Wuyts, Rachel S. Somerville, Natascha M. Förster Schreiber, Reinhard Genzel, Eric F. Bell, Gabe Brammer, Avishai Dekel, Sandra M. Faber, Henry C. Ferguson, Norman A. Grogin, Dale D. Kocevski, Anton M. Koekemoer, Dieter Lutz, Elizabeth J. McGrath, Ivelina Momcheva, Erica J. Nelson, Joel R. Primack, David J. Rosario, Rosalind E. Skelton, Linda J. Tacconi, Pieter G. van Dokkum, and Katherine E. Whitaker. Bulge Growth and Quenching since z = 2.5 in CANDELS/3D-HST. *ApJ*, 788(1):11, June 2014. .

Kyle R. Stewart, James S. Bullock, Risa H. Wechsler, and Ariyeh H. Maller. Gas-rich Mergers in LCDM: Disk Survivability and the Baryonic Assembly of Galaxies. *ApJ*, 702(1):307–317, September 2009b. .

Shiyin Shen, H. J. Mo, Simon D. M. White, Michael R. Blanton, Guinevere Kauffmann, Wolfgang Voges, J. Brinkmann, and Istvan Csabai. The size distribution of galaxies in the Sloan Digital Sky Survey. *MNRAS*, 343(3):978–994, August 2003. .

C. Tonini, A. Lapi, F. Shankar, and P. Salucci. Measuring the Spin of Spiral Galaxies. *ApJ*, 638(1):L13–L16, February 2006. .

I. M. Whiley, A. Aragón-Salamanca, G. De Lucia, A. von der Linden, S. P. Bamford, P. Best, M. N. Bremer, P. Jablonka, O. Johnson, B. Milvang-Jensen, S. Noll, B. M. Poggianti, G. Rudnick, R. Saglia, S. White, and D. Zaritsky. The evolution of the brightest cluster galaxies since z $\sim$1 from the ESO Distant Cluster Survey (EDisCS). *MNRAS*, 387(3):1253–1263, July 2008. .

Chris A. Collins, John P. Stott, Matt Hilton, Scott T. Kay, S. Adam Stanford, Michael Davidson, Mark Hosmer, Ben Hoyle, Andrew Liddle, Ed Lloyd-Davies, Robert G. Mann, Nicola Mehrtens, Christopher J. Miller, Robert C. Nichol, A. Kathy Romer, Martin Sahlén, Pedro T. P. Viana, and Michael J. West. Early assembly of the most massive galaxies. *Nature*, 458(7238):603–606, April 2009. .

J. P. Stott, C. A. Collins, M. Sahlén, M. Hilton, E. Lloyd-Davies, D. Capozzi, M. Hosmer, A. R. Liddle, N. Mehrtens, C. J. Miller, A. K. Romer, S. A. Stanford, P. T. P. Viana, M. Davidson, B. Hoyle, S. T. Kay, and R. C. Nichol. The XMM Cluster Survey: The Build-up of Stellar Mass in Brightest Cluster Galaxies at High Redshift. *ApJ*, 718(1): 23–30, July 2010. .

C. Lidman, J. Suherli, A. Muzzin, G. Wilson, R. Demarco, S. Brough, A. Rettura, J. Cox, A. DeGroot, H. K. C. Yee, D. Gilbank, H. Hoekstra, M. Balogh, E. Ellingson, A. Hicks, J. Nantais, A. Noble, M. Lacy, J. Surace, and T. Webb. Evidence for significant growth in the stellar mass of brightest cluster galaxies over the past 10 billion years. *MNRAS*, 427(1):550–568, November 2012. .

Sabine Bellstedt, Chris Lidman, Adam Muzzin, Marijn Franx, Susanna Guatelli, Allison R. Hill, Henk Hoekstra, Noah Kurinsky, Ivo Labbe, Danilo Marchesini, Z. Cemile Marsan, Mitra Safavi-Naeini, Cristóbal Sifón, Mauro Stefanon, Jesse van de Sande, Pieter van Dokkum, and Catherine Weigel. The evolution in the stellar mass of brightest cluster galaxies over the past 10 billion years. *MNRAS*, 460(3):2862–2874, August 2016. .

Yen-Ting Lin, Bau-Ching Hsieh, Sheng-Chieh Lin, Masamune Oguri, Kai-Feng Chen, Masayuki Tanaka, I. Non Chiu, Song Huang, Tadayuki Kodama, Alexie Leauthaud, Surhud More, Atsushi J. Nishizawa, Kevin Bundy, Lihwai Lin, and Satoshi Miyazaki. First Results on the Cluster Galaxy Population from the Subaru Hyper Suprime-Cam Survey. III. Brightest Cluster Galaxies, Stellar Mass Distribution, and Active Galaxies. *ApJ*, 851(2):139, December 2017. .

Y. Zhang, C. J. Miller, P. Rooney, A. Bermeo, A. K. Romer, C. Vergara cervantes, E. S. Rykoff, C. Hennig, R. Das, T. Mckay, J. Song, H. Wilcox, D. Bacon, S. L. Bridle, C. Collins, C. Conselice, M. Hilton, B. Hoyle, S. Kay, A. R. Liddle, R. G. Mann, N. Mehrtens, J. Mayers, R. C. Nichol, M. Sahlen, J. Stott, P. T. P. Viana, R. H. Wechsler, T. Abbott, F. B. Abdalla, S. Allam, A. Benoit-levy, D. Brooks, E. Buckley-geer, D. L. Burke, A. Carnero rosell, M. Carrasco kind, J. Carretero, F. J. Castander, M. Crocce, C. E. Cunha, C. B. Dandrea, L. N. Da costa, H. T. Diehl, J. P. Dietrich, T. F. Eifler, B. Flaugher, P. Fosalba, J. Garcia-bellido, E. Gaztanaga, D. W. Gerdes, D. Gruen, R. A. Gruendl, J. Gschwend, G. Gutierrez, K. Honscheid, D. J. James, T. Jeltema, K. Kuehn, N. Kuropatkin, M. Lima, H. Lin, M. A. G. Maia, M. March, J. L. Marshall, P. Melchior, F. Menanteau, R. Miquel, R. L. C. Ogando, A. A. Plazas, E. Sanchez, M. Schubnell, I. Sevilla-noarbe, M. Smith, M. Soares-santos, F. Sobreira, E. Suchyta, M. E. C. Swanson, G. Tarle, and A. R. Walker. Galaxies in X-ray Selected Clusters and Groups in Dark Energy Survey Data II: Hierarchical Bayesian Modeling of the Red-Sequence Galaxy Luminosity Function. *arXiv e-prints*, art. arXiv:1710.05908, October 2017.

Joel Leja, Pieter G. van Dokkum, Marijn Franx, and Katherine E. Whitaker. Reconciling the Observed Star-forming Sequence with the Observed Stellar Mass Function. *ApJ*, 798(2):115, January 2015. .

Bianca M. Poggianti, Alessia Moretti, Marco Gullieuszik, Jacopo Fritz, Yara Jaffé, Daniela Bettoni, Giovanni Fasano, Callum Bellhouse, George Hau, Benedetta Vulcani, Andrea Biviano, Alessandro Omizzolo, Angela Paccagnella, Mauro D'Onofrio, Antonio Cava, Y. K. Sheen, Warrick Couch, and Matt Owers. GASP. I. Gas Stripping Phenomena in Galaxies with MUSE. *ApJ*, 844(1):48, July 2017. .

A. Franchetto, B. Vulcani, B. M. Poggianti, M. Gullieuszik, M. Mingozzi, A. Moretti, N. Tomicic, J. Fritz, D. Bettoni, and Y. L. Jaffe. VizieR Online Data Catalog: GAs Stripping Phenomena in galaxies with MUSE (Franchetto+, 2020). *VizieR Online Data Catalog*, art. J/ApJ/895/106, September 2021. .

Nina Akerman, Stephanie Tonnesen, Bianca M Poggianti, Rory Smith, Antonino Marasco, Andrea Kulier, Ancla Müller, and Benedetta Vulcani. The Surprising Lack of Effect from Stellar Feedback on the Gas Stripping Rate from Massive Jellyfish Galaxies. *arXiv e-prints*, art. arXiv:2311.04964, November 2023. .

Carlo Cannarozzo, Alexie Leauthaud, Grecco A. Oyarzún, Carlo Nipoti, Benedikt Diemer, Song Huang, Vicente Rodriguez-Gomez, Alessandro Sonnenfeld, and Kevin Bundy. The contribution of in-situ and ex-situ star formation in early-type galaxies: MaNGA versus IllustrisTNG. *MNRAS*, October 2022. .

Sebastian Trujillo-Gomez, J. M. Diederik Kruijssen, Joel Pfeffer, Marta Reina-Campos, Robert A. Crain, Nate Bastian, and Ivan Cabrera-Ziri. In-situ or accreted? Using deep learning to infer the origin of extragalactic globular clusters from observables. *arXiv e-prints*, art. arXiv:2301.05716, January 2023.

Piero Madau and Mark Dickinson. Cosmic Star-Formation History. *ARA&A*, 52:415–486, August 2014. .

Sownak Bose, Daniel J. Eisenstein, Lars Hernquist, Annalisa Pillepich, Dylan Nelson, Federico Marinacci, Volker Springel, and Mark Vogelsberger. Revealing the galaxy-halo connection in IllustrisTNG. *MNRAS*, 490(4):5693–5711, December 2019. .

Cheqiu Lyu, Yingjie Peng, Yipeng Jing, Xiaohu Yang, Luis C. Ho, Alvio Renzini, Bitao Wang, Kai Wang, Bingxiao Xu, Dingyi Zhao, Jing Dou, Qiusheng Gu, Roberto Maiolino, Filippo Mannucci, and Feng Yuan. From Halos to Galaxies. VII. The Connections between Stellar Mass Growth History, Quenching History, and Halo Assembly History for Central Galaxies. *ApJ*, 959(1):5, December 2023. .

G. Rodighiero, A. Renzini, E. Daddi, I. Baronchelli, S. Berta, G. Cresci, A. Franceschini, C. Gruppioni, D. Lutz, C. Mancini, P. Santini, G. Zamorani, J. Silverman, D. Kashino, P. Andreani, A. Cimatti, H. Domínguez Sánchez, E. Le Floch, B. Magnelli, P. Popesso, and F. Pozzi. A multiwavelength consensus on the main sequence of star-forming galaxies at z $\sim$ 2. *MNRAS*, 443(1):19–30, September 2014. .

W. J. Pearson, L. Wang, P. D. Hurley, K. Małek, V. Buat, D. Burgarella, D. Farrah, S. J. Oliver, D. J. B. Smith, and F. F. S. van der Tak. Main sequence of star forming galaxies beyond the Herschel confusion limit. *A&A*, 615:A146, July 2018. .

Nicholas Lee, D. B. Sanders, Caitlin M. Casey, Sune Toft, N. Z. Scoville, Chao-Ling Hung, Emeric Le Floc'h, Olivier Ilbert, H. Jabran Zahid, Hervé Aussel, Peter Capak, Jeyhan S. Kartaltepe, Lisa J. Kewley, Yanxia Li, Kevin Schawinski, Kartik Sheth, and Quanbao Xiao. A Turnover in the Galaxy Main Sequence of Star Formation at M $_*$ $\sim 10^{10}$ M $_\odot$ for Redshifts z < 1.3. *ApJ*, 801(2):80, March 2015. .

Adam R. Tomczak, Ryan F. Quadri, Kim-Vy H. Tran, Ivo Labbé, Caroline M. S. Straatman, Casey Papovich, Karl Glazebrook, Rebecca Allen, Gabreil B. Brammer, Michael

Cowley, Mark Dickinson, David Elbaz, Hanae Inami, Glenn G. Kacprzak, Glenn E. Morrison, Themiya Nanayakkara, S. Eric Persson, Glen A. Rees, Brett Salmon, Corentin Schreiber, Lee R. Spitler, and Katherine E. Whitaker. The SFR-M* Relation and Empirical Star-Formation Histories from ZFOURGE* at 0.5 < z < 4. *ApJ*, 817 (2):118, February 2016. .

Jessica E. Thorne, Aaron S. G. Robotham, Luke J. M. Davies, Sabine Bellstedt, Simon P. Driver, Matías Bravo, Malcolm N. Bremer, Benne W. Holwerda, Andrew M. Hopkins, Claudia del P. Lagos, Steven Phillipps, Malgorzata Siudek, Edward N. Taylor, and Angus H. Wright. Deep Extragalactic VIsible Legacy Survey (DEVILS): SED fitting in the D10-COSMOS field and the evolution of the stellar mass function and SFR-$M_\star$ relation. *MNRAS*, 505(1):540–567, July 2021. .

M. Bernardi, F. Shankar, J. B. Hyde, S. Mei, F. Marulli, and R. K. Sheth. Galaxy luminosities, stellar masses, sizes, velocity dispersions as a function of morphological type. *MNRAS*, 404(4):2087–2122, June 2010. .

Martina Donnari, Annalisa Pillepich, Dylan Nelson, Mark Vogelsberger, Shy Genel, Rainer Weinberger, Federico Marinacci, Volker Springel, and Lars Hernquist. The star formation activity of IllustrisTNG galaxies: main sequence, UVJ diagram, quenched fractions, and systematics. *MNRAS*, 485(4):4817–4840, June 2019. .

Abdolhosein Hashemizadeh, Simon P. Driver, Luke J. M. Davies, Aaron S. G. Robotham, Sabine Bellstedt, Rogier A. Windhorst, Malcolm Bremer, Steven Phillipps, Matt Jarvis, Benne W. Holwerda, Claudia del P. Lagos, Soheil Koushan, Malgorzata Siudek, Natasha Maddox, Jessica E. Thorne, and Pascal Elahi. Deep extragalactic visible legacy survey (DEVILS): stellar mass growth by morphological type since z = 1. *MNRAS*, 505(1):136–160, July 2021. .

Mireia Montes. The faint light in groups and clusters of galaxies. *Nature Astronomy*, 6: 308–316, March 2022. .

Michael D. Gregg and Michael J. West. Galaxy disruption as the origin of intracluster light in the Coma cluster of galaxies. *Nature*, 396(6711):549–552, December 1998. .

J. Christopher Mihos, Paul Harding, John Feldmeier, and Heather Morrison. Diffuse Light in the Virgo Cluster. *ApJ*, 631(1):L41–L44, September 2005. .

E. Contini, S. K. Yi, and X. Kang. The different growth pathways of brightest cluster galaxies and intracluster light. *MNRAS*, 479(1):932–944, September 2018. .

Chiara Tonini, Maksym Bernyk, Darren Croton, Claudia Maraston, and Daniel Thomas. The Evolution of Brightest Cluster Galaxies in a Hierarchical Universe. *ApJ*, 759(1): 43, November 2012. .

G. Murante, M. Arnaboldi, O. Gerhard, S. Borgani, L. M. Cheng, A. Diaferio, K. Dolag, L. Moscardini, G. Tormen, L. Tornatore, and P. Tozzi. The Diffuse Light in Simulations of Galaxy Clusters. *ApJ*, 607(2):L83–L86, June 2004. .

Yen-Ting Lin and Joseph J. Mohr. K-band Properties of Galaxy Clusters and Groups: Brightest Cluster Galaxies and Intracluster Light. *ApJ*, 617(2):879–895, December 2004. .

Chris W. Purcell, James S. Bullock, and Andrew R. Zentner. Shredded Galaxies as the Source of Diffuse Intrahalo Light on Varying Scales. *ApJ*, 666(1):20–33, September 2007. .

K. Dolag, G. Murante, and S. Borgani. Dynamical difference between the cD galaxy and the diffuse, stellar component in simulated galaxy clusters. *MNRAS*, 405(3): 1544–1559, July 2010. .

Weiguang Cui, G. Murante, P. Monaco, S. Borgani, G. L. Granato, M. Killedar, G. De Lucia, V. Presotto, and K. Dolag. Characterizing diffused stellar light in simulated galaxy clusters. *MNRAS*, 437(1):816–830, January 2014. .

Sarah Brough, Syeda Lammim Ahad, Yannick M. Bahe, Amaël Ellien, Anthony H. Gonzalez, Yolanda Jiménez-Teja, Lucas C. Kimmig, Garreth Martin, Cristina Martínez-Lombilla, Mireia Montes, Annalisa Pillepich, Rossella Ragusa, Rhea-Silvia Remus, Chris A. Collins, Johan H. Knapen, and J. Chris Mihos. Preparing for low surface brightness science with the Vera C. Rubin Observatory: A Comparison of Observable and Simulated Intracluster Light Fractions. *arXiv e-prints*, art. arXiv:2311.18016, November 2023. .

A. van der Wel, M. Franx, P. G. van Dokkum, R. E. Skelton, I. G. Momcheva, K. E. Whitaker, G. B. Brammer, E. F. Bell, H. W. Rix, S. Wuyts, H. C. Ferguson, B. P. Holden, G. Barro, A. M. Koekemoer, Yu-Yen Chang, E. J. McGrath, B. Häussler, A. Dekel, P. Behroozi, M. Fumagalli, J. Leja, B. F. Lundgren, M. V. Maseda, E. J. Nelson, D. A. Wake, S. G. Patel, I. Labbé, S. M. Faber, N. A. Grogin, and D. D. Kocevski. 3D-HST+CANDELS: The Evolution of the Galaxy Size-Mass Distribution since z = 3. *ApJ*, 788(1):28, June 2014. .

Pieter G. van Dokkum, Erica June Nelson, Marijn Franx, Pascal Oesch, Ivelina Momcheva, Gabriel Brammer, Natascha M. Förster Schreiber, Rosalind E. Skelton, Katherine E. Whitaker, Arjen van der Wel, Rachel Bezanson, Mattia Fumagalli, Garth D. Illingworth, Mariska Kriek, Joel Leja, and Stijn Wuyts. Forming Compact Massive Galaxies. *ApJ*, 813(1):23, November 2015. .

Shannon G. Patel, Yu Xuan Hong, Ryan F. Quadri, Bradford P. Holden, and Rik J. Williams. A Comparison of the Most Massive Quiescent Galaxies from z $\sim$ 3 to the Present: Slow Evolution in Size, and spheroid-dominated. *ApJ*, 839(2):127, April 2017. .

Lamiya A. Mowla, Pieter van Dokkum, Gabriel B. Brammer, Ivelina Momcheva, Arjen van der Wel, Katherine Whitaker, Erica Nelson, Rachel Bezanson, Adam Muzzin, Marijn Franx, John MacKenty, Joel Leja, Mariska Kriek, and Danilo Marchesini. COSMOS-DASH: The Evolution of the Galaxy Size-Mass Relation since z $\sim$ 3 from New Wide-field WFC3 Imaging Combined with CANDELS/3D-HST. *ApJ*, 880(1):57, July 2019. .

L. Zanisi, F. Shankar, M. Bernardi, S. Mei, and M. Huertas-Company. The size function of massive satellites from the R_e-R_h and M_{star}-M_h relations: constraining the role of environment. *MNRAS*, 505(1):L84–L89, July 2021. .

G. Yang, W. N. Brandt, F. Vito, C. T. J. Chen, J. R. Trump, B. Luo, M. Y. Sun, Y. Q. Xue, A. M. Koekemoer, D. P. Schneider, C. Vignali, and J. X. Wang. Linking black hole growth with host galaxies: the accretion-stellar mass relation and its cosmic evolution. *MNRAS*, 475(2):1887–1911, April 2018. .

Benjamin L. Davis, Alister W. Graham, and Ewan Cameron. Black Hole Mass Scaling Relations for Spiral Galaxies. II. M_{BH}-$M_{*,tot}$ and M_{BH}-$M_{*,disk}$. *ApJ*, 869(2):113, December 2018. .

Agnese Cherubini. A semi-empirical model to constrain the growth of supermassive black holes. *Master's Degree thesis*, Università degli Studi di Padova. 2022.

Hakim Atek, Iryna Chemerynska, Bingjie Wang, Lukas J. Furtak, Andrea Weibel, Pascal Oesch, John R. Weaver, Ivo Labbé, Rachel Bezanson, Pieter van Dokkum, Adi Zitrin, Pratika Dayal, Christina C. Williams, Themiya Nannayakkara, Sedona H. Price, Gabriel Brammer, Andy D. Goulding, Joel Leja, Danilo Marchesini, Erica J. Nelson, Richard Pan, and Katherine E. Whitaker. JWST UNCOVER: discovery of z > 9 galaxy candidates behind the lensing cluster Abell 2744. *MNRAS*, 524(4):5486–5496, October 2023. .

Ryan Endsley, Daniel P. Stark, Lily Whitler, Michael W. Topping, Zuyi Chen, Adèle Plat, John Chisholm, and Stéphane Charlot. A JWST/NIRCam study of key contributors to reionization: the star-forming and ionizing properties of UV-faint z 7-8 galaxies. *MNRAS*, 524(2):2312–2330, September 2023. .

Ivo Labbe, Jenny E. Greene, Rachel Bezanson, Seiji Fujimoto, Lukas J. Furtak, Andy D. Goulding, Jorryt Matthee, Rohan P. Naidu, Pascal A. Oesch, Hakim Atek, Gabriel Brammer, Iryna Chemerynska, Dan Coe, Sam E. Cutler, Pratika Dayal, Robert Feldmann, Marijn Franx, Karl Glazebrook, Joel Leja, Danilo Marchesini, Michael Maseda, Themiya Nanayakkara, Erica J. Nelson, Richard Pan, Casey Papovich, Sedona H. Price, Katherine A. Suess, Bingjie Wang, Katherine E. Whitaker, Christina C. Williams, and Adi Zitrin. UNCOVER: Candidate Red Active Galactic Nuclei at 3<z<7 with JWST and ALMA. *arXiv e-prints*, art. arXiv:2306.07320, June 2023. .

Erica J. Nelson, Katherine A. Suess, Rachel Bezanson, Sedona H. Price, Pieter van Dokkum, Joel Leja, Bingjie Wang, Katherine E. Whitaker, Ivo Labbé, Laia Barrufet, Gabriel Brammer, Daniel J. Eisenstein, Justus Gibson, Abigail I. Hartley, Benjamin D. Johnson, Kasper E. Heintz, Elijah Mathews, Tim B. Miller, Pascal A. Oesch, Lester Sandles, David J. Setton, Joshua S. Speagle, Sandro Tacchella, Ken-ichi Tadaki, Hannah Übler, and John. R. Weaver. JWST Reveals a Population of Ultrared, Flattened Galaxies at $2 \lesssim z \lesssim 6$ Previously Missed by HST. *ApJ*, 948(2):L18, May 2023. .

Francisco Prada, Anatoly A. Klypin, Antonio J. Cuesta, Juan E. Betancort-Rijo, and Joel Primack. Halo concentrations in the standard Λ cold dark matter cosmology. *MNRAS*, 423(4):3018–3030, July 2012. .

Anatoly Klypin, Gustavo Yepes, Stefan Gottlöber, Francisco Prada, and Steffen Heß. MultiDark simulations: the story of dark matter halo concentrations and density profiles. *MNRAS*, 457(4):4340–4359, April 2016. .

G. Rodighiero, E. Daddi, I. Baronchelli, A. Cimatti, A. Renzini, H. Aussel, P. Popesso, D. Lutz, P. Andreani, S. Berta, A. Cava, D. Elbaz, A. Feltre, A. Fontana, N. M. Förster Schreiber, A. Franceschini, R. Genzel, A. Grazian, C. Gruppioni, O. Ilbert, E. Le Floch, G. Magdis, M. Magliocchetti, B. Magnelli, R. Maiolino, H. McCracken, R. Nordon, A. Poglitsch, P. Santini, F. Pozzi, L. Riguccini, L. J. Tacconi, S. Wuyts, and G. Zamorani. The Lesser Role of Starbursts in Star Formation at z = 2. *ApJ*, 739(2): L40, October 2011. .

C. Gruppioni, F. Pozzi, G. Rodighiero, I. Delvecchio, S. Berta, L. Pozzetti, G. Zamorani, P. Andreani, A. Cimatti, O. Ilbert, E. Le Floc'h, D. Lutz, B. Magnelli, L. Marchetti, P. Monaco, R. Nordon, S. Oliver, P. Popesso, L. Riguccini, I. Roseboom, D. J. Rosario, M. Sargent, M. Vaccari, B. Altieri, H. Aussel, A. Bongiovanni, J. Cepa, E. Daddi, H. Domínguez-Sánchez, D. Elbaz, N. Förster Schreiber, R. Genzel, A. Iribarrem, M. Magliocchetti, R. Maiolino, A. Poglitsch, A. Pérez García, M. Sanchez-Portal, E. Sturm, L. Tacconi, I. Valtchanov, A. Amblard, V. Arumugam, M. Bethermin, J. Bock, A. Boselli, V. Buat, D. Burgarella, N. Castro-Rodríguez, A. Cava, P. Chanial, D. L. Clements, A. Conley, A. Cooray, C. D. Dowell, E. Dwek, S. Eales, A. Franceschini, J. Glenn, M. Griffin, E. Hatziminaoglou, E. Ibar, K. Isaak, R. J. Ivison, G. Lagache, L. Levenson, N. Lu, S. Madden, B. Maffei, G. Mainetti, H. T. Nguyen, B. O'Halloran, M. J. Page, P. Panuzzo, A. Papageorgiou, C. P. Pearson, I. Pérez-Fournon, M. Pohlen, D. Rigopoulou, M. Rowan-Robinson, B. Schulz, D. Scott, N. Seymour, D. L. Shupe, A. J. Smith, J. A. Stevens, M. Symeonidis, M. Trichas, K. E. Tugwell, L. Vigroux, L. Wang, G. Wright, C. K. Xu, M. Zemcov, S. Bardelli, M. Carollo, T. Contini, O. Le Févre, S. Lilly, V. Mainieri, A. Renzini, M. Scodeggio, and E. Zucca. The Herschel PEP/HerMES luminosity function - I. Probing the evolution of PACS selected Galaxies to $z \simeq 4$. *MNRAS*, 432(1):23–52, June 2013. .

B. Magnelli, P. Popesso, S. Berta, F. Pozzi, D. Elbaz, D. Lutz, M. Dickinson, B. Altieri, P. Andreani, H. Aussel, M. Béthermin, A. Bongiovanni, J. Cepa, V. Charmandaris, R. R. Chary, A. Cimatti, E. Daddi, N. M. Förster Schreiber, R. Genzel, C. Gruppioni, M. Harwit, H. S. Hwang, R. J. Ivison, G. Magdis, R. Maiolino, E. Murphy, R. Nordon, M. Pannella, A. Pérez García, A. Poglitsch, D. Rosario, M. Sanchez-Portal, P. Santini, D. Scott, E. Sturm, L. J. Tacconi, and I. Valtchanov. The deepest Herschel-PACS far-infrared survey: number counts and infrared luminosity functions from combined PEP/GOODS-H observations. *A&A*, 553:A132, May 2013. .

M. P. Koprowski, J. S. Dunlop, M. J. Michałowski, K. E. K. Coppin, J. E. Geach, R. J. McLure, D. Scott, and P. P. van der Werf. The evolving far-IR galaxy luminosity function and dust-obscured star formation rate density out to z$\simeq$5. *MNRAS*, 471(4): 4155–4169, November 2017. .

C. Gruppioni, M. Béthermin, F. Loiacono, O. Le Fèvre, P. Capak, P. Cassata, A. L. Faisst, D. Schaerer, J. Silverman, L. Yan, S. Bardelli, M. Boquien, R. Carraro, A. Cimatti, M. Dessauges-Zavadsky, M. Ginolfi, S. Fujimoto, N. P. Hathi, G. C. Jones, Y. Khusanova, A. M. Koekemoer, G. Lagache, B. C. Lemaux, P. A. Oesch, F. Pozzi, D. A. Riechers, G. Rodighiero, M. Romano, M. Talia, L. Vallini, D. Vergani, G. Zamorani, and E. Zucca. The ALPINE-ALMA [CII] survey. The nature, luminosity function, and star formation history of dusty galaxies up to z $\simeq$ 6. *A&A*, 643:A8, November 2020. .

K. Kohno, S. Fujimoto, A. Tsujita, V. Kokorev, G. Brammer, G. E. Magdis, F. Valentino, N. Laporte, Fengwu Sun, E. Egami, F. E. Bauer, A. Guerrero, N. Nagar, K. I. Caputi, G. B. Caminha, J. B. Jolly, K. K. Knudsen, R. Uematsu, Y. Ueda, M. Oguri, A. Zitrin, M. Ouchi, Y. Ono, J. Gonzalez-Lopez, J. Richard, I. Smail, D. Coe, M. Postman, L. Bradley, A. M. Koekemoer, A. M. Munoz Arancibia, M. Dessauges-Zavadsky, D. Espada, H. Umehata, B. Hatsukade, F. Egusa, K. Shimasaku, K. Matsui-Morokuma, W. H. Wang, T. Wang, Y. Ao, A. J. Baker, Minju M. Lee, C. del P. Lagos, D. H. Hughes, and ALCS collaboration. Unbiased surveys of dust-enshrouded galaxies using ALMA. *arXiv e-prints*, art. arXiv:2305.15126, May 2023. .

V. Picouet, S. Arnouts, E. Le Floc'h, T. Moutard, K. Kraljic, O. Ilbert, M. Sawicki, G. Desprez, C. Laigle, D. Schiminovich, S. de la Torre, S. Gwyn, H. J. McCracken, Y. Dubois, R. Davé, S. Toft, J. R. Weaver, M. Shuntov, and O. B. Kauffmann. HSC-CLAUDS survey: The star formation rate functions since z $\sim$ 2 and comparison with hydrodynamical simulations. *A&A*, 675:A164, July 2023. .

Hiroaki Aihara, Yusra AlSayyad, Makoto Ando, Robert Armstrong, James Bosch, Eiichi Egami, Hisanori Furusawa, Junko Furusawa, Andy Goulding, Yuichi Harikane, Chiaki Hikage, Paul T. P. Ho, Bau-Ching Hsieh, Song Huang, Hiroyuki Ikeda, Masatoshi Imanishi, Kei Ito, Ikuru Iwata, Anton T. Jaelani, Ryota Kakuma, Kojiro Kawana, Satoshi Kikuta, Umi Kobayashi, Michitaro Koike, Yutaka Komiyama, Xiangchong Li, Yongming Liang, Yen-Ting Lin, Wentao Luo, Robert Lupton, Nate B. Lust, Lauren A.

MacArthur, Yoshiki Matsuoka, Sogo Mineo, Hironao Miyatake, Satoshi Miyazaki, Surhud More, Ryoma Murata, Shigeru V. Namiki, Atsushi J. Nishizawa, Masamune Oguri, Nobuhiro Okabe, Sakurako Okamoto, Yuki Okura, Yoshiaki Ono, Masato Onodera, Masafusa Onoue, Ken Osato, Masami Ouchi, Takatoshi Shibuya, Michael A. Strauss, Naoshi Sugiyama, Yasushi Suto, Masahiro Takada, Yuhei Takagi, Tadafumi Takata, Satoshi Takita, Masayuki Tanaka, Tsuyoshi Terai, Yoshiki Toba, Hisakazu Uchiyama, Yousuke Utsumi, Shiang-Yu Wang, Wenting Wang, and Yoshihiko Yamada. Second data release of the Hyper Suprime-Cam Subaru Strategic Program. *PASJ*, 71(6):114, December 2019. .

Marcin Sawicki, Stephane Arnouts, Jiasheng Huang, Jean Coupon, Anneya Golob, Stephen Gwyn, Sebastien Foucaud, Thibaud Moutard, Ikuru Iwata, Chengze Liu, Lingjian Chen, Guillaume Desprez, Yuichi Harikane, Yoshiaki Ono, Michael A. Strauss, Masayuki Tanaka, Nathalie Thibert, Michael Balogh, Kevin Bundy, Scott Chapman, James E. Gunn, Bau-Ching Hsieh, Olivier Ilbert, Yipeng Jing, Olivier LeFèvre, Cheng Li, Yuichi Matsuda, Satoshi Miyazaki, Tohru Nagao, Atsushi J. Nishizawa, Masami Ouchi, Kazuhiro Shimasaku, John Silverman, Sylvain de la Torre, Laurence Tresse, Wei-Hao Wang, Chris J. Willott, Toru Yamada, Xiaohu Yang, and Howard K. C. Yee. The CFHT large area U-band deep survey (CLAUDS). *MNRAS*, 489(4):5202–5217, November 2019. .

Zhen-Yi Cai, Andrea Lapi, Alessandro Bressan, Gianfranco De Zotti, Mattia Negrello, and Luigi Danese. A Physical Model for the Evolving Ultraviolet Luminosity Function of High Redshift Galaxies and their Contribution to the Cosmic Reionization. *ApJ*, 785(1):65, April 2014. .

N. J. Adams, R. A. A. Bowler, M. J. Jarvis, R. G. Varadaraj, and B. Häußler. The total rest-frame UV luminosity function from 3 < z < 5: a simultaneous study of AGN and galaxies from -28 < M_{UV} < -16. *MNRAS*, 523(1):327–346, July 2023. .

J. Aird, A. L. Coil, and A. Georgakakis. X-rays across the galaxy population - II. The distribution of AGN accretion rates as a function of stellar mass and redshift. *MNRAS*, 474:1225–1249, January 2018. .

R. Carraro, G. Rodighiero, P. Cassata, M. Brusa, F. Shankar, I. Baronchelli, E. Daddi, I. Delvecchio, A. Franceschini, R. Griffiths, C. Gruppioni, E. López-Navas, C. Mancini, S. Marchesi, M. Negrello, A. Puglisi, E. Sani, and H. Suh. Coevolution of black hole accretion and star formation in galaxies up to z = 3.5. *A&A*, 642:A65, October 2020. .

A. Marconi, G. Risaliti, R. Gilli, L. K. Hunt, R. Maiolino, and M. Salvati. Local supermassive black holes, relics of active galactic nuclei and the X-ray background. *MNRAS*, 351(1):169–185, June 2004. .

Themiya Nanayakkara, James Esdaile, Karl Glazebrook, Juan M. Espejo Salcedo, Mark Durre, and Colin Jacobs. Massive high-redshift quiescent galaxies with JWST. *PASA*, 39:e002, January 2022. .

A. C. Carnall, D. J. McLeod, R. J. McLure, J. S. Dunlop, R. Begley, F. Cullen, C. T. Donnan, M. L. Hamadouche, S. M. Jewell, E. W. Jones, C. L. Pollock, and V. Wild. A surprising abundance of massive quiescent galaxies at $3 < z < 5$ in the first data from JWST CEERS. *MNRAS*, 520(3):3974–3985, April 2023. .

Francesco Valentino, Gabriel Brammer, Katriona M. L. Gould, Vasily Kokorev, Seiji Fujimoto, Christian Kragh Jespersen, Aswin P. Vijayan, John R. Weaver, Kei Ito, Masayuki Tanaka, Olivier Ilbert, Georgios E. Magdis, Katherine E. Whitaker, Andreas L. Faisst, Anna Gallazzi, Steven Gillman, Clara Giménez-Arteaga, Carlos Gómez-Guijarro, Mariko Kubo, Kasper E. Heintz, Michaela Hirschmann, Pascal Oesch, Masato Onodera, Francesca Rizzo, Minju Lee, Victoria Strait, and Sune Toft. An Atlas of Color-selected Quiescent Galaxies at $z > 3$ in Public JWST Fields. *ApJ*, 947(1):20, April 2023. .

Tibor Dome, Sandro Tacchella, Anastasia Fialkov, Daniel Ceverino, Avishai Dekel, Omri Ginzburg, Sharon Lapiner, and Tobias J. Looser. Mini-quenching of z = 4-8 galaxies by bursty star formation. *MNRAS*, 527(2):2139–2151, January 2024. .

A. Schulze and L. Wisotzki. Low redshift AGN in the Hamburg/ESO Survey . II. The active black hole mass function and the distribution function of Eddington ratios. *A&A*, 516:A87, June 2010. .

A. D. Goulding, D. M. Alexander, B. D. Lehmer, and J. R. Mullaney. Towards a complete census of active galactic nuclei in nearby galaxies: the incidence of growing black holes. *MNRAS*, 406(1):597–611, July 2010. .

Francesco Shankar, David H. Weinberg, and Jordi Miralda-Escudé. Accretion-driven evolution of black holes: Eddington ratios, duty cycles and active galaxy fractions. *MNRAS*, 428(1):421–446, January 2013b. .

A. Georgakakis, J. Aird, A. Schulze, T. Dwelly, M. Salvato, K. Nandra, A. Merloni, and D. P. Schneider. Observational constraints on the specific accretion-rate distribution of X-ray-selected AGNs. *MNRAS*, 471(2):1976–2001, October 2017. .

Zhong-yi Man, Ying-jie Peng, Xu Kong, Ke-xin Guo, Cheng-peng Zhang, and Jing Dou. The dependence of AGN activity on environment in SDSS. *MNRAS*, 488(1):89–98, September 2019. .

Christopher Marsden, Francesco Shankar, Mariangela Bernardi, Ravi K. Sheth, Hao Fu, and Andrea Lapi. The weak dependence of velocity dispersion on disk fractions, mass-to-light ratio and redshift: Implications for galaxy and black hole evolution. *MNRAS*, December 2021. .

Ziwen Zhang, Huiyuan Wang, Wentao Luo, Houjun Mo, Jun Zhang, Xiaohu Yang, Hao Li, and Qinxun Li. Halo Mass-observable Proxy Scaling Relations and Their Dependencies on Galaxy and Group Properties. *ApJ*, 960(1):71, January 2024. .

Philip F. Hopkins, Lars Hernquist, Thomas J. Cox, Tiziana Di Matteo, Brant Robertson, and Volker Springel. A Unified, Merger-driven Model of the Origin of Starbursts, Quasars, the Cosmic X-Ray Background, Supermassive Black Holes, and Galaxy Spheroids. *ApJS*, 163(1):1–49, March 2006. .

Marta Volonteri, Hugo Pfister, Ricarda S. Beckmann, Yohan Dubois, Monica Colpi, Christopher J. Conselice, Massimo Dotti, Garreth Martin, Ryan Jackson, Katarina Kraljic, Christophe Pichon, Maxime Trebitsch, Sukyoung K. Yi, Julien Devriendt, and Sébastien Peirani. Black hole mergers from dwarf to massive galaxies with the NewHorizon and Horizon-AGN simulations. *MNRAS*, 498(2):2219–2238, October 2020. .

Tian-Chi Zhang, Qi Guo, Yan Qu, and Liang Gao. The role of mergers and gas accretion in black hole growth and galaxy evolution. *Research in Astronomy and Astrophysics*, 21 (8):212, October 2021. .

J. Christopher Mihos and Lars Hernquist. Gasdynamics and Starbursts in Major Mergers. *ApJ*, 464:641, June 1996. .

Philip F. Hopkins, Lars Hernquist, Thomas J. Cox, and Dušan Kereš. A Cosmological Framework for the Co-Evolution of Quasars, Supermassive Black Holes, and Elliptical Galaxies. I. Galaxy Mergers and Quasar Activity. *ApJS*, 175(2):356–389, April 2008. .

Martin Sparre and Volker Springel. Zooming in on major mergers: dense, starbursting gas in cosmological simulations. *MNRAS*, 462(3):2418–2430, November 2016. .

Tiziana Di Matteo, Volker Springel, and Lars Hernquist. Energy input from quasars regulates the growth and activity of black holes and their host galaxies. *Nature*, 433 (7026):604–607, February 2005. .

Philip F. Hopkins and Lars Hernquist. A Characteristic Division Between the Fueling of Quasars and Seyferts: Five Simple Tests. *ApJ*, 694(1):599–609, March 2009. .

Ezequiel Treister, Priyamvada Natarajan, David B. Sanders, C. Megan Urry, Kevin Schawinski, and Jeyhan Kartaltepe. Major Galaxy Mergers and the Growth of Supermassive Black Holes in Quasars. *Science*, 328(5978):600, April 2010. .

E. Treister, K. Schawinski, C. M. Urry, and B. D. Simmons. Major Galaxy Mergers Only Trigger the Most Luminous Active Galactic Nuclei. *ApJ*, 758(2):L39, October 2012. .

L. Ciotti and G. Bertin. Analytical properties of the $R^{1/m}$ law. *A&A*, 352:447–451, December 1999. .

M. Huertas-Company, S. Mei, F. Shankar, L. Delaye, A. Raichoor, G. Covone, A. Finoguenov, J. P. Kneib, Fèvre O. Le, and M. Povic. The evolution of the mass-size relation for early-type galaxies from z $\sim$ 1 to the present: dependence on environment, mass range and detailed morphology. *MNRAS*, 428(2):1715–1742, January 2013. .

Song Huang, Alexie Leauthaud, Jenny E. Greene, Kevin Bundy, Yen-Ting Lin, Masayuki Tanaka, Satoshi Miyazaki, and Yutaka Komiyama. Individual stellar haloes of massive galaxies measured to 100 kpc at 0.3 < z < 0.5 using Hyper Suprime-Cam. *MNRAS*, 475(3):3348–3368, April 2018. .

M. Bernardi, H. Domínguez Sánchez, J. R. Brownstein, N. Drory, and R. K. Sheth. Galaxy properties as revealed by MaNGA - II. Differences in stellar populations of slow and fast rotator ellipticals and dependence on environment. *MNRAS*, 489(4): 5633–5652, November 2019. .

H. Domínguez Sánchez, M. Bernardi, F. Nikakhtar, B. Margalef-Bentabol, and R. K. Sheth. Galaxy properties as revealed by MaNGA - III. Kinematic profiles and stellar population gradients in S0s. *MNRAS*, 495(3):2894–2908, July 2020. .

Dimitri A. Gadotti. Structural properties of pseudo-bulges, classical bulges and elliptical galaxies: a Sloan Digital Sky Survey perspective. *MNRAS*, 393(4):1531–1552, March 2009. .

David B. Fisher and Niv Drory. Bulges of Nearby Galaxies with Spitzer: Scaling Relations in Pseudobulges and Classical Bulges. *ApJ*, 716(2):942–969, June 2010. .

F. Shankar, F. Marulli, S. Mathur, M. Bernardi, and F. Bournaud. Black holes in pseudobulges: demography and models. *A&A*, 540:A23, April 2012. .

M. Franco, D. Elbaz, M. Béthermin, B. Magnelli, C. Schreiber, L. Ciesla, M. Dickinson, N. Nagar, J. Silverman, E. Daddi, D. M. Alexander, T. Wang, M. Pannella, E. Le Floc'h, A. Pope, M. Giavalisco, A. J. Maury, F. Bournaud, R. Chary, R. Demarco, H. Ferguson, S. L. Finkelstein, H. Inami, D. Iono, S. Juneau, G. Lagache, R. Leiton, L. Lin, G. Magdis, H. Messias, K. Motohara, J. Mullaney, K. Okumura, C. Papovich, J. Pforr, W. Rujopakarn, M. Sargent, X. Shu, and L. Zhou. GOODS-ALMA: 1.1 mm galaxy survey. I. Source catalog and optically dark galaxies. *A&A*, 620:A152, December 2018. .

Tao Wang. ALMA unveils massive galaxies at z>3 that are hidden from Hubble. In *ALMA2019: Science Results and Cross-Facility Synergies*, page 6, December 2019. .

Margherita Talia, Andrea Cimatti, Marika Giulietti, Gianni Zamorani, Matthieu Bethermin, Andreas Faisst, Olivier Le Fèvre, and Vernesa Smolçić. Illuminating the Dark Side of Cosmic Star Formation Two Billion Years after the Big Bang. *ApJ*, 909(1):23, March 2021. .

L. Barrufet, P. A. Oesch, A. Weibel, G. Brammer, R. Bezanson, R. Bouwens, Y. Fudamoto, V. Gonzalez, R. Gottumukkala, G. Illingworth, K. E. Heintz, B. Holden, I. Labbe, D. Magee, R. P. Naidu, E. Nelson, M. Stefanon, R. Smit, P. van Dokkum, J. R. Weaver, and C. C. Williams. Unveiling the nature of infrared bright, optically dark galaxies with early JWST data. *MNRAS*, 522(1):449–456, June 2023. .

W. J. Pearson, F. Pistis, M. Figueira, K. Małek, T. Moutard, D. Vergani, and A. Pollo. Influence of star-forming galaxy selection on the galaxy main sequence. *A&A*, 679: A35, November 2023. .

Joel Leja, Benjamin D. Johnson, Charlie Conroy, Pieter van Dokkum, Joshua S. Speagle, Gabriel Brammer, Ivelina Momcheva, Rosalind Skelton, Katherine E. Whitaker, Marijn Franx, and Erica J. Nelson. An Older, More Quiescent Universe from Panchromatic SED Fitting of the 3D-HST Survey. *ApJ*, 877(2):140, June 2019b. .

Ewald Puchwein, Volker Springel, Debora Sijacki, and Klaus Dolag. Intracluster stars in simulations with active galactic nucleus feedback. *MNRAS*, 406(2):936–951, August 2010. .

Emanuele Contini. On the Origin and Evolution of the Intra-Cluster Light: A Brief Review of the Most Recent Developments. *Galaxies*, 9(3):60, August 2021. .

Mireia Montes and Ignacio Trujillo. Intracluster light: a luminous tracer for dark matter in clusters of galaxies. *MNRAS*, 482(2):2838–2851, January 2019. .

E. Contini and Q. Gu. On the Mass Distribution of the Intracluster Light in Galaxy Groups and Clusters. *ApJ*, 901(2):128, October 2020. .

E. Contini, S. Jeon, J. Rhee, S. Han, and S. K. Yi. The Intracluster Light and its Link with the Dynamical State of the Host Group/Cluster: the Role of the Halo Concentration. *arXiv e-prints*, art. arXiv:2310.03263, October 2023.

A. Katsianis, E. Tescari, G. Blanc, and M. Sargent. The evolution of the star formation rate function and cosmic star formation rate density of galaxies at z $\sim$ 1-4. *MNRAS*, 464(4):4977–4994, February 2017. .

Asa F. L. Bluck, Christopher J. Conselice, Katherine Ormerod, Joanna M. Piotrowska, Nathan Adams, Duncan Austin, Joseph Caruana, K. J. Duncan, Leonardo Ferreira, Paul Goubert, Thomas Harvey, James Trussler, and Roberto Maiolino. Galaxy quenching at the high redshift frontier: A fundamental test of cosmological models in the early universe with JWST-CEERS. *arXiv e-prints*, art. arXiv:2311.02526, November 2023b. .

Justin W. Cole, Casey Papovich, Steven L. Finkelstein, Micaela B. Bagley, Mark Dickinson, Kartheik G. Iyer, L. Y. Aaron Yung, Laure Ciesla, Ricardo O. Amorin, Pablo Arrabal Haro, Rachana Bhatawdekar, Antonello Calabro, Nikko J. Cleri, Alexander de la

Vega, Avishai Dekel, Ryan Endsley, Eric Gawiser, Mauro Giavalisco, Nimish P. Hathi, Michaela Hirschmann, Benne W. Holwerda, Jeyhan S. Kartaltepe, Anton M. Koekemoer, Ray A. Lucas, Sara Mascia, Bahram Mobasher, Pablo G. Perez-Gonzalez, Giulia Rodighiero, Kaila Ronayne, Sandro Tachhella, Benjamin J. Weiner, and Stephen M. Wilkins. CEERS: Increasing Scatter along the Star-Forming Main Sequence Indicates Early Galaxies Form in Bursts. *arXiv e-prints*, art. arXiv:2312.10152, December 2023. .

Andrew Ptak and LSST Galaxies Collaboration. Galaxy Evolution with LSST. In *American Astronomical Society Meeting Abstracts #217*, volume 217 of *American Astronomical Society Meeting Abstracts*, page 252.16, January 2011.

Jonathan P. Gardner, John C. Mather, Mark Clampin, Rene Doyon, Matthew A. Greenhouse, Heidi B. Hammel, John B. Hutchings, Peter Jakobsen, Simon J. Lilly, Knox S. Long, Jonathan I. Lunine, Mark J. McCaughrean, Matt Mountain, John Nella, George H. Rieke, Marcia J. Rieke, Hans-Walter Rix, Eric P. Smith, George Sonneborn, Massimo Stiavelli, H. S. Stockman, Rogier A. Windhorst, and Gillian S. Wright. The James Webb Space Telescope. *Space Sci. Rev.*, 123(4):485–606, April 2006. .

J. Amiaux, R. Scaramella, Y. Mellier, B. Altieri, C. Burigana, Antonio Da Silva, P. Gomez, J. Hoar, R. Laureijs, E. Maiorano, D. Magalhães Oliveira, F. Renk, G. Saavedra Criado, I. Tereno, J. L. Auguères, J. Brinchmann, M. Cropper, L. Duvet, A. Ealet, P. Franzetti, B. Garilli, P. Gondoin, L. Guzzo, H. Hoekstra, R. Holmes, K. Jahnke, T. Kitching, M. Meneghetti, W. Percival, and S. Warren. Euclid mission: building of a reference survey. In Mark C. Clampin, Giovanni G. Fazio, Howard A. MacEwen, and Jr. Oschmann, Jacobus M., editors, *Space Telescopes and Instrumentation 2012: Optical, Infrared, and Millimeter Wave*, volume 8442 of *Society of Photo-Optical Instrumentation Engineers (SPIE) Conference Series*, page 84420Z, September 2012. .